Study on mechanical property of hydrogels based on relaxation behavior by reversible cross-links

A Doctoral Thesis

by

Subaru Konishi

Submitted to

The Graduate School of Science, Osaka University

February 2023

Acknowledgment

This work was carried out from 2017 to 2023 under the direction of Professor Dr. Yoshinori Takashima, Professor Dr. Hiroyasu Yamaguchi, and Professor Dr. Akira Harada at the Department of Macromolecular Science, Graduate School of Science, Osaka University. The author expresses deep gratitude to Professor Dr. Yoshinori Takashima, Professor Dr. Hiroyasu Yamaguchi, and Professor Dr. Akira Harada for accurate and kind guidance throughout the study. Furthermore, the author also thanks Lecturer Dr. Motofumi Osaki, Assistant professor Dr. Junsu Park, Assistant professor Dr. Yuichiro Kobayashi, and Project researcher Dr. Ryohei Ikura for their continuing help, warm encouragement, and kind advices.

Grateful acknowledgements are made to Professor Dr. Tadashi Inoue and Associate Professor Dr. Osamu Urakawa in Osaka University, for their permission and cooperation of rheological measurements, which gave me essential data on polymer dynamics. The author would like to acknowledgement to Associate Professor Dr. Go Watanabe in Kitasato University, Lecturer Dr. Takuya Katashima in The University of Tokyo, and Professor Dr. Go Matsuba in Yamagata University for collaboration works. They provided important results on my research by Quantum chemical calculations, DMA, SAXS measurements. Without their cooperation, my research would lack direct structural data. The author also appreciates Assistant Professor Dr. Takashi Nakamura in University of Tsukuba for the collaboration to investigate polymeric materials based on metal-ligand chemistry.

Members of analytical instrument faculty cooperated with my research. In particular, Dr. Naoya Inazumi, Mr. Yasuto Todokoro, and Mr. Kazushi Kawamura helped NMR measurements, ITC measurements, and FT-IR, respectively.

The author also appreciates all members of Takashima, Yamaguchi, Inoue, and Hashidzume laboratories for their cooperation and friendship. And their various research were good chances for the author to be familiar with varied research fields. At last, the author would like to appreciate to all colleagues, friends, and family for their help and encouragements.

February 2023

Subaru Konishi

Contents

Chapter 1
General Introduction

1.1. Chemistry of non-covalent bonds

Non-covalent bonds mean intramolecular or intermolecular interactions and differ from covalent bonds that share electron pairs. Depending on the type of interaction, these bonds are categorized into ionic bonding, metal-ligand coordination, hydrogen bonding, host-guest complexation, hydrophobic interactions, π-π interactions, and so on.

The characteristics of non-covalent bonds are usually quantified by several parameters, including thermodynamic parameters, kinetic parameters, and the binding energy. **Table 1-1** shows the association constant (equilibrium constant, K_a) and binding energy (E_b) of non-covalent bonds summarized from several reviews.[1–5]

Table 1-1. Binding energy (E_b) and association constant (K_a) of various non-covalent bonds.

Type of interaction		E_b (kJ mol^{-1})	K_a (M^{-1})
Covalent bonding		**100-450**	**—**
Ionic interactions		**200-300**	**—**
Metal-ligand coordination		**0-400**	**< 10^{37}-10^{40}**
Hydrogen bonding		**4-120**	**≤ 10^{9}**
Host-guest complexations	**Cyclodextrin**	**5-25**	**10^{3}-10^{5}**
	Cucurbituril	**20-40**	**≤ 10^{15}**
π-π stacking		**~ 10**	**10^{1}-10^{2}**
Hydrophobic interactions		**< 10**	**—**

In contrast, the association rate constant (k_a) and dissociation rate constant (k_d) vary with the structures of the binding motifs.[6,7] For example, **Figure 1-1** shows the relation between the K_a and k_d of dimerization and 1:1 complexation for hydrogen bonding and host-guest complexations. We can see the relation of $k_d \sim K_a^{-1}$ in many reaction systems. Note that the thermodynamics and kinetics of non-covalent bonds are highly dependent not only on the structures of the binding motifs but also on the external environment, such as the temperature and solvent.

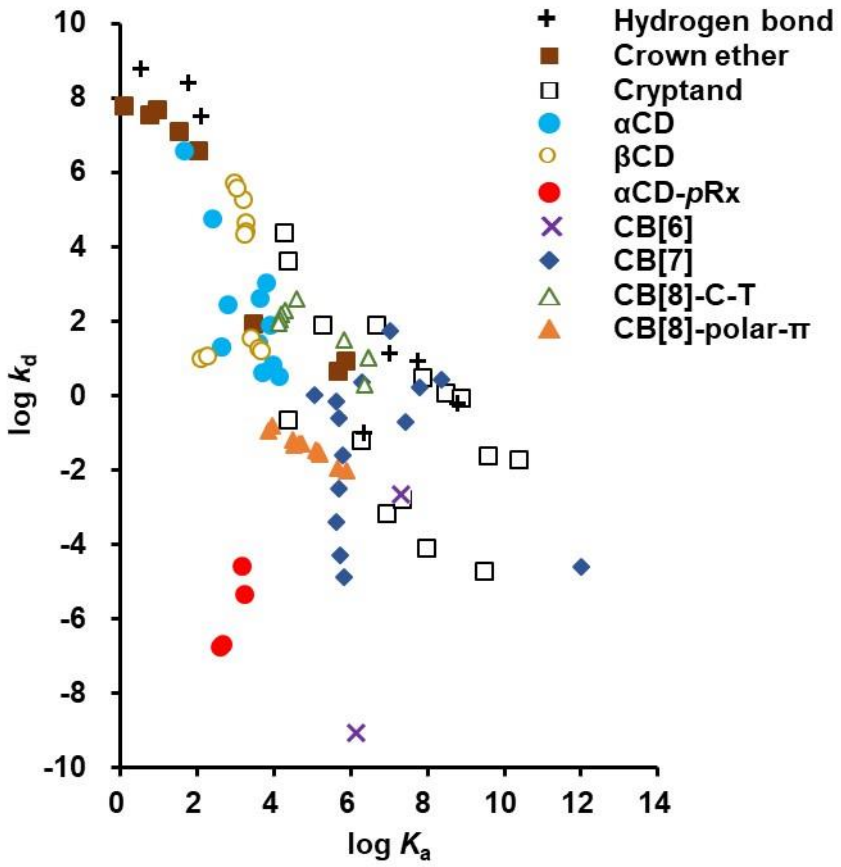

Figure 1-1. Comparison of the dissociation rate constant (k_d [s^{-1}]) and K_a [M^{-1}] of dimerization and 1:1 complexation for different non-covalent bonds, including hydrogen bonds[8–10], as well as host-guest complexation based on crown ethers[11–14], cryptands[15,16], α-cyclodextrin (αCD)[17–19], β-cyclodextrin (βCD)[17,20–24], and cucurbit[*n*]urils (CB[6][25], CB[7][25–29], and CB[8]). αCD-*p*Rx[30–32] indicates a formation of [2]*pseudo*-rotaxane with an alkyl axis containing cation moieties at both ends. CB[8]-C-T[33,34] and CB[8]-polar-π[35] indicate CB[8]-mediated charge-transfer interactions and polar-π interactions, respectively.

Host-guest complexation means complex formation in which a cyclic host molecule incorporates guest molecules with a suitable size for its cavity. Host-guest complexation is caused by a cooperative effect of several interactions, e.g. electrostatic interactions, ion-dipole interactions, hydrophobic interactions, and van der Waals forces. Cyclodextrins (CDs) are water-soluble and cyclic host molecules composed of D-glucose units linked by α-1,4 bonds. Three major CDs having 6, 7, and 8 D-glucose units are called αCD, βCD, and γCD, respectively. CDs form host-guest complexes by including hydrophobic guest molecules in their cavities.[36,37]

As shown in **Figure 1-1**, 1:1 host-guest complexation of CDs with hydrophobic molecules usually exhibits relatively low association constants ($K_a = 10^2 \sim 10^4$ M^{-1}) and high dissociation rate constants ($k_d = 10^1 \sim 10^6$ s^{-1}). Additionally, some studies revealed that introducing different functional groups to the end of an axis molecule decreased the kinetics of the formation of the *pseudo*-rotaxane of CD with the axis (represented as αCD-*p*Rx in **Figure 1-1**) while maintaining the K_a value. **Table 1-2** shows the K_a, k_a, and k_d of the *pseudo*-rotaxane of αCD. Threading/dethreading of αCD along the dodecamethylenediamine axis occurs faster than the NMR time scale. However, the introduction of cation groups to both ends of the axis slows the rate constants of αCD.[30–32,38,39] Although the trimethylammonium cation, pyridinium cation, and viologen dication groups can pass through αCD,[40–43] including cationic units directly in its cavity is difficult due to their electrostatic instability. Therefore, cations at the end of the axis function as a potential barrier that slows the kinetics of host-guest complexation. An increase in the positive charge density and steric hindrance decreases k_a and k_d more.

Table 1-2. Chemical structures of cation-modified alkyl guests, association constants (K_a), and association/dissociation rate constants (k_a and k_d) of the inclusion complexes with αCD.

Guest	K_a / M^{-1}	k_a / $s^{-1}M^{-1}$	k_d / s^{-1}	T / °C	ref.
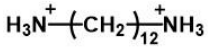 $N^+C_{12}N^+$	**7400**	**n.d.[a]**	**n.d.**	**25**	**[40]**
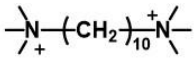 $Me_3N^+C_{11}N^+Me_3$	**1540**	**3.6×10^{-2}**	**2.4×10^{-5}**	**25**	**[30]**
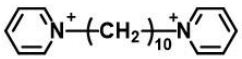 $Py^+C_{10}Py^+$	**2200**	**n.d.**	**n.d.**	**5.0**	**[41]**
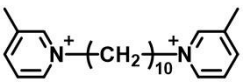	**n.d.**	**n.d.**	**n.d.**	**25**	**[31]**
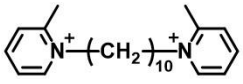	**490**	**9.3×10^{-5}**	**1.9×10^{-7}**	**25**	**[31]**
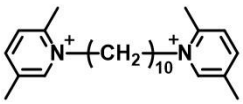	**430**	**7.3×10^{-5}**	**1.7×10^{-7}**	**25**	**[31]**
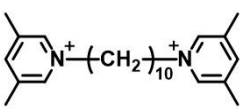	**not form[b]**	**not form**	**not form**	**25**	**[31]**

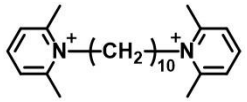	not form	not form	not form	25	[31]
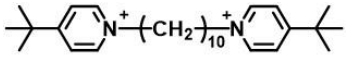 tbPy^{+}C$_{10}$Py^{+}tb	1800	4.2×10^{-4}	4.2×10^{-6}	25	[32]
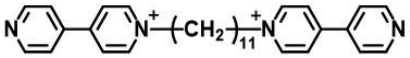 V^{+}C$_{11}$V^{+}	4050	n.d.	n.d.	25	[43]
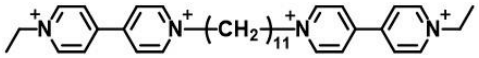 EtV^{2+}C$_{11}$V^{2+}Et	230	n.d.	n.d.	25	[43]
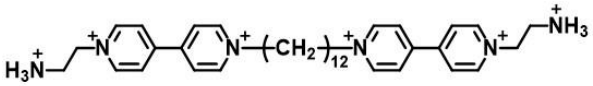 AV^{3+}C$_{12}$AV^{3+}	n.d.	5.0×10^{-5} [c]	n.d.	30	[38]

*[a] These values could not be determined because the reactions occurred too fast. [b] These molecules could not form inclusion complexes. [c] This value was calculated from the reanalysis data of the reference.[38]

1.2. Functional polymeric materials with reversible cross-links

Non-covalent bonds can be formed not only between low-molecular-weight compounds but also between macromolecules. Various non-covalent bonds between polymers act as cross-links to give supramolecular polymer networks and materials. The cross-links formed by non-covalent bonds are called reversible cross-links since they reversibly associate and dissociate based on chemistry of non-covalent bonds. Generally, the thermodynamics of non-covalent bonds directly affect the *degree* of cross-linking, and the kinetics affect the *dynamic nature* of cross-links and polymer networks.[3,44,45] In addition to various non-covalent bonds, including those involving ionic interactions,[46–50] coordination bonding,[51] hydrogen bonding,[52,53] hydrophobic interactions,[54,55] and host-guest interactions,[56–65] dynamic covalent bonds[66] also form reversible cross-links.

Depending on the chemical properties and reversibility of the cross-links, polymeric materials can exhibit various functions, such as toughening, self-healing,[67–72] stimuli-responsiveness,[73–75] shape-memory effects,[76–78] and controlled mechanical properties.[1,79,80] Considering the direct relation of reversible cross-links and functionalities, the parameters of non-covalent bonds should also be important in designing functional polymeric materials.

1.3. Energy dissipation mechanisms for tough materials (gels and networks)

Hydrogels, which are defined as three-dimensional polymeric materials containing water, are abundant in nature. Natural hydrogels (cartilage, tendon, polysaccharides, *etc.*) usually show extreme mechanical properties.[81–85] These properties come from elaborate and sophisticated designs, such as precise sequences, hierarchical structures, combinations of different functional groups, and multiscale components.[1,80,86]

In contrast, synthetic hydrogels are easily prepared by a traditional method such as free radical polymerization with chemical cross-links.[87,88] Furthermore, the physical properties and functionalities of the hydrogels can be modified depending on the characteristics of the compounds used. However, the mechanical performance of synthetic hydrogels is usually poorer than that of natural hydrogels due to their deficient heterogeneous network, low friction between polymers, and resulting stress concentration around short polymer chains.[89,90] To address this issue, substantial developments in mechanical properties have been made in the field of polymeric materials by approximating an ideal polymer network or adopting mechanisms for dissipating energy from the environment.[1,79,80,91–95] The strategy of approximating an ideal polymer network has been achieved for tetra(polyethylene glycol) (tetra-PEG) gels[96–99] and slide-ring gels.[100–104] Homogeneous structures are realized for the former gels by a highly stoichiometric and symmetric gelation process. In the latter gels, cross-linking points slide along the chain to equalize the force and reduce the heterogeneity under deformation. These hydrogels show high extensibility.

Energy dissipation mechanisms in tough hydrogels include the fracture of polymer chains, the transformation of domains in polymer chains or cross-links, the fracture and pullout of fibers or fillers in composites, and the dissociation of reversible cross-links.[79,91,105] These mechanisms were incorporated into different strategies, such as multiple network gels,[90,106–111] nanocomposite gels,[112–118] polyrotaxane gels,[119–121] and rotaxane cross-linked gels.[122–124]

Figure 1-2 shows a schematic of the mechanism of energy dissipation by reversible cross-links. The reversible cross-links can dissociate when a polymeric material is under mechanical stress. The dissociation relaxes the stretched polymer chains and leads to the dissipation of energy from the polymer network, high stretchability of the polymer network, and eventually toughening of the materials.[79] The author has become interested in investigating the energy dissipation mechanism and relaxation phenomena in terms of the parameters of non-covalent bonds. For example, the author expects that the kinetics parameter of non-covalent bonds will affect the frequency of energy dissipation in polymeric materials over a certain timescale.

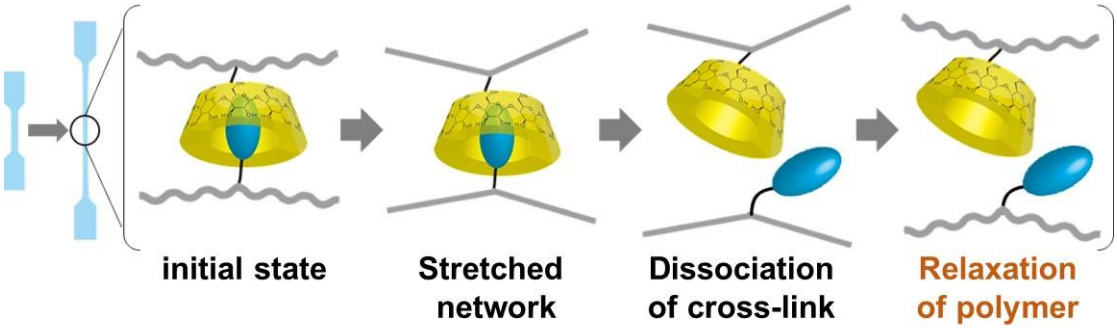

Figure 1-2. Schematic of energy dissipation through the relaxation behavior of reversible cross-links.

1.4. Macroscopic behavior of polymeric materials with reversible cross-links

1.4.1. Change in the relaxation time of supramolecular polymeric materials induced by the kinetics of non-covalent bonds

As described above, the kinetics of non-covalent bonds should affect the *dynamic nature* of supramolecular polymer networks. Several physical models have been developed to predict the viscoelastic properties of supramolecular polymer networks: 'living' polymer theory by Cates *et al.*,[125] sticky-Rouse theory by Baxandall,[126] and sticky-reptation theory by Leibler, Rubinstein, and Colby.[127] There are two important timescales to characterize the dynamics of supramolecular polymer networks. One is the timescale of association/dissociation of reversible cross-links, and the other is that of relaxation of polymer chains or chain segments. Many studies have experimentally demonstrated that the former timescale τ_b is profoundly affected by the kinetics of non-covalent bonds ($\tau_b \approx k_d^{-1}$), not the thermodynamics. Details of the models and experimental findings have been reviewed in several reports,[3,6,44,45,95,128,129] so the author only introduces one example here.

A series of works by Craig and coworkers are representative works that demonstrated the quantitative relation between the kinetics of non-covalent bonds and the macroscopic dynamic properties of supramolecular polymers.[130–132] They designed poly(4-vinylpyridine) (PVP) networks with reversible cross-links by metal-ligand coordination in DMSO. The point of their works was independent control of the kinetics and thermodynamics of cross-links by using the steric hindrance effect. They used 4 types of reversible cross-links composed of the pyridyl moiety of PVP and bis(Pd^{2+}- or Pt^{2+}-pincer). The steric hindrance effect of substituents on the pincer structure with methyl or ethyl groups led to large changes in the exchange rate constants by two orders of magnitude, without significant changes in the K_a of each metal. Therefore,

the effect of the kinetics of cross-links could be studied independently of the thermodynamics. The remarkable result is that the viscoelastic properties of PVP networks scaled exactly with the k_d of low-molecular model compounds analyzed by NMR spectroscopy. The frequency-dependent storage modulus and viscosity of the four different PVP networks were reduced to a master curve by simply rescaling the frequency with k_d^{-1}, regardless of the large difference in K_a between Pd^{2+} and Pt^{2+} ($K_a = 10^1$ and 10^3 M^{-1}, respectively). This clearly identified that the kinetics of reversible cross-links dominantly determined the viscoelastic properties of supramolecular polymer networks.

These results were supported by individual studies using hydrogen bonding motifs,[8] metal-histidine complexes,[133,134] the CB[7] complex,[29] the CB[8] complex,[35,64] DNA duplexes,[135] boronic ester bond,[136] and so on. Control of the viscoelastic properties of supramolecular polymer networks has been achieved using the kinetics of non-covalent bonds in various studies and continues to attract much attention.

1.4.2. Change in the mechanical properties of polymeric materials induced by dynamics

Given that supramolecular polymeric networks have frequency-dependent viscoelastic characteristics, the idea that the mechanical properties of supramolecular hydrogels with reversible cross-links should exhibit strain rate dependence seems natural. However, the author feels that the relation between the strain rate and toughening of hydrogels with reversible cross-links has not been well discussed.

A strong dependence of the mechanical behavior on the strain rate has been observed in dual cross-link hydrogels that combine permanent covalent cross-links and reversible cross-links in a single network.[91] One example is the nanocomposite hydrogel combining silica nanoparticles and a chemically cross-linked poly(*N*,*N*-dimethylacrylamide) network developed by Marcellan *et al*.[137] A large strain mechanical cycling test of the hybrid hydrogel was performed at different strain rates, where the maximum strain was set to ~0.3, and the strain rate was set to 3×10^{-4}, 0.06, or 0.6 s^{-1}. The stiffness and energy dissipated during the cycling test strongly depended on the applied strain rate: the hydrogels showed low stiffness and hysteresis at low strain rates (similar to a chemical network) and high stiffness and hysteresis at high strain rates (similar to a viscoelastic hybrid network). The time-dependent dissipative mechanism was attributed to the timescale of "sacrificial" silica/polymer interactions. Such a dependence on the strain rate indicated that "toughening mechanisms operating at standard strain rates, as often reported,

maybe quite different at slower or larger strain rates." Furthermore, a model for the time-dependent behavior of a dual cross-link gel was developed by Narita and Hui *et al.*[138,139]

A different example is tough and viscoelastic hydrogels cross-linked by ionic interactions in Gong's group: polyampholyte hydrogels.[46] In polyampholyte hydrogels, two types of multiple ionic bonds with different strengths are formed. One is the strong interchain bonds that act as quasi-permanent cross-links to impart elasticity. The other is weak inter- and intrachain bonds, which serve as reversible cross-links to dissipate energy. The tensile behavior of the polyampholyte hydrogels in the equilibrated state depended on the initial strain rate, indicating that their viscoelastic feature contributed to a high shock-absorption ratio and toughness.[46,48] Further investigation found that the hysteresis energy at large strain obtained at different strain rates and temperatures could be reduced to a single master curve by adopting time–temperature superposition.[50] This interesting result means that the linear viscoelasticity is also applicable to the bulk energy dissipation in the large deformation regime, and the dissociation of ionic bonds is thermally activated and hardly depends on the applied strain.

The above findings in dual cross-linked hydrogels suggest that both the strain rate and dynamics of reversible cross-links affect the mechanical properties of the hydrogels. Such discussions should be extended to the energy dissipation mechanism in other supramolecular hydrogels with reversible cross-links. Recently, Chen, Cao, and Tan *et al.* developed tetra-PEG hydrogels cross-linked by host-guest complexation of CB[7] with hexanoate-isoquinoline (HIQ).[29] The dynamics of reversible CB[7]-HIQ cross-links were tuned by the pH, ranging from 10^{-1} to 10^{3} s. Although the dependence on the strain rate was not investigated, they showed how the work of fracture during tensile tests was correlated with the dynamics of CB[7]-HIQ cross-links by tuning the pH. The hydrogels showed distinct mechanical behaviors, from a soft-and-weak type at low pH to a soft-but-tough type at neutral pH and a hard-but-brittle type at high pH. At pH 6–8, the hydrogels exhibited relatively high work of fracture. In this pH range, the lifetime of cross-links (33~3200 s) was close to the timescale of tensile tests (~10^{2} s). Therefore, they concluded that maximal toughness could be achieved when the lifetime of reversible cross-links matched the experimental network deformation timescale.

As described in the previous section, techniques to control the viscoelastic behavior of polymer networks by engineering the kinetics of binding motifs are developing. Therefore, more quantitative discussions and evidence in terms of the chemistry of non-covalent bonds will be needed to design the mechanical properties and functionalities of supramolecular polymeric materials.

1.5. Scope and outline of this thesis

This thesis addresses the material design based on the quantitative parameters of non-covalent bonds. In particular, the author focuses on the relation between the viscoelastic relaxation time and the mechanical properties of supramolecular polymeric materials.

In Chapter 2, the viscoelastic and mechanical properties of supramolecular hydrogels cross-linked by host-guest complexation are presented. Complexation of αCDs with cation-terminated alkyl chain guests was used to obtain reversible cross-links in the hydrogels. The second-order average viscoelastic relaxation time ($<\tau>_w$) of the hydrogels widely varied from 1.8 s to 9.5 × 10^3 s depending on the structure, charge density, and bulkiness of the cationic moieties. The author demonstrated the viscoelastic behavior of reversible cross-links under tensile testing by using the relaxation time and initial strain rate and demonstrated their effect on the toughness and stiffness of the hydrogels (**Figure 1-3**). The toughness drastically increased on the timescale where the reversible cross-links behaved as viscoelastic bodies. The importance of designing the dynamics of reversible cross-links to improve the toughness was revealed.

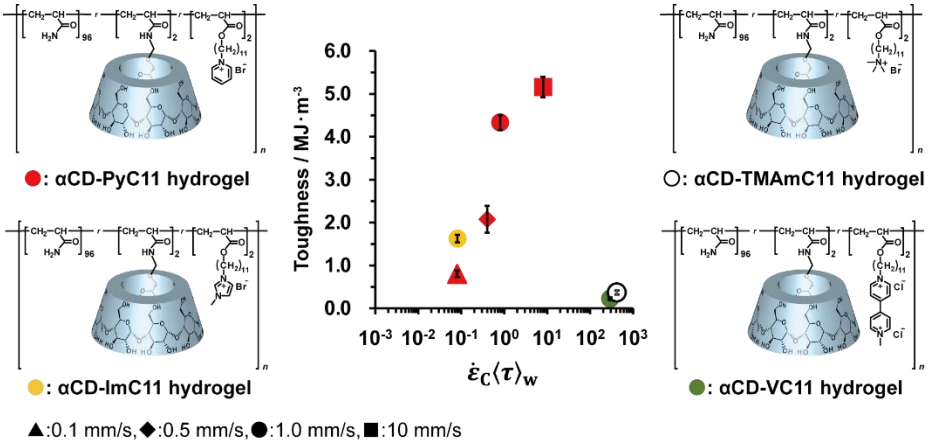

Figure 1-3. Relation among the toughness, relaxation time, and strain rate of supramolecular hydrogels.

In Chapter 3, the viscoelasticity and mechanical toughness of supramolecular hydrogels consisting of two kinetically distinct reversible cross-links provided by host-guest interactions are investigated (**Figure 1-4**). Linear viscoelastic measurements clarified that the two kinds of cross-links independently relaxed and that the combined hydrogels showed a hierarchy of relaxation behaviors over wide timescales. The hydrogels combining fast and slowly reversible cross-links showed a toughness several times as high as that of other hydrogels. The dependence of the hysteresis properties on the induced strain revealed that the tough hydrogels with fast and slow cross-links effectively dissipated more mechanical energy at large strains.

This suggests that the fast and slow cross-links dissociated at small and large strains, respectively, and the stepwise relaxations improved the toughness.

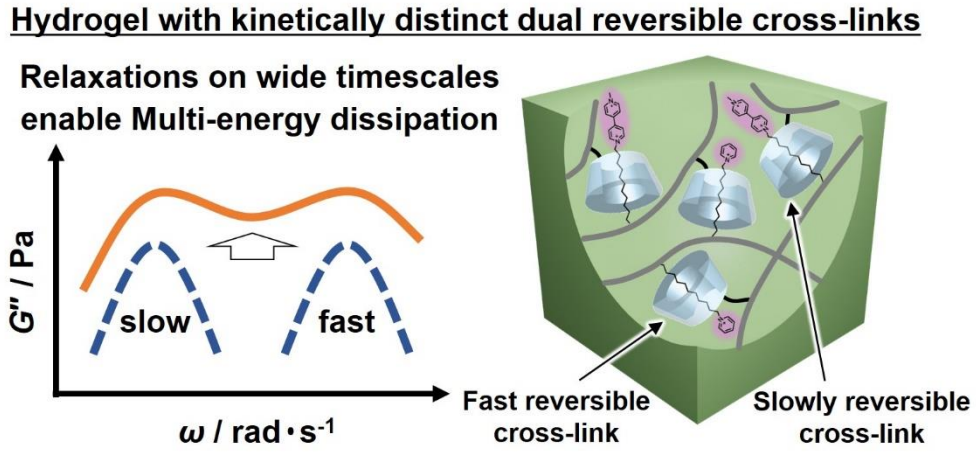

Figure 1-4. Schematics of a supramolecular hydrogel with kinetically distinct dual reversible cross-links and expected viscoelastic relaxation.

In Chapter 4, supramolecular hydrogels cross-linked by metal-ligand complexes with different kinetics are studied to investigate the universality of the relation between the relaxation time and toughness of hydrogels discovered in the previous chapters (**Figure 1-5**). The reversible cross-links were composed of complexes of transition metals with 2,2′-bipyridyl units. The author investigated the relation between the relaxation time and toughness of metal-ligand-type hydrogels and compared it with the results in Chapter 2.

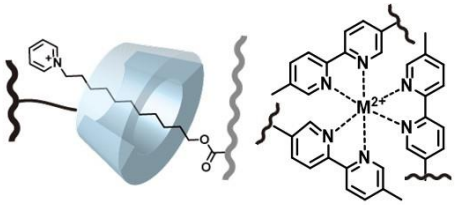

	Host-guest complexation	Metal-ligand Coordination
Structure	1:1	1:1 ~ 1:3
K_a	$K_1 \approx 10^3$	$K_1K_2K_3 \approx 10^{20}$
k_d	n.d.	(variable)
$\langle\tau\rangle_w$	10^1 ~ 10^3 s	(variable)

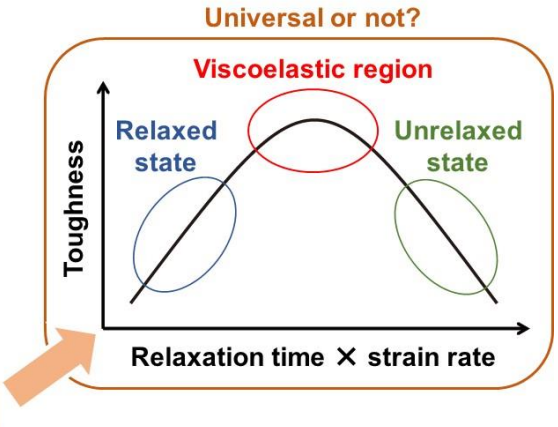

Figure 1-5. The comparison of hydrogels cross-linked by host-guest complexations with those cross-linked by metal-ligand coordination to investigate the relation between relaxation time and tensile toughness.

References

(1) Zhao, X.; Chen, X.; Yuk, H.; Lin, S.; Liu, X.; Parada, G. Soft Materials by Design: Unconventional Polymer Networks Give Extreme Properties. *Chem. Rev.* **2021**, *121* (8), 4309–4372.

(2) Rodin, M.; Li, J.; Kuckling, D. Dually Cross-Linked Single Networks: Structures and Applications. *Chem. Soc. Rev.* **2021**, *50* (14), 8147–8177.

(3) Appel, E. A.; del Barrio, J.; Loh, X. J.; Scherman, O. A. Supramolecular Polymeric Hydrogels. *Chem. Soc. Rev.* **2012**, *41* (18), 6195–6214.

(4) Khare, E.; Holten-Andersen, N.; Buehler, M. J. Transition-Metal Coordinate Bonds for Bioinspired Macromolecules with Tunable Mechanical Properties. *Nature Reviews Materials*. Springer US 2021, pp 421–436.

(5) Shi, L.; Ding, P.; Wang, Y.; Zhang, Y.; Ossipov, D.; Hilborn, J. Self-Healing Polymeric Hydrogel Formed by Metal–Ligand Coordination Assembly: Design, Fabrication, and Biomedical Applications. *Macromol. Rapid Commun.* **2019**, *40* (7), 1–18.

(6) Chen, H.; Tong, K. The Contributions of Supramolecular Kinetics to Dynamics of Supramolecular Polymers. *Chempluschem* **2022**, *87*, e202200279.

(7) Bohne, C. Supramolecular Dynamics. *Chem. Soc. Rev.* **2014**, *43* (12), 4037–4050.

(8) Sijbesma, R. P.; Beijer, F. H.; Brunsveld, L.; Folmer, B. J. B.; Hirschberg, J. H. K. K.; Lange, R. F. M.; Lowe, J. K. L.; Meijer, E. W. Reversible Polymers Formed from Self-Complementary Monomers Using Quadruple Hydrogen Bonding. *Science* **1997**, *278* (5343), 1601–1604.

(9) Hammes, G. G.; Park, A. C. Kinetic Studies of Hydrogen Bonding. 1-Cyclohexyluracil and 9-Ethyladenine. *J. Am. Chem. Soc.* **1968**, *90* (15), 4151–4157.

(10) Söntjens, S. H. M.; Sijbesma, R. P.; Van Genderen, M. H. P.; Meijer, E. W. Stability and Lifetime of Quadruply Hydrogen Bonded 2-Ureido-4[1H]-Pyrimidinone Dimers. *J. Am. Chem. Soc.* **2000**, *122* (31), 7487–7493.

(11) Liesegang, G. W.; Farrow, M. M.; Purdie, N.; Eyring, E. M. Ultrasonic Absorption Kinetic Studies of the Complexation of Aqueous Potassium and Cesium Ions by 18-Crown-6. *J. Am. Chem. Soc.* **1976**, *98* (22), 6905–6908.

(12) Liesegang, G. W.; Farrow, M. M.; Arce Vazquez, F.; Purdie, N.; Eyring, E. M. Ultrasonic Absorption Kinetic Studies of the Complexation of Aqueous Lithium(1+), Sodium(1+), Rubidium(1+), Thallium(1+), Silver(1+), Ammonium(1+), and Calcium(2+) Ions by 18-Crown-6. *J. Am. Chem. Soc.* **1977**, *99* (10), 3240–3243.

(13) Cox, B. G.; Firman, P.; Schneider, I.; Schneider, H. Rates and Equilibria of Alkaline-Earth-Metal Complexes with Diaza Crown Ethers in Methanol. *Inorg. Chem.* **1988**, *27* (22), 4018–4021.

(14) Cox, B. G.; Firman, P.; Schneider, H. Thermodynamic and Kinetic Studies on Complex Formation of Alkaline Earth Metal Ions with Diaza-Crown Ethers in Methanol. *Inorganica Chim. Acta* **1983**, *69* (C), 161–166.

(15) Cox, B. G.; Stroka, J.; Schneider, H. Kinetics of Alkali Metal Complex Formation with Cryptands in Methanol. *J. Am. Chem. Soc.* **1978**, *100* (15), 4746–4749.

(16) Cox, B. G.; Schneider, H. The Acid Catalyzed Dissociation of Metal Cryptate Complexes. *J. Am. Chem. Soc.* **1977**, *99* (8), 2809–2811.

(17) Nau, W. M.; Zhang, X. An Exceedingly Long-Lived Fluorescent State as a Distinct Structural and Dynamic Probe for Supramolecular Association: An Exploratory Study of Host- Guest Complexation by Cyclodextrins. *J. Am. Chem. Soc.* **1999**, *121* (35), 8022–8032.

(18) Formation, T. Inclusion Compounds . XIX . La The Formation of Inclusion Thermodynamics and Kinetics. *J. Am. Chem. Soc.* **1967**, *89* (5), 14–20.

(19) Park, J. W. Kinetics and Mechanism of Cyclodextrin Inclusion Complexation Incorporating Bidirectional Inclusion and Formation of Orientational Isomers. *J. Phys. Chem. B* **2006**, *110* (49), 24915–24922.

(20) Barros, T. C.; Stefaniak, K.; Holzwarth, J. F.; Bohne, C. Complexation of Naphthylethanols with β-Cyclodextrin. *J. Phys. Chem. A* **1998**, *102* (28), 5639–5651

(21) Yim, C. T.; Zhu, X. X.; Brown, G. R. Kinetics of Inclusion Reactions of β-Cyclodextrin with Several Dihydroxycholate Ions Studied by NMR Spectroscopy. *J. Phys. Chem. B* **1999**, *103* (3), 597–602.

(22) Zheng, P.; Li, Z.; Tong, L.; Lu, R. Study of Inclusion Complexes of Cyclodextrins with Orange II. *J. Incl. Phenom.* **2002**, *43* (3–4), 183–186.

(23) Matsue, T.; Evans, D. H.; Osa, T.; Kobayashi, N. Electron-Transfer Reactions Associated with Host-Guest Complexation. Oxidation of Ferrocenecarboxylic Acid in the Presence of β-Cyclodextrin. *J. Am. Chem. Soc.* **1985**, *107* (12), 3411–3417.

(24) Wang, Y.; Mendoza, S.; Kaifer, A. E. Electrochemical Reduction of Cobaltocenium in the Presence of β-Cyclodextrin. *Inorg. Chem.* **1998**, *37* (2), 317–320.

(25) Mukhopadhyay, P.; Zavalij, P. Y.; Isaacs, L. High Fidelity Kinetic Self-Sorting in Multi-Component Systems Based on Guests with Multiple Binding Epitopes. *J. Am. Chem. Soc.* **2006**, *128* (43), 14093–14102.
(26) Tang, H.; Fuentealba, D.; Ko, Y. H.; Selvapalam, N.; Kim, K.; Bohne, C. Guest Binding Dynamics with Cucurbit[7]Uril in the Presence of Cations. *J. Am. Chem. Soc.* **2011**, *133* (50), 20623–20633.
(27) Miskolczy, Z.; Biczók, L.; Jablonkai, I. Kinetics of the Reversible Inclusion of Flavopereirine in Cucurbit[7]Uril. *Phys. Chem. Chem. Phys.* **2017**, *19* (1), 766–773.
(28) Miskolczy, Z.; Megyesi, M.; Toke, O.; Biczók, L. Change of the Kinetics of Inclusion in Cucurbit[7]Uril upon Hydrogenation and Methylation of Palmatine. *Phys. Chem. Chem. Phys.* **2019**, *21* (9), 4912–4919.
(29) Chen, H.; Zhang, J.; Yu, W.; Cao, Y.; Cao, Z.; Tan, Y. Control Viscoelasticity of Polymer Networks with Crosslinks of Superposed Fast and Slow Dynamics. *Angew. Chemie - Int. Ed.* **2021**, *60* (41), 22332–22338.
(30) Herrmann, W.; Keller, B.; Wenz, G. Kinetics and Thermodynamics of the Inclusion of Ionene-6,10 in α-Cyclodextrin in an Aqueous Solution. *Macromolecules* **1997**, *30* (17), 4966–4972.
(31) Oshikiri, T.; Takashima, Y.; Yamaguchi, H.; Harada, A. Face-Selective [2]- and [3]Rotaxanes: Kinetic Control of the Threading Direction of Cyclodextrins. *Chem. - A Eur. J.* **2007**, *13* (25), 7091–7098.
(32) Macartney, D. H. The Self-Assembly of a [2]Pseudorotaxane of α-Cyclodextrin by the Slippage Mechanism. *J. Chem. Soc. Perkin Trans. 2* **1996**, No. 12, 2775–2778.
(33) Appel, E. A.; Biedermann, F.; Hoogland, D.; Del Barrio, J.; Driscoll, M. D.; Hay, S.; Wales, D. J.; Scherman, O. A. Decoupled Associative and Dissociative Processes in Strong yet Highly Dynamic Host-Guest Complexes. *J. Am. Chem. Soc.* **2017**, *139* (37), 12985–12993.
(34) Appel, E. A.; Forster, R. A.; Koutsioubas, A.; Toprakcioglu, C.; Scherman, O. A. Activation Energies Control the Macroscopic Properties of Physically Cross-Linked Materials. *Angew. Chemie - Int. Ed.* **2014**, *53* (38), 10038–10043.
(35) Huang, Z.; Chen, X.; O'Neill, S. J. K.; Wu, G.; Whitaker, D. J.; Li, J.; McCune, J. A.; Scherman, O. A. Highly Compressible Glass-like Supramolecular Polymer Networks. *Nat. Mater.* **2022**, *21* (1), 103–109.
(36) Szejtli, J. Introduction and General Overview of Cyclodextrin Chemistry. *Chem. Rev.* **1998**, *98* (5), 1743–1753.
(37) Harada, A. *Supramolecular Polymer Chemistry*; Wiley-VCH: Weinheim, 2012.
(38) Kawaguchi, Y.; Harada, A. An Electric Trap: A New Method for Entrapping Cyclodextrin in a Rotaxane Structure. *J. Am. Chem. Soc.* **2000**, *122* (15), 3797–3798.
(39) Kawaguchi, Y.; Harada, A. A Cyclodextrin-Based Molecular Shuttle Containing Energetically Favored and Disfavored Portions in Its Dumbbell Component. *Org. Lett.* **2000**, *2* (10), 1353–1356.
(40) Li, J.; Harada, A.; Kamachi, M. Formation of Inclusion Complexes of Oligoethylene and Its Derivatives with α-Cyclodextrin. *Bull. Chem. Soc. Jpn.* **1994**, *67* (10), 2808–2818.
(41) Saito, H.; Yonemura, H.; Nakamura, H.; Matsuo, T. Stability and Exchange Properties of Through-Ring Cyclodextrin Complexes. Effects of Chain Length in Polymethylene Bis[1-Pyridinium] as Guest Molecules. *Chemistry Letters*. **1990**, 535–538.
(42) Yonemura, H.; Kasahara, M.; Saito, H.; Nakamura, H.; Matsuo, T. Spectroscopic Studies on Exchange Properties in Through-Ring Cyclodextrin Complexes of Carbazole-Viologen Linked Compounds: Effects of Spacer Chain Length. *J. Phys. Chem.* **1992**, *96* (14), 5765–5770.
(43) Castro, R.; Godínez, L. A.; Criss, C. M.; Kaifer, A. E. Host Properties of α-Cyclodextrin and a Water-Soluble Calix[6]Arene Probed with Dimeric Bipyridinium Guests. *J. Org. Chem.* **1997**, *62* (15), 4928–4935.
(44) Serpe, M. J.; Craig, S. L. Physical Organic Chemistry of Supramolecular Polymers. *Langmuir* **2007**, *23* (4), 1626–1634.
(45) Seiffert, S.; Sprakel, J. Physical Chemistry of Supramolecular Polymer Networks. *Chem. Soc. Rev.* **2012**, *41* (2), 909–930.
(46) Sun, T. L.; Kurokawa, T.; Kuroda, S.; Ihsan, A. Bin; Akasaki, T.; Sato, K.; Haque, M. A.; Nakajima, T.; Gong, J. P. Physical Hydrogels Composed of Polyampholytes Demonstrate High Toughness and Viscoelasticity. *Nat. Mater.* **2013**, *12* (10), 932–937.
(47) Luo, F.; Sun, T. L.; Nakajima, T.; Kurokawa, T.; Zhao, Y.; Sato, K.; Ihsan, A. Bin; Li, X.; Guo, H.; Gong, J. P. Oppositely Charged Polyelectrolytes Form Tough, Self-Healing, and Rebuildable Hydrogels. *Adv. Mater.* **2015**, *27* (17), 2722–2727.
(48) Sun, T. L.; Luo, F.; Kurokawa, T.; Karobi, S. N.; Nakajima, T.; Gong, J. P. Molecular Structure of Self-Healing Polyampholyte Hydrogels Analyzed from Tensile Behaviors. *Soft Matter* **2015**, *11* (48), 9355–9366.
(49) Ihsan, A. Bin; Sun, T. L.; Kurokawa, T.; Karobi, S. N.; Nakajima, T.; Nonoyama, T.; Roy, C. K.; Luo, F.; Gong, J. P. Self-Healing Behaviors of Tough Polyampholyte Hydrogels. *Macromolecules* **2016**, *49* (11), 4245–4252.
(50) Sun, T. L.; Luo, F.; Hong, W.; Cui, K.; Huang, Y.; Zhang, H. J.; King, D. R.; Kurokawa, T.; Nakajima, T.; Gong, J. P. Bulk Energy Dissipation Mechanism for the Fracture of Tough and Self-Healing Hydrogels.

Macromolecules **2017**, *50* (7), 2923–2931.
(51) Lin, P.; Ma, S.; Wang, X.; Zhou, F. Molecularly Engineered Dual-Crosslinked Hydrogel with Ultrahigh Mechanical Strength, Toughness, and Good Self-Recovery. *Adv. Mater.* **2015**, *27* (12), 2054–2059.
(52) Percec, V.; Bera, T. K.; Butera, R. J. A New Strategy for the Preparation of Supramolecular Neutral Hydrogels. *Biomacromolecules* **2002**, *3* (2), 272–279.
(53) Guo, M.; Pitet, L. M.; Wyss, H. M.; Vos, M.; Dankers, P. Y. W.; Meijer, E. W. Tough Stimuli-Responsive Supramolecular Hydrogels with Hydrogen-Bonding Network Junctions. *J. Am. Chem. Soc.* **2014**, *136* (19), 6969–6977.
(54) Abdurrahmanoglu, S.; Can, V.; Okay, O. Design of High-Toughness Polyacrylamide Hydrogels by Hydrophobic Modification. *Polymer* **2009**, *50* (23), 5449–5455.
(55) Hao, J.; Weiss, R. A. Viscoelastic and Mechanical Behavior of Hydrophobically Modified Hydrogels. *Macromolecules* **2011**, *44* (23), 9390–9398.
(56) Appel, E. A.; Biedermann, F.; Rauwald, U.; Jones, S. T.; Zayed, J. M.; Scherman, O. A. Supramolecular Cross-Linked Networks via Host-Guest Complexation with Cucurbit[8]Uril. *J. Am. Chem. Soc.* **2010**, *132* (40), 14251–14260.
(57) Appel, E. A.; Loh, X. J.; Jones, S. T.; Biedermann, F.; Dreiss, C. A.; Scherman, O. A. Ultrahigh-Water-Content Supramolecular Hydrogels Exhibiting Multistimuli Responsiveness. *J. Am. Chem. Soc.* **2012**, *134* (28), 11767–11773.
(58) Liu, J.; Tan, C. S. Y.; Yu, Z.; Lan, Y.; Abell, C.; Scherman, O. A. Biomimetic Supramolecular Polymer Networks Exhibiting Both Toughness and Self-Recovery. *Adv. Mater.* **2017**, *29* (10), 1604951.
(59) Liu, J.; Scherman, O. A. Cucurbit[n]Uril Supramolecular Hydrogel Networks as Tough and Healable Adhesives. *Adv. Funct. Mater.* **2018**, *28* (21), 1–6.
(60) Liu, J.; Tan, C. S. Y.; Yu, Z.; Li, N.; Abell, C.; Scherman, O. A. Tough Supramolecular Polymer Networks with Extreme Stretchability and Fast Room-Temperature Self-Healing. *Adv. Mater.* **2017**, *29* (22), 1–7.
(61) Ni, M.; Zhang, N.; Xia, W.; Wu, X.; Yao, C.; Liu, X.; Hu, X. Y.; Lin, C.; Wang, L. Dramatically Promoted Swelling of a Hydrogel by Pillar[6]Arene-Ferrocene Complexation with Multistimuli Responsiveness. *J. Am. Chem. Soc.* **2016**, *138* (20), 6643–6649.
(62) Schmidt, B. V. K. J.; Barner-Kowollik, C. Dynamic Macromolecular Material Design—The Versatility of Cyclodextrin-Based Host–Guest Chemistry. *Angew. Chemie - Int. Ed.* **2017**, *56* (29), 8350–8369.
(63) Sinawang, G.; Osaki, M.; Takashima, Y.; Yamaguchi, H.; Harada, A. Supramolecular Self-Healing Materials from Non-Covalent Cross-Linking Host–Guest Interactions. *Chem. Commun.* **2020**, *56* (32), 4381–4395.
(64) Tan, C. S. Y.; Agmon, G.; Liu, J.; Hoogland, D.; Janeček, E. R.; Appel, E. A.; Scherman, O. A. Distinguishing Relaxation Dynamics in Transiently Crosslinked Polymeric Networks. *Polym. Chem.* **2017**, *8* (35), 5336–5343.
(65) Zhang, M.; Xu, D.; Yan, X.; Chen, J.; Dong, S.; Zheng, B.; Huang, F. Self-Healing Supramolecular Gels Formed by Crown Ether Based Host-Guest Interactions. *Angew. Chemie - Int. Ed.* **2012**, *51* (28), 7011–7015.
(66) Chakma, P.; Konkolewicz, D. Dynamic Covalent Bonds in Polymeric Materials. *Angew. Chemie - Int. Ed.* **2019**, *58* (29), 9682–9695.
(67) Herbst, F.; Döhler, D.; Michael, P.; Binder, W. H. Self-Healing Polymers via Supramolecular Forces. *Macromol. Rapid Commun.* **2013**, *34* (3), 203–220.
(68) Taylor, D. L.; in het Panhuis, M. Self-Healing Hydrogels. *Adv. Mater.* **2016**, *28* (41), 9060–9093.
(69) Campanella, A.; Döhler, D.; Binder, W. H. Self-Healing in Supramolecular Polymers. *Macromol. Rapid Commun.* **2018**, *39* (17), 1–19.
(70) Wang, S.; Urban, M. W. Self-Healing Polymers. *Nat. Rev. Mater.* **2020**, *5*, 562–583.
(71) Sinawang, G.; Osaki, M.; Takashima, Y.; Yamaguchi, H.; Harada, A. Supramolecular Self-Healing Materials from Non-Covalent Cross-Linking Host-Guest Interactions. *Chem. Commun.* **2020**, *56* (32), 4381–4395.
(72) Ikura, R.; Park, J.; Osaki, M.; Yamaguchi, H.; Harada, A.; Takashima, Y. Design of Self-Healing and Self-Restoring Materials Utilizing Reversible and Movable Crosslinks. *NPG Asia Mater.* **2022**, *14* (1), 1–17.
(73) Yan, X.; Wang, F.; Zheng, B.; Huang, F. Stimuli-Responsive Supramolecular Polymeric Materials. *Chem. Soc. Rev.* **2012**, *41* (18), 6042–6065.
(74) Herbert, K. M.; Schrettl, S.; Rowan, S. J.; Weder, C. 50th Anniversary Perspective: Solid-State Multistimuli, Multiresponsive Polymeric Materials. *Macromolecules* **2017**, *50* (22), 8845–8870.
(75) Vázquez-González, M.; Willner, I. Stimuli-Responsive Biomolecule-Based Hydrogels and Their Applications. *Angew. Chemie - Int. Ed.* **2020**, *59* (36), 15342–15377.
(76) Löwenberg, C.; Balk, M.; Wischke, C.; Behl, M.; Lendlein, A. Shape-Memory Hydrogels: Evolution of Structural Principles To Enable Shape Switching of Hydrophilic Polymer Networks. *Acc. Chem. Res.* **2017**,

50 (4), 723–732.
(77) Lu, W.; Le, X.; Zhang, J.; Huang, Y.; Chen, T. Supramolecular Shape Memory Hydrogels: A New Bridge between Stimuli-Responsive Polymers and Supramolecular Chemistry. *Chem. Soc. Rev.* **2017**, *46* (5), 1284–1294.
(78) Shang, J.; Le, X.; Zhang, J.; Chen, T.; Theato, P. Trends in Polymeric Shape Memory Hydrogels and Hydrogel Actuators. *Polym. Chem.* **2019**, *10* (9), 1036–1055.
(79) Zhao, X. Multi-Scale Multi-Mechanism Design of Tough Hydrogels: Building Dissipation into Stretchy Networks. *Soft Matter* **2014**, *10* (5), 672–687.
(80) Fan, H.; Gong, J. P. Fabrication of Bioinspired Hydrogels: Challenges and Opportunities. *Macromolecules* **2020**, *53* (8), 2769–2782.
(81) Wegst, U. G. K.; Ashby, M. F. The Mechanical Efficiency of Natural Materials. *Philos. Mag.* **2004**, *84* (21), 2167–2186.
(82) Ashby, M. F. The CES EduPack Database of Natural and Man-Made Materials. *Cambridge Univ.* **2008**, *1*, 1–26.
(83) Chen, Q.; Liang, S.; Thouas, G. A. Elastomeric Biomaterials for Tissue Engineering. *Prog. Polym. Sci.* **2013**, *38* (3–4), 584–671.
(84) Calvert, P. Hydrogels for Soft Machines. *Adv. Mater.* **2009**, *21* (7), 743–756.
(85) Guimarães, C. F.; Gasperini, L.; Marques, A. P.; Reis, R. L. The Stiffness of Living Tissues and Its Implications for Tissue Engineering. *Nat. Rev. Mater.* **2020**, *5* (5), 351–370.
(86) Huang, W.; Restrepo, D.; Jung, J. Y.; Su, F. Y.; Liu, Z.; Ritchie, R. O.; McKittrick, J.; Zavattieri, P.; Kisailus, D. Multiscale Toughening Mechanisms in Biological Materials and Bioinspired Designs. *Adv. Mater.* **2019**, *31* (43), 1901561.
(87) Hennink, W. E.; van Nostrum, C. F. Novel Crosslinking Methods to Design Hydrogels. *Adv. Drug Deliv. Rev.* **2002**, *54* (1), 13–36.
(88) Buwalda, S. J.; Boere, K. W. M.; Dijkstra, P. J.; Feijen, J.; Vermonden, T.; Hennink, W. E. Hydrogels in a Historical Perspective: From Simple Networks to Smart Materials. *J. Control. Release* **2014**, *190*, 254–273.
(89) Bastide, J.; Leibler, L. Large-Scale Heterogeneities in Randomly Cross-Linked Networks. *Macromolecules* **1988**, *21* (8), 2647–2649.
(90) Gong, J. P. Why Are Double Network Hydrogels so Tough? *Soft Matter* **2010**, *6* (12), 2583–2590.
(91) Creton, C. 50th Anniversary Perspective: Networks and Gels: Soft but Dynamic and Tough. *Macromolecules* **2017**, *50* (21), 8297–8316.
(92) Means, A. K.; Grunlan, M. A. Modern Strategies to Achieve Tissue-Mimetic, Mechanically Robust Hydrogels. *ACS Macro Lett.* **2019**, *8* (6), 705–713.
(93) Peak, C. W.; Wilker, J. J.; Schmidt, G. A Review on Tough and Sticky Hydrogels. *Colloid Polym. Sci.* **2013**, *291* (9), 2031–2047.
(94) Zhang, Y. S.; Khademhosseini, A. Advances in Engineering Hydrogels. *Science* **2017**, *356* (6337), eaaf3627.
(95) Li, Y.; Zhu, C.; Dong, Y.; Liu, D. Supramolecular Hydrogels: Mechanical Strengthening with Dynamics. *Polymer* **2020**, *210* (June), 122993.
(96) Sakai, T.; Matsunaga, T.; Yamamoto, Y.; Ito, C.; Yoshida, R.; Suzuki, S.; Sasaki, N.; Shibayama, M.; Chung, U. Il. Design and Fabrication of a High-Strength Hydrogel with Ideally Homogeneous Network Structure from Tetrahedron-like Macromonomers. *Macromolecules* **2008**, *41* (14), 5379–5384.
(97) Kondo, S.; Hiroi, T.; Han, Y. S.; Kim, T. H.; Shibayama, M.; Chung, U. Il; Sakai, T. Reliable Hydrogel with Mechanical "Fuse Link" in an Aqueous Environment. *Adv. Mater.* **2015**, *27* (45), 7407–7411.
(98) Parada, G. A.; Zhao, X. Ideal Reversible Polymer Networks. *Soft Matter* **2018**, *14* (25), 5186–5196.
(99) Lin, S.; Ni, J.; Zheng, D.; Zhao, X. Fracture and Fatigue of Ideal Polymer Networks. *Extrem. Mech. Lett.* **2021**, *48*, 101399.
(100) Okumura, Y.; Ito, K. The Polyrotaxane Gel: A Topological Gel by Figure-of-Eight Cross-links. *Adv. Mater.* **2001**, *13* (7), 485–487.
(101) Ito, K. Novel Cross-Linking Concept of Polymer Network: Synthesis, Structure, and Properties of Slide-Ring Gels with Freely Movable Junctions. *Polym. J.* **2007**, *39* (6), 489–499.
(102) Bin Imran, A.; Esaki, K.; Gotoh, H.; Seki, T.; Ito, K.; Sakai, Y.; Takeoka, Y. Extremely Stretchable Thermosensitive Hydrogels by Introducing Slide-Ring Polyrotaxane Cross-Linkers and Ionic Groups into the Polymer Network. *Nat. Commun.* **2014**, *5*, 1–8.
(103) Wang, W.; Zhao, D.; Yang, J.; Nishi, T.; Ito, K.; Zhao, X.; Zhang, L. Novel Slide-Ring Material/Natural Rubber Composites with High Damping Property. *Sci. Rep.* **2016**, *6* (1), 22810.
(104) Zheng, S. Y.; Liu, C.; Jiang, L.; Lin, J.; Qian, J.; Mayumi, K.; Wu, Z. L.; Ito, K.; Zheng, Q. Slide-Ring Cross-Links Mediated Tough Metallosupramolecular Hydrogels with Superior Self-Recoverability. *Macromolecules* **2019**, *52*, 6748–6755.
(105) Clancy, A. J.; Anthony, D. B.; De Luca, F. Metal Mimics: Lightweight, Strong, and Tough Nanocomposites

and Nanomaterial Assemblies. *ACS Appl. Mater. Interfaces* **2020**, *12* (14), 15955–15975.
(106) Gong, J. P.; Katsuyama, Y.; Kurokawa, T.; Osada, Y. Double-Network Hydrogels with Extremely High Mechanical Strength. *Adv. Mater.* **2003**, *15* (14), 1155–1158.
(107) Sun, J. Y.; Zhao, X.; Illeperuma, W. R. K.; Chaudhuri, O.; Oh, K. H.; Mooney, D. J.; Vlassak, J. J.; Suo, Z. Highly Stretchable and Tough Hydrogels. *Nature* **2012**, *489* (7414), 133–136.
(108) Li, J.; Illeperuma, W. R. K.; Suo, Z.; Vlassak, J. J. Hybrid Hydrogels with Extremely High Stiffness and Toughness. *ACS Macro Lett.* **2014**, *3* (6), 520–523.
(109) Ducrot, E.; Chen, Y.; Bulters, M.; Sijbesma, R. P.; Creton, C. Toughening Elastomers with Sacrificial Bonds and Watching Them Break. *Science* **2014**, *344* (6180), 186–189.
(110) Sato, K.; Nakajima, T.; Hisamatsu, T.; Nonoyama, T.; Kurokawa, T.; Gong, J. P. Phase-Separation-Induced Anomalous Stiffening, Toughening, and Self-Healing of Polyacrylamide Gels. *Adv. Mater.* **2015**, *27* (43), 6990–6998.
(111) Kamio, E.; Yasui, T.; Iida, Y.; Gong, J. P.; Matsuyama, H. Inorganic/Organic Double-Network Gels Containing Ionic Liquids. *Adv. Mater.* **2017**, *29* (47), 1–8.
(112) Haraguchi, K.; Takehisa, T. Nanocomposite Hydrogels: A Unique Organic-Inorganic Network Structure with Extraordinary Mechanical, Optical, and Swelling/De-Swelling Properties. *Adv. Mater.* **2002**, *14* (16), 1120–1124.
(113) Haraguchi, K.; Farnworth, R.; Ohbayashi, A.; Takehisa, T. Compositional Effects on Mechanical Properties of Nanocomposite Hydrogels Composed of Poly(N,N-Dimethylacrylamide) and Clay. *Macromolecules* **2003**, *36* (15), 5732–5741.
(114) Li, H. J.; Jiang, H.; Haraguchi, K. Ultrastiff, Thermoresponsive Nanocomposite Hydrogels Composed of Ternary Polymer-Clay-Silica Networks. *Macromolecules* **2018**, *51* (2), 529–539.
(115) Haraguchi, K.; Shimizu, S.; Tanaka, S. Instant Strong Adhesive Behavior of Nanocomposite Gels toward Hydrophilic Porous Materials. *Langmuir* **2018**, *34* (29), 8480–8488.
(116) Haraguchi, K.; Kimura, Y.; Shimizu, S. Reversible Generation of Large Retractive Tensile Forces in Isometric Chemo-Mechanical Actuators Composed of Nanocomposite Hydrogels and Aqueous NaCl Solutions. *Soft Matter* **2018**, *14* (6), 927–933.
(117) Wang, Q.; Mynar, J. L.; Yoshida, M.; Lee, E.; Lee, M.; Okuro, K.; Kinbara, K.; Aida, T. High-Water-Content Mouldable Hydrogels by Mixing Clay and a Dendritic Molecular Binder. *Nature* **2010**, *463* (7279), 339–343.
(118) Lin, W. C.; Fan, W.; Marcellan, A.; Hourdet, D.; Creton, C. Large Strain and Fracture Properties of Poly(Dimethylacrylamide)/Silica Hybrid Hydrogels. *Macromolecules* **2010**, *43* (5), 2554–2563.
(119) Harada, A.; Li, J.; Kamachi, M. The Molecular Necklace: A Rotaxane Containing Many Threaded α-Cyclodextrins. *Nature* **1992**, *356* (6367), 325–327.
(120) Harada, A.; Li, J.; Kamachi, M. Synthesis of a Tubular Polymer from Threaded Cyclodextrins. *Nature* **1993**, *364* (6437), 516–518.
(121) Li, J.; Harada, A.; Kamachi, M. Sol–Gel Transition during Inclusion Complex Formation between α-Cyclodextrin and High Molecular Weight Poly(Ethylene Glycol)s in Aqueous Solution. *Polym. J.* **1994**, *26* (9), 1019–1026.
(122) Nakahata, M.; Mori, S.; Takashima, Y.; Yamaguchi, H.; Harada, A. Self-Healing Materials Formed by Cross-Linked Polyrotaxanes with Reversible Bonds. *Chem* **2016**, *1* (5), 766–775.
(123) Sawada, J.; Aoki, D.; Kuzume, M.; Nakazono, K.; Otsuka, H.; Takata, T. A Vinylic Rotaxane Cross-Linker for Toughened Network Polymers from the Radical Polymerization of Vinyl Monomers. *Polym. Chem.* **2017**, *8* (12), 1878–1881.
(124) Sawada, J.; Aoki, D.; Sun, Y.; Nakajima, K.; Takata, T. Effect of Coexisting Covalent Cross-Links on the Properties of Rotaxane-Cross-Linked Polymers. *ACS Appl. Polym. Mater.* **2020**, *2* (3), 1061–1064.
(125) Cates, M. E. Reptation of Living Polymers: Dynamics of Entangled Polymers in the Presence of Reversible Chain-Scission Reactions. *Macromolecules* **1987**, *20* (9), 2289–2296.
(126) Baxandall, L. G. Dynamics of Reversibly Crosslinked Chains. *Macromolecules* **1989**, *22* (4), 1982–1988.
(127) Leibler, L.; Rubinstein, M.; Colby, R. H. Dynamics of Reversible Networks. *Macromolecules* **1991**, *24* (16), 4701–4707.
(128) Golkaram, M.; Loos, K. A Critical Approach to Polymer Dynamics in Supramolecular Polymers. *Macromolecules* **2019**, *52* (24), 9427–9444.
(129) Wu, S.; Chen, Q. Advances and New Opportunities in the Rheology of Physically and Chemically Reversible Polymers. *Macromolecules* **2022**, *55* (3), 697–714.
(130) Yount, W. C.; Loveless, D. M.; Craig, S. L. Small-Molecule Dynamics and Mechanisms Underlying the Macroscopic Mechanical Properties of Coordinatively Cross-Linked Polymer Networks. *J. Am. Chem. Soc.* **2005**, *127* (41), 14488–14496.
(131) Yount, W. C.; Loveless, D. M.; Craig, S. L. Strong Means Slow: Dynamic Contributions to the Bulk

Mechanical Properties of Supramolecular Networks. *Angew. Chemie - Int. Ed.* **2005**, *44* (18), 2746–2748.
(132) Yount, W. C.; Juwarker, H.; Craig, S. L. Orthogonal Control of Dissociation Dynamics Relative to Thermodynamics in a Main-Chain Reversible Polymer. *J. Am. Chem. Soc.* **2003**, *125* (50), 15302–15303.
(133) Grindy, S. C.; Learsch, R.; Mozhdehi, D.; Cheng, J.; Barrett, D. G.; Guan, Z.; Messersmith, P. B.; Holten-Andersen, N. Control of Hierarchical Polymer Mechanics with Bioinspired Metal-Coordination Dynamics. *Nat. Mater.* **2015**, *14* (12), 1210–1216.
(134) Ahmadi, M.; Seiffert, S. Thermodynamic Control over Energy Dissipation Modes in Dual-Network Hydrogels Based on Metal-Ligand Coordination. *Soft Matter* **2020**, *16* (9), 2332–2341.
(135) Ohira, M.; Katashima, T.; Naito, M.; Aoki, D.; Yoshikawa, Y.; Iwase, H.; Takata, S. ichi; Miyata, K.; Chung, U. il; Sakai, T.; et al. Star-Polymer–DNA Gels Showing Highly Predictable and Tunable Mechanical Responses. *Adv. Mater.* **2022**, *34* (13), 1–9.
(136) Katashima, T.; Kudo, R.; Naito, M.; Nagatoishi, S.; Miyata, K.; Chung, U. Il; Tsumoto, K.; Sakai, T. Experimental Comparison of Bond Lifetime and Viscoelastic Relaxation in Transient Networks with Well-Controlled Structures. *ACS Macro Lett.* **2022**, *11* (6), 753–759.
(137) Rose, S.; Dizeux, A.; Narita, T.; Hourdet, D.; Marcellan, A. Time Dependence of Dissipative and Recovery Processes in Nanohybrid Hydrogels. *Macromolecules* **2013**, *46* (10), 4095–4104.
(138) Long, R.; Mayumi, K.; Creton, C.; Narita, T.; Hui, C. Y. Time Dependent Behavior of a Dual Cross-Link Self-Healing Gel: Theory and Experiments. *Macromolecules* **2014**, *47* (20), 7243–7250.
(139) Mayumi, K.; Marcellan, A.; Ducouret, G.; Creton, C.; Narita, T. Stress-Strain Relationship of Highly Stretchable Dual Cross-Link Gels: Separability of Strain and Time Effect. *ACS Macro Lett.* **2013**, *2* (12), 1065–1068.

Chapter 2

Design and Mechanical Properties of Supramolecular Polymeric Materials Based on Host-Guest Complexations: the Relation between Relaxation Time and Toughness

2.1. Introduction

Chapter 1 showed that functional polymeric materials based on reversible cross-links had been developed due to their unique mechanical and responsive properties. In particular, the association/dissociation of the reversible bond is widely known to improve the toughness of polymeric materials.

Takashima and Harada *et al.* previously reported supramolecular hydrogels cross-linked by host-guest complexations of CDs with alkyl guests on the polymer side chain.[1,2] The CD cavity size and shape and the charge of the guest unit affect the mechanical properties of the material. Based the previous works, the combination of host/guest molecules with a high association constant (K_a) did not give supramolecular hydrogels with a high toughness (G_f), but the Young's modulus (E) of the hydrogel at a certain strain rate was increased. On the other hand, increasing the charge at the end of the alkyl guest unit effectively improved G_f, which is closely related to the kinetics of the threading/dethreading of the CD units.

In this chapter, the author hypothesize that the kinetics of CD units affect viscoelastic relaxation time (τ) of hydrogels, and τ can be tuned to control G_f and E in host/guest supramolecular hydrogels. Actually, the dynamics of reversible cross-linking point are well known to have an impact on the dynamics and mechanics of transient polymer networks.[3–8] **Figure 2-1a** shows the trend between G_f and E in covalently cross-linked materials. High E should result in a very small fracture strain and a small G_f. This trend corresponds to the Lake-Thomas model[9–11], which estimates that fracture energy of covalently cross-linked hydrogels is generally proportional to $E^{-1/2}$. In contrast, from the viewpoint of viscoelastic dynamics, a suitable E would give viscoelastic materials with the highest G_f. If the viscoelastic hydrogel has a mechanical relaxation process with a relaxation time τ, G_f should be low under a low strain rate $\dot{\varepsilon}_C$ ($\tau \times \dot{\varepsilon}_C \ll 1$) due to the low loss modulus (G''). By applying a high $\dot{\varepsilon}_C$ ($\tau \times \dot{\varepsilon}_C \gg 1$), G_f also decreases because of the low G''. If host/guest supramolecular hydrogels with a maximum G'' at the frequency corresponding to $\dot{\varepsilon}_C$ are prepared by tuning τ, we will obtain materials with the highest G_f (**Figure 2-1b**). Of course, E is also related to $\tau \times \dot{\varepsilon}_C$ (**Figure 2-1c**). At $\tau \times \dot{\varepsilon}_C > 1$, E significantly increases to a steady state.

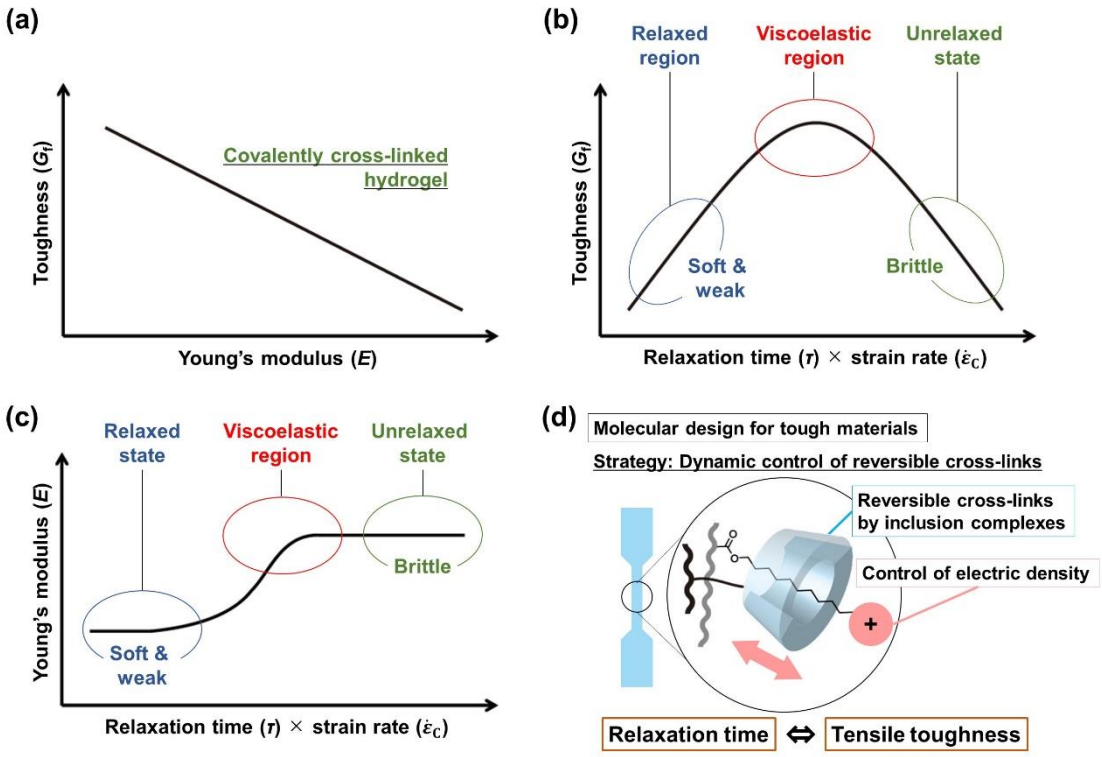

Figure 2-1. The design concept of supramolecular hydrogels. (a) The trend between toughness (G_f) and Young's modulus (E) of covalently cross-linked hydrogels. (b) Dependence of G_f of viscoelastic hydrogels with various relaxation times on $\tau \times \dot{\varepsilon}_C$. (c) Dependence of E on $\tau \times \dot{\varepsilon}_C$. (d) Schematic of the reversible cross-linking points in these materials.

Herein, the author studied the relationship between the τ value of the reversible bonds and G_f in supramolecular hydrogels. The author experimentally demonstrated G_f in relation to the τ value of the reversible bonds and the observation time scale. To control the τ value, we designed a reversible cross-linking point using CDs, alkyl chains, and cations (**Figure 2-1d**). Tuning the viscoelasticity of the reversible cross-linking points based on the $\tau \times \dot{\varepsilon}_C$ values improved G_f of the supramolecular hydrogels (**Figure 2-2**).

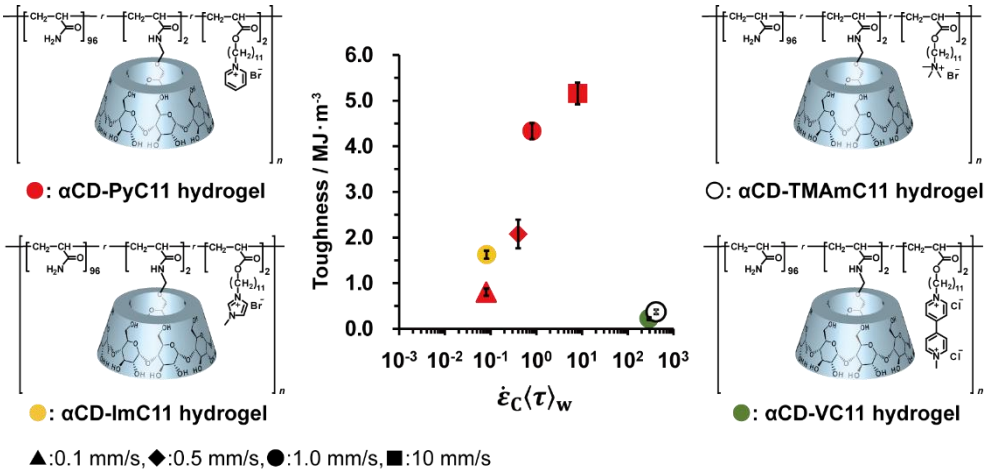

Figure 2-2. The relation between $\tau \times \dot{\varepsilon}_C$ and G_f of the supramolecular hydrogels.

2.2. Experimental

2.2.1. Materials

Acrylamide (AAm) and *N*-(hydroxymethyl)acrylamide were purchased from Wako Pure Chemical Industries, Ltd. α-Cyclodextrin (αCD) and β-cyclodextrin (βCD) were obtained from Junsei Chemical Co. Ltd. Acetone, methanol, diethyl ether, ethyl acetate, acrylic acid, hydrochloric acid, sodium hydroxide, sodium sulfate, *p*-toluenesulfonic acid monohydrate, potassium peroxodisulfate (KPS), *N,N,N′,N′*–tetramethylethylenediamine (TEMED), 1-methylimidazole and pyridine were purchased from Nacalai Tesque Inc. Dimethyl sulfoxide-d_6 (DMSO–d_6) was obtained from Merck & Co., Inc. Chloroform-*d* ($CDCl_3$) and deuterium oxide (D_2O) were obtained from EURISO-TOP. 4,4'-Bipyridyl and trimethylamine (in acetonitrile) were purchased from Tokyo Kasei. Sodium 3-(trimethylsilyl)-1-propanesulfonate (DSS) was purchased from Sigma-Aldrich. The water used for the preparation of the aqueous solutions was purified with a Millipore Elix 5 system. Other reagents were used without further purification. Acrylamido-methyl ether-modified αCD and βCD (αCDAAmMe and βCDAAmMe) and 4-(11-acryloyloxyundecyl)-4'-(methyl)-bipyridinium dichloride (VC11 monomer) were prepared according to previous reports by Takashima and Harada, *et al*.[1,2]

2.2.2. Measurements

Nuclear magnetic resonance (NMR) spectroscopy: ^1H and ^{13}C NMR spectra were recorded with a JEOL JNM–ECA 400 NMR spectrometer (400 MHz) and a JEOL JNM–ECA 500 NMR spectrometer (500 MHz). Solid–state ^1H field gradient magic angle spinning (FG-MAS) NMR spectra were recorded with a JEOL JNM–ECA 400 NMR spectrometer (400 MHz, with a sample spinning rate of 7 kHz). 2-dimensional ^1H Rotating-frame Overhauser effect spectroscopy (2D ROESY) NMR spectra were performed at 600 MHz with an Agilent VNS600 NMR spectrometer. All chemical shifts were referenced to the residual solvent peaks as internal standards (for ^1H NMR: δ = 0 ppm for tetramethylsilane (TMS), 2.49 ppm for DMSO–d_6, 4.79 ppm for D_2O, and 7.26 ppm for $CDCl_3$, ^{13}C NMR: δ = 0 ppm for TMS and DSS, 39.5 ppm for DMSO–d_6, and 77.0 ppm for $CDCl_3$).

Mass spectroscopy: Matrix-assisted LASER desorption/ionization time-of-flight mass spectrometry (MALDI-TOF MS) was conducted on a Bruker autoflex speed mass spectrometer using 2,5-dihydroxy-benzoic acid as a matrix. Electrospray ionization-linear ion trap-orbitrap

(ESI-LIT-orbitrap) mass spectroscopy was conducted on a Thermo Fisher Scientific Orbitrap XL using methanol as solvent.

Fourier-transform infrared (FT-IR) spectroscopy: FT-IR spectra were acquired using a JASCO FT/IR–410 spectrometer.

Isothermal titration calorimetry (ITC): ITC measurements were performed by Malvern MicroCal iTC200 system.

Tensile test: Tensile tests were performed on a universal testing machine [Autograph AG-X plus (Shimadzu Co.)] equipped with a 20 N load cell and 1 N clip grips. The hydrogels were prepared using type 4 dumbbell-shaped Teflon mold following the JIS K6251 standard. The thickness of the prepared hydrogel was 2.4 mm. The initial sample length (L_0) for tensile tests was defined as the distance between the clip jigs, and its value was approximately 23 mm. Nominal stress and nominal strain were recorded during tensile tests, and these were used thereafter as 'stress' and 'strain', respectively. Based on the stress-strain curves, fracture strength and strain were defined as the maximum stress and strain before the stress decreased. Toughness (G_f) was calculated from the integral of the stress-strain curve and the fracture strain was set as the upper limit of the integral. Young's modulus (E) was calculated from the initial slope of the stress-strain curve at a range between 3%–8% strain. The error bars (standard deviation) for toughness and the Young's modulus were calculated from the results of more than three experiments.

Rheological measurement: Dynamic viscoelasticity and stress-relaxation properties were measured using an Anton Paar MCR302 rheometer with a parallel-plate fixture (8 mm in diameter). An angular frequency (ω) sweep from 0.1 to 100 rad/s was performed using a parallel-plate fixture with 8 mm in diameter over a temperature range of 0–45 °C. Stress-relaxation tests were performed at 25 °C. The shear strain amplitudes (γ) applied in both ω sweep and stress-relaxation tests were within the range of linear viscoelasticity. Details of the analysis method are described below.

2.2.3. Preparation of guest monomers

The author prepared three new compounds, ImC11, PyC11, and TMAmC11. Here, only synthesis procedures are described. Details of characterization are shown in the author's Original Paper 1.

Preparation of 3-(11-acryloyloxyundecyl)-1-methyl-imidazolium bromide (ImC11)

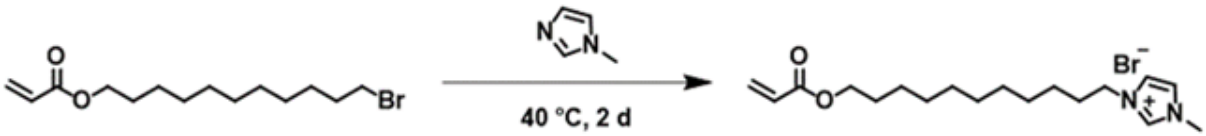

Scheme. 2-1. Preparation of ImC11.

Scheme. 2-1 shows the preparation of ImC11. 4-(11-Acryloyloxyundecyl)-4'-bipyridinium bromide (5.77 g, 19 mmol) was dissolved in 1-methylimidazole (1.5 mL, 19 mmol), and the solution was stirred for 2 days at 40 °C. The resulting solution was poured into diethyl ether to precipitate the crude product, which was collected by filtration and washed with diethyl ether. ImC11 was obtained as white solid (6.47 g, 88% yield).

Preparation of 1-(11-acryloyloxyundecyl)-pyridinium bromide (PyC11)

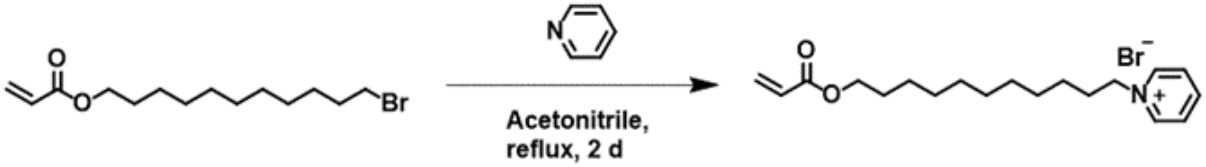

Scheme. 2-2. Preparation of PyC11.

Scheme. 2-2 shows the preparation of PyC11. 4-(11-Acryloyloxyundecyl)-4'-bipyridinium bromide (3.05 g, 10 mmol) and pyridine (1.58 g, 20 mmol) were dissolved in acetonitrile (20 mL), and the solution was refluxed for 2 days. The resulting solution was poured into diethyl ether to precipitate the crude product, which was filtrated and washed with diethyl ether. PyC11 was obtained as white solid (2.75 g, 72% yield).

Preparation of 11-Acryloyloxyundecyl trimethylammonium bromide (TMAmC11)

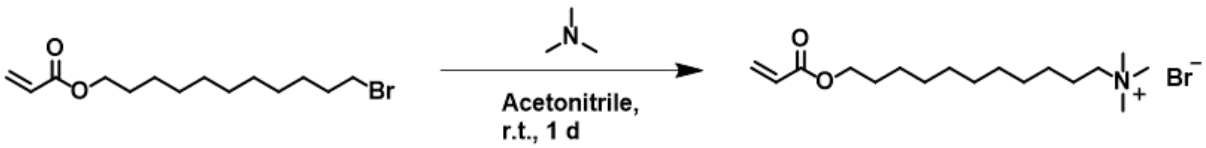

Scheme. 2-3. Preparation of TMAmC11.

Scheme. 2-3 shows the preparation of TMAmC11. Trimethylamine in acetonitrile (2.0 M, 10 mL, 20 mmol) was added to a solution of 4-(11-acryloyloxyundecyl)-4'-bipyridinium bromide (2.02 g, 6.6 mmol) in acetonitrile (10 mL), and the solution was stirred at r.t. for 1 day. After the resulting solution was evaporated, the residue was dissolved in methanol and poured into diethyl ether to precipitate the product. TMAmC11 was separated from the mixture by centrifugation and obtained as white solid (2.16 g, 89% yield).

2.2.4. Formation of the inclusion complexes of αCDAAmMe with guest monomers

To confirm the formation of the inclusion complex of αCDAAmMe with ImC11, PyC11, or TMAmC11 monomers, the mixture of the αCDAAmMe and guest monomers in D_2O were analyzed by 2D ^1H rotating-frame Overhauser effect spectroscopy (ROESY) NMR.

Figure2-3 shows the 2D ROESY NMR spectrum of the mixture of αCD with ImC11 in D_2O. Correlations were observed between the inner protons ($C^{3,5,6}H$) of the αCD residues and the protons of the methylene groups (j, k, and l) of ImC11, indicating that the alkyl group of ImC11 is included in the αCDAAmMe. Similar results of PyC11 and TMAmC11 were confirmed (see the author's Original Paper 1).

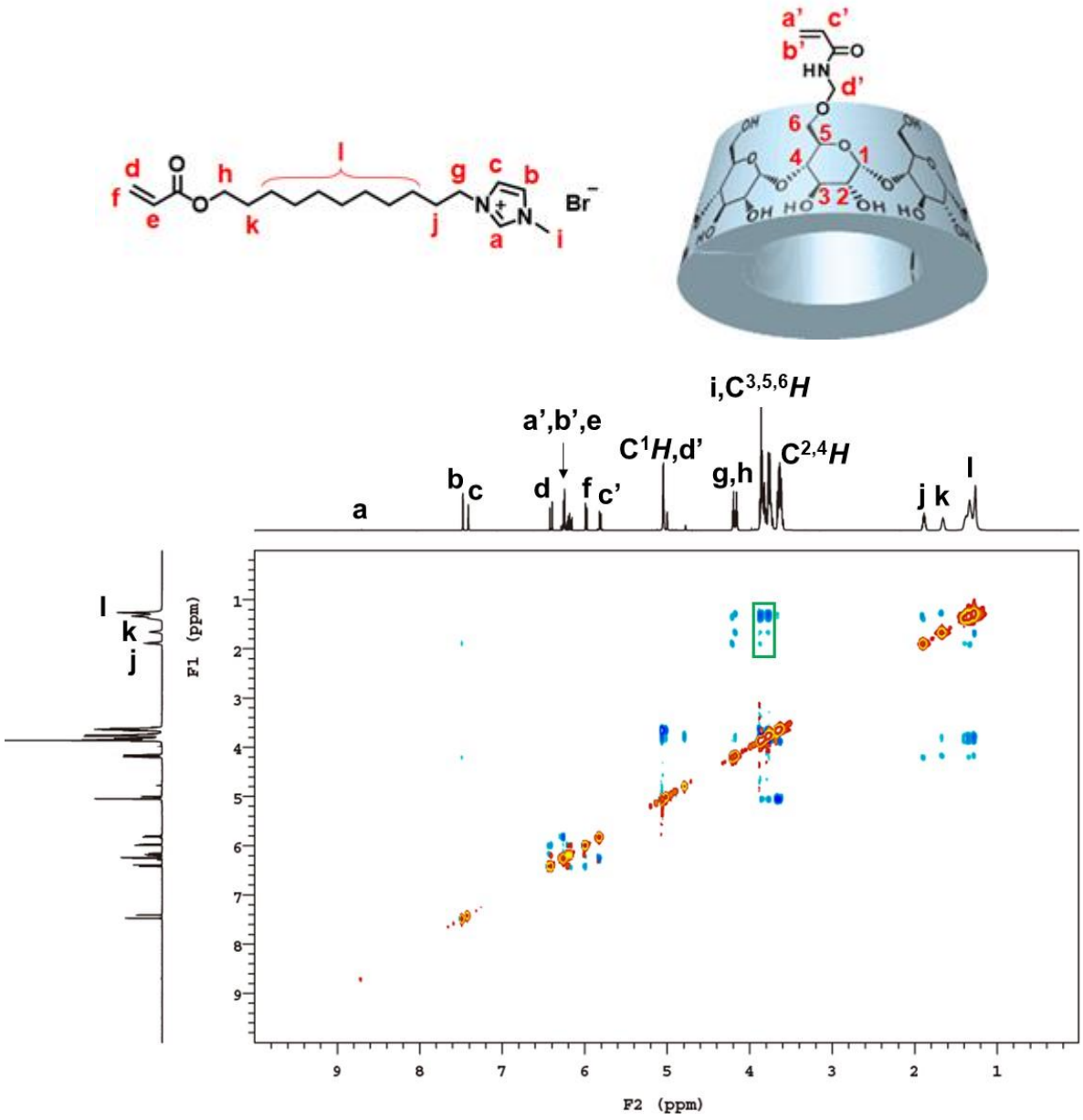

Figure 2-3. 600 MHz 2D ROESY NMR spectrum of a mixture of αCDAAmMe (10 mM) and ImC11 (10 mM) in D_2O at 30 °C.

2.2.5. Association constant of the inclusion complex of αCDAAmMe and guest monomers

^{1}H NMR measurements were performed to estimate the association constant (K_a) of 1:1 complexation between αCDAAmMe and guest monomers using nonlinear least-squares method. All chemical shifts were referenced to the residual solvent peaks of deuterated DMSO as external standards (δ = 2.49 ppm). $\Delta\delta_{obs}$ was plotted as a function of $[H]_0/[G]_0$. Fitting equation (1) as shown below was used to determine K_a. Details of the NMR spectra and analyses are shown in the author's Original Paper 1. The average values of K_a for ImC11 and PyC11 were calculated as (1.7 ± 0.35) × 10^3 and (1.7 ± 0.51) × 10^3 M^{-1}, respectively.

$$\Delta\delta_{obs} = \frac{\Delta\delta_{max}}{2K_a[G]_0}\left[1 + K_a[H]_0 + K_a[G]_0 - \left\{(1 + K_a[H]_0 + K_a[G]_0)^2 - 4{K_a}^2[H]_0[G]_0\right\}^{1/2}\right] \quad (1)$$

$\Delta\delta_{obs}$: Observed change in chemical shift

$\Delta\delta_{max}$: Maximum change in chemical shift (fitting parameter)

K_a: Association constant (fitting parameter)

$[H]_0$: Concentration of host

$[G]_0$: Concentration of guest (fixed parameter)

K_a of αCDAAmMe with C12 could not be estimated due to hydrophobicity of C12 and the inclusion complex. Therefore, I referred to K_a of αCD with *n*-dodecyl(ester)-acrylamide polymer (1200 M^{-1}).[12]

K_a of αCDAAmMe with VC11 was calculated as 3.5 × 10^3 M^{-1} in Harada's previous work.[13]

We cited K_a of αCD with N^1,N^1,N^1,N^{10},N^{10},N^{10}-hexamethyldecane-1,10-diaminium (1540 M^{-1})[14] as a model of αCDAAmMe with TMAmC11.

2.2.6. Preparation of the supramolecular hydrogels

Five kinds of reversibly cross-linked supramolecular hydrogels (αCD-R hydrogels), αCD-C12, αCD-ImC11, αCD-PyC11, αCD-VC11 and αCD-TMAmC11 hydrogels, were prepared (**Figures 2-4a and 2-4b**).

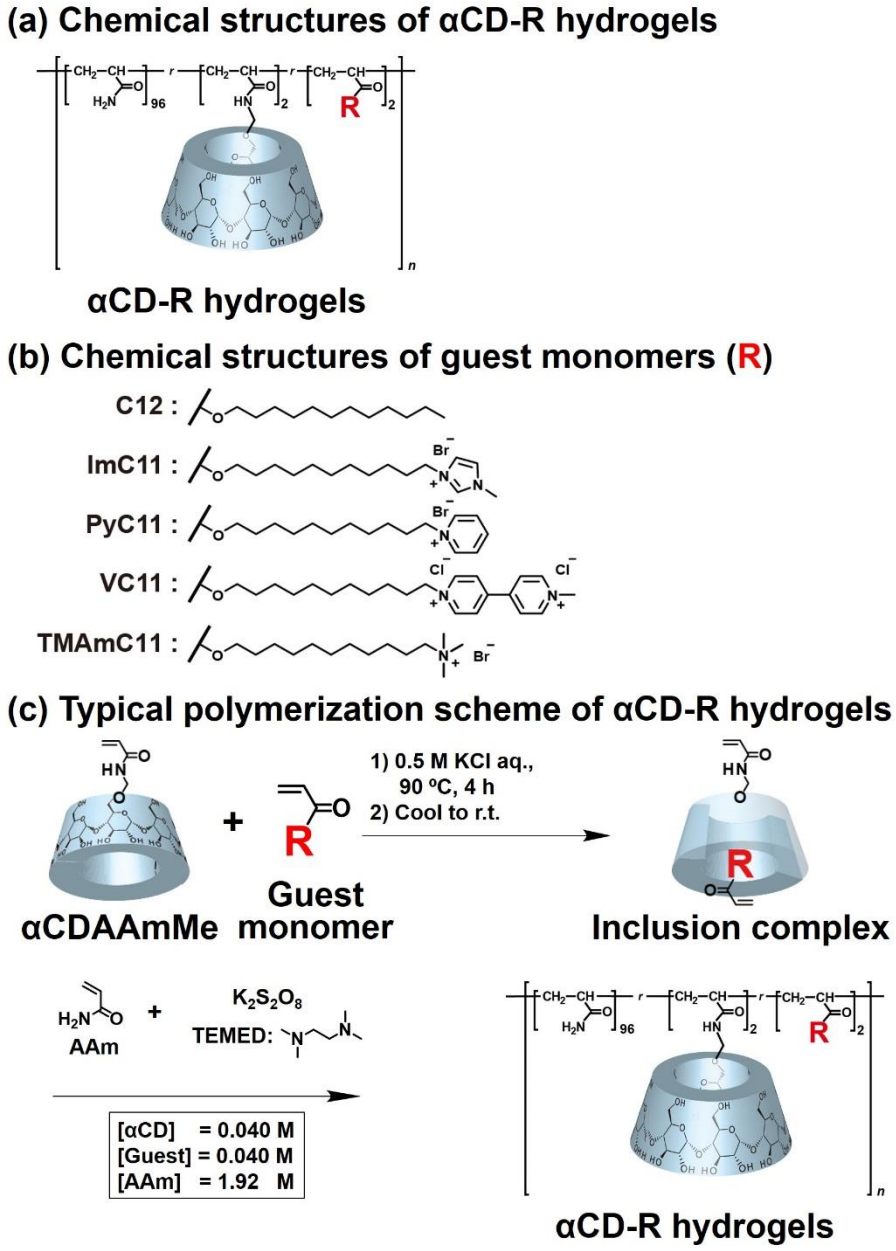

Figure 2-4. (a) Chemical structures of the αCD-R hydrogels. **(b)** Chemical structures of the guest monomers. **(c)** Typical polymerization scheme for the αCD-R hydrogels.

The αCD-R hydrogels have cation-terminated or nonion linear alkyl chain guests (R) as well as αCD moiety on the polymer side chain. Complexes of the αCD with alkyl moieties act as reversible cross-links in the hydrogel state. **Figure 2-4b** shows the chemical structures of the cationic guest units. The linear alkyl chain units function as molecular recognition sites for αCD, while the cationic groups function as electric traps.[15] The guest units of the αCD-C12 hydrogel have no cationic units. The αCD-ImC11 and αCD-PyC11 hydrogels have imidazolium and pyridinium (monocation) units, respectively. Viologen (dication) units were introduced into the αCD-VC11 hydrogel to increase the electric density. The αCD-TMAmC11 hydrogel have bulky trimethylammonium (monocation) units that show the effect of steric hindrance on αCD. The increase in the electric density or steric hindrance on the cationic moiety decreases the kinetic rate in the association/dissociation equilibrium of the αCD/R complex.

Figure 2-4c shows a general preparation method of the αCD-R hydrogels by radical copolymerization. αCDAAmMe (2 mol%) and R-acrylate monomers (2 mol%) were mixed in 0.5 M potassium chloride (KCl) aqueous solution for 4 hours at 90 °C to form the host-guest inclusion complexes. These complex monomers, αCDAAmMe/C12, αCDAAmMe/ImC11, αCDAAmMe/PyC11, αCDAAmMe/VC11, and αCDAAmMe/TMAmC11 were copolymerized with acrylamide (AAm; 96 mol%) at a total monomer concentration of 2 mol/L by using potassium persulfate ($K_2S_2O_4$, 1 mol%) and *N*,*N*,*N*′,*N*′-tetramethylethylenediamine (TEMED, 1 mol%) at room temperature to give the αCD-R hydrogels. Details of the reagents and solutions are presented in **Tables 2-1–2-5**.

Table 2-1. Amount of reagents and solvents used in the preparation of the αCD-C12 hydrogel.

	KCl aq. /mL	AAm /mg	αCDAAmMe /mg	C12 /mg	KPS /mg	TEMED /μL
αCD-C12 hydrogel	2.0	273	84.5	18.9	10.8	5.96

Table 2-2. Amount of reagents and solvents used in the preparation of the αCD-ImC11 hydrogel.

	KCl aq. /mL	AAm /mg	αCDAAmMe /mg	ImC11 /mg	KPS /mg	TEMED /μL
αCD-ImC11 hydrogel	2.0	273	84.5	31.0	10.8	5.96

Table 2-3. Amount of reagents and solvents used in the preparation of the αCD-PyC11 hydrogel.

	KCl aq. /mL	AAm /mg	αCDAAmMe /mg	PyC11 /mg	KPS /mg	TEMED /μL
αCD-PyC11 hydrogel	2.0	273	84.5	30.8	10.8	5.96

Table 2-4. Amount of reagents and solvents used in the preparation of the αCD-VC11 hydrogel.

	KCl aq. /mL	AAm /mg	αCDAAmMe /mg	VC11 /mg	KPS /mg	TEMED /μL
αCD-VC11 hydrogel	2.0	273	84.5	37.4	10.8	5.96

Table 2-5. Amount of reagents and solvents used in the preparation of the αCD-TMAmC11 hydrogel.

	KCl aq. /mL	AAm /mg	αCDAAmMe /mg	TMAmC11 /mg	KPS /mg	TEMED /μL
αCD-TMAmC11 hydrogel	2.0	273	84.5	29.1	10.8	5.96

2.2.7. Characterization of the supramolecular hydrogels

Fourier transform infrared (FT-IR) and ^{1}H field gradient magic angle spinning (FG-MAS) NMR spectroscopic analyses were used to structurally characterize the αCD-R hydrogels.

FT-IR spectra

Please see the author's Original Paper 1 for details of methods and FT-IR spectra of the αCD-R hydrogels. In short, absorption by O-H stretching, N-H stretching, C-H stretching, C=O stretching, and N-H bending was observed, indicating the formation of poly(acrylamide) main chain.

FG-MAS NMR spectra

The as-prepared αCD-R hydrogels were freeze-dried, immersed in D_2O, and analyzed by FG-MAS spectroscopy. For example, **Figure 2-5** shows the NMR spectra of the αCD-ImC11 hydrogel. This shows the presence of αCDAAmMe, cationic guest, and AAm units in the αCD-R hydrogel. The protons on the double bond of αCDAAmMe and the cationic guest monomers disappeared, indicating that a predefined monomer ratio was introduced into the αCD-R hydrogels. FG-MAS NMR spectra of the other αCD-R hydrogels were shown in the author's Original Paper 1, and similar results were confirmed.

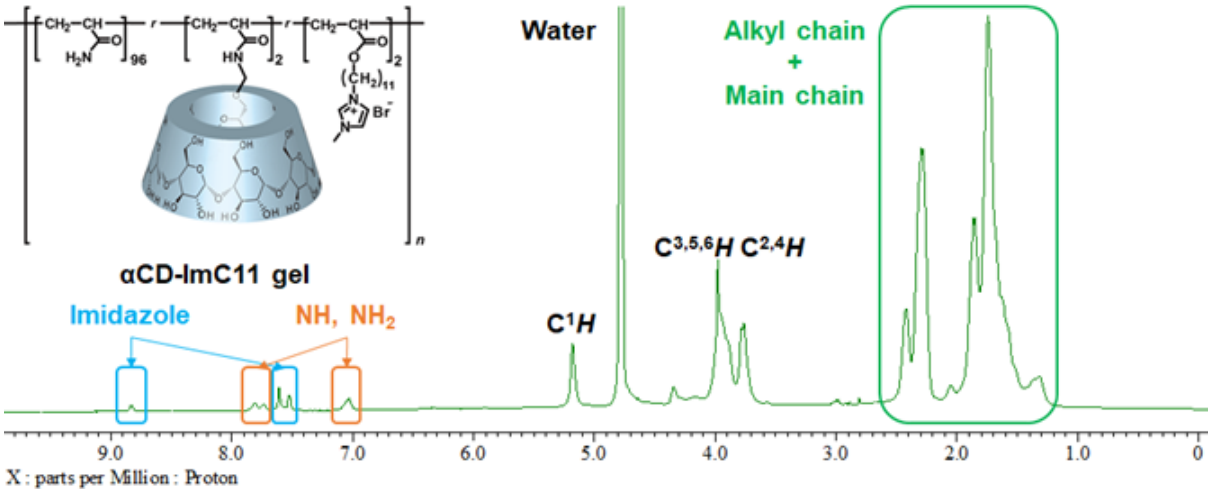

Figure 2-5. 400 MHz ^{1}H FG-MAS NMR spectrum of the αCD-ImC11 hydrogel (immersed in D_2O) at 25 °C. The frequency of the magic angle spinning was 7 kHz.

Amount of each residues
In the preparation: [αCD] / [ImC11] / [AAm] = 2.0 / 2.0 / 96.0.
Calculated from the spectrum: [αCD] / [ImC11] / [AAm] = 1.5 / 1.8 / 96.7.

2.3. Results and discussion

2.3.1. Mechanical properties of the αCD-R hydrogels

Uniaxial tensile tests (tensile rate: 1.0 mm/s, 25 °C) were used to evaluate the mechanical properties of the αCD-R hydrogels (**Figure 2-6**). **Figure 2-6b** shows a photograph of the αCD-R hydrogels prepared using type 4 dumbbell-shaped Teflon mold following the JIS K6251 standard. The αCD-ImC11, αCD-PyC11, αCD-VC11 and αCD-TMAmC11 hydrogels were transparent, while the αCD-C12 hydrogel was not. The turbidity of the αCD-C12 hydrogel is derived from the microcrystals of the inclusion complex of the αCD/C12 monomers and the formation of the nanosized hydrogel.

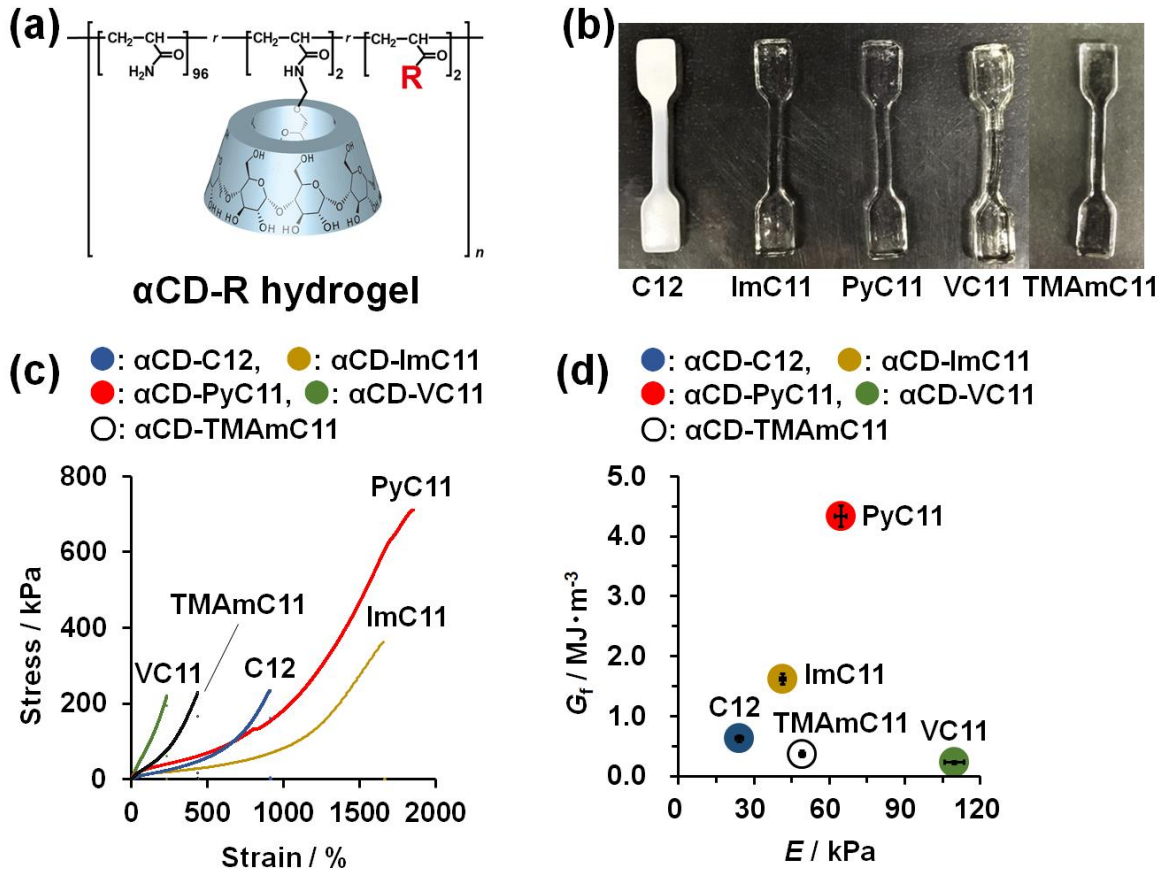

Figure 2-6. (a) Chemical structure of the αCD-R hydrogels. **(b)** Photograph of the as-prepared αCD-R hydrogels. **(c)** Stress-strain curves of the αCD-R hydrogels at a tensile rate of 1.0 mm/s. **(d)** Plots of toughness (G_f) and Young's modulus (E) for the αCD-R hydrogels; αCD-C12 hydrogel: G_f = 0.62 ± 0.05 MJ/m^3 and E = 24 ± 1.4 kPa; αCD-ImC11 hydrogel: G_f = 1.62 ± 0.09 MJ/m^3 and E = 41 ± 1.2 kPa; αCD-PyC11 hydrogel: G_f = 4.33 ± 0.18 MJ/m^3 and E = 64 ± 2.2 kPa; αCD-VC11 hydrogel: G_f = 0.22 ± 0.03 MJ/m^3 and E = 110 ± 4.0 kPa; and αCD-TMAmC11 hydrogel: G_f = 0.37 ± 0.05 MJ/m^3 and E = 49 ± 1.0 kPa.

Figure 2-6c shows typical nominal stress-nominal strain curves of the αCD-R hydrogels. G_f was calculated from the integral of the stress-strain curve, and E was calculated from the initial slope of the stress-strain curve in the range between 3%–8% strain. Detailed results of tensile tests for the αCD-R hydrogels are shown in **Figure 2-7**.

Figure 2-6d shows the relation between G_f and E, which varied with the structure of the reversible cross-links. The error bars (standard deviation) were calculated from more than three experiments. The αCD-C12 hydrogel showed low G_f and E. In the cases of the αCD-ImC11 and αCD-PyC11 hydrogels, which had monocationic moieties, both G_f and E were higher than those of the αCD-C12 hydrogel. In particular, the αCD-PyC11 hydrogel exhibited the highest G_f (4.33 ± 0.18 MJ/m^3). Unexpectedly, although the charge numbers of the cation species in the ImC11 and PyC11 units were the same, the mechanical properties (G_f and E) of the αCD-ImC11 and αCD-PyC11 hydrogels were significantly different. The αCD-VC11 hydrogel bearing dicationic moieties showed the highest E but the lowest G_f. Similarly, in the case of the αCD-TMAmC11 hydrogel bearing bulky monocationic moieties, E was higher than that of the αCD- C12 hydrogel, but G_f decreased. I wondered why the G_f of the αCD-PyC11 hydrogel was higher than that of the αCD-VC11 hydrogel because the hydrogels have the same alkyl chain length. I suppose that K_a or τ may be major contributors to G_f and E of the αCD-R hydrogels.

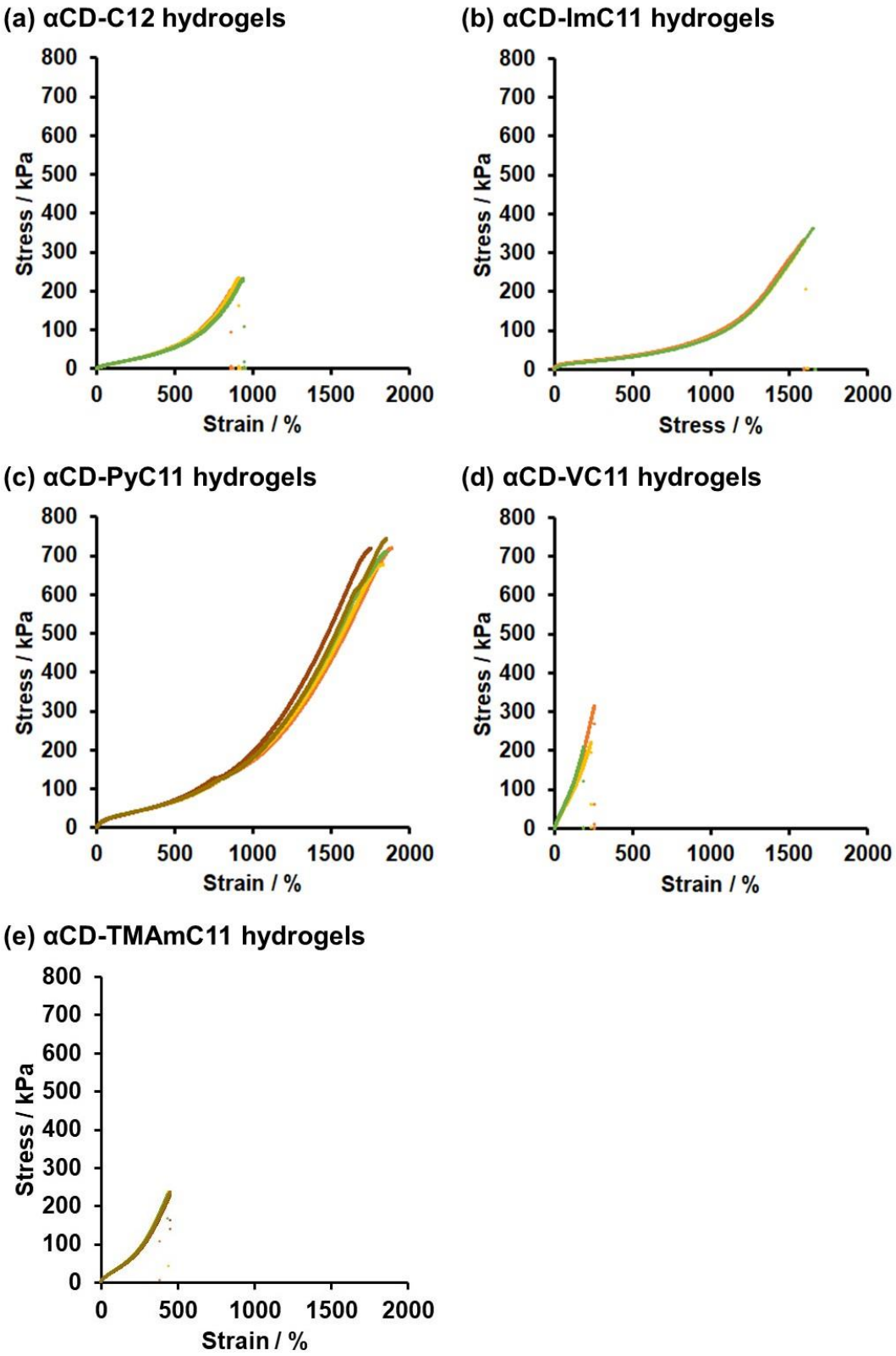

Figure 2-7. Stress-strain curves of **(a)** αCD-C12 hydrogels, **(b)** αCD-ImC11 hydrogels, **(c)** αCD-PyC11 hydrogels, **(d)** αCD-VC11 hydrogels, and **(e)** αCD-TMAmC11 hydrogels at 25 °C at a tensile rate of 1.0 mm/s.

2.3.2. Relationship between the mechanical properties and association constant

The author investigated the effects of K_a between the αCDAAmMe host and the corresponding guest monomers on G_f and E of the αCD-R hydrogels (**Figure 2-8**). **Figure 2-8a** summarizes the K_a values calculated from the ^{1}H NMR spectra shown in Section 2.2.5.

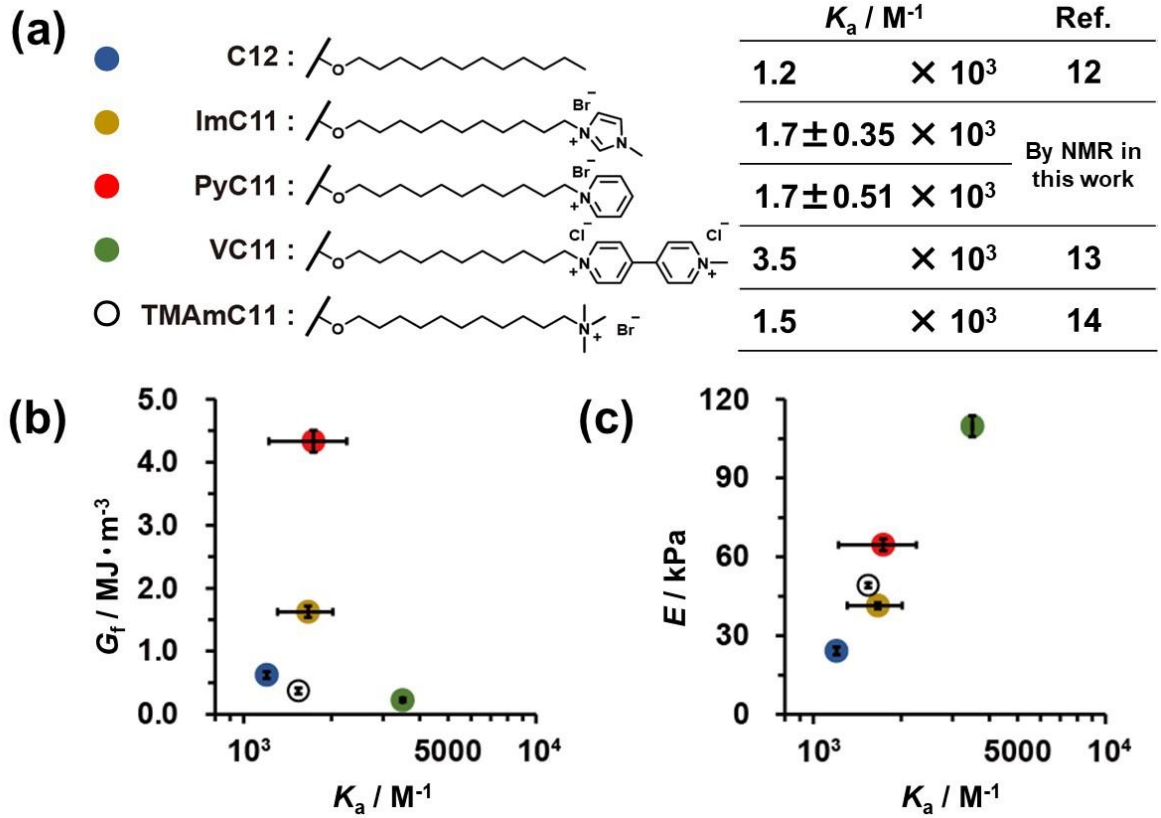

Figure 2-8. (a) Association constants (K_a) of αCDAAmMe with guest units in aqueous solutions. K_a of the αCDAAmMe unit with the C12 unit is 1200 M^{-1} by using αCD and *n*-dodecyl(ester)-acrylamide polymer.[12] Those with ImC11 and PyC11 were determined by NMR in this study. That with VC11 was calculated in Yamaguchi's work.[13] K_a of αCD with N^1,N^1,N^1,N^{10},N^{10},N^{10}-hexamethyldecane-1,10-diaminium (1540 M^{-1})[14] was cited as a model of αCDAAmMe with TMAmC11. **(b)** G_f of the αCD-R hydrogels against K_a. **(c)** E of the αCD-R hydrogels against K_a.

Figure 2-8b shows the relation between K_a and G_f. The K_a values of the αCD-C12, αCD-ImC11, αCD-PyC11, αCD-VC11, and αCD-TMAmC11 complexes were in almost the same order in the range of 1.2–3.5 × 10^3 M^{-1}. On the other hand, the αCD-PyC11 hydrogel exhibited a high G_f (4.3 MJ/m^3), but the others showed low G_f values (< 2.0 MJ/m^3) even with the same K_a. This result indicates that K_a does not affect the G_f of the αCD-R hydrogels.

Figure 2-8c shows the relation between K_a and E of the αCD-R hydrogels. The order of the E values is αCD-C12 < αCD-ImC11 < αCD-TMAmC11 < αCD-PyC11 < αCD-VC11 hydrogels. E is generally proportional to the cross-linking density. To consider the effect of K_a on the cross-linking density of the αCD-R hydrogels, the complexation ratio was calculated from equation (3) using the K_a value and a preset concentration of the host and guest molecules. **Figure 2-9** shows the theoretical curve of complexation ratio when $[H]_0$ and $[G]_0$ are 0.040 M.

$$Complexation\ ratio\ (\%) = \frac{100[\mathrm{Complex}]}{[H]_0} = \frac{50\left\{[H]_0 + [G]_0 - K_a^{-1} - \sqrt{([H]_0 + [G_0] - K_a^{-1})^2 - 4[H]_0[G]_0}\right\}}{[H_0]} \quad (3)$$

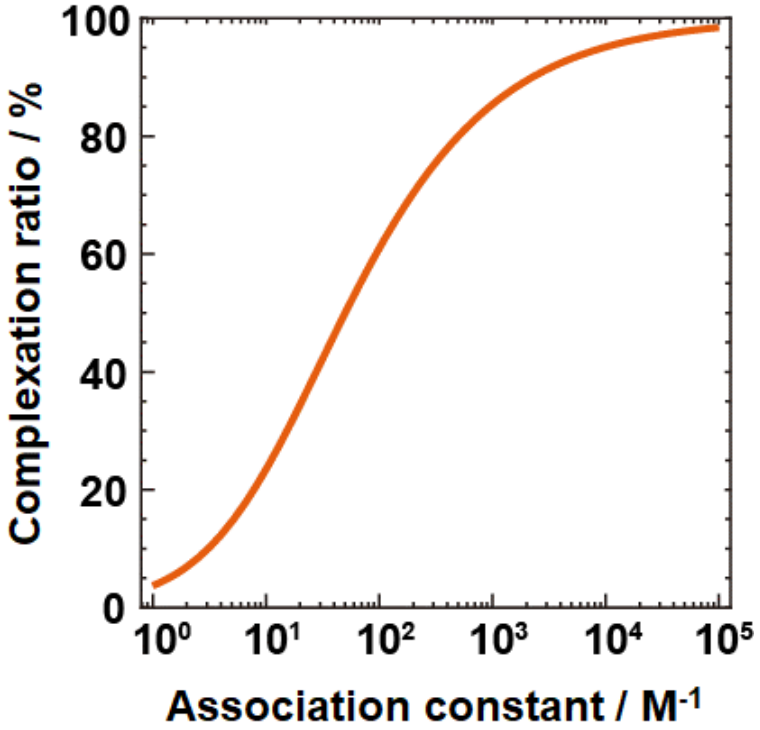

Figure 2-9. A theoretical curve depicting the K_a dependence of the 1:1 complexation ratio when $[H]_0$ and $[G]_0$ are 0.040 M.

When the range of K_a was 1.2–3.5 × 10^3 M^{-1}, the theoretical concentration of the inclusion complex in the αCD-R hydrogel was estimated to be 0.035–0.037 mol/L, indicating that the cross-linking density of the αCD-R hydrogels was almost the same. The range of theoretical concentrations of the inclusion complexes was smaller than the range of E values of the αCD-R hydrogels. The above result suggests that the effect of K_a on E was relatively small. Therefore, the author hypothesize that the threading/dethreading kinetics of the CD units is mainly affected G_f and E.

2.3.3. Relation between the mechanical properties and the partial atomic charges of the cationic moieties

To assess the threading/dethreading kinetics of CD units, we evaluated the potential barrier of the cationic species by using charge density analysis. The partial atomic charges on ImC11, PyC11, VC11, and TMAmC11 were calculated using the restrained electrostatic potential (RESP)[16] methodology based on quantum chemical calculations at the B3LYP level using the 6-31G(d,p) basis set in Gaussian 09 Rev. E01[17] (**Figures 2-10–2-13 and 2-14a**). These calculations were performed by Associate Professor Dr. Go Watanabe in Kitasato University.

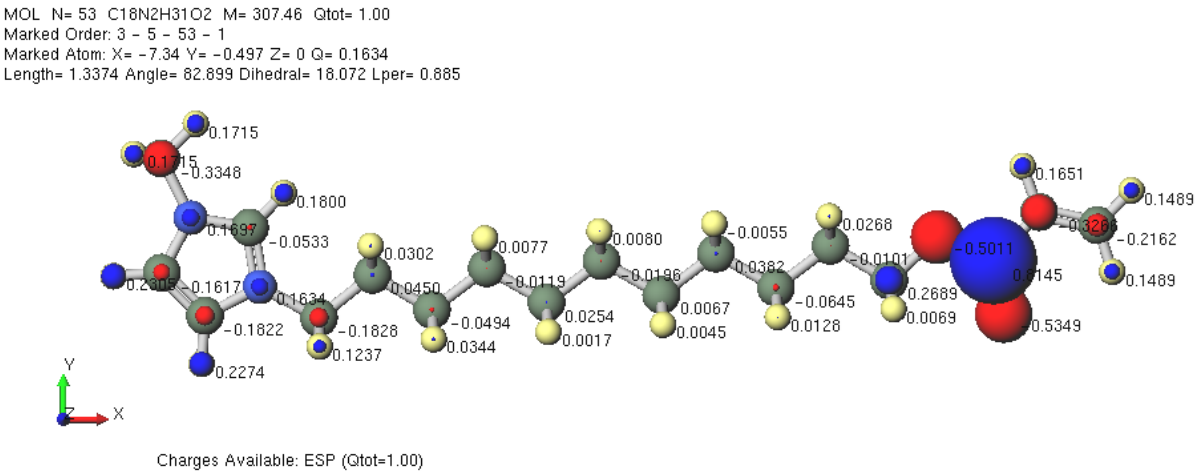

Figure 2-10. The RESP partial atomic charges in ImC11 monomer.

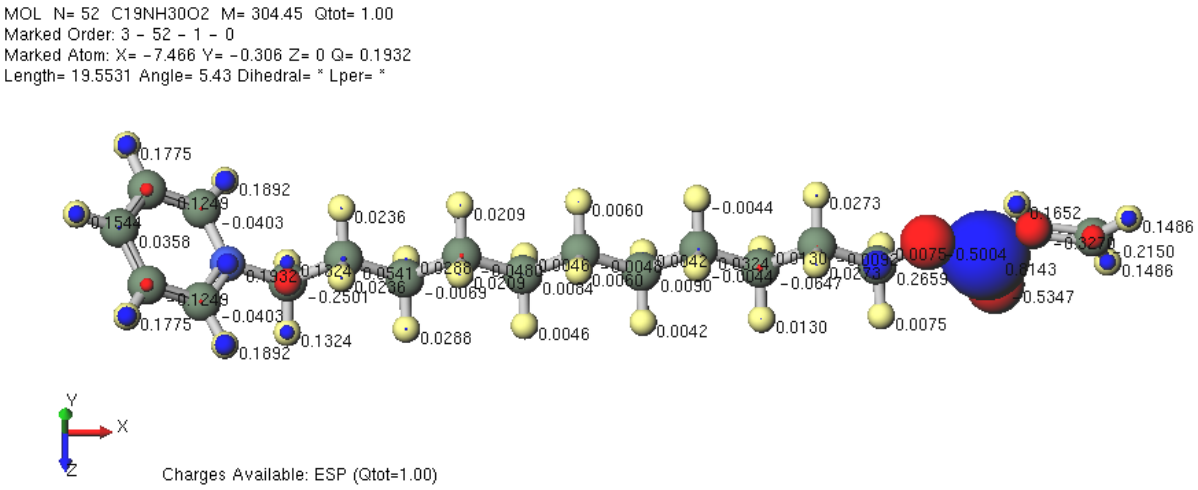

Figure 2-11. The RESP partial atomic charges in PyC11 monomer.

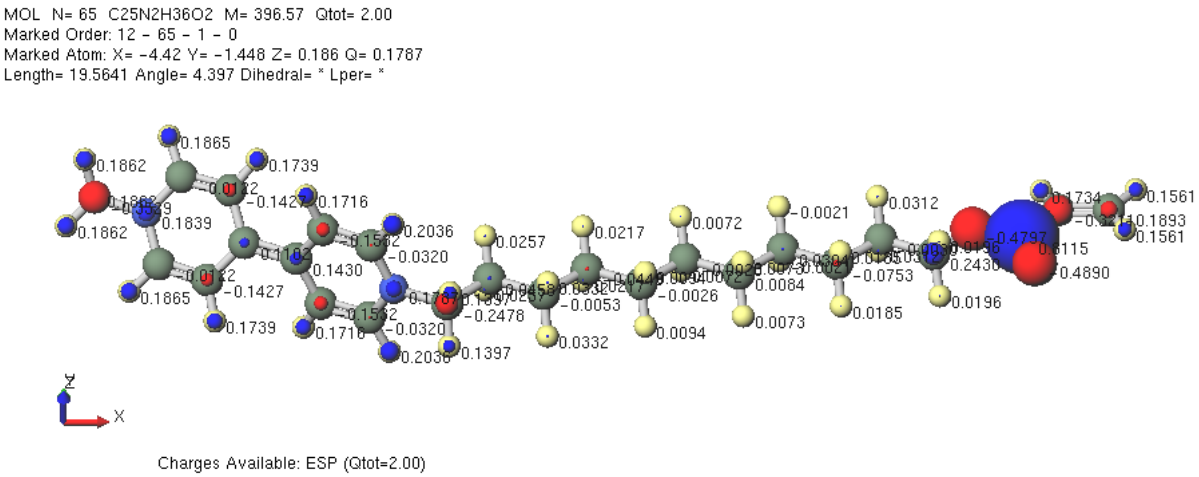

Figure 2-12. The RESP partial atomic charges in VC11 monomer.

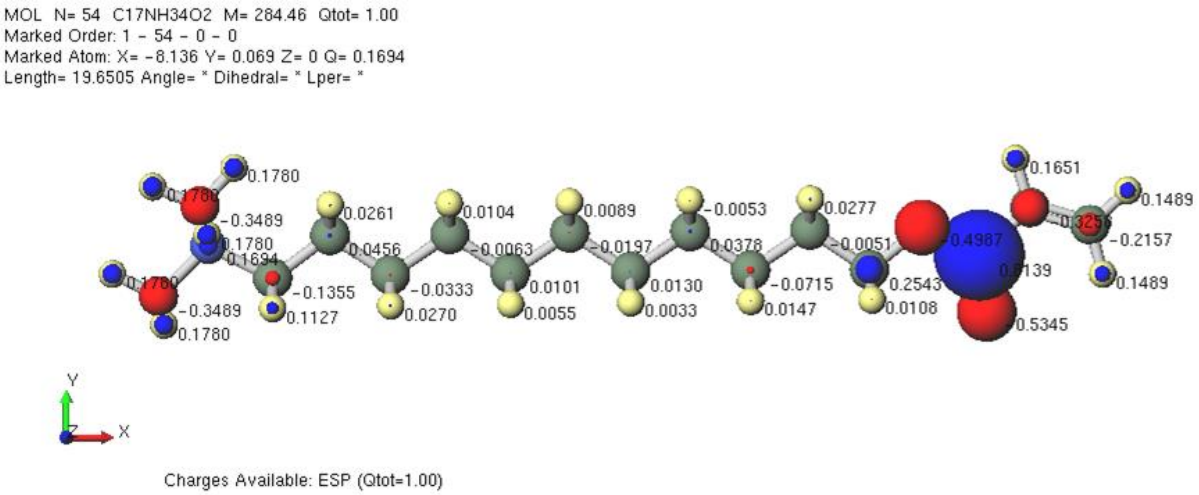

Figure 2-13. The RESP partial atomic charges in TMAmC11 monomer.

Figure 2-14a shows that RESP partial atomic charges on quaternary ammonium cations (N^+) increased in the order of ImC11 < TMAmC11 < PyC11 < VC11. The potential barrier (electric instability) between the CD units and the cationic units should increase in the same order.

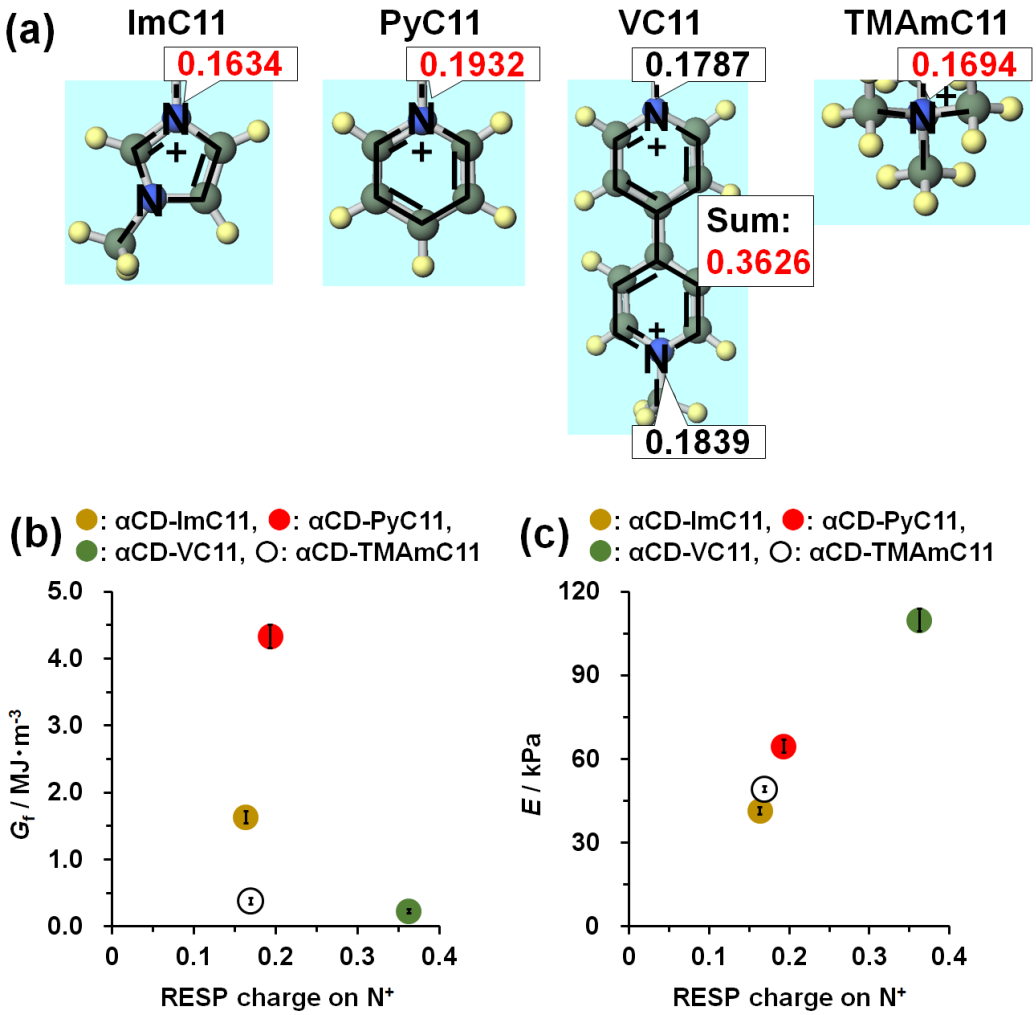

Figure 2-14. (a) The RESP partial atomic charges on N^+ in ImC11, PyC11, VC11 and TMAmC11 monomers. The charges on N^+ are shown in the boxes. **(b)** Plots of G_f and the RESP charges on N^+. **(c)** Plots of E and the RESP charges on N^+.

A clear correlation between the RESP charges on N^+ and the mechanical properties was observed. G_f reached its maximum at a RESP charge of approximately 0.2–0.3 (**Figure 2-14b**), indicating that a suitable RESP charge should give the highest G_f. E increased with RESP charge (**Figure 2-14c**), indicating that the RESP charge directly affects the stiffness of the αCD-R hydrogels. The RESP charge is closely related to the activation energy of the kinetics of the threading/dethreading CD units. These relations suggest that the kinetics of the threading/dethreading of the CD units, in other words, the lifetime of the reversible cross-links, has a major impact on the G_f and E of the αCD-R hydrogels. It is to be noted that not only the RESP charge but also steric hindrance of the TMAmC11 should influence G_f and E of the αCD-TMAmC11 hydrogel.

2.3.4. Linear viscoelastic measurement of the αCD-R hydrogels

To determine the relaxation time of the αCD-R hydrogels, dynamic viscoelastic measurements and stress-relaxation tests of sheet-like samples with thickness of ~ 1 mm were performed. **Figures 2-15–2-19** show results of angular frequency sweeps from 0.1 to 100 rad/s using the parallel-plate fixture with 8 mm in diameter in a temperature range of 0–45 °C. **Figures 2-15c–2-19c** show the frequency (ω) dependence of the storage modulus (G'), loss modulus (G''), and loss factor (tan δ) at different temperatures, which followed the time-temperature superposition to give the master curves referenced at 25 °C (**Figures 2-15d–2-19d**). Second-order average relaxation times ($\langle\tau\rangle_w$) were estimated by fitting master curves of G' and G'' with the generalized Maxwellian model (equations (4)–(6)), except for the αCD-C12, αCD-VC11, and αCD-TMAmC11 hydrogels. **Tables 2-6 and 2-7** shows the results of fitting for the αCD-ImC11 and αCD-PyC11 hydrogels.

$$G' = \sum_{p=1}^{N} G_p \frac{\omega^2 {\tau_p}^2}{1 + \omega^2 {\tau_p}^2} + G_N \tag{4}$$

$$G'' = \sum_{p=1}^{N} G_p \frac{\omega \tau_p}{1 + \omega^2 {\tau_p}^2} \tag{5}$$

$$\langle\tau\rangle_w = \frac{\sum_{p=1}^{N} G_p {\tau_p}^2}{\sum_{p=1}^{N} G_p \tau_p} \tag{6}$$

G_p: Relaxation strength in the p^{th} relaxation mode.

τ_p: Relaxation time in the p^{th} relaxation mode.

G_N: Terminal modulus.

The apparent activation energy ΔE_a was calculated from the Arrhenius equation (7), where a_T was the shift factor, R was the ideal gas constant, and A was a constant.

$$a_T = A e^{-\frac{\Delta E_a}{RT}} \tag{7}$$

Equation (7) was converted to equation (8). **Figures 2-15e–2-29e** show Arrhenius plots of the logarithm of a_T and inverse of T using eq. (8).

$$\ln a_T = \frac{\Delta E_a}{R}\left(\frac{1}{T} - \frac{1}{T_0}\right) \tag{8}$$

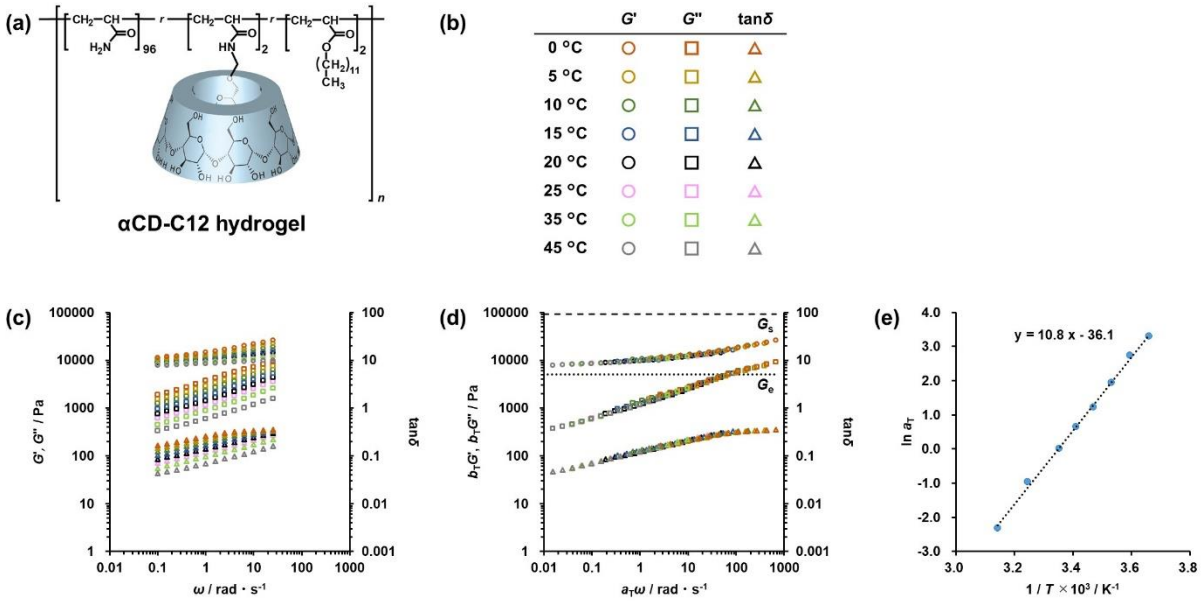

Figure 2-15. (a) Chemical structure of the αCD-C12 hydrogel. **(b)** Symbols for G', G'', and tan δ defined at each temperature. **(c)** Angular frequency dependence of G', G'', and tan δ. **(d)** Master curves of G', G'', and tan δ of the αCD-C12 hydrogel referenced at 25 °C. **(e)** The Arrhenius plot of a_T.

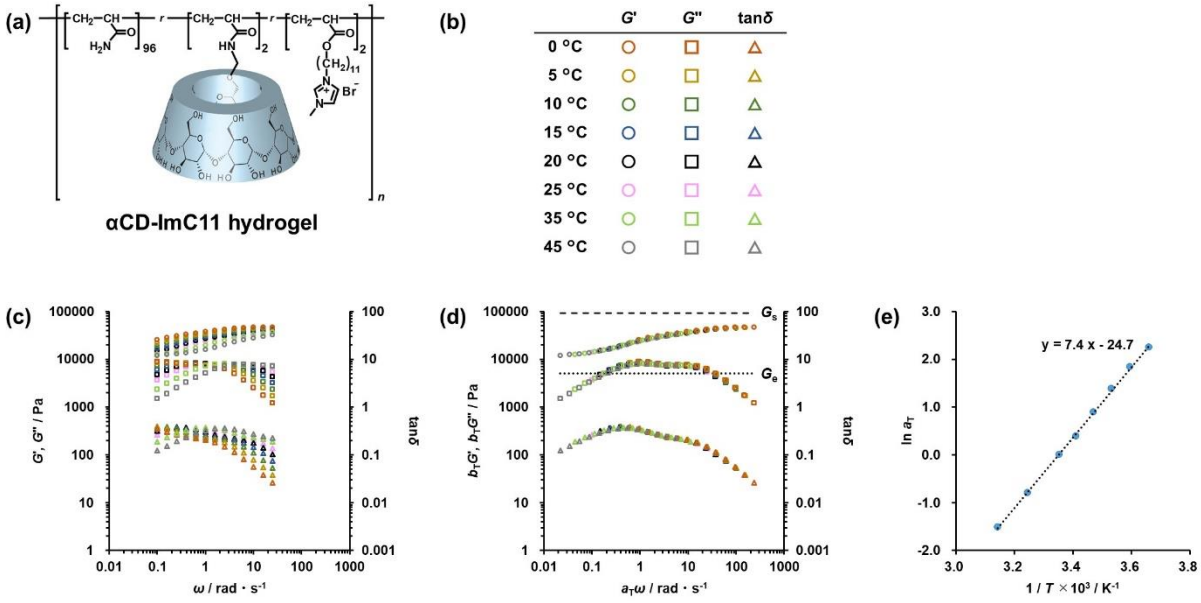

Figure 2-16. (a) Chemical structure of the αCD-ImC11 hydrogel. **(b)** Symbols for G', G'', and tan δ defined at each temperature. **(c)** Angular frequency dependence of G', G'', and tan δ. **(d)** Master curves of G', G'', and tan δ of the αCD-ImC11 hydrogel referenced at 25 °C. **(e)** The Arrhenius plot of a_T.

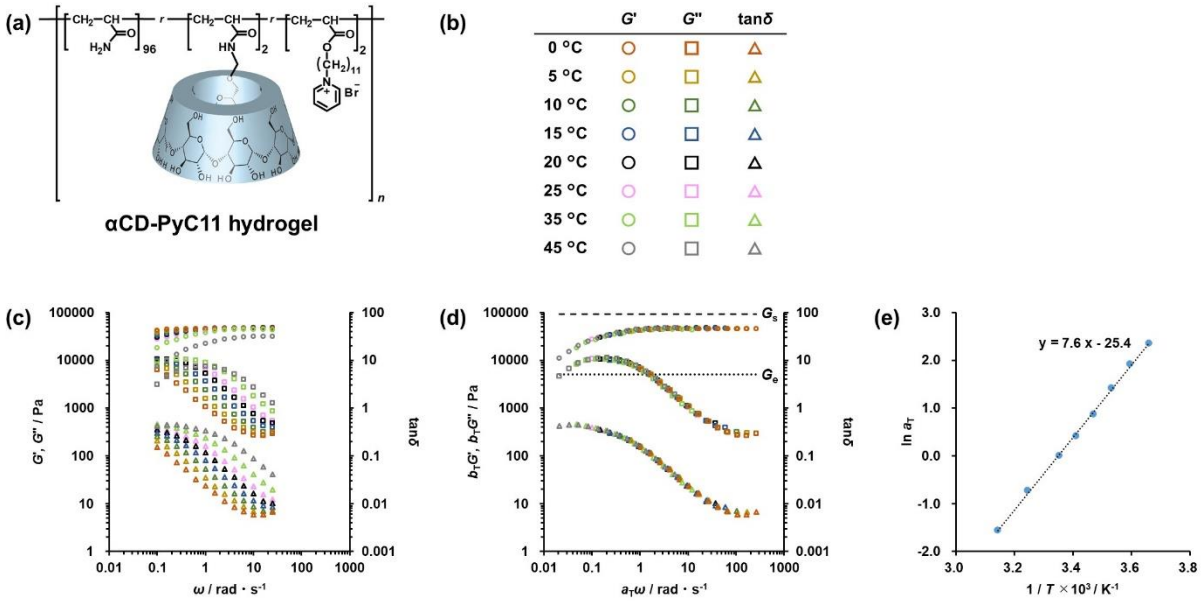

Figure 2-17. (a) Chemical structure of the αCD-PyC11 hydrogel. **(b)** Symbols for G', G'' and tan δ defined at each temperature. **(c)** Angular frequency dependence of G', G'', and tan δ. **(d)** Master curves of G', G'', and tan δ of the αCD-PyC11 hydrogel referenced at 25 °C. **(e)** The Arrhenius plot of a_T.

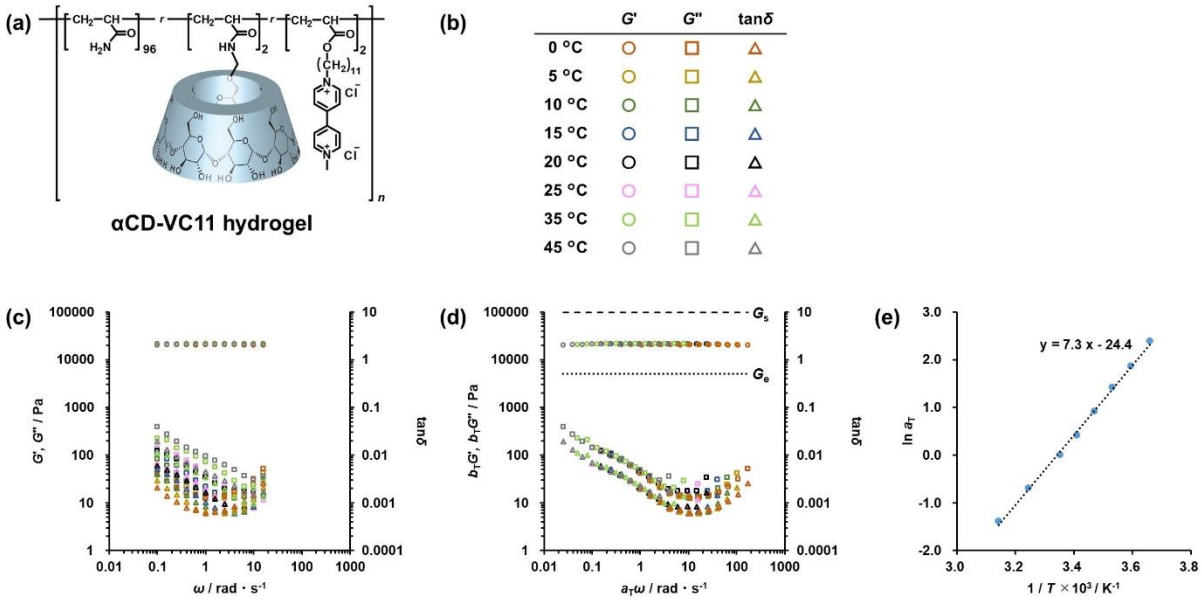

Figure 2-18. (a) Chemical structure of the αCD-VC11 hydrogel. **(b)** Symbols for G', G'', and tan δ defined at each temperature. **(c)** Angular frequency dependence of G', G'', and tan δ. **(d)** Master curves of G', G'', and tan δ of the αCD-VC11 hydrogel referenced at 25 °C. **(e)** The Arrhenius plot of a_T.

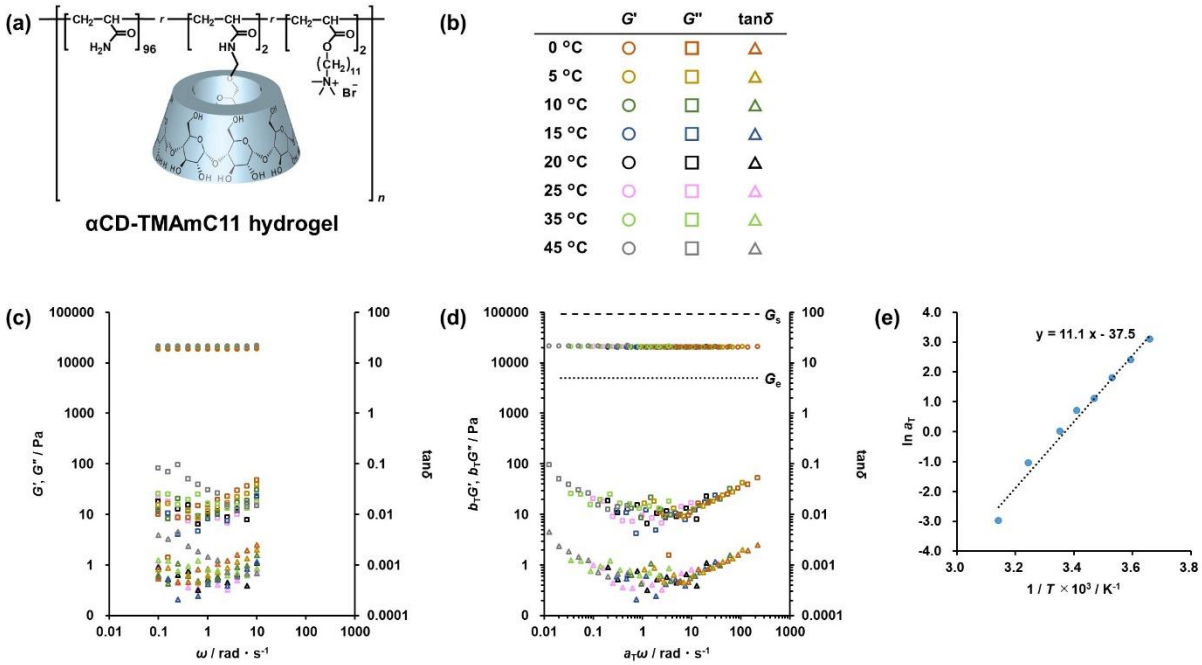

Figure 2-19. (a) Chemical structure of the αCD-TMAmC11 hydrogel. **(b)** Symbols for G', G'', and tan δ defined at each temperature. **(c)** Angular frequency dependence of G', G'', and tan δ. **(d)** Master curves of G', G'', and tan δ of the αCD-TMAmC11 hydrogel referenced at 25 °C. **(e)** The Arrhenius plot of a_T.

Table 2-6. Parameters G_p and τ_p used for curve fitting of the master curves of G' and G'' of the αCD-ImC11 hydrogel.

mode	**1**	**2**	**3**	**4**	**5**	**6**	**7**	G_N
G_p **/ Pa**	15353	15405	-	-	-	-	-	12600
τ_p **/ s**	0.102	1.948	-	-	-	-	-	-

Table 2-7. Parameters G_p and τ_p used for curve fitting of the master curves of G' and G'' of the αCD-PyC11 hydrogel.

mode	**1**	**2**	**3**	**4**	**5**	**6**	**7**	G_N
G_p **/ Pa**	14493	23250	-	-	-	-	-	7734
τ_p **/ s**	2.204	19.35	-	-	-	-	-	-

The master curves of the αCD-R hydrogels were explained by the sticky reptation model, which considers that the stickers retard the global diffusion of the entangled chains (reptation).[18,19] **Figures 2-15d–2-19d** show theoretical lines for the plateau values from the entanglements (G_e: dotted line). The dashed lines (G_s in **Figures 2-15d–2-19d**) represent those from the entanglements and reversible cross-links (host-guest cross-links). G_e was experimentally estimated to be about 5.0×10^3 Pa from the rubbery plateau level of G' for the entangled polyacrylamide solution.[19] G_s is the theoretical G' derived from the sticky reptation model, in which the entangled polymer network is assumed to be cross-linked by host-guest inclusion complexes as sticking points. G_s was calculated with a following equation (9), where v_s was the number density of temporary cross-linking points (stickers) and k_B was Boltzmann constant.

$$G_s = v_s k_B T + G_e \quad (9)$$

Assuming that all the inclusion complexes in the αCD-R hydrogel acted as stickers, we roughly estimated G_s to be about $9.1–9.6 \times 10^4$ Pa at 25 °C, based on the concentration of αCDAAmMe and guest monomer, and K_a.

The observed G' of the αCD-R hydrogels increased with increasing ω from G_e to G_s, indicating that the αCD-R hydrogels are the entanglement-dominant networks with sticky points, and the G' value is derived from the entanglement of the polyacrylamide chains and the host-guest interactions. Therefore, the increase in G' is due to the inclusion complexes as sticking points, suggesting that the observed relaxation modes of the αCD-R hydrogels are derived from the association and dissociation of the reversible cross-linking points formed by the inclusion complexes. It should be noted that the level of G_s does not agree with the plateau modulus at high frequency limit. This deviation is attributed to connectivity defects including intramolecular connection, which does not contribute to elasticity.

To detect the relaxation time of the αCD-VC11 hydrogel, stress-relaxation tests were performed with the rheometer MCR302 (**Figure 2-20**). The relaxation modulus ($G(t)$) was fitted with the following equation using seven relaxation modes (**Table 2-8)**.

$$G(t) = \sum_{p=1}^{N} G_p e^{-\frac{t}{\tau_p}} + G_{\mathrm{N}} \tag{10}$$

Based on obtained parameters, we deduced the complex moduli (**Figure 2-21**). Calculated values, especially G', agrees with the experimentally obtained complex moduli, indicating that the stress relaxation tests were successfully performed in the linear viscoelastic range. $<\tau>_{\mathrm{w}}$ was calculated as 6.6×10^3 s with equation (6).

For the same reason, the stress-relaxation test of the αCD-TMAmC11 hydrogel was performed (**Figures 2-22 and 2-23, Table 2-9**). The result was fitted with equation (10) using a relaxation mode and $<\tau>_{\mathrm{w}}$ was calculated as 9.5×10^3 s with equation (6).

Table 2-8. Parameters G_{p} and τ_{p} used for curve fitting of $G(t)$ of the αCD-VC11 hydrogel.

mode	**1**	**2**	**3**	**4**	**5**	**6**	**7**	$\boldsymbol{G_{\mathrm{N}}}$
$\boldsymbol{G_{\mathrm{p}}}$ **/ Pa**	3256	2497	4137	4491	1658	1198	414	7964
$\boldsymbol{\tau_{\mathrm{p}}}$ **/ s**	1309	1350	5255	7099	7698	9006	10089	-

Table 2-9. Parameters G_{p} and τ_{p} used for curve fitting of $G(t)$ of the αCD-TMAmC11 hydrogel.

mode	**1**	**2**	**3**	**4**	**5**	**6**	**7**	$\boldsymbol{G_{\mathrm{N}}}$
$\boldsymbol{G_{\mathrm{p}}}$ **/ Pa**	16899	-	-	-	-	-	-	-
$\boldsymbol{\tau_{\mathrm{p}}}$ **/ s**	9455	-	-	-	-	-	-	-

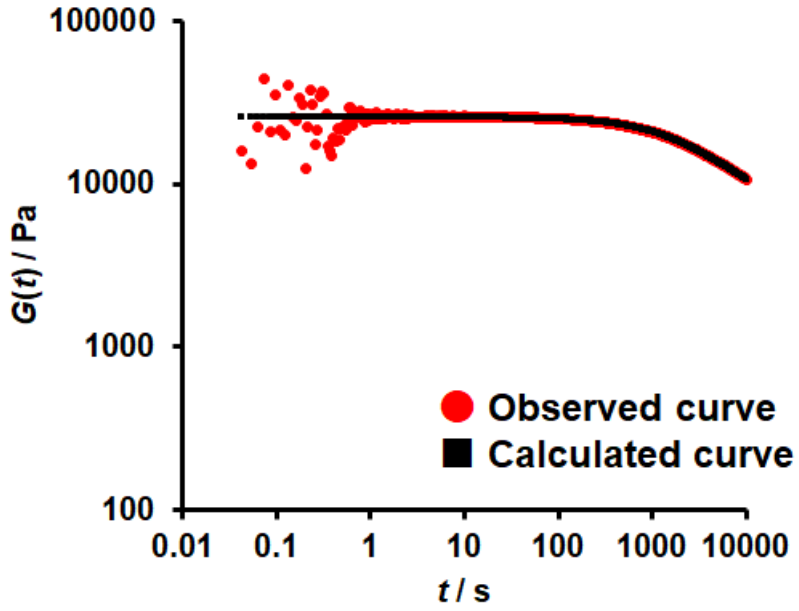

Figure 2-20. (a) Stress-relaxation curves of the αCD-VC11 hydrogel (γ = 0.4%, T = 25 °C).

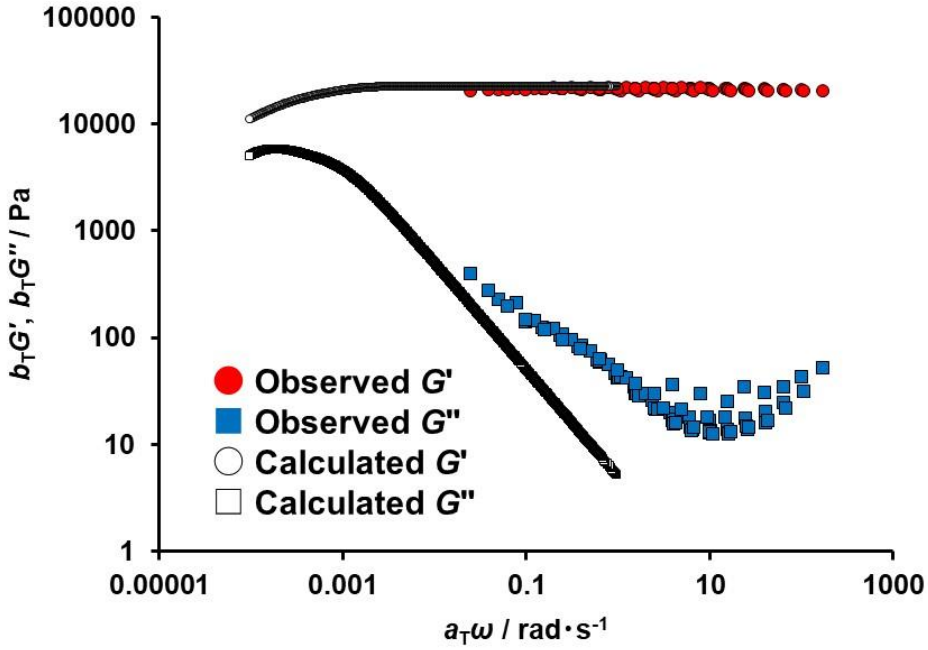

Figure 2-21. The comparison between calculated moduli and master curves of G' and G'' of the αCD-VC11 hydrogel.

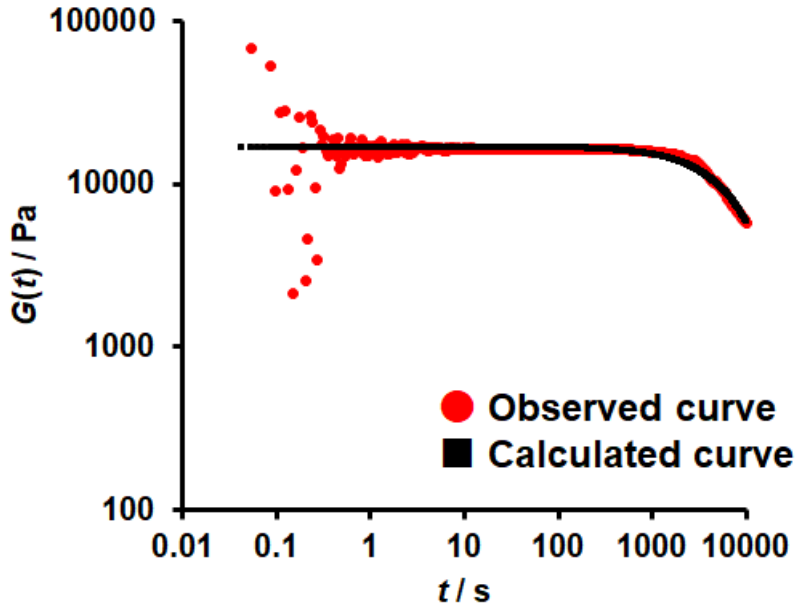

Figure 2-22. Stress-relaxation curves of the αCD-TMAmC11 hydrogel (γ = 0.6%, T = 25 °C).

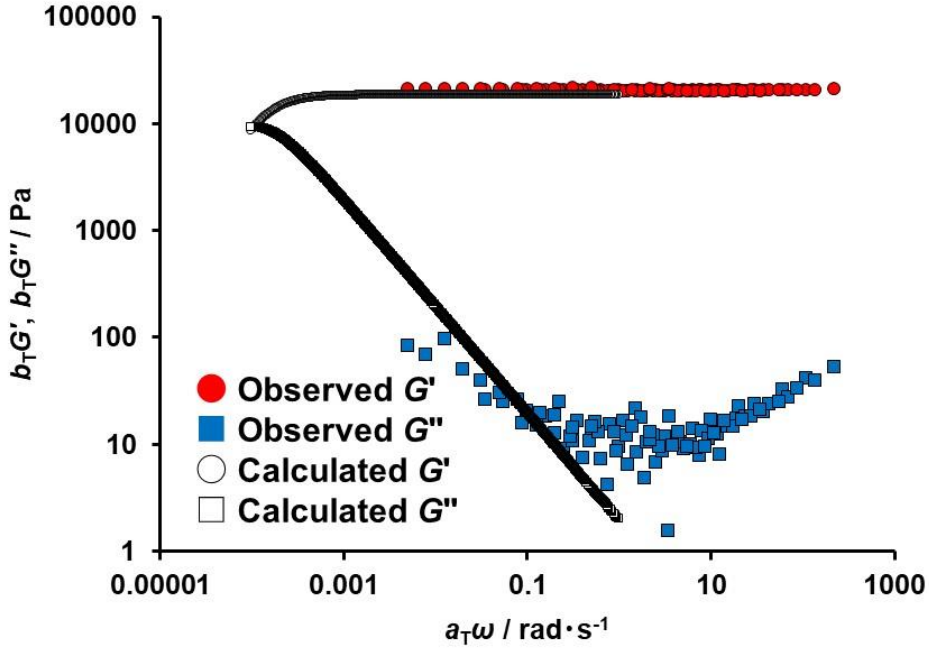

Figure 2-23. The comparison between calculated moduli and master curves of G' and G'' of the αCD-TMAmC11 hydrogel.

As shown in **Figures 2-24–26** and **Tables 2-10–2-12**, stress-relaxation tests of the αCD-C12, αCD-ImC11, and αCD-PyC11 hydrogels were similarly performed in the linear viscoelastic range. These $G(t)$ monotonically decreased, and the calculated G' reached the secondary rubbery plateau region in the range of $\omega < 0.1$ rad/s. These low plateau moduli were about $5.1–9.5 \times 10^3$ Pa and correspond to the plateau modulus derived from the entangled polymer strand (G_e). On the other hand, as described above, the plateau moduli in high ω region were originating from the temporary cross-linked polymer network (G_s). These viscoelastic properties of the αCD-R hydrogels support that the relaxation characteristics of the αCD-R hydrogels are well explained by the sticky reptation model.

Table 2-10. Parameters G_p and τ_p used for curve fitting of $G(t)$ of the αCD-C12 hydrogel.

mode	**1**	**2**	**3**	**4**	**5**	**6**	**7**	G_N
G_p **/ Pa**	1200	702.0	392.3	188.6	-	-	-	3008
τ_p **/ s**	2.573	21.62	226.0	3994	-	-	-	-

Table 2-11. Parameters G_p and τ_p used for curve fitting of $G(t)$ of the αCD-ImC11 hydrogel.

mode	**1**	**2**	**3**	**4**	**5**	**6**	**7**	G_N
G_p **/ Pa**	12361	13827	3984	1305	-	-	-	9511
τ_p **/ s**	0.1520	1.464	13.04	432.8	-	-	-	-

Table 2-12. Parameters G_p and τ_p used for curve fitting of $G(t)$ of the αCD-PyC11 hydrogel.

mode	**1**	**2**	**3**	**4**	**5**	**6**	**7**	G_N
G_p **/ Pa**	16141	12477	4111	2704	-	-	-	5156
τ_p **/ s**	3.714	22.28	157.8	2384	-	-	-	-

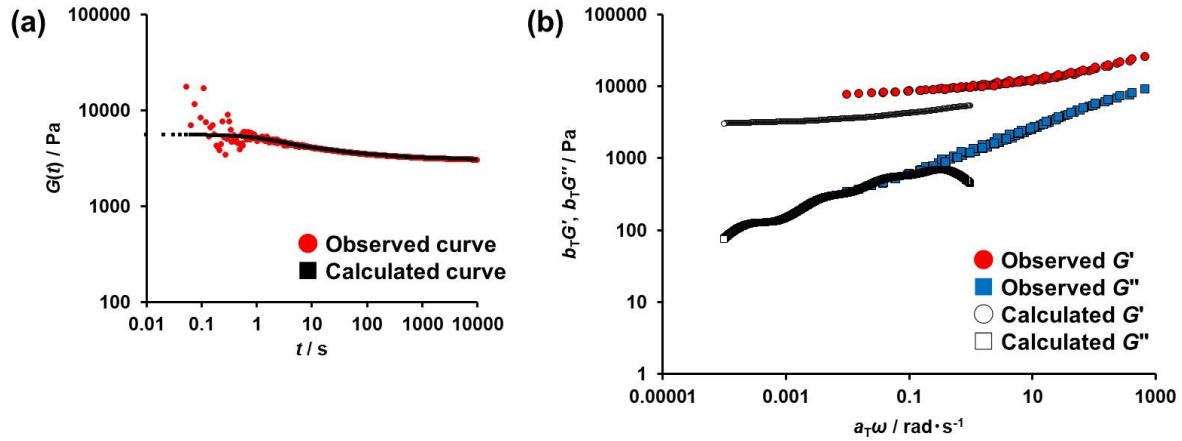

Figure 2-24. (a) Stress-relaxation curves of the αCD-C12 hydrogel (γ = 3%, T = 25 °C). **(b)** The comparison between calculated moduli and master curves of G' and G'' of the αCD-C12 hydrogel.

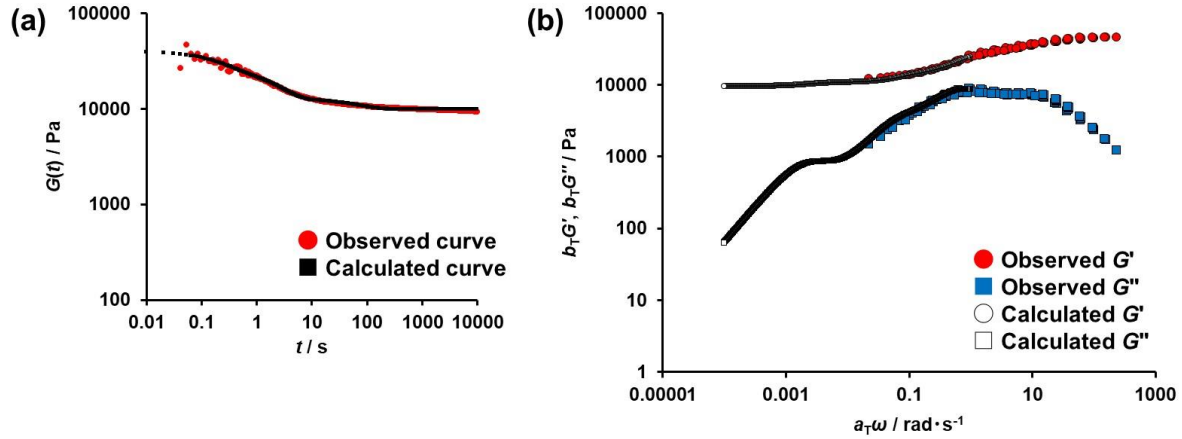

Figure 2-25. (a) Stress-relaxation curves of the αCD-ImC11 hydrogel (γ = 3%, T = 25 °C). **(b)** The comparison between calculated moduli and master curves of G' and G'' of the αCD-ImC11 hydrogel.

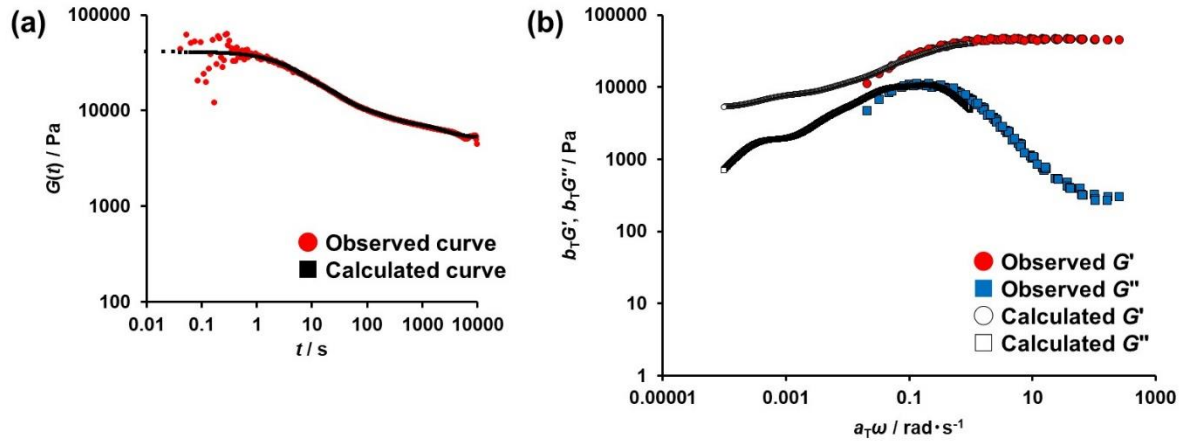

Figure 2-26. (a) Stress-relaxation curves of the αCD-PyC11 hydrogel (γ = 3%, T = 25 °C). **(b)** The comparison between calculated moduli and master curves of G' and G'' of the αCD-PyC11 hydrogel.

2.3.5. Relationship between $<\tau>_w$ of the αCD-R hydrogels and RESP charges

Calculated τ, $<\tau>_w$ and ΔE_a were summarized in **Table 2-13**. The αCD-C12 hydrogel did not show distinct relaxation modes, but its G'' was in proportion to $\omega^{0.5}$ in the high frequency region, which is derived from the Rouse modes of the polymer network.[20] The longest relaxation time (τ) of the Rouse modes of the αCD-C12 hydrogel was estimated as about 2×10^{-3} s by curve fitting using the generalized Maxwellian model, because τ attributed to the host-guest cross-linking points (stickers) should be faster than that of the Rouse modes. $<\tau>_w$ values of the αCD-ImC11, αCD-PyC11, αCD-VC11, and αCD-TMAmC11 hydrogels were 1.8, 18, and 6.6×10^3, 9.5×10^3 s, respectively.

Table 2-13. Relaxation time (τ), second-order average relaxation times ($<\tau>_w$) and apparent activation energy (ΔE_a) of the αCD-R hydrogels.

	αCD-C12 hydrogel	**αCD-ImC11 hydrogel**	**αCD-PyC11 hydrogel**	**αCD-VC11 hydrogel**	**αCD-TMAmC11 hydrogel**
τ	n/a (< 0.01 s)	0.10 s 1.9 s	2.2 s 19 s	5.3×10^3 s	9.5×10^3 s
$<\tau>_w$	n/a	1.8 s	18 s	6.6×10^3 s	9.5×10^3 s
ΔE_a	84 kJ/mol	59 kJ/mol	63 kJ/mol	61 kJ/mol	92 kJ/mol

Figure 2-27 shows the relation between $<\tau>_w$ and RESP charge on N^+ of the cationic unit. $<\tau>_w$ linearly increased with the RESP charges on N^+, except for the αCD-TMAmC11 hydrogel. The relation between $<\tau>_w$ and the RESP charge supports the above idea of the lifetime of the reversible cross-linking points. The αCD-TMAmC11 hydrogel showed the longest $<\tau>_w$ although the RESP charge on N^+ was similar to ImC11. This is mainly attributed to the large steric hindrance effect of TMAmC11 on αCD.

On the other hand, ΔE_a in **Table 2-11** was almost the same among the αCD-ImC11, αCD-PyC11, αCD-VC11 hydrogels. ΔE_a is one of the measures of the temperature dependence of the relaxation, which is not the life time of the stickers. This result also supports that the life time of the stickers is determined by the RESP fitted charge, resulting in the direct effect on the viscoelastic relaxation time. Noted that ΔE_a of the αCD-C12 hydrogel was higher than the others, which is attributed to the fact that the αCD-C12 hydrogel was turbid.

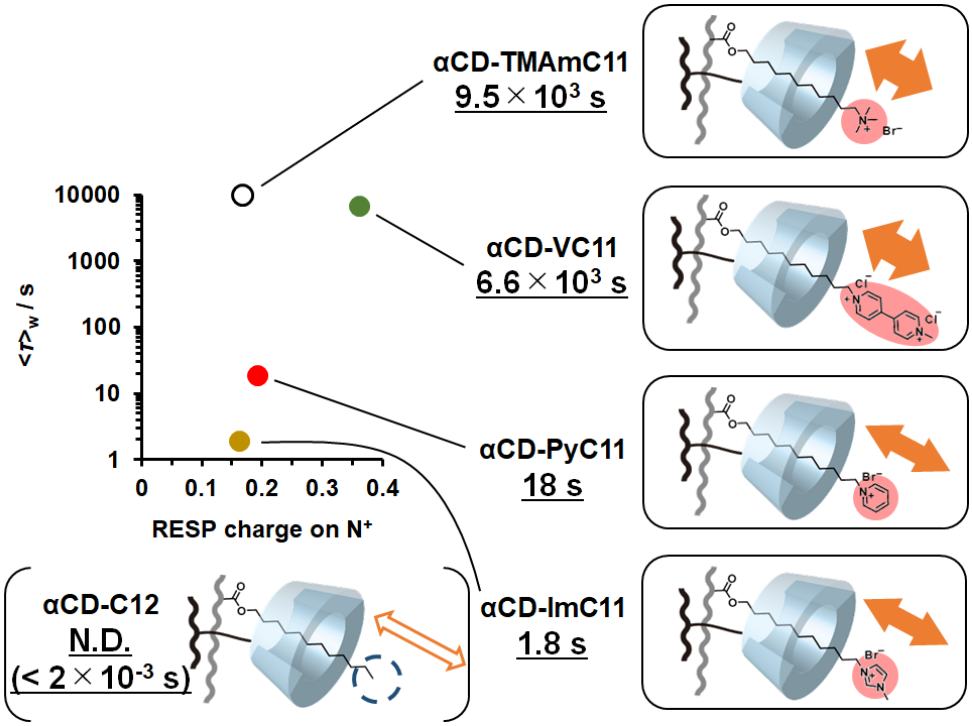

Figure 2-27. Plots of the second-order relaxation time ($<\tau>_w$) and RESP charges on N^+, and schematic of the reversible cross-linking points of the αCD-R hydrogels.

Furthermore, the trend of $<\tau>_w$ of the αCD-R hydrogels is consistent with the following kinetics studies of complexation behaviors of αCD in an aqueous solution system. Association/dissociation rates (k_1 and k_{-1}) in complexation with alkyl chains through tricationic[15] or bulky cationic[14,21,22] groups could be determined, because the threading motions are too slow on the NMR time scale. On the other hand, complexation through mono- or dicationic groups with low steric hindrance were so fast that k_1 and k_{-1} could not be estimated by NMR spectroscopy.[15,21,23] These results indicate that the kinetics of the threading/dethreading of the CD units directly affected the viscoelastic properties of the αCD-R hydrogels, and that the increment of E accompanied by the RESP charge is attributed to the delay of the viscoelastic relaxation time.

2.3.6. Relationship between the mechanical properties and the viscoelastic properties of the αCD-R hydrogels

The linear viscoelastic measurements revealed distinct relaxation times derived from the reversible cross-linking points. Furthermore, the relation between RESP charges and mechanical properties (**Figure 2-14**) suggested that the lifetime of the reversible cross-links had a major impact on the G_f and E of the αCD-R hydrogels. To investigate the effect of relaxation time in more detail, additional tensile tests of the αCD-PyC11 hydrogel at different tensile rates (0.10, 0.50, and 10 mm/s) were performed (**Figure 2-28**). Mechanical properties of the αCD-PyC11 hydrogels varied with the tensile rate.

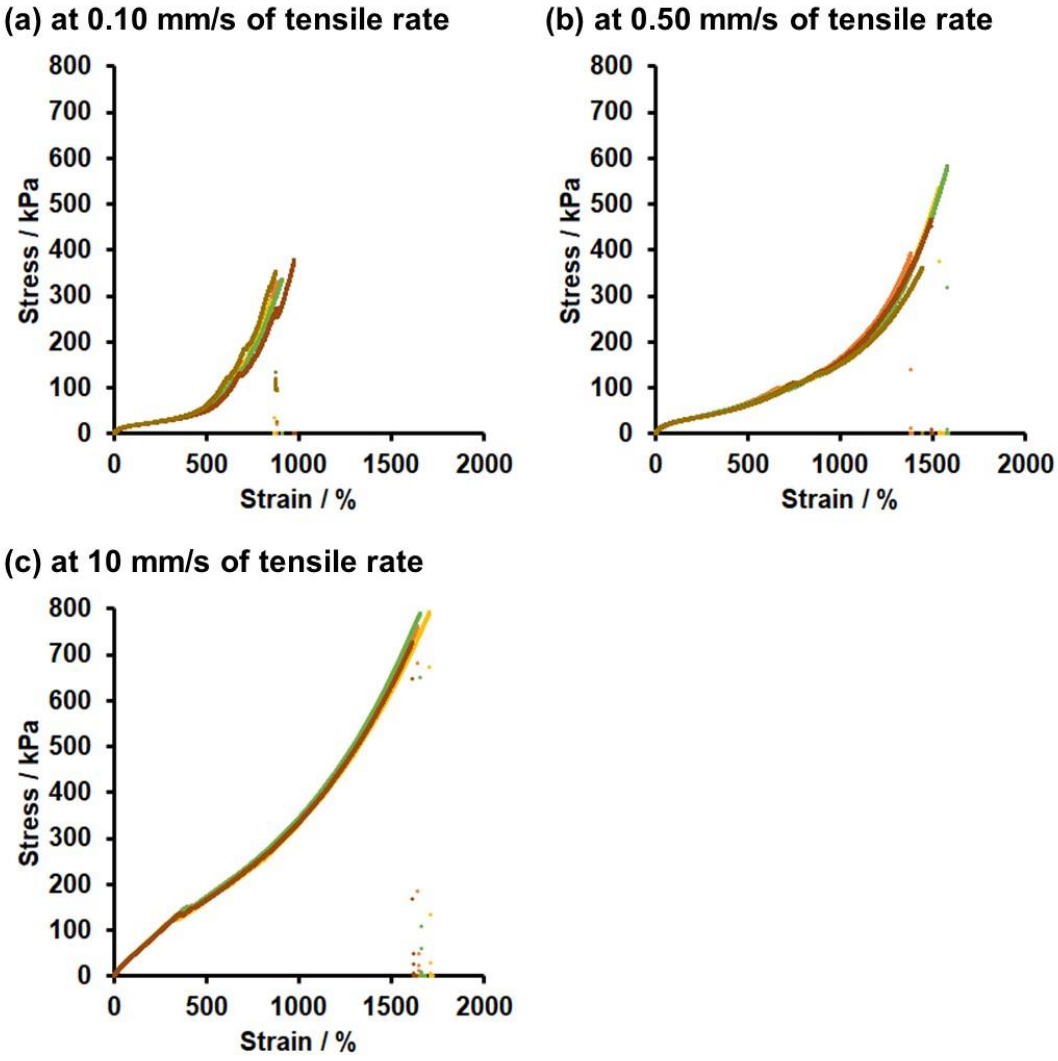

Figure 2-28. Stress-strain curves of the αCD-PyC11 hydrogel at 25 °C at different tensile rates, **(a)** at 0.10 mm/s, **(b)** at 0.50 mm/s, and **(c)** at 10 mm/s.

The author focused on strain rate during tensile tests and $<\tau>_w$ to investigate the relation among mechanical properties and viscoelastic properties of the αCD-R hydrogels (**Figure 2-29**).

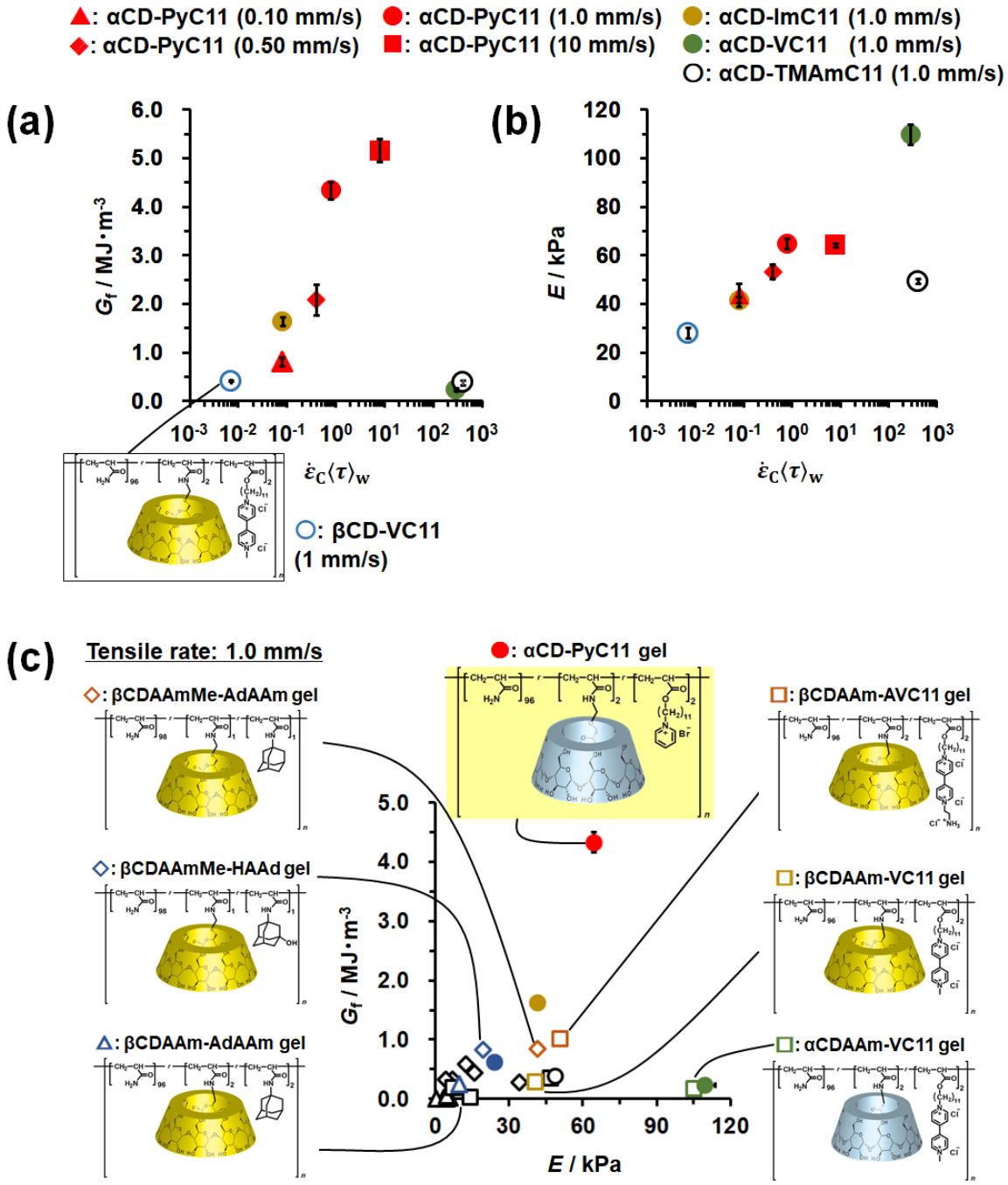

Figure 2-29. (a) Plots of G_f and $\dot{\varepsilon}_C\langle\tau\rangle_w$ of the αCD-R hydrogels. **(b)** Plots of the E and $\dot{\varepsilon}_C\langle\tau\rangle_w$ of the αCD-R hydrogels. The true strain rate decreases with increasing strain. For example, true $\dot{\varepsilon}_C\langle\tau\rangle_w$ at a strain of 1000% will be one-tenth of the initial $\dot{\varepsilon}_C\langle\tau\rangle_w$ **(c)** Plots of G_f and E of the host-guest hydrogels in this work (filled circle) and previous achievements (open triangle,[24] diamond,[2] and square[1]).

Figure 2-29a demonstrates the viscoelastic behavior of the reversible cross-linking points under tensile testing, showing its relation with G_f. **Figure 2-29b** demonstrates the relation between the viscoelastic behavior and E. The X-axis shows the product of $<\tau>_w$ and the nominal strain rate ($\dot{\varepsilon}_C$), which corresponds to the Weissenberg number: a dimensionless parameter that characterizes the behavior of a viscoelastic body during a deformation process. $\dot{\varepsilon}_C$ is calculated from the tensile speed (v) and initial length of a sample (L_0) as

$$\dot{\varepsilon}_C \equiv \frac{d\varepsilon_c}{dt} \sim \frac{d}{dt}(\lambda - 1) = \frac{v}{L_0}$$

Figure 2-29a shows that G_f reached its maximum within $\dot{\varepsilon}_C\langle\tau\rangle_w$ of 1~10. At a tensile rate of 1.0 mm/s (circles), $\dot{\varepsilon}_C\langle\tau\rangle_w$ of the αCD-ImC11, αCD-PyC11, and αCD-VC11 hydrogels were 0.081, 0.80, and 290, respectively. When $\dot{\varepsilon}_C\langle\tau\rangle_w$ of the αCD-R hydrogels was in the range of 1~10, the αCD-R hydrogels acted as viscoelastic bodies. The αCD-R hydrogels with $\dot{\varepsilon}_C\langle\tau\rangle_w$ = 1~10 showed high G_f values, indicating that the viscoelastic body showed high G_f. G_f of the αCD-PyC11 hydrogel was dependent on the tensile rate (0.10, 0.50, 1.0, and 10 mm/s). In particular, G_f of the αCD-PyC11 hydrogel was highest (5.2 MJ/m^3) at a tensile rate of 10 mm/s (red square: $\dot{\varepsilon}_C\langle\tau\rangle_w$ = 8.0). On the other hand, G_f of the αCD-PyC11 hydrogel drastically decreased at tensile rates of 0.50 mm/s (red diamond: $\dot{\varepsilon}_C\langle\tau\rangle_w$ = 0.40) or 0.10 (red triangle: $\dot{\varepsilon}_C\langle\tau\rangle_w$ = 0.080), and the hydrogel acted as a viscous body at $\dot{\varepsilon}_C\langle\tau\rangle_w < 1$. G_f of the αCD-ImC11 and αCD-VC11 hydrogels decreased outside the range of $\dot{\varepsilon}_C\langle\tau\rangle_w$ = 1~10, in which the αCD-ImC11, αCD-VC11 and αCD-TMAmC11 hydrogels acted as the viscous body ($\dot{\varepsilon}_C\langle\tau\rangle_w < 1$) and the elastic body ($\dot{\varepsilon}_C\langle\tau\rangle_w > 10$), respectively. These results indicate that the linear viscoelastic properties strongly influence the mechanical toughness of the αCD-R hydrogels.

Figure 2-29b shows the relation between $\dot{\varepsilon}_C\langle\tau\rangle_w$ and E. The tensile rate dependence of E for the αCD-PyC11 hydrogel correlated E with the linear viscoelastic spectra. E of the αCD-PyC11 hydrogel increased with increasing $\dot{\varepsilon}_C\langle\tau\rangle_w$ in the range of $\dot{\varepsilon}_C\langle\tau\rangle_w < 1$ and reached a steady value at $\dot{\varepsilon}_C\langle\tau\rangle_w > 1$. This result is consistent with the ω dependence of G' of the αCD-PyC11 hydrogel (**Figure 2-17d**), indicating that the αCD-PyC11 hydrogel acted as a viscoelastic body at $\dot{\varepsilon}_C\langle\tau\rangle_w \sim 1$.

Interestingly, in **Figures 2-29a and 2-29b**, the βCD-VC11 hydrogel (blue open circle), which was reported by Harada *et al.*,[1,13] was compared with the αCD-R hydrogels by using $\dot{\varepsilon}_C\langle\tau\rangle_w$. G_f and E of the βCD-VC11 hydrogel were lower than those of the αCD-ImC11 and αCD-PyC11 hydrogels due to lower $\dot{\varepsilon}_C\langle\tau\rangle_w$. In particular, the βCD-VC11 hydrogel, which has the same VC11 guest unit, was a viscous body. On the other hand, as described above, αCD-

VC11 acted as the elastic body to show low G_f. This is the opposite result, as it depends on the cavity size of the CDs. This parameter, $\dot{\varepsilon}_C\langle\tau\rangle_w$, enables us to evaluate various CD-based hydrogels at different tensile rates in a similar way.

Figure 2-29c shows the relation between G_f and E of the host-guest hydrogels developed in this work and in our previous work as they were strained at 1 mm/s.[1,2,24] The αCD-PyC11 hydrogels achieved higher G_f compared to those of our previous works. G_f of the βCDAAmMe-AdAAm hydrogel was low due to its short τ of stickers (~ 2×10^{-4} s)[2,19], whereas the βCDAAmMe-AdAAm hydrogel has self-healing properties, and the K_a of the βCD-Ad complex is high. G_f and E of the αCDAAm-VC11 hydrogel are similar to those of the αCD-VC11 hydrogel due to the long τ, which is derived from the large potential barrier of the VC11 unit against the αCD unit.

As mentioned above, the kinetics of the threading/dethreading of the CD units strongly influences the lifetime of the reversible cross-linking points. The relationship between the lifetime and the tensile rate drastically changed the G_f and E of the αCD-R hydrogels. Molecular design focusing on the lifetime of the reversible cross-linking points is important to improve the G_f of supramolecular hydrogels.

2.4. Conclusion

The author prepared five kinds of reversible-cross-linked αCD-R hydrogels (αCD-C12, αCD-ImC11, αCD-PyC11, αCD-VC11, and αCD-TMAmC11 hydrogels) and investigated the relations between the lifetime ($<\tau>_w$) of the reversible cross-linking points and the mechanical properties (G_f and E). The inclusion complex of the αCD unit and the cation-terminated linear alkyl chain unit on the polymer side chain functioned as a reversible cross-linking point. Quantum chemical calculations and linear viscoelastic measurements revealed that $<\tau>_w$ was controlled by the kinetics of the threading/dethreading of the αCD units, which was influenced by the potential barrier of the cationic units. The author demonstrated the effect of the viscoelastic behavior of the reversible cross-linking points on G_f of the αCD-R hydrogels using a dimensionless parameter $\dot{\varepsilon}_C\langle\tau\rangle_w$. The αCD-R hydrogels exhibited high G_f within $\dot{\varepsilon}_C\langle\tau\rangle_w$ of 1~10, where the reversible cross-linking points acted as viscoelastic bodies and G'' of the hydrogels was high. The author found that G_f within $\dot{\varepsilon}_C\langle\tau\rangle_w$ of 1~10 showed a local maximum because the observed G'' of the αCD-R hydrogels represents the energy dissipated by dissociation of the reversible cross-linking points. In the region of $\dot{\varepsilon}_C\langle\tau\rangle_w << 1$, only the entangled polymer network contributes to G_f because the inclusion complexes in the viscous state cannot contribute to energy dispersion. On the other hand, in the region of $\dot{\varepsilon}_C\langle\tau\rangle_w > 10$, the inclusion complexes behave like fixed cross-links, resulting in brittleness, similar to a conventional chemically cross-linked network. On the basis of these results, we have to design a molecular structure focusing on relaxation behavior, *i.e.,* the lifetime of the reversible cross-linking points, to achieve tough materials.

References

(1) Takashima, Y.; Otani, K.; Kobayashi, Y.; Aramoto, H.; Nakahata, M.; Yamaguchi, H.; Harada, A. Mechanical Properties of Supramolecular Polymeric Materials Formed by Cyclodextrins as Host Molecules and Cationic Alkyl Guest Molecules on the Polymer Side Chain. *Macromolecules* **2018**, *51* (16), 6318–6326.

(2) Takashima, Y.; Sawa, Y.; Iwaso, K.; Nakahata, M.; Yamaguchi, H.; Harada, A. Supramolecular Materials Cross-Linked by Host-Guest Inclusion Complexes: The Effect of Side Chain Molecules on Mechanical Properties. *Macromolecules* **2017**, *50* (8), 3254–3261.

(3) Yount, W. C.; Loveless, D. M.; Craig, S. L. Small-Molecule Dynamics and Mechanisms Underlying the Macroscopic Mechanical Properties of Coordinatively Cross-Linked Polymer Networks. *J. Am. Chem. Soc.* **2005**, *127* (41), 14488–14496.

(4) Serpe, M. J.; Craig, S. L. Physical Organic Chemistry of Supramolecular Polymers. *Langmuir* **2007**, *23* (4), 1626–1634.

(5) Seiffert, S.; Sprakel, J. Physical Chemistry of Supramolecular Polymer Networks. *Chem. Soc. Rev.* **2012**, *41* (2), 909–930.

(6) Grindy, S. C.; Learsch, R.; Mozhdehi, D.; Cheng, J.; Barrett, D. G.; Guan, Z.; Messersmith, P. B.; Holten-Andersen, N. Control of Hierarchical Polymer Mechanics with Bioinspired Metal-Coordination Dynamics. *Nat. Mater.* **2015**, *14* (12), 1210–1216.

(7) Yesilyurt, V.; Ayoob, A. M.; Appel, E. A.; Borenstein, J. T.; Langer, R.; Anderson, D. G. Mixed Reversible Covalent Crosslink Kinetics Enable Precise, Hierarchical Mechanical Tuning of Hydrogel Networks. *Adv. Mater.* **2017**, *29* (19), 1–6.

(8) Tan, C. S. Y.; Agmon, G.; Liu, J.; Hoogland, D.; Janeček, E. R.; Appel, E. A.; Scherman, O. A. Distinguishing Relaxation Dynamics in Transiently Crosslinked Polymeric Networks. *Polym. Chem.* **2017**, *8* (35), 5336–5343.

(9) Lake G. J.; Thomas A. G. The Strength of Highly Elastic Materials. *Proc. R. Soc. London, Ser. A* **1967**, *300* (1460), 108–119.

(10) Akagi, Y.; Sakurai, H.; Gong, J. P.; Chung, U.; Sakai, T. Fracture Energy of Polymer Gels with Controlled Network Structures. *J. Chem. Phys.* **2013**, *139* (14), 144905.

(11) Liu, C.; Kadono, H.; Mayumi, K.; Kato, K.; Yokoyama, H.; Ito, K. Unusual Fracture Behavior of Slide-Ring Gels with Movable Cross-Links. *ACS Macro Lett.* **2017**, *6* (12), 1409–1413.

(12) Yamaguchi, H.; Kobayashi, R.; Takashima, Y.; Hashidzume, A.; Harada, A. Self-Assembly of Gels through Molecular Recognition of Cyclodextrins: Shape Selectivity for Linear and Cyclic Guest Molecules. *Macromolecules* **2011**, *44* (8), 2395–2399.

(13) Aramoto, H.; Osaki, M.; Konishi, S.; Ueda, C.; Kobayashi, Y.; Takashima, Y.; Harada, A.; Yamaguchi, H. Redox-Responsive Supramolecular Polymeric Networks Having Double-Threaded Inclusion Complexes. *Chem. Sci.* **2020**, *11* (17), 4322–4331.

(14) Herrmann, W.; Keller, B.; Wenz, G. Kinetics and Thermodynamics of the Inclusion of Ionene-6,10 in α-Cyclodextrin in an Aqueous Solution. *Macromolecules* **1997**, *30* (17), 4966–4972.

(15) Kawaguchi, Y.; Harada, A. An Electric Trap: A New Method for Entrapping Cyclodextrin in a Rotaxane Structure. *J. Am. Chem. Soc.* **2000**, *122* (15), 3797–3798.

(16) Bayly, C. I.; Cieplak, P.; Cornell, W. D.; Kollman, P. A. A Well-Behaved Electrostatic Potential Based Method Using Charge Restraints for Deriving Atomic Charges: The RESP Model. *J. Phys. Chem.* **1993**, *97* (40), 10269–10280.

(17) Frisch, M. J.; Trucks, G. W.; Schlegel, H. B.; Scuseria, G. E.; Robb, M. A.; Cheeseman, J. R.; Scalmani, G.; Barone, V.; Mennucci, B.; Petersson, G. A.; et al. Gaussian 09. Gaussian Inc.: Wallingford CT **2009**.

(18) Leibler, L.; Rubinstein, M.; Colby, R. H. Dynamics of Reversible Networks. *Macromolecules* **1991**, *24* (16), 4701–4707.

(19) Kashiwagi, Y.; Katashima, T.; Nakahata, M.; Takashima, Y.; Harada, A.; Inoue, T. Linear Viscoelastic Studies on a Transient Network Formed by Host–Guest Interaction. *J. Polym. Sci. Part B Polym. Phys.* **2018**, *56* (15), 1109–1117.

(20) Rouse, P. E. A Theory of the Linear Viscoelastic Properties of Dilute Solutions of Coiling Polymers. *J. Chem. Phys.* **1953**, *21* (7), 1272–1280.

(21) Oshikiri, T.; Takashima, Y.; Yamaguchi, H.; Harada, A. Face-Selective [2]- and [3]Rotaxanes: Kinetic Control of the Threading Direction of Cyclodextrins. *Chem. - A Eur. J.* **2007**, *13* (25), 7091–7098.

(22) Macartney, D. H. The Self-Assembly of a [2]Pseudorotaxane of α-Cyclodextrin by the Slippage Mechanism. *J. Chem. Soc. Perkin Trans. 2* **1996**, *12*, 2775–2778.

(23) Castro, R.; Godínez, L. A.; Criss, C. M.; Kaifer, A. E. Host Properties of α-Cyclodextrin and a Water-Soluble Calix[6]Arene Probed with Dimeric Bipyridinium Guests. *J. Org. Chem.* **1997**, *62* (15), 4928–4935.

(24) Nakahata, M.; Takashima, Y.; Harada, A. Highly Flexible, Tough, and Self-Healing Supramolecular Polymeric Materials Using Host-Guest Interaction. *Macromol. Rapid Commun.* **2016**, *37* (1), 86–92.

Chapter 3

Multi-Energy Dissipation Mechanisms in Supramolecular Hydrogels with Fast and Slow Relaxation Modes

3.1. Introduction

The previous chapter, Chapter 2, showed the importance of the viscoelastic behavior of reversible cross-links to improve the toughness of the αCD-R (2, 2) hydrogels. When the toughness increased, the loss modulus (G'') of the hydrogel was high. Therefore, the author hypothesized that high cross-linking density and corresponding high G'' might give tougher hydrogel. However, the αCD-R hydrogels with high cross-linking density actually showed high Young's modulus and low toughness. A high value of G'' did not overcome the trade-off problem between modulus and toughness. Next, the author proposed combining two or more kinds of reversible cross-links to improve toughness.

Inspired by the different features of non-covalent bonds, combinations of several kinds of reversible cross-links in a single network have attracted much attention as a way to establish more highly functional materials.[1] Such hydrogels containing two kinds of reversible cross-links are called dual physically cross-linked hydrogels. While many of them were designed for effective self-healing[2–5] and multi-stimuli responsiveness[6–12], some hydrogels cross-linked by metal-ligand coordination[13,14], hydrogen bonding[15,16], or ionic interactions[17,18] have exhibited outstanding mechanical properties, probably due to their high binding energies.[2,19–24] For diverse hydrogels as well as dual physically cross-linked hydrogels, there is no known set of general principles with which to design properties and functionality.[25–28]

In addition, different reversible cross-links usually associate and dissociate with different timescales.[29–38] Therefore, a combination of different reversible cross-links also influences the viscoelastic properties of dual physically cross-linked hydrogels, where the dynamics of reversible cross-links with different timescales may produce a specific response to the external deformation.[39–43] Although the dynamics should be related to the energy dissipation mechanisms and toughness of the hydrogels, only a few studies on the quantitative relationships between dynamics and toughness have been reported.[36,38,44–51]

In this chapter, the author shows the relation between a combination of different molecular mobility and toughness values for supramolecular hydrogels (**Figure 3-1**). To do this, hydrogels with dual reversible cross-links by using host-guest complexation of α-cyclodextrins (αCDs) and cation-terminated alkyl chain guests were prepared. The author focused on the

viscoelastic relaxation time (τ) as a parameter for the molecular mobility of reversible cross-links. τ is defined as the characteristic time required for the modulus or stress to decrease to the value divided by Napier's constant under stress. Therefore, it will be useful for the discussion of energy dissipation in polymer materials as it closely relates to mechanical phenomena. Depending on the structure of the host-guest complex and the kinetics of bond breaking, the reversible cross-links show distinct second-order average relaxation times ($<\tau>_w$).[36] Previously, in the case of the hydrogel with one type of reversible cross-link, the author demonstrated the balance between $<\tau>_w$ and initial strain rate was important to improve toughness. By contrast, supramolecular hydrogels consisting of two different host-guest cross-links are expected to show unique relaxation behaviors on wide timescales. We investigated the effects of combined reversible cross-links with different $<\tau>_w$ values on the viscoelastic and the mechanical properties of supramolecular hydrogels to design an effective energy dissipation mechanism.

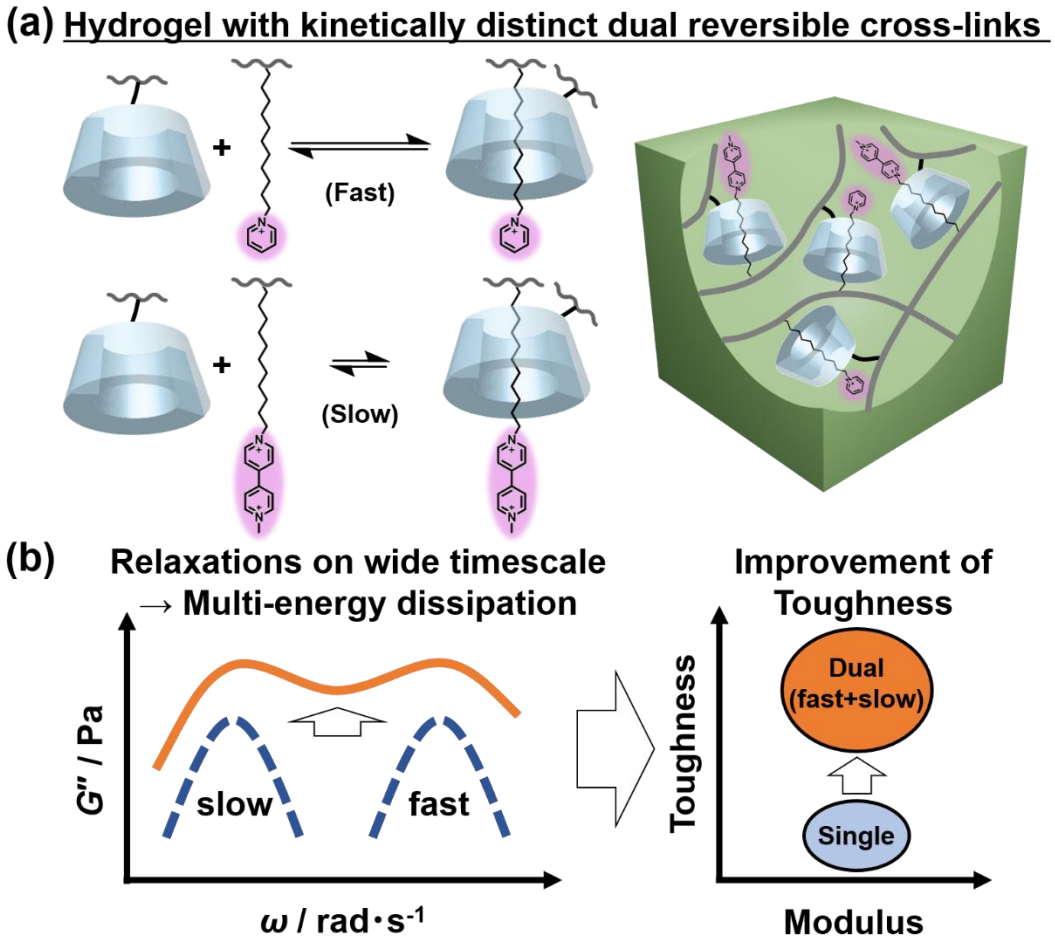

Figure 3-1. Conceptual figure for Chapter 3. **(a)** Schematic of a supramolecular hydrogel with two reversible cross-links exhibiting distinct kinetics. **(b)** Schematics for viscoelastic relaxation of the supramolecular hydrogels and the corresponding high toughness.

3.2. Experimental

Materials

N,N'–Methylenebis(acrylamide) (MBAAm), was purchased from Nacalai Tesque Inc. Acrylamido-methyl ether-modified αCD (αCDAAmMe), 3-(11-acryloyloxyundecyl)-1-methyl-imidazolium bromide (ImC11 monomer), 1-(11-acryloyloxyundecyl)-pyridinium bromide (PyC11 monomer), 4-(11-acryloyloxyundecyl)-4'-(methyl)-bipyridinium dichloride (VC11 monomer), and 11-acryloyloxyundecyl trimethylammonium bromide (TMAmC11 monomer) were prepared according to previous reports by Harada *et al*.[35,36,52,53] Other reagents were the same as described in Chapter 2.

Measurements

^{1}H and ^{13}C nuclear magnetic resonance (NMR) spectroscopy: ^{1}H and ^{13}C NMR spectra, solid-state ^{1}H field gradient magic angle spinning (FG-MAS) NMR spectra, and 2-Dimensional ^{1}H-^{1}H Nuclear Overhauser Effect spectroscopy (2D NOESY) NMR spectra were recorded in the similar manner as in Chapter 2. The mixing time for 2D NOESY NMR was set to 500 ms.

Fourier transform infrared (FT-IR) spectroscopy: FT-IR spectra were acquired at room temperature using a JASCO FT/IR–6100 spectrometer in the wavenumber range 600 to 4000 cm^{-1} via the attenuated total reflection (ATR) method using a ZnSe prism.

Tensile tests: Tensile tests and cyclic tensile tests were performed on a universal testing machine [Autograph AG-X plus (Shimadzu Co.)] equipped with a 20 N load cell and 1 N clip grips. The size of hydrogels and conditions for tensile tests were the same as shown in Chapter 2. For cyclic tensile tests, the hydrogels were stretched and recovered at approximately 25 °C with a tensile rate of 1 mm/s without intervals. Then, the maximum strains were set to 16%, 32%, 48%, 64% and 80% of the fracture strain of each hydrogel. The hysteresis ratio at each cycle was calculated using equation (1). The error bars for the hysteresis areas and hysteresis ratios were calculated from more than three experiments.

$$\text{Hysteresis ratio (\%)} = \frac{\text{Hysteresis area}}{\text{Supplied work under loading}} \times 100 \qquad (1)$$

Rheological measurements: Dynamic viscoelasticity and stress-relaxation properties were measured using an Anton Paar MCR302 rheometer with a parallel-plate fixture (8 mm in diameter). Measuring conditions were the same as described in Chapter 2.

Small-angle X-ray scattering (SAXS) measurements: The internal structures of the hydrogels under stretching were analyzed by SAXS with a tensile device at the BL40B2 beamline of SPring-8, Nishiharima, Japan. The wavelength of the incident X-ray beams was 0.10 nm. The sample-to-detector lengths were 2000 and 2282 mm. Type 4 dumbbell-shaped hydrogels with thicknesses of approximately 1 or 2.4 mm were prepared and cut to 15 mm lengths to fit the tensile device. They were stretched at room temperature with a tensile rate of 0.63 mm/s to adjust the initial strain rates to values similar to those of the tensile tests. When the strain (ε_c) of the hydrogel reached 0%, 50%, 100%, 200%, 300% and 400%, the strain was fixed for 90~120 s, and then the SAXS profiles were recorded. The obtained 1D SAXS profiles were converted into absolute intensity (I_{abs}) with equation (2) to eliminate the effects of exposure time (t_e), transmittance (T) and thickness of gels (Z). In concrete terms, the 1D SAXS profiles of the hydrogels and background were normalized with t_e, T and Z. Then, assuming affine deformation of the hydrogels, the thickness at each ε_c was theoretically corrected by the initial thickness (Z_0) and ε_c with equation (3). Note that the detection efficiency of the measuring device was not taken into account.

$$Absolute\ intensity\ (I_{\mathrm{abs}}) = \frac{Obtained\ profile}{t_{\mathrm{e}}TZ} - \frac{background}{t_{\mathrm{e}}Z} \tag{2}$$

$$Z = \frac{Z_0}{\sqrt{1+\varepsilon_{\mathrm{C}}}} \tag{3}$$

3.2.1. Preparation of the αCD-R_1-R_2 (2, 1, 1) hydrogels

The author prepared supramolecular hydrogels with dual or single reversible cross-links based on host-guest complexation between αCD (host) and various cation-terminated alkyl chains (guest molecules, R). The hydrogels with dual reversible cross-links were named αCD-R_1-R_2 (2, 1, 1) hydrogels (**Figure 3-2a**). They have a poly(acrylamide) main chain and two kinds of host-guest units in the polymer side chains. (2, 1, 1) denotes the feed molar ratio of αCD, R_1, and R_2 units, respectively. Those with one type of host-guest cross-link, named αCD-R (2, 2) hydrogels.

The αCD-R_1-R_2 (2, 1, 1) and αCD-R (2, 2) hydrogels were prepared by radical copolymerization with a redox initiator system according to our previous reports[35,36,54]. **Figure 3-2c** shows a preparation method of the αCD-ImC11-PyC11 (2, 1, 1) hydrogel as a typical polymerization scheme for the former hydrogels. The αCD monomer (αCDAAmMe) and two guest monomers with different cation end groups (R monomers) were sonicated in a 0.5 M potassium chloride (KCl) solution at 50 °C for one hour to form two different 1:1 inclusion complexes. Because the K_a values of the R monomers and their molar concentrations were almost the same, each R_1 and R_2 monomers could form similar amounts of complexes with αCDAAmMe. The acrylamide (AAm) main monomer and potassium persulfate (KPS) were added to the resulting solution. Then, the total concentration of monomers was set to 2 M. The molar ratios of αCDAAmMe, R_1, R_2, AAm, and KPS were 2.0, 1.0, 1.0, 96 and 1.0 mol%, respectively. Finally, 1.0 mol% of *N*,*N*,*N*′,*N*′-tetramethylethylenediamine (TEMED) was added. The solution was shaken quickly and poured into a Teflon mold to start gelation. The solution gelated within 5 minutes to give a self-standing hydrogel. Details of the reagents and solutions are summarized in **Tables 3-1–3-10**. The αCD-R_1-R_2 (2, 1, 1) hydrogels containing VC11 were light yellow and transparent, and the others were colorless and transparent.

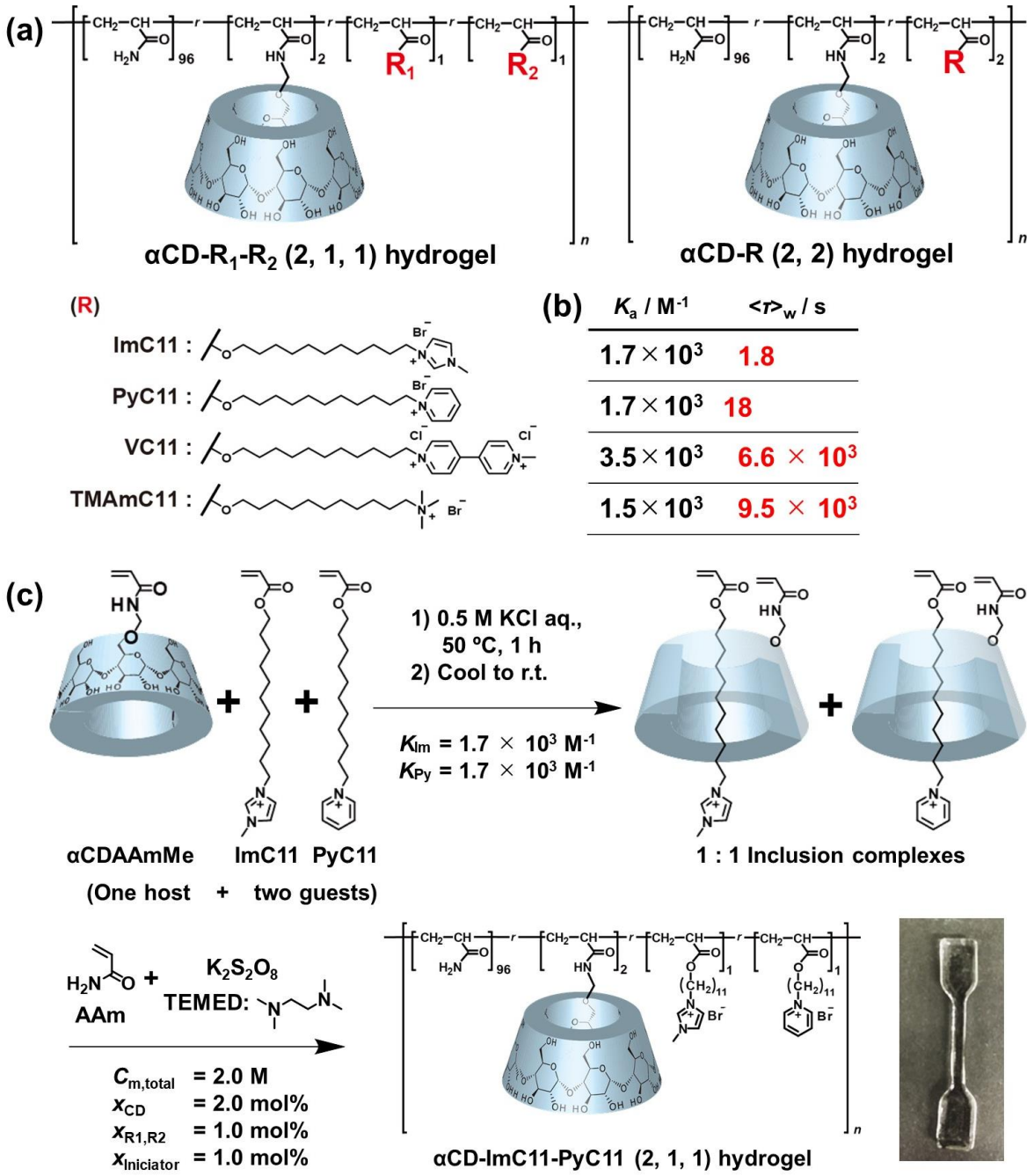

Figure 3-2. (a) Chemical structures of the αCD-R_1-R_2 (2, 1, 1) and αCD-R (2, 2) hydrogels. **(b)** Association constant (K_a) of αCDAAmMe with cation-terminated alkyl (R) monomers and the second-order average relaxation time ($<\tau>_w$) of the corresponding αCD-R crosslink. K_a was measured in previous studies.[35,36,55] **(c)** Typical preparation scheme and a picture of the αCD-ImC11-PyC11 (2, 1, 1) hydrogel. Other αCD-R_1-R_2 (2, 1, 1) and αCD-R (2, 2) hydrogels were prepared in a similar way.

Table 3-1. Amounts of reagents and solvents used in the preparation of the αCD-ImC11-PyC11 (2, 1, 1) hydrogel.

	KCl aq. /mL	AAm /mg	αCDAAmMe /mg	ImC11 /mg	PyC11 /mg	KPS /mg	TEMED /μL
αCD-ImC11-PyC11 (2, 1, 1) hydrogel	2.0	273	84.5	15.5	15.4	10.8	6.0

Table 3-2. Amounts of reagents and solvents used in the preparation of the αCD-ImC11-VC11 (2, 1, 1) hydrogel.

	KCl aq. /mL	AAm /mg	αCDAAmMe /mg	ImC11 /mg	VC11 /mg	KPS /mg	TEMED /μL
αCD-ImC11-VC11 (2, 1, 1) hydrogel	2.0	273	84.5	15.5	18.7	10.8	6.0

Table 3-3. Amounts of reagents and solvents used in the preparation of the αCD-ImC11-TMAmC11 (2, 1, 1) hydrogel.

	KCl aq. /mL	AAm /mg	αCDAAmMe /mg	ImC11 /mg	TMAmC11 /mg	KPS /mg	TEMED /μL
αCD-ImC11-TMAmC11 (2, 1, 1) hydrogel	2.0	273	84.5	15.5	14.6	10.8	6.0

Table 3-4. Amounts of reagents and solvents used in the preparation of the αCD-PyC11-VC11 (2, 1, 1) hydrogel.

	KCl aq. /mL	AAm /mg	αCDAAmMe /mg	PyC11 /mg	VC11 /mg	KPS /mg	TEMED /μL
αCD-PyC11-VC11 (2, 1, 1) hydrogel	2.0	273	84.5	15.4	18.7	10.8	6.0

Table 3-5. Amounts of reagents and solvents used in the preparation of the αCD-PyC11-TMAmC11 (2, 1, 1) hydrogel.

	KCl aq. /mL	AAm /mg	αCDAAmMe /mg	PyC11 /mg	TMAmC11 /mg	KPS /mg	TEMED /μL
αCD-PyC11-TMAmC11 (2, 1, 1) hydrogel	2.0	273	84.5	15.4	14.6	10.8	6.0

Table 3-6. Amounts of reagents and solvents used in the preparation of the αCD-VC11-TMAmC11 (2, 1, 1) hydrogel.

	KCl aq. /mL	AAm /mg	αCDAAmMe /mg	VC11 /mg	TMAmC11 /mg	KPS /mg	TEMED /μL
αCD-VC11-TMAmC11 (2, 1, 1) hydrogel	2.0	273	84.5	18.7	14.6	10.8	6.0

Table 3-7. Amounts of reagents and solvents used in the preparation of the αCD-ImC11- (2, 2) hydrogel.

	KCl aq. /mL	AAm /mg	αCDAAmMe /mg	ImC11 /mg	KPS /mg	TEMED /μL
αCD-ImC11 (2, 2) hydrogel	2.0	273	84.5	31.0	10.8	6.0

Table 3-8. Amounts of reagents and solvents used in the preparation of the αCD-PyC11 (2, 2) hydrogel.

	KCl aq. /mL	AAm /mg	αCDAAmMe /mg	PyC11 /mg	KPS /mg	TEMED /μL
αCD-PyC11 (2, 2) hydrogel	2.0	273	84.5	30.8	10.8	6.0

Table 3-9. Amounts of reagents and solvents used in the preparation of the αCD-VC11 (2, 2) hydrogel.

	KCl aq. /mL	AAm /mg	αCDAAmMe /mg	VC11 /mg	KPS /mg	TEMED /μL
αCD-VC11 (2, 2) hydrogel	2.0	273	84.5	37.4	10.8	6.0

Table 3-10. Amounts of reagents and solvents used in the preparation of the αCD-TMAmC11 (2, 2) hydrogel.

	KCl aq. /mL	AAm /mg	αCDAAmMe /mg	TMAmC11 /mg	KPS /mg	TEMED /μL
αCD-TMAmC11 (2, 2) hydrogel	2.0	273	84.5	29.1	10.8	6.0

3.3. Results

3.3.1. Characteristics of the αCD-R_1-R_2 hydrogels

The αCDs can include the linear alkyl chains in their cavities to form 1:1 inclusion complexes,[56,57] which act as reversible cross-links in the supramolecular hydrogels.[58–62] In contrast, cations have difficulty forming the inclusion complex directly due to electrostatic instability toward CDs but can also pass through the cavity of an αCD.[63,64] Therefore, cations at the alkyl end slow the kinetics for reactions of host-guest complexes of αCD with alkyl chains,[65,66] which leads to longer relaxation times (τ) for the αCD-R cross-links.[36] Furthermore, the high electric charge and bulkiness of cations make the τ values of the αCD-R cross-links longer. Here, four kinds of cation-terminated alkyl monomers, ImC11, PyC11, VC11, and TMAmC11 were prepared (**Figure 3-2a**). They have undecyl guest units and four different cationic units at the terminal imidazole (Im), pyridine (Py), viologen (V) and trimethylammonium (TMAm) groups. Their association constants (K_a) with αCDAAmMe monomers in aqueous solutions and the second-order average relaxation times ($<\tau>_w$) of the corresponding αCD-R cross-links in the αCD-R (2, 2) hydrogels are summarized in **Figure 3-2b**. Because dissociations of the αCD-R cross-links show several relaxation modes,[36] the author simply use $<\tau>_w$ to explain the difference in dynamics for each αCD-R cross-link. $<\tau>_w$ is the average value of τ determined by considering the values of relaxation strength (G) and τ (eq. (7) in Chapter 2). While the values of K_a were almost the same, those of $<\tau>_w$ varied depending on the structures of the cations. $<\tau>_w$ for the αCD-ImC11 and αCD- PyC11 cross-links, which bore monocationic units, were relatively short at 1.8 and 18 s. When dicationic VC11 or bulky monocationic TMAmC11 was used, however, $<\tau>_w$ for the αCD-VC11 and αCD-TMAmC11 cross-links were extraordinarily long at 6.6×10^3 and 9.5×10^3 s, respectively.

Characterization of the αCD-R_1-R_2 hydrogels by IR and NMR spectroscopy

FT-IR spectra

FT-IR difference spectra of the αCD-R_1-R_2 (2, 1, 1) hydrogels swollen in D_2O were recorded at room temperature in the attenuated total reflection (ATR) method using a ZnSe prism. Details of the method and FT-IR difference spectra are shown in the author's Original Paper 2. Absorption by O-H stretching, N-H stretching, C-H stretching, C=O stretching, and N-H bending was observed. The observed peaks in the difference spectra of the αCD-R_1-R_2 hydrogels mainly reflected the poly(acrylamide) main chain. Analyses of the αCD-R (2, 2) hydrogels by FT-IR spectroscopy were reported in Chapter 2.[36]

FG-MAS NMR spectra

The as-prepared αCD-R_1-R_2 (2, 1, 1) hydrogels were freeze-dried, immersed in D_2O, and analyzed by FG-MAS spectroscopy. For example, **Figure 3-3** shows the NMR spectra of the αCD-ImC11-PyC11 (2, 1, 1) hydrogel.

All of the units were confirmed, and the molar ratios of each unit were calculated from the FG-MAS NMR spectra. Their values were almost identical to the feed molar ratios, indicating that predefined molar ratios were introduced into the αCD-ImC11-PyC11 (2, 1, 1) hydrogel. Similar results of other αCD-R_1-R_2 (2, 1, 1) hydrogels were confirmed (see the author's Original Paper 2). The αCD-R (2, 2) hydrogels were analyzed in the Chapter 2.[36]

2D ^{1}H-^{1}H NOESY NMR spectra

To confirm the formation of inclusion complexes serving as cross-links in the αCD-R_1-R_2 (2, 1, 1) hydrogels, the hydrogels swollen in D_2O were analyzed by 2-dimensional nuclear Overhauser effect spectroscopy (2D NOESY). The as-prepared αCD-R_1-R_2 (2, 1, 1) hydrogels were swollen in water to eliminate excess KCl. The swollen hydrogels were cut into small pieces and dried with flowing air in a windy oven at 60 °C for 20 hours. The dried gels were immersed in D_2O in NMR tubes and analyzed by 2D ^{1}H-^{1}H NOESY NMR spectroscopy (600 MHz, 25 °C, mixing time = 500 ms). **Figure 3-4** shows the NOESY NMR spectrum of the αCD-ImC11-PyC11 (2, 1, 1) hydrogel. The other spectra of the αCD-R_1-R_2 (2, 1, 1) hydrogels are shown in the author's Original Paper 2.

In all spectra, the protons of undecyl units showed NOE correlations to inner protons ($C^{3,5,6}H$) of the αCD units. This result indicates that the alkyl chains of R guests were included in the cavity of αCD and formed reversible cross-links in the hydrogels.

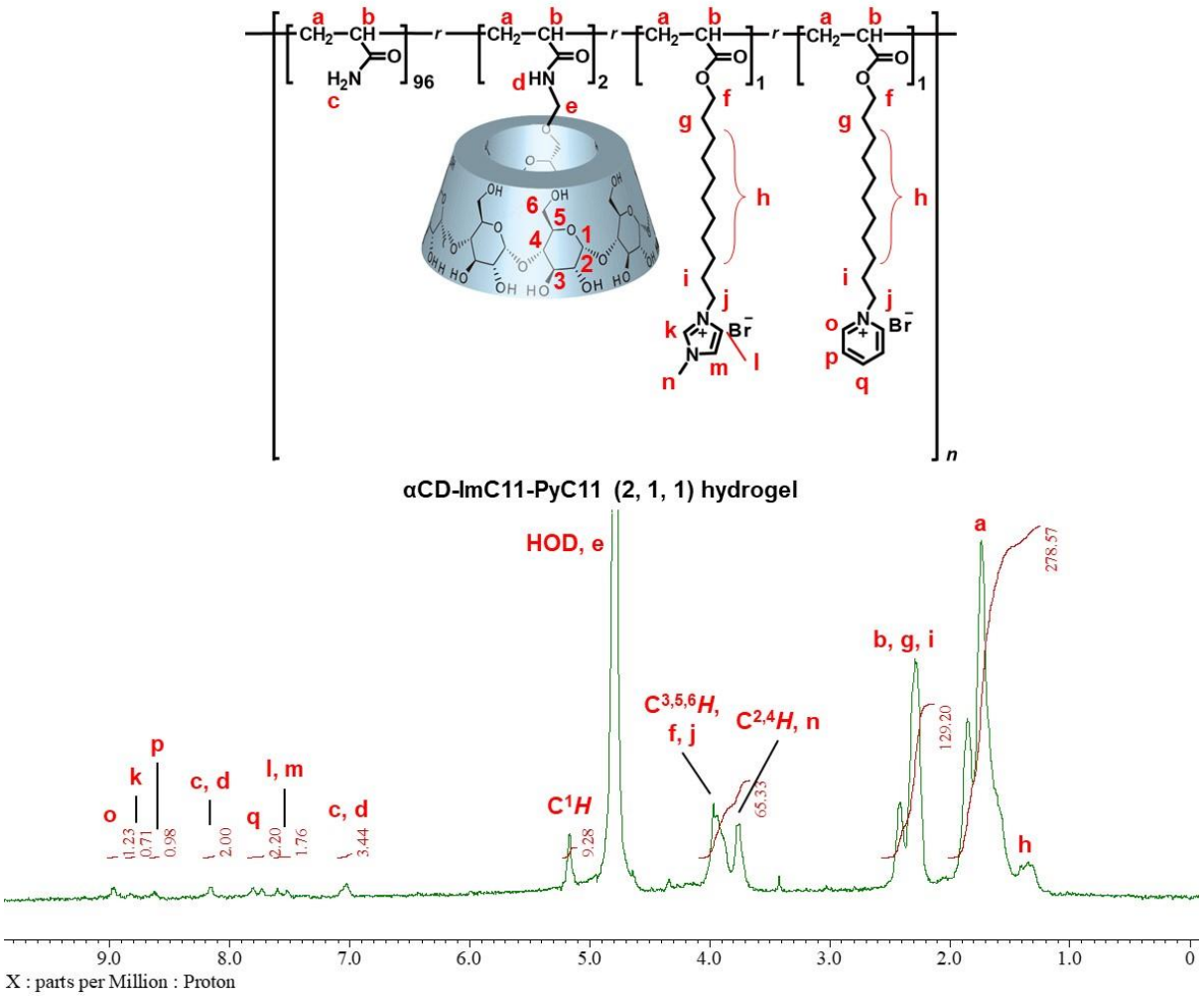

Figure 3-3. 400 MHz ^{1}H FG-MAS NMR spectrum of the αCD-ImC11-PyC11 (2, 1, 1) hydrogel immersed in D_2O at 25 °C. The frequency of the magic angle spinning was 7 kHz.

Amount of each residue

In the preparation: [AAm]/[αCD]/[ImC11]/[PyC11] = 96.0/2.0/1.0/1.0.

Calculated from the spectrum: [AAm]/[αCD]/[ImC11]/[PyC11] = 97.2/1.2/0.8/0.8.

^{1}H NMR: δ = 8.96, 8.83, 8.63, 8.16, 7.76, 7.56, 7.03, 5.17, 4.04–3.82, 3.82–3.68, 2.58–2.10, 2.00–1.46, 1.46–1.20.

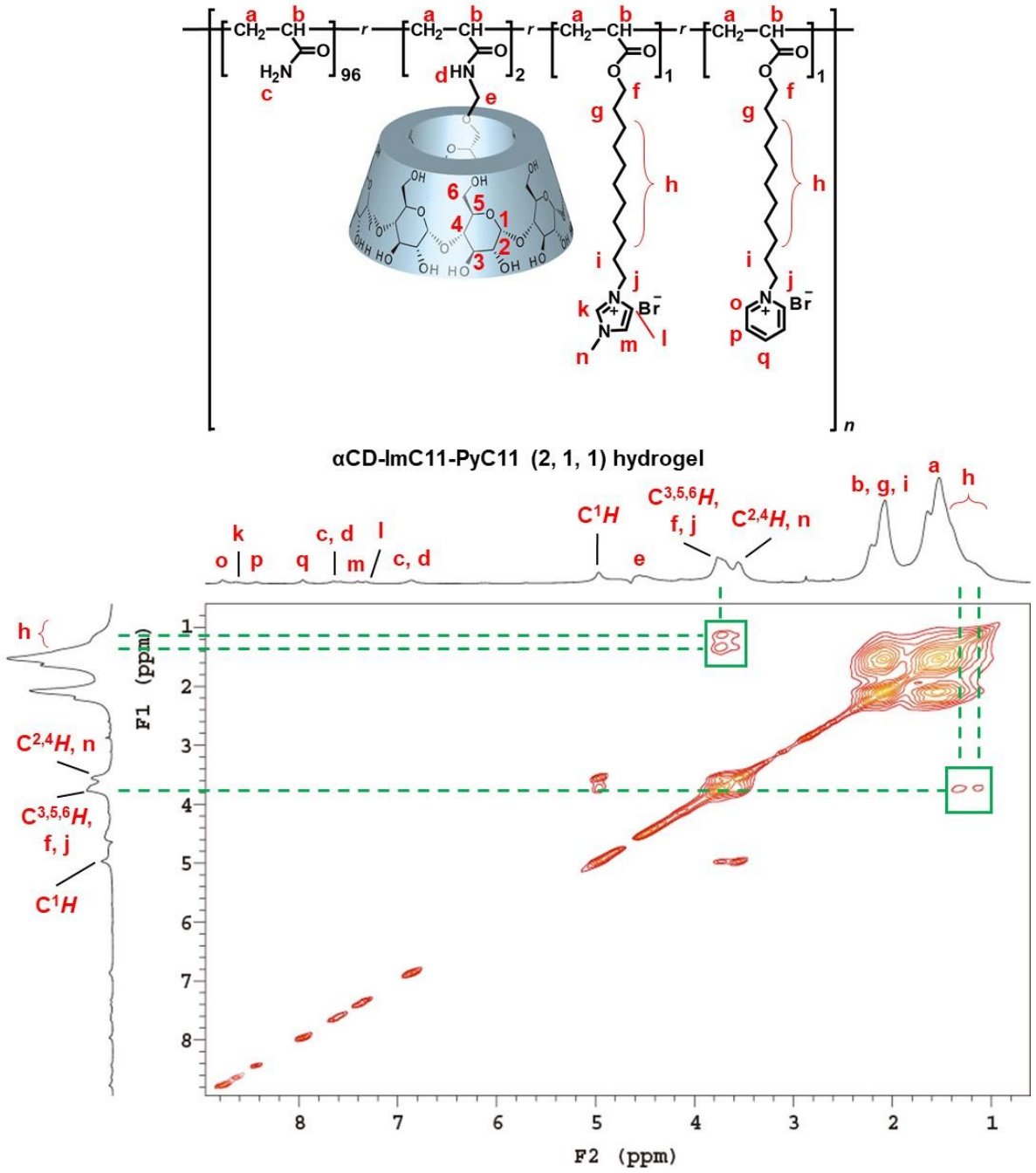

Figure 3-4. 600 MHz 2D ^{1}H-^{1}H NOESY NMR spectrum of the αCD-ImC11-PyC11 (2, 1, 1) hydrogel in D_2O at 25 °C. NOE correlation peaks between undecyl units and inner protons of αCDs are indicated with green boxes. To suppress the water peak, we performed presaturation and diffusion filter processes.

3.3.2. Mechanical properties of the αCD-R_1-R_2 hydrogels

The mechanical properties of the αCD-R_1-R_2 (2, 1, 1) and αCD-R (2, 2) hydrogels were evaluated with uniaxial tensile tests (tensile speed = 1.0 mm/s, room temperature = approximately 25 °C) (**Figures 3-5 and 3-6**). **Figure 3-5a** shows representative stress-strain curves of the αCD-R_1-R_2 (2, 1, 1) and αCD-R (2, 2) hydrogels. The entire results of the curves are shown in **Figure 3-6**.

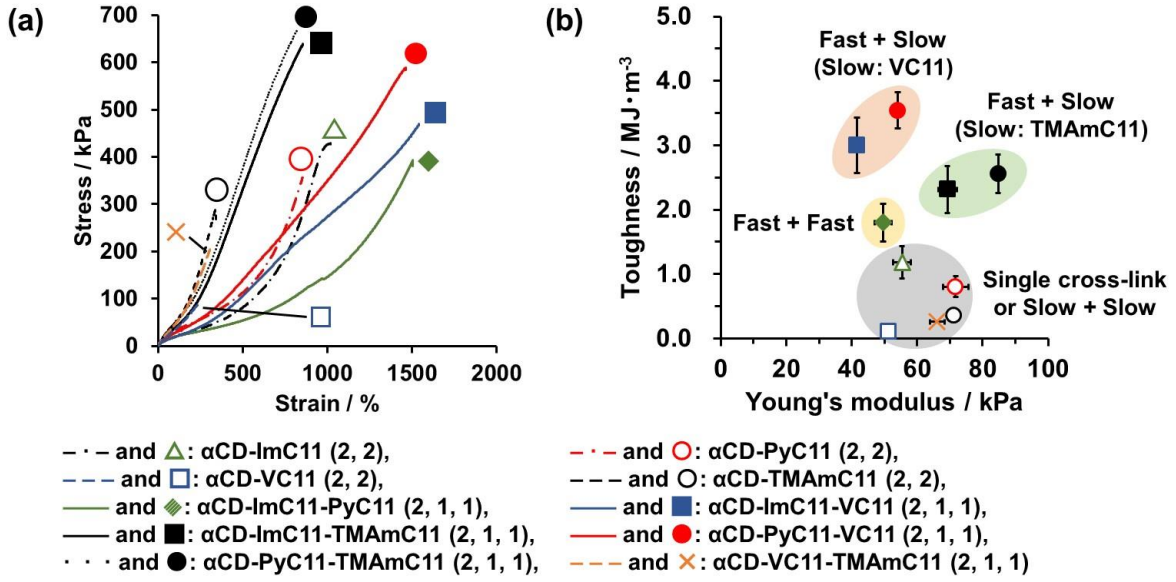

Figure 3-5. Mechanical properties of the αCD-R_1-R_2 (2, 1, 1) and αCD-R (2, 2) hydrogels. **(a)** Stress–strain curves. **(b)** Plots of toughness and Young's modulus. αCD-ImC11 (2, 2): black chain line and green open triangle (△). αCD-PyC11 (2, 2): red chain line and red open circle (○). αCD-VC11 (2, 2): blue dashed line and blue open square (□). αCD-TMAmC11: black dashed line and black open circle (○). αCD-ImC11-PyC11 (2, 1, 1): green solid line and green filled diamond (◆). αCD-ImC11-VC11 (2, 1, 1): blue solid line and blue filled square (■). αCD-ImC11-TMAmC11 (2, 1, 1): black solid line and black filled square (■). αCD-PyC11-VC11 (2, 1, 1): red solid line and red filled circle (●). αCD-PyC11-TMAmC11 (2, 1, 1): black dotted line and black filled circle (●). αCD-VC11-TMAmC11 (2, 1, 1): orange dashed line and orange cross mark (×).

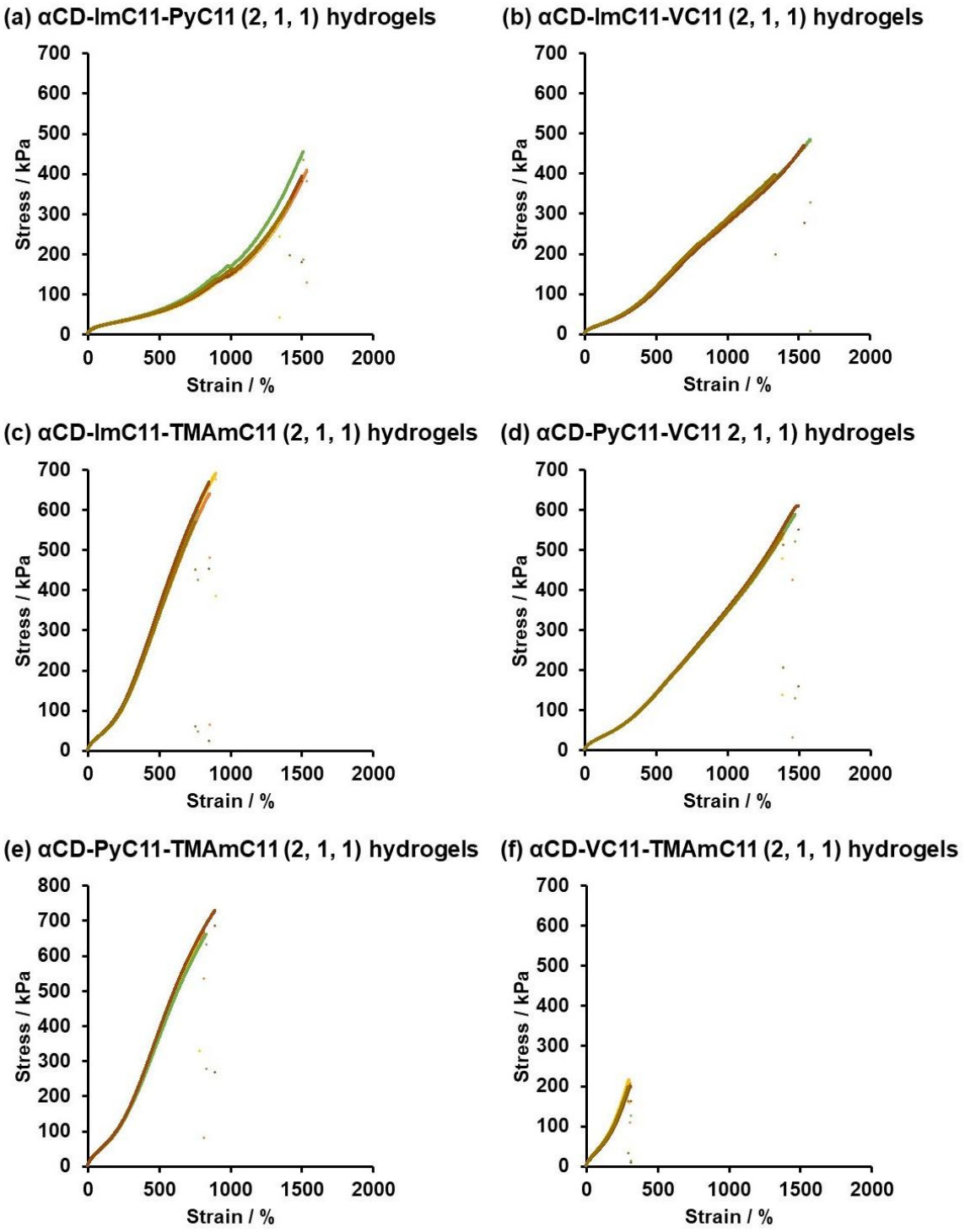

Figure 3-6. Stress-strain curves of the αCD-R_1-R_2 (2, 1, 1) hydrogels at 25 °C at a tensile rate of 1.0 mm/s. **(a)** αCD-ImC11-PyC11 (2, 1, 1) hydrogel (n = 5), **(b)** αCD-ImC11-VC11 (2, 1, 1) hydrogel (n = 3), **(c)** αCD-ImC11-TMAmC11 (2, 1, 1) hydrogel (n = 5), **(d)** αCD-PyC11-VC11 (2, 1, 1) hydrogel (n = 5), **(e)** αCD-PyC11-TMAmC11 (2, 1, 1) hydrogel (n = 4), and (f) αCD-VC11-TMAmC11 (2, 1, 1) hydrogel (n = 5).

The author calculated toughness by integrating the obtained stress-strain curves and Young's modulus from the initial slope of the curves. **Figure 3-5b** shows the plots of toughness and Young's modulus. The toughness values varied with the structures of the reversible cross-links, while Young's moduli were almost the same. In particular, four of the hydrogels, the αCD-ImC11-VC11 (2, 1, 1), αCD-ImC11-TMAmC11 (2, 1, 1), αCD-PyC11-VC11 (2, 1, 1) and αCD-PyC11-TMAmC11 (2, 1, 1) hydrogels, showed relatively high toughness values (2.3~3.5 MJ/m^3). The hydrogels consisted of combinations of reversible cross-links with short $<\tau>_w$ of 1~10 s and long $<\tau>_w$ of > 1000 s. In particular, the toughness of the αCD-PyC11-VC11 (2, 1, 1) hydrogel (3.5 MJ/m^3) was 3-4 times larger than those of the αCD-PyC11 (2, 2) and αCD-VC11 (2, 2) hydrogels (0.80 and 0.10 MJ/m^3, respectively). On the other hand, in the case of the αCD-ImC11-PyC11 (2, 1, 1) hydrogel containing two fast reversible cross-links, the toughness was moderate (1.8 MJ/m^3). The αCD-VC11-TMAmC11 (2, 1, 1) hydrogel with two slowly reversible cross-links was weak (0.26 MJ/m^3). It was revealed that a combination of fast and slowly reversible cross-links significantly improved toughness while maintaining Young's modulus.

3.3.3. Linear viscoelasticity of the αCD-R_1-R_2 (2, 1, 1) hydrogels

Measurement and Analysis

Dynamic viscoelastic measurements and stress-relaxation tests of sheet-like samples with thicknesses of ~ 1 mm were performed with an Anton Paar MCR302 rheometer to evaluate how the combination of reversible cross-links affected the relaxation behaviors of the αCD-R_1-R_2 (2, 1, 1) hydrogels (**Figures 3-7–3-12**). An angular frequency (ω) sweep was performed from 0.1 to 100 rad/s using a parallel-plate fixture 8 mm in diameter at a temperature range of 0–45 °C (**Figures 3-7c–3-12c**). The shear strain amplitudes (γ) for all tests were within the range of linear viscoelasticity. The results for the αCD-R_1-R_2 (2, 1, 1) hydrogels at different temperatures and frequencies followed the time-temperature superposition principle to give master curves. The author supposed that temperature only changed the relaxation rate while keeping the microstructure and the mode of molecular motion that induced viscoelastic relaxation unchanged in the experimental window. Therefore, the time-temperature superposition was applicable.

Figures 3-7d–3-12d show the master curves for the storage modulus (G'), loss modulus (G'') and loss factor (tan δ) referenced at 25 °C and the Arrhenius plot depicting the temperature dependence of the shift factors (a_T) for each sample. **Figures 3-7e–3-12e** show Arrhenius plots of the logarithm of a_T and the inverse of T. To detect long relaxation times of the αCD-R_1-R_2 (2, 1, 1) hydrogels, stress-relaxation tests were also performed with an MCR302 rheometer at 25 °C (**Figure 3-7f–3-12f**).

These viscoelastic curves were analyzed in the same manner as in Chapter 2 to estimate relaxation modes (G_p and τ_p), terminal modulus (G_N), apparent activation energy (ΔE_a), and second-order average relaxation times ($<\tau>_w$). Parameters G_p, τ_p, and G_N obtained from the master curves and stress-relaxation curves are summarized in **Tables 3-11–3-21**. The results for the αCD-R (2, 2) hydrogels were reported in Chapter 2.[36]

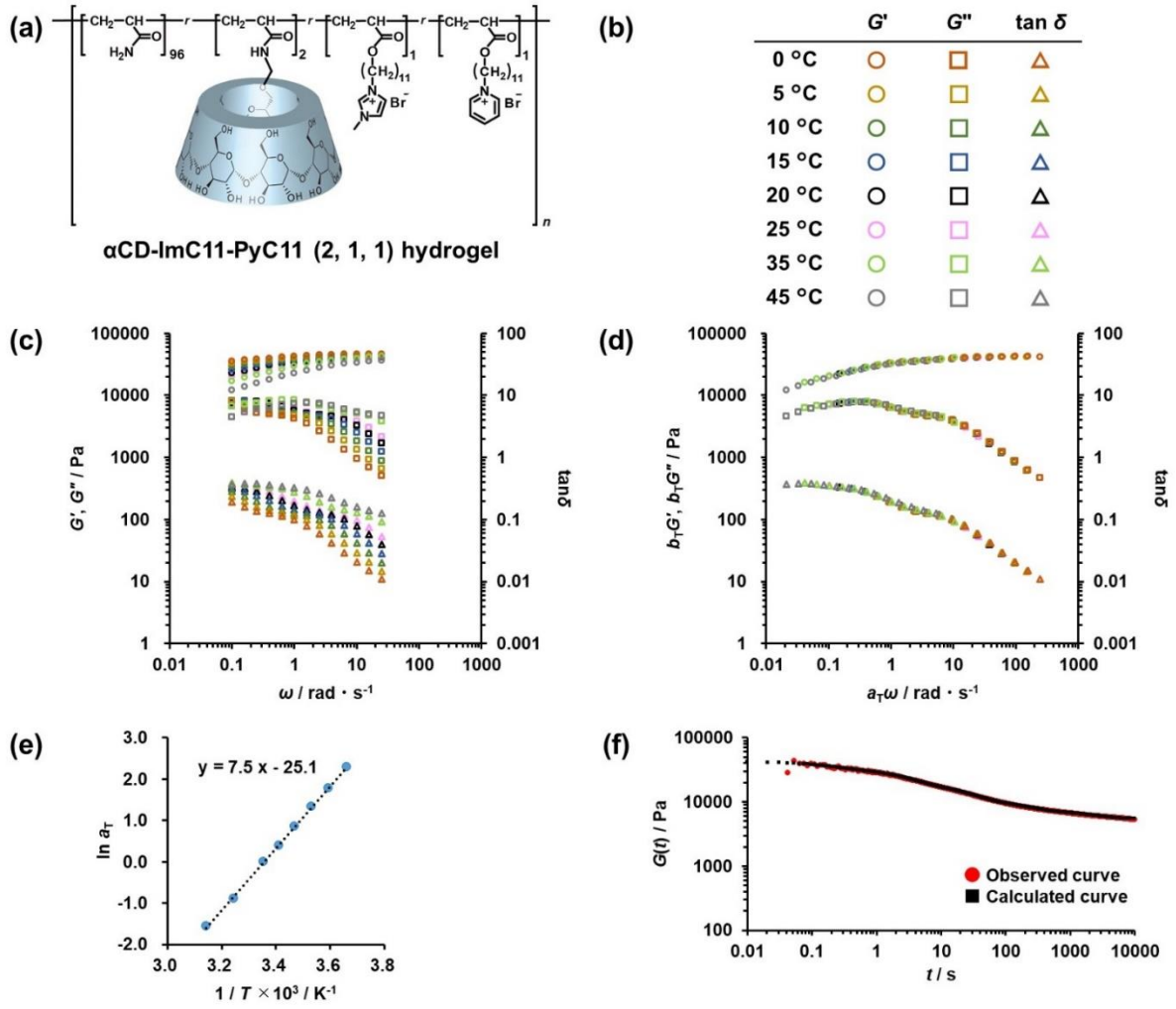

Figure 3-7. (a) Chemical structure of the αCD-ImC11-PyC11 (2, 1, 1) hydrogel. **(b)** Symbols for G', G'', and tan δ defined at each temperature. **(c)** Angular frequency dependence of G', G'', and tan δ (amplitude strain (γ) = 1%). **(d)** Master curves of G', G'', and tan δ for the αCD-ImC11-PyC11 (2, 1, 1) hydrogel referenced to 25 °C. **(e)** The Arrhenius plot of a_T used for superposition. **(f)** The stress-relaxation curve of the αCD-ImC11-PyC11 (2, 1, 1) hydrogel (γ = 3%, T = 25 °C) and curve fitting.

Table. 3-11. Parameters G_p and τ_p used for fitting of the master curves of G' and G'' of the αCD-ImC11-PyC11 (2, 1, 1) hydrogel.

mode	1	2	3	4	5	6	7	G_N
G_p / Pa	7727	13037	10989	-	-	-	-	10492
τ_p / s	0.156	2.388	21.31	-	-	-	-	-

Table 3-12. Parameters G_p and τ_p used for fitting of the $G(t)$ of the αCD-ImC11-PyC11 (2, 1, 1) hydrogel.

mode	1	2	3	4	5	6	7	G_N
G_p / Pa	8863	13259	8734	3463	1937	-	-	5367
τ_p / s	0.200	2.843	25.45	189.2	2420	-	-	-

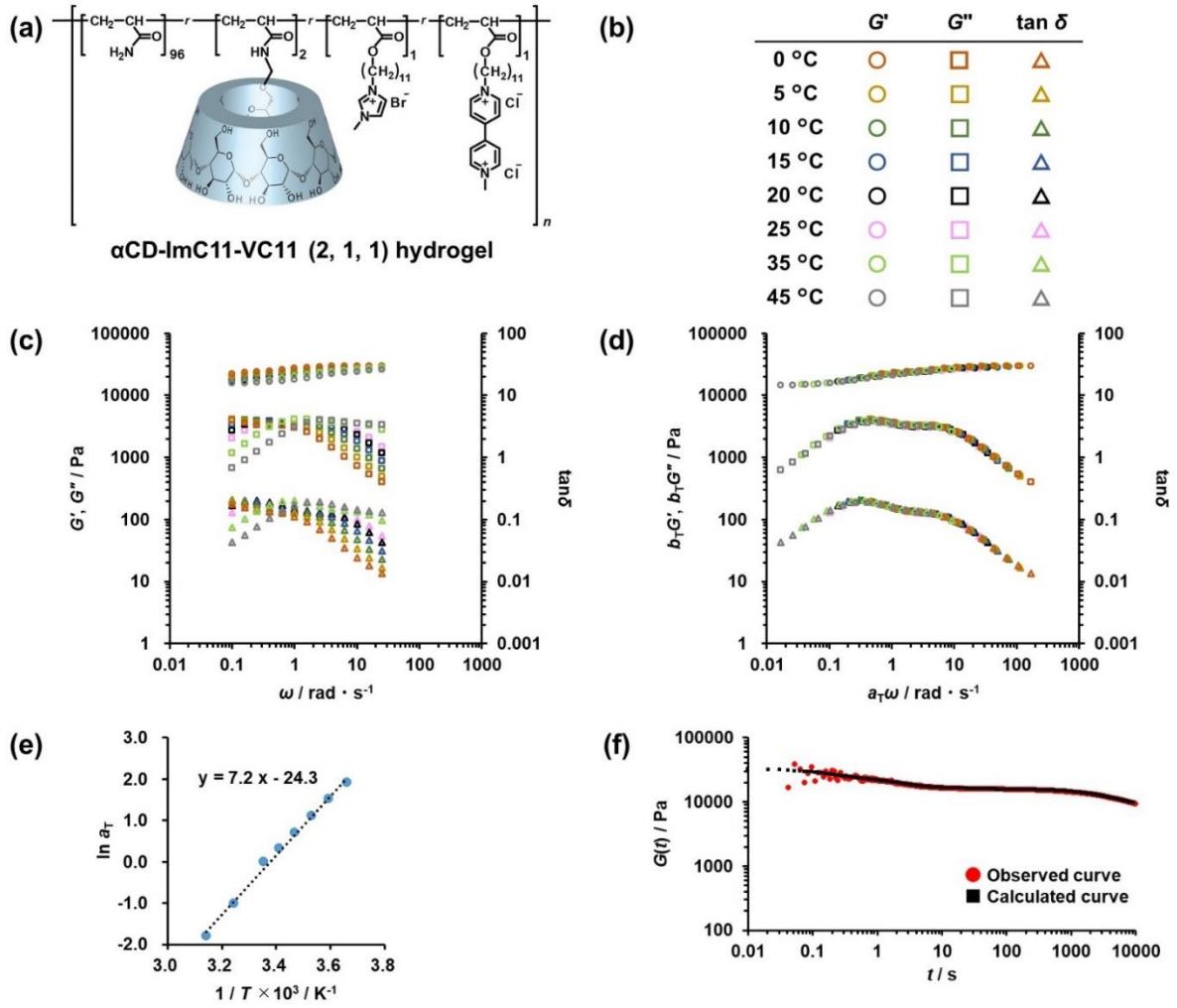

Figure 3-8. (a) Chemical structure of the αCD-ImC11-VC11 (2, 1, 1) hydrogel. **(b)** Symbols for G', G'', and tan δ defined at each temperature. **(c)** Angular frequency dependence of G', G'', and tan δ (γ = 1%). **(d)** Master curves of G', G'', and tan δ for the αCD-ImC11-VC11 (2, 1, 1) hydrogel referenced to 25 °C. **(e)** Arrhenius plot of a_T used for superposition. **(f)** Stress-relaxation curve of the αCD-ImC11-VC11 (2, 1, 1) hydrogel (γ = 3%, T = 25 °C) and curve fitting.

Table 3-13. Parameters G_p and τ_p used for fitting of the master curves of G' and G'' of the αCD-ImC11-VC11 (2, 1, 1) hydrogel.

mode	1	2	3	4	5	6	7	G_N
G_p / Pa	6025	7890	-	-	-	-	-	15008
τ_p / s	0.163	2.860	-	-	-	-	-	-

Table 3-14. Parameters G_p and τ_p used for fitting of $G(t)$ of the αCD-ImC11-VC11 (2, 1, 1) hydrogel.

mode	1	2	3	4	5	6	7	G_N
G_p / Pa	8000	7778	1019	7002	-	-	-	8660
τ_p / s	0.180	2.195	26.71	4650	-	-	-	-

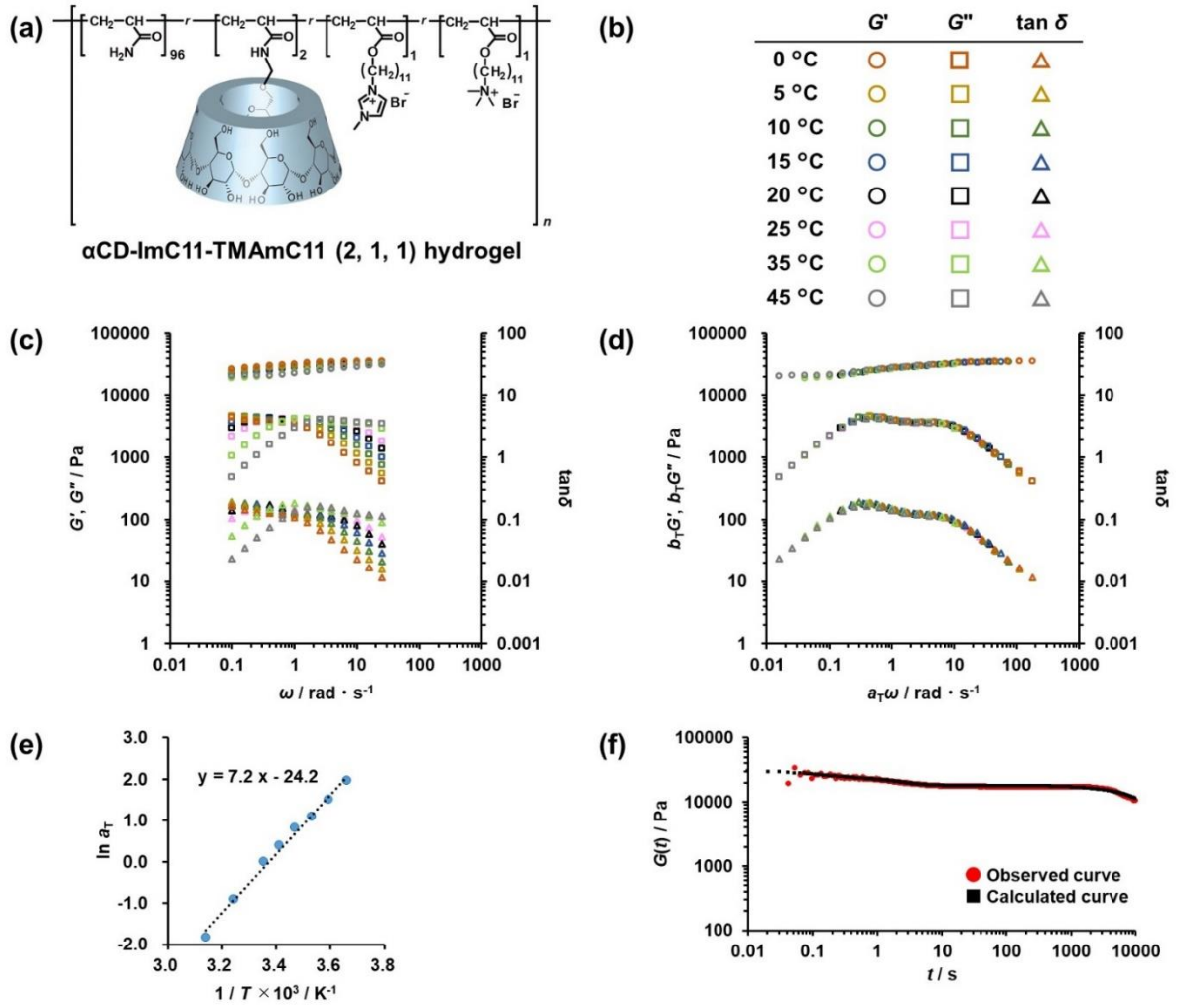

Figure 3-9. (a) Chemical structure of the αCD-ImC11-TMAmC11 (2, 1, 1) hydrogel. **(b)** Symbols for G', G'', and tan δ defined at each temperature. **(c)** Angular frequency dependence of G', G'', and tan δ (γ = 1%). **(d)** Master curves of G', G'', and tan δ for the αCD-ImC11-TMAmC11 (2, 1, 1) hydrogel referenced to 25 °C. **(e)** Arrhenius plot of a_T used for superposition. **(f)** Stress-relaxation curve of the αCD-ImC11-TMAmC11 (2, 1, 1) hydrogel (γ = 3%, T = 25 °C) and curve fitting.

Table 3-15. Parameters G_p and τ_p used for fitting of the master curves of G' and G'' of the αCD-ImC11-TMAmC11 (2, 1, 1) hydrogel.

mode	1	2	3	4	5	6	7	G_N
G_p / Pa	6270	8253	-	-	-	-	-	20455
τ_p / s	0.156	2.368	-	-	-	-	-	-

Table 3-16. Parameters G_p and τ_p used for fitting of $G(t)$ of the αCD-ImC11-TMAmC11 (2, 1, 1) hydrogel.

mode	1	2	3	4	5	6	7	G_N
G_p / Pa	5460	6885	17696	-	-	-	-	0
τ_p / s	0.127	2.214	21668	-	-	-	-	-

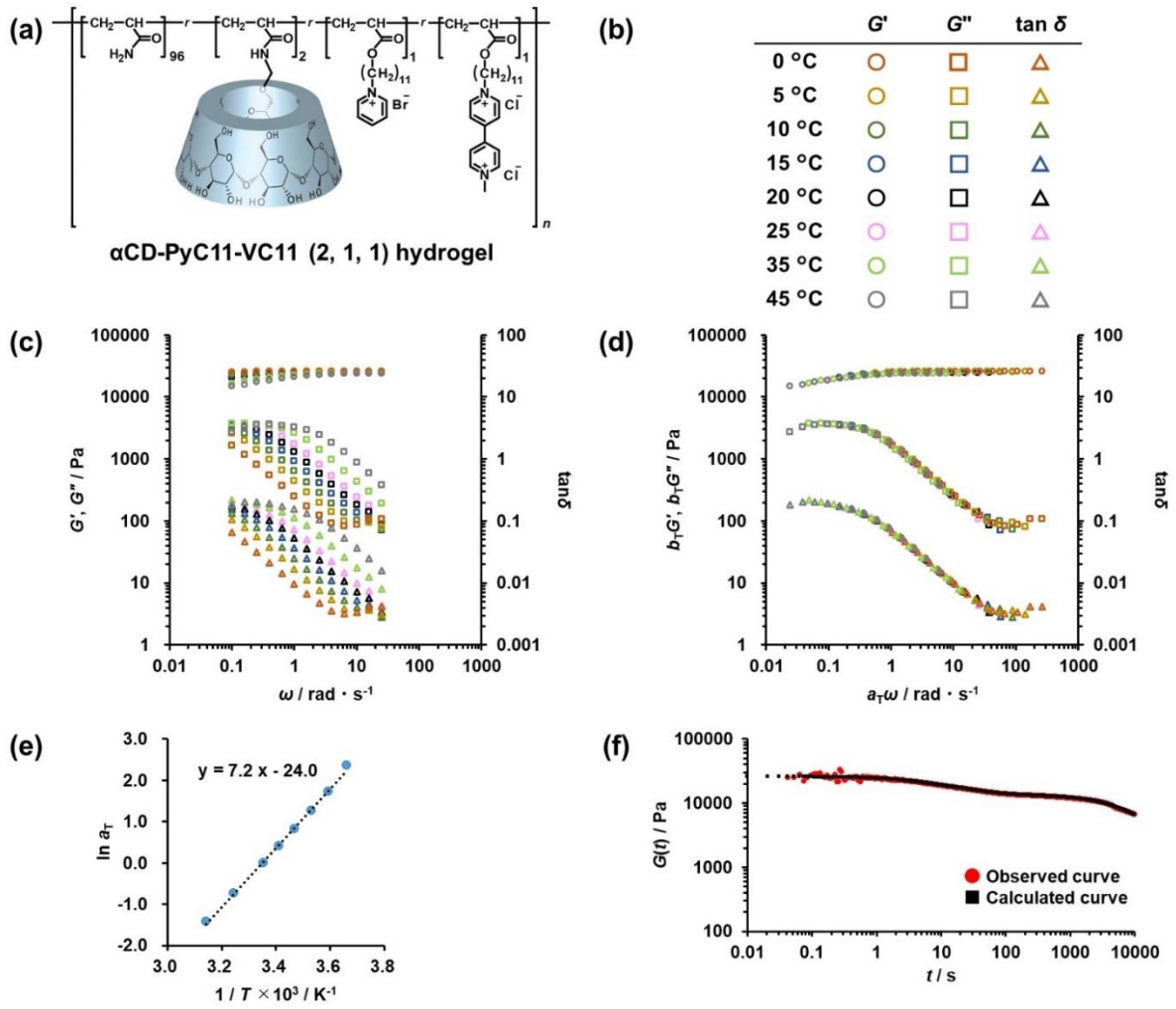

Figure 3-10. (a) Chemical structure of the αCD-PyC11-VC11 (2, 1, 1) hydrogel. **(b)** Symbols for G', G'', and tan δ defined at each temperature. **(c)** Angular frequency dependence of G', G'', and tan δ (γ = 1%). **(d)** Master curves of G', G'', and tan δ for the αCD-PyC11-VC11 (2, 1, 1) hydrogel referenced to 25 °C. **(e)** Arrhenius plot of a_T used for superposition. **(f)** Stress-relaxation curve of the αCD-PyC11-VC11 (2, 1, 1) hydrogel (γ = 3%, T = 25 °C) and curve fitting.

Table 3-17. Parameters G_p and τ_p used for fitting of the master curves of G' and G'' of the αCD-PyC11-VC11 (2, 1, 1) hydrogel.

mode	**1**	**2**	**3**	**4**	**5**	**6**	**7**	G_N
G_p **/ Pa**	4467	6639	-	-	-	-	-	14146
τ_p **/ s**	2.436	15.81	-	-	-	-	-	-

Table 3-18. Parameters G_p and τ_p used for fitting of $G(t)$ of the αCD-PyC11-VC11 (2, 1, 1) hydrogel.

mode	**1**	**2**	**3**	**4**	**5**	**6**	**7**	G_N
G_p **/ Pa**	5161	5686	1410	8749	-	-	-	4463
τ_p **/ s**	4.074	26.09	115.4	7014	-	-	-	-

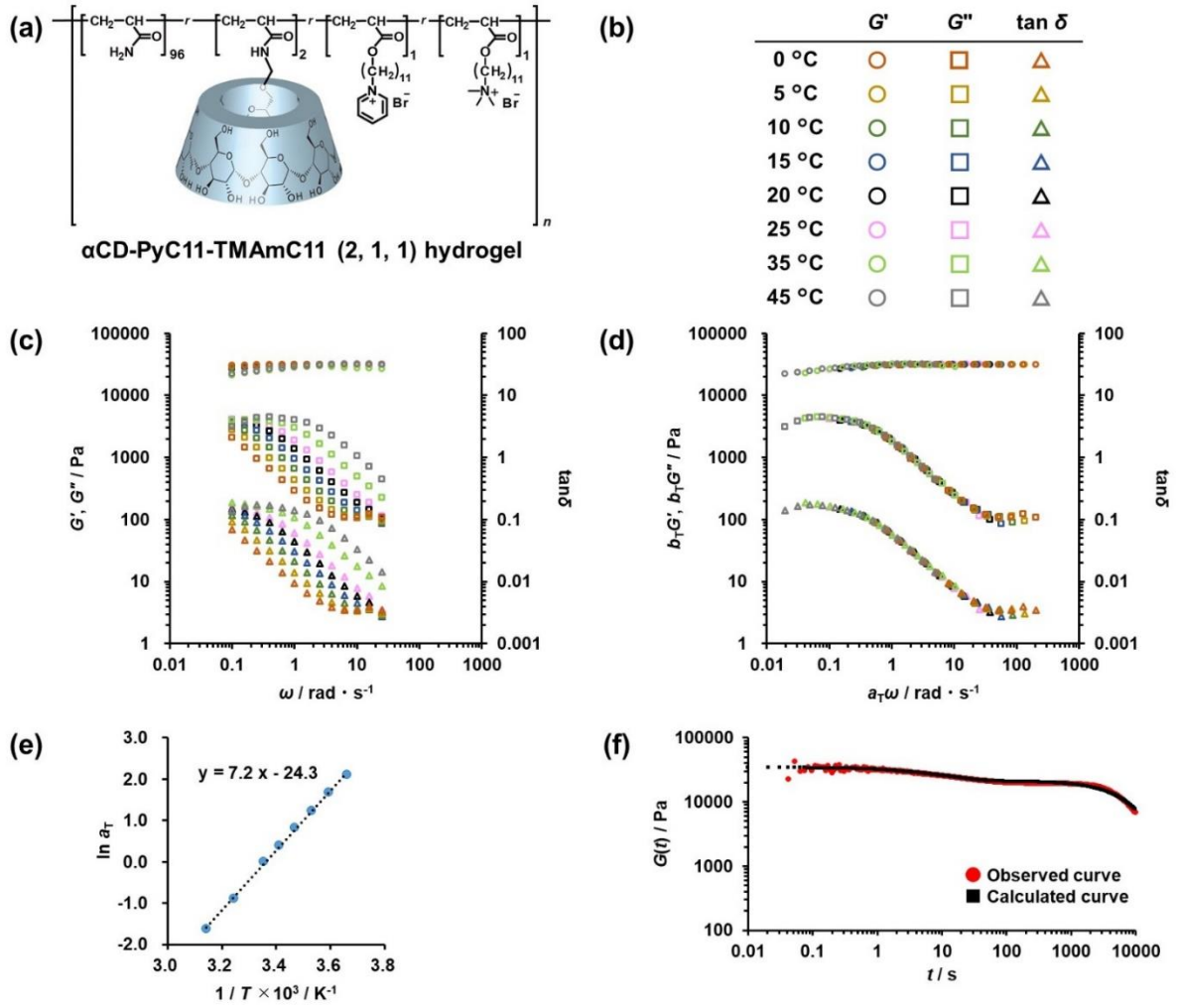

Figure 3-11. (a) Chemical structure of the αCD-PyC11-TMAmC11 (2, 1, 1) hydrogel. **(b)** Symbols for G', G'', and tan δ defined at each temperature. **(c)** Angular frequency dependence of G', G'', and tan δ (γ = 1%). **(d)** Master curves of G', G'', and tan δ for the αCD-PyC11-TMAmC11 (2, 1, 1) hydrogel referenced to 25 °C. **(e)** Arrhenius plot of a_T used for superposition. **(f)** Stress-relaxation curve of the αCD-PyC11-TMAmC11 (2, 1, 1) hydrogel (γ = 2%, T = 25 °C) and curve fitting.

Table 3-19. Parameters G_p and τ_p used for fitting of the master curves of G' and G'' of the αCD-PyC11-TMAmC11 (2, 1, 1) hydrogel.

mode	1	2	3	4	5	6	7	G_N
G_p / Pa	4800	7617	-	-	-	-	-	20000
τ_p / s	2.897	20.53	-	-	-	-	-	-

Table 3-20. Parameters G_p and τ_p used for fitting of $G(t)$ of the αCD-PyC11-TMAmC11 (2, 1, 1) hydrogel.

mode	1	2	3	4	5	6	7	G_N
G_p / Pa	4448	8392	20818	-	-	-	-	0
τ_p / s	2.409	17.12	9821	-	-	-	-	-

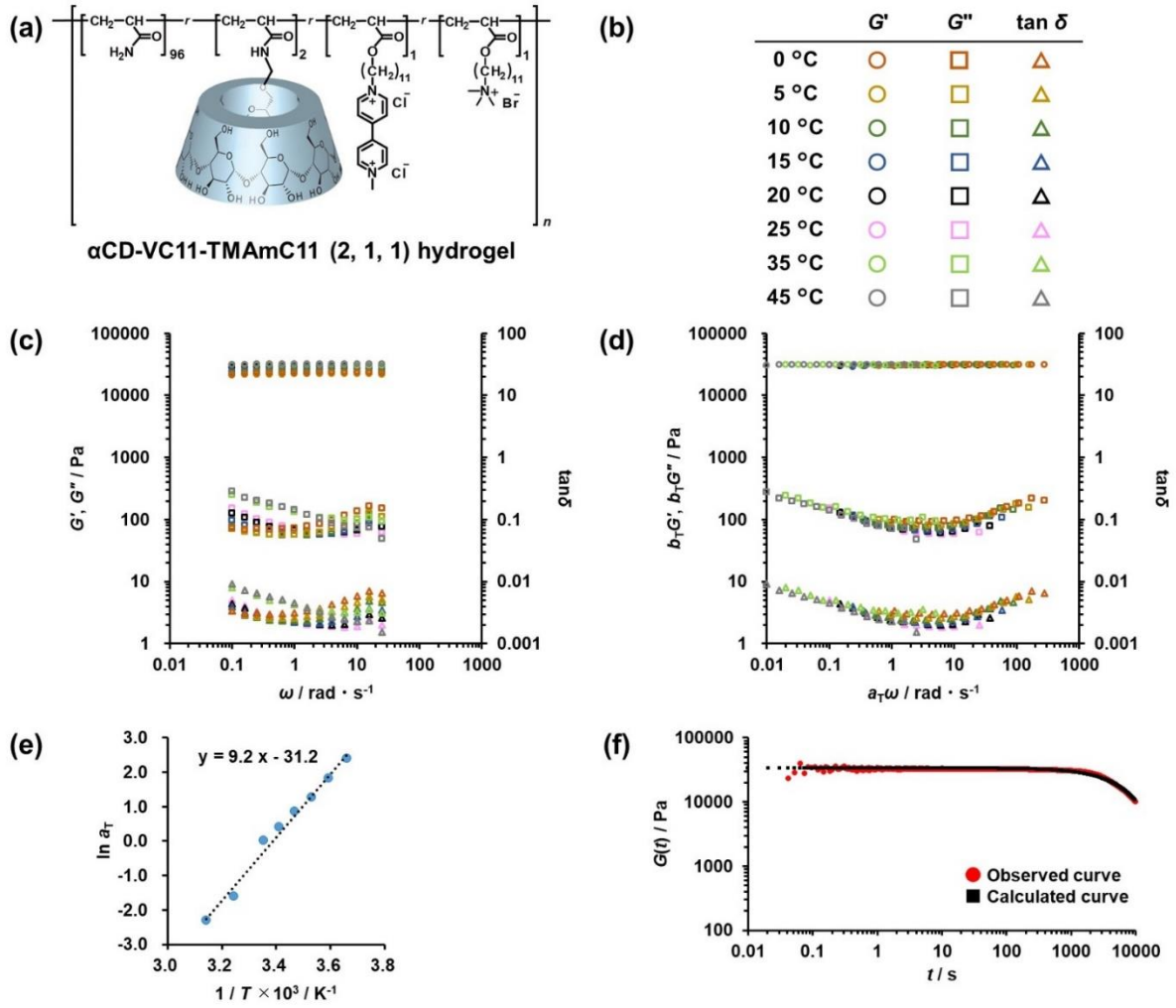

Figure 3-12. (a) Chemical structure of the αCD-VC11-TMAmC11 (2, 1, 1) hydrogel. **(b)** Symbols for G', G'', and tan δ defined at each temperature. **(c)** Angular frequency dependence of G', G'', and tan δ (γ = 0.8%). **(d)** Master curves of G', G'', and tan δ of the αCD-VC11-TMAmC11 (2, 1, 1) hydrogel referenced to 25 °C. **(e)** Arrhenius plot of a_T used for superposition. **(f)** Stress-relaxation curve of the αCD-VC11-TMAmC11 (2, 1, 1) hydrogel (γ = 2%, T = 25 °C) and curve fitting.

Table 3-21. Parameters G_p and τ_p used for fitting of $G(t)$ of the αCD-VC11-TMAmC11 (2, 1, 1) hydrogel.

mode	**1**	**2**	**3**	**4**	**5**	**6**	**7**	G_N
G_p **/ Pa**	8801	2411	-	-	-	-	-	0
τ_p **/ s**	7094	9403	-	-	-	-	-	-

* Fitting master curves of G' and G'' of the αCD-VC11-TMAmC11 (2, 1, 1) hydrogel was not performed.

The calculated ΔE_a values are summarized in **Table 3-22**. ΔE_a was almost the same for the αCD-R_1-R_2 (2, 1, 1) hydrogels. ΔE_a is one of the measures for the temperature dependence of relaxation, which is not the lifetime of the sticker. The αCD-R_1-R_2 (2, 1, 1) hydrogels showed similar values of ΔE_a, whereas their relaxation times were different. This result suggests that the lifetimes of the stickers are determined by the electrostatic instability of cation units, resulting in a direct effect on the viscoelastic relaxation time. Note that ΔE_a of the αCD-VC11-TMAmC11 (2, 1, 1) hydrogel was slightly higher than the others, which may be attributed to the elastic network cross-linked by the αCD-VC11 and αCD-TMAmC11 cross-links.

Table 3-22. Results for ΔE_a of the αCD-R_1-R_2 (2, 1, 1) hydrogels.

Sample	ΔE_a / kJ/mol
αCD-ImC11-PyC11 (2, 1, 1)	59.6
αCD-ImC11-VC11 (2, 1, 1)	59.7
αCD-ImC11-TMAmC11 (2, 1, 1)	59.6
αCD-PyC11-VC11 (2, 1, 1)	59.6
αCD-PyC11-TMAmC11 (2, 1, 1)	60.1
αCD-VC11-TMAmC11 (2, 1, 1)	76.4

Result of viscoelasticity

Figure 3-13 shows a comparison of the αCD-PyC11-VC11 (2, 1, 1), αCD-PyC11 (2, 2) and αCD-VC11 (2, 2) hydrogels. According to the Chapter 2 and Inoue's work[36,67], viscoelasticity of the αCD-R_1-R_2 (2, 1, 1) hydrogels αCD-R (2, 2) hydrogels can be explained by the stick reptation model.[68] Storage moduli (G') of the hydrogels show rubbery plateaus originating from the network formed by αCD-R cross-links in high angular frequency (ω) region. In the low ω (or long time) region where the cross-links dissociate, G' reduces to the second plateau derived from entanglements through the Rouse mode. Note that the terminal relaxation of chain reptation is not observed in the present experimental window because the cross-links retard the reptation process.

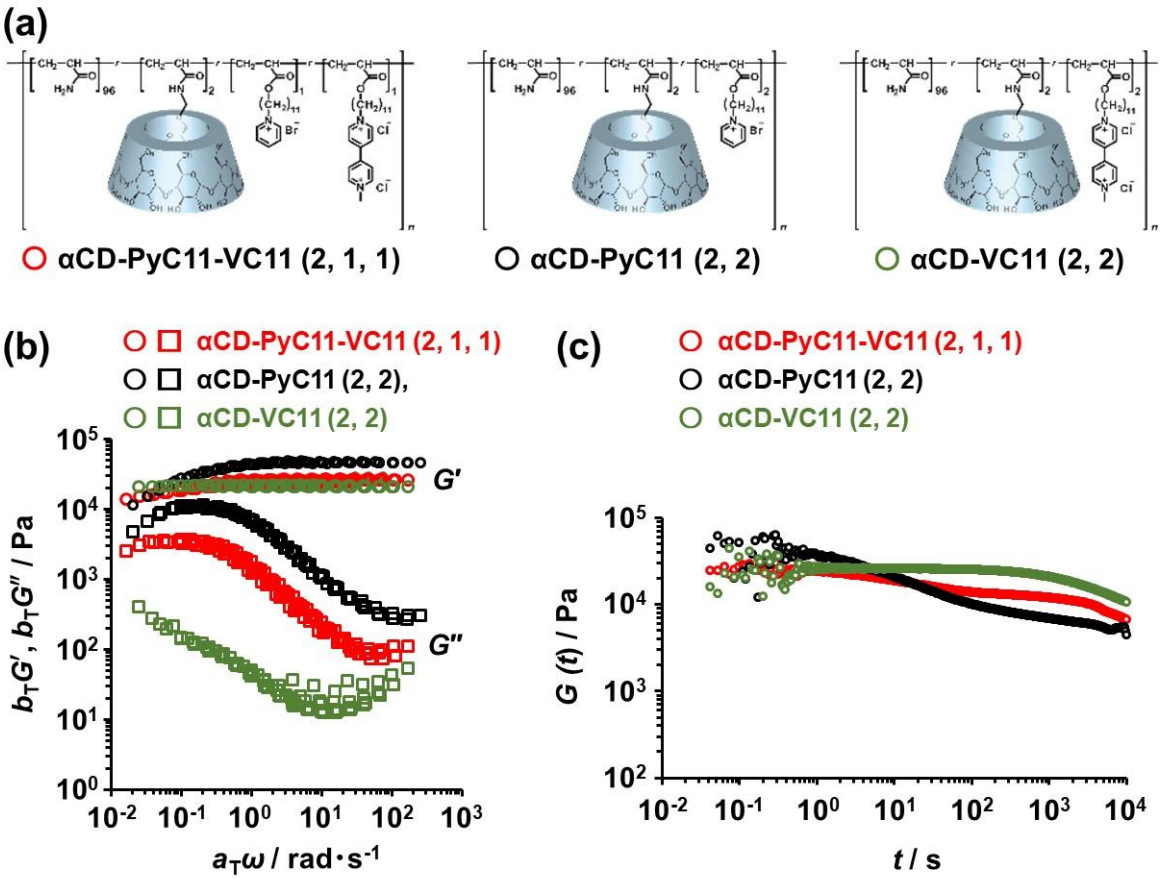

Figure 3-13. Representative viscoelastic characteristics of the αCD-R_1-R_2 (2, 1, 1) and αCD-R (2, 2) hydrogels. **(a)** Chemical structures of the αCD-PyC11-VC11 (2, 1, 1), αCD-PyC11 (2, 2) and αCD-VC11 (2, 2) hydrogels. **(b)** Comparison of the master curves referenced at 25 °C. **(c)** Comparison of stress-relaxation curves at 25 °C.

In the master curves (**Figure 3-13b**), the αCD-PyC11-VC11 (2, 1, 1) and αCD-PyC11 (2, 2) hydrogels showed similar relaxation modes at $\omega = 10^{-1}$~10^{0} rad/s derived from αCD-PyC11 cross-links, while the αCD-VC11 (2, 2) hydrogel did not show relaxation in this ω range. In stress-relaxation curves (**Figure 3-13c**), the αCD-PyC11-VC11 (2, 1, 1) hydrogel showed gradual relaxation similar to that of the αCD-PyC11 (2, 2) hydrogel in the short time region (~up to 100 s), whereas it showed a plateau and slower relaxation mode similar to those of the αCD-VC11 (2, 2) hydrogel in a long time (10^{3}~10^{4} s) region. These results indicated that the αCD-PyC11-VC11 (2, 1, 1) hydrogel had combined relaxation modes derived from each network comprising αCD-PyC11 and αCD-VC11 cross-links. In other words, the relaxation of each αCD-R cross-links in the αCD-PyC11-VC11 (2, 1, 1) hydrogel should occur independently.

To discuss the details, these master curves and relaxation curves were analyzed with the generalized Maxwell model (**Tables 3-11–3-21**). **Table 3-23** shows the combined results for the relaxation modes calculated from both curves. In this section, the author discusses τ and G of the individual relaxation modes but not $<\tau>_w$ because a comparison of individual relaxation modes is enough to examine the combined effects of the αCD-R cross-links on the relaxation behaviors of the αCD-R_1-R_2 (2, 1, 1) hydrogels. As shown in **Table 3-23**, for example, the αCD-PyC11- VC11 (2, 1, 1) hydrogel indeed had short relaxation times (2.4 and 16 s) for the 2nd and 3rd relaxation modes, which were in accordance with τ_2 and τ_3 of the αCD-PyC11 (2, 2) hydrogel. On the other hand, it showed a long relaxation time (τ_5, 7.0×10^{3} s) consistent with τ_5 of the αCD-VC11 (2, 2) hydrogel. It is convincing that the relaxation strengths (G_2, G_3, and G_5) of the αCD-PyC11-VC11 (2, 1, 1) hydrogel were smaller than G_2 and G_3 of the αCD-PyC11 (2, 2) and G_5 of the αCD-VC11 (2, 2) hydrogels because the αCD-PyC11-VC11 (2, 1, 1) hydrogel contained 1 mol% content for both PyC11 and VC11 units compared with 2 mol% in the αCD-R (2, 2) hydrogels.

The above features were generalized for other αCD-R_1-R_2 (2, 1, 1) hydrogels. The αCD-R_1-R_2 (2, 1, 1) hydrogels exhibited independent relaxations derived from dissociations of αCD-R_1 and αCD-R_2 cross-links. These results indicated that the αCD-R_1 and αCD-R_2 cross-links always dissociated with different timescales and dissipated mechanical energy in the αCD-R_1-R_2 hydrogel, at least in the linear viscoelastic range.

Table 3-23. Relaxation strength (G_p), relaxation time (τ_p) in the p^{th} relaxation mode and terminal modulus (G_N) used for curve fitting of the αCD-R_1-R_2 (2, 1, 1) and αCD-R (2, 2) hydrogels.

Sample	G_1, τ_1 [Pa], [s]	G_2, τ_2 [Pa], [s]	G_3, τ_3 [Pa], [s]	G_4, τ_4 [Pa], [s]	G_5, τ_5 [Pa], [s]	G_N [Pa]
αCD-ImC11 (2, 2)	1.4×10^4, 0.09	1.5×10^4, 1.6	3.4×10^3, 11	1.3×10^3, 1.2×10^2	5.2×10^2, 3.3×10^3	9.5×10^3
αCD-PyC11 (2, 2)	-	1.4×10^4, 2.2	2.3×10^4, 19	4.1×10^3, 1.6×10^2	2.7×10^3, 2.4×10^3	5.2×10^3
αCD-VC11 (2, 2)	-	-	-	4.7×10^3, 1.0×10^3	1.2×10^4, 5.5×10^3	8.7×10^3
αCD-TMAmC11 (2, 2)	-	-	-	-	1.7×10^4, 9.5×10^3	0
αCD-ImC11-PyC11 (2, 1, 1)	7.3×10^3, 0.16	1.3×10^4, 2.4	1.1×10^4, 21	3.5×10^3, 1.9×10^2	1.9×10^3, 2.4×10^3	5.4×10^3
αCD-ImC11-VC11 (2, 1, 1)	6.0×10^3, 0.16	7.9×10^3, 2.9	1.0×10^3, 27	-	7.0×10^3, 4.6×10^3	8.7×10^3
αCD-ImC11-TMAmC11 (2, 1, 1)	6.3×10^3, 0.16	8.2×10^3, 2.4	-	-	1.8×10^4, 2.2×10^4	0
αCD-PyC11-VC11 (2, 1, 1)	-	4.5×10^3, 2.4	6.6×10^3, 16	1.4×10^3, 1.2×10^2	8.7×10^3, 7.0×10^3	4.5×10^3
αCD-PyC11-TMAmC11 (2, 1, 1)	-	4.8×10^3, 2.9	7.6×10^3, 20	-	2.1×10^4, 9.8×10^3	0
αCD-VC11-TMAmC11 (2, 1, 1)	-	-	-	8.8×10^3, 7.1×10^3	2.4×10^4, 9.4×10^3	0

3.3.4. Mechanical hysteresis of the αCD-R_1-R_2 hydrogels

Linear viscoelastic measurements revealed independent relaxations of αCD-R_1 and αCD-R_2 cross-links in the αCD-R_1-R_2 (2, 1, 1) hydrogels. To directly evaluate their energy dissipation capabilities during stretching, the author performed cyclic tensile tests at a tensile rate of 1 mm/s without intervals and calculated the hysteresis areas and ratios of the αCD-R_1-R_2 (2, 1, 1) and αCD-R (2, 2) hydrogels from the surrounding area with cyclic stress–strain curves (**Figures 3-14–3-16**). Then, the number of cycles was five, and the maximum strains for each cycle were set to 16%, 32%, 48%, 64% and 80% of the fracture strain of each hydrogel. **Figure 3-16a–c** shows cyclic stress–strain curves for the αCD-PyC11-VC11 (2, 1, 1), αCD-PyC11 (2, 2), and αCD-VC11 (2, 2) hydrogels. They showed different stress–strain curves during the cyclic tensile tests.

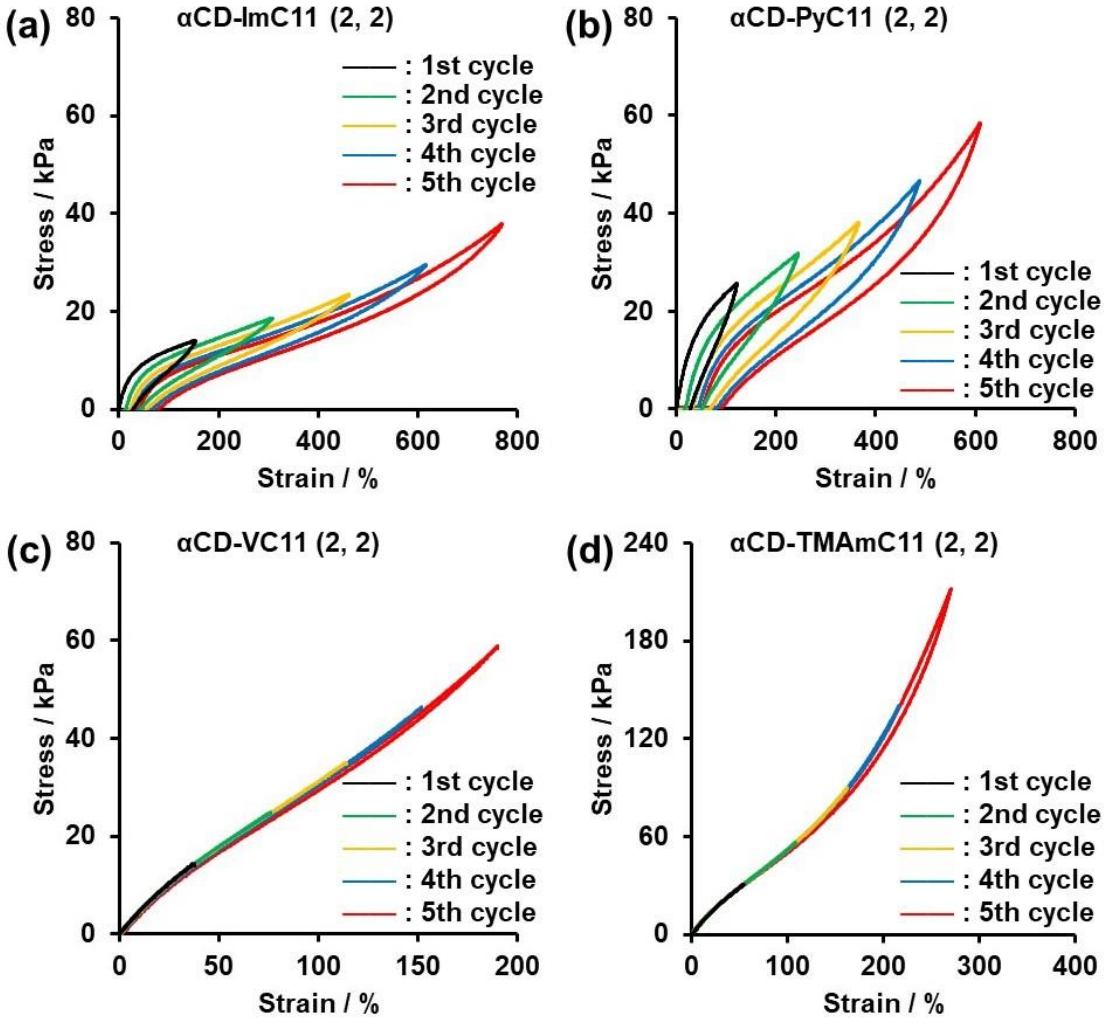

Figure 3-14. Cyclic stress–strain curves of **(a)** αCD-ImC11 (2, 2), **(b)** αCD-PyC11 (2, 2), **(c)** αCD-VC11 (2, 2), and **(d)** αCD-TMAmC11 (2, 2) hydrogels. Maximum strains were set to 16%, 32%, 48%, 64% and 80% of the fracture strain of each gel.

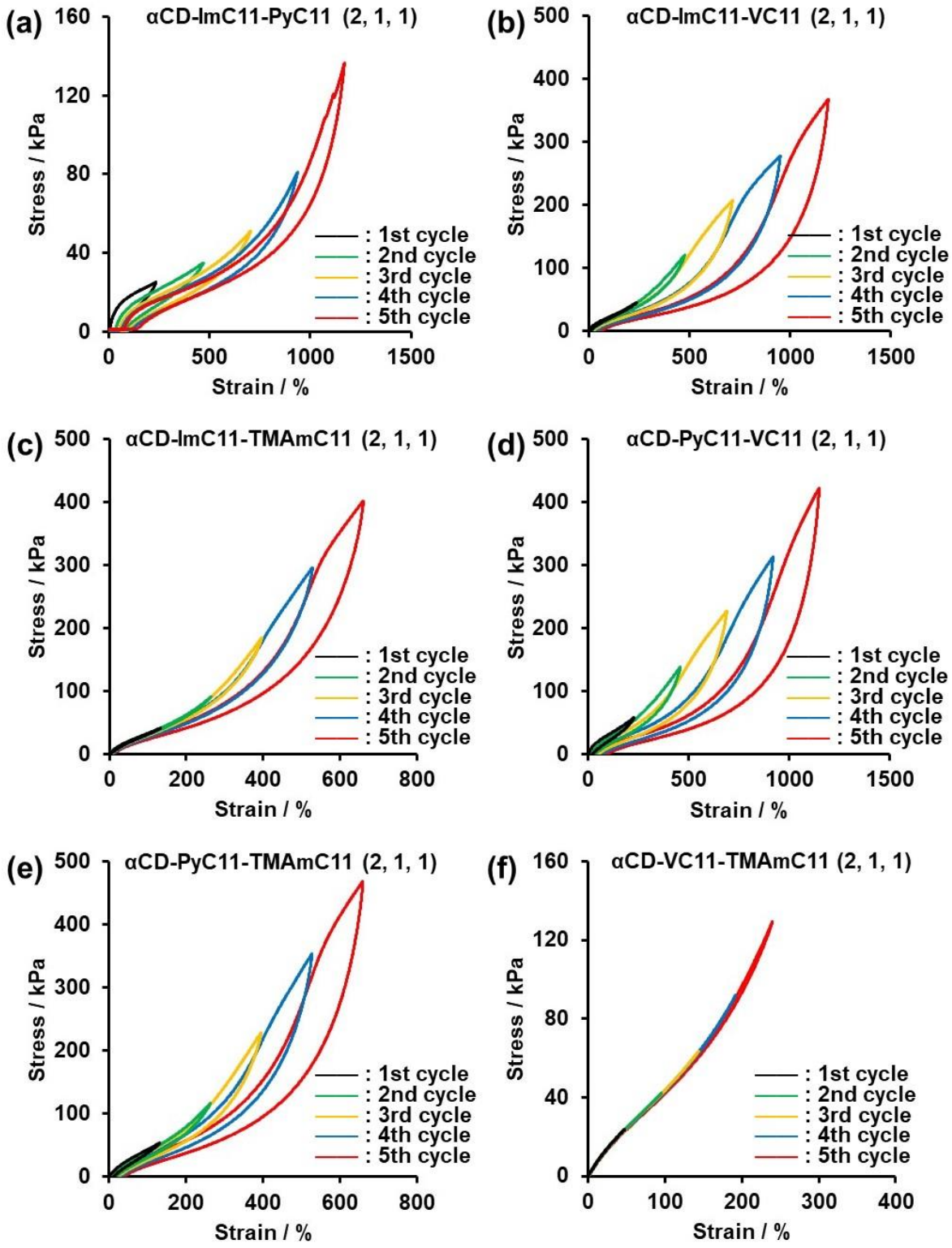

Figure 3-15. Cyclic stress–strain curves of **(a)** αCD-ImC11-PyC11 (2, 1, 1), **(b)** αCD-ImC11-VC11 (2, 1, 1), **(c)** αCD-ImC11-TMAmC11 (2, 1, 1), **(d)** αCD-PyC11-VC11 (2, 1, 1), **(e)** αCD-PyC11-TMAmC11 (2, 1, 1), and **(f)** αCD-VC11-TMAmC11 (2, 1, 1) hydrogels. Maximum strains were set to 16%, 32%, 48%, 64% and 80% of the fracture strain of each gel.

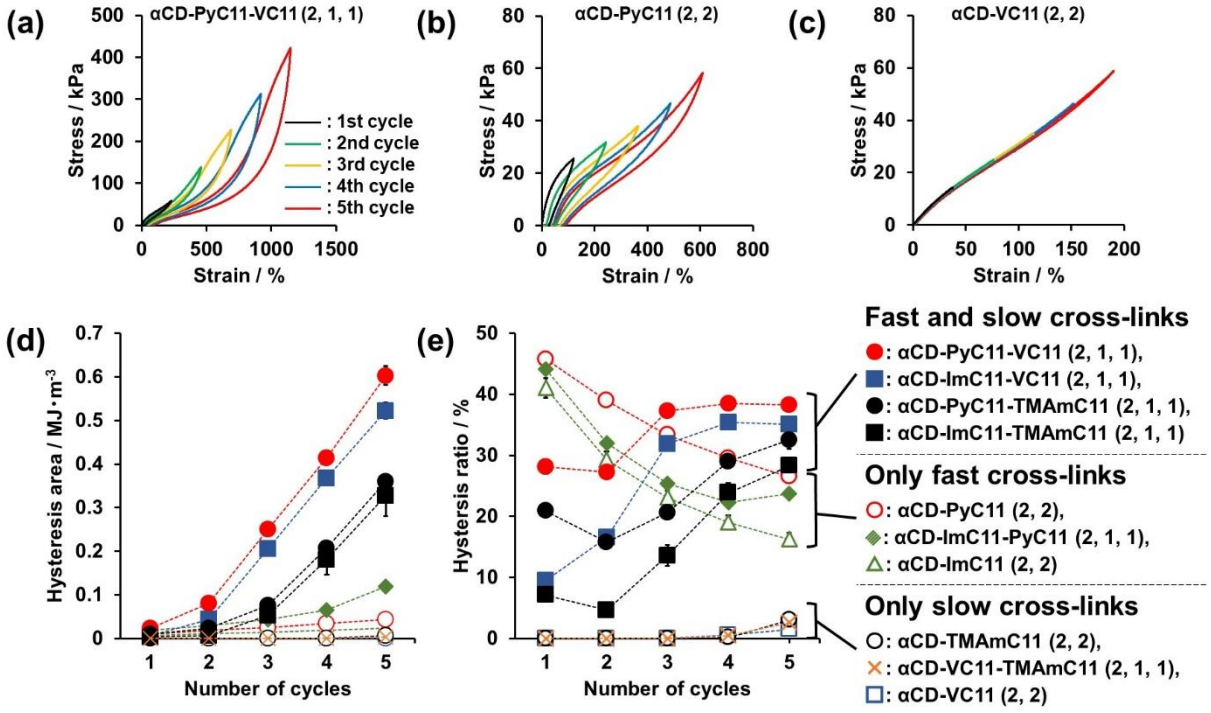

Figure 3-16. Hysteresis properties of the αCD-R_1-R_2 (2, 1, 1) and αCD-R (2, 2) hydrogels. Representative cyclic stress–strain curves of **(a)** αCD-PyC11-VC11 (2, 1, 1), **(b)** αCD-PyC11 (2, 2) and **(c)** αCD-VC11 (2, 2) hydrogels. Maximum strains were set to 16%, 32%, 48%, 64%, and 80% of the fracture strain of each hydrogel. **(d)** Hysteresis areas at each cycle of the αCD-R_1-R_2 (2, 1, 1) and αCD-R (2, 2) hydrogels. **(e)** Hysteresis ratios at each cycle of the αCD-R_1-R_2 (2, 1, 1) and αCD-R (2, 2) hydrogels.

To discuss the energy dissipation mechanism and changes in the hydrogels under stretching in detail, the author investigated the changes in hysteresis properties with the number of cycles. **Figure 3-16d** shows the dependence of the hysteresis area on the number of cycles. In all αCD-R_1-R_2 (2, 1, 1) and αCD-R (2, 2) hydrogels, hysteresis losses increased with increases in the number of cycles. The order of the hysteresis area was in accord with that of the toughness in **Figure 3-5b**. This implied that more mechanical energy was dissipated in tougher αCD-R_1-R_2 (2, 1, 1) and αCD-R (2, 2) hydrogels.

Figure 3-16e shows the dependence of the hysteresis ratio on the number of cycles. Interestingly, the dependence was divided into three categories according to a combination of dynamics of the αCD-R cross-links. First, in the cases of αCD-ImC11 (2, 2), αCD-PyC11 (2, 2), and αCD-ImC11-PyC11 (2, 1, 1) hydrogels, which had only fast reversible cross-links, the hysteresis ratios decreased with increasing numbers of cycles. For example, the hysteresis ratio of the αCD-ImC11-PyC11 (2, 1, 1) hydrogel in the first cycle was 44%, and it decreased to 24% in the fifth cycle. This dependence indicated that fast dissociating αCD-R cross-links (with short $<\tau>_w$) effectively dissipated much energy at low strain due to the viscoelastic behavior of cross-links, while the capability for energy dissipation decreased gradually at large strain due to a decrease in the strain rate. The strain rate is defined with the constant tensile speed (1 mm/s) and sample length during stretching (L):

$$\text{Strain rate} \,/\, \text{s}^{-1} = \frac{\text{Tensile speed}}{\text{Sample length}} = \frac{1}{L}$$

Second, the αCD-VC11 (2, 2), αCD-TMAmC11 (2, 2), and αCD-VC11-TMAmC11 (2, 1, 1) hydrogels with only slowly reversible cross-links showed zero or very low (~ 3%) hysteresis ratios regardless of the number of guest types. This meant that the slowly reversible αCD-R cross-links entirely acted as elastic bodies and could not dissipate mechanical energy.

Finally, the four αCD-R_1-R_2 (2, 1, 1) hydrogels with fast and slowly reversible cross-links (R_1 = ImC11 or PyC11, R_2 = VC11 or TMAmC11) showed unique changes in hysteresis ratios. Their hysteresis ratios at the first and second cycles were moderately high (lower than those of hydrogels with only fast reversible cross-link). However, they increased from the third to fifth cycles. This result indicated that the four αCD-R_1-R_2 (2, 1, 1) hydrogels dissipated more mechanical energy at large strain than at low strain. The author considered that these specific hysteresis ratios contributed to toughening the αCD-R_1-R_2 (2, 1, 1) hydrogels, such as the αCD-PyC11-VC11 (2, 1, 1) hydrogel.

In short, tough αCD-R_1-R_2 (2, 1, 1) hydrogels with fast and slow cross-links showed high hysteresis ratios at large strains. On the other hand, the hydrogels with only fast cross-links showed decreases in the hysteresis ratios with increasing strain, and the hydrogels with only slow cross-links showed very low hysteresis ratios. Therefore, the slow αCD-R_2 cross-links in the αCD-R_1-R_2 (2, 1, 1) hydrogels should increase the hysteresis ratios at large strains.

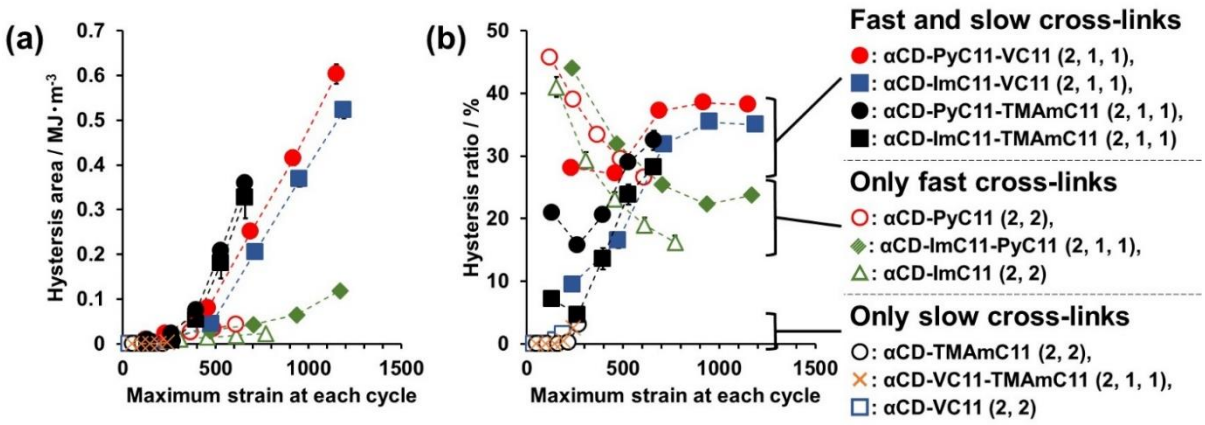

Figure 3-17. (a) Relation between hysteresis areas and maximum strains at each cycle for the αCD-R_1-R_2 (2, 1, 1) and αCD-R (2, 2) hydrogels. **(b)** Relation between hysteresis ratios and maximum strains at each cycle for the αCD-R_1-R_2 (2, 1, 1) and αCD-R (2, 2) hydrogels.

Figure 3-17 shows the relation between hysteresis properties and maximum strains as a supplementary data. It makes it easier to compare the hydrogels with similar fracture strains, such as αCD-PyC11-VC11 (2, 1, 1), αCD-ImC11-VC11 (2, 1, 1), and αCD-ImC11-PyC11 (2, 1, 1) hydrogels. Comparison of the three hydrogels, for instance, show more clearly the difference in hysteresis between hydrogels with fast and slow cross-links and those with only fast cross-links. Furthermore, **Figure 3-17** also informs us that hysteresis area, hysteresis ratio, and their dependences on strain changed universally depending on the combination of dynamics of reversible cross-links.

In addition, the hysteresis of the supramolecular hydrogel with reversible cross-links should be dependent on the deformation rate as described in Section 1.4.2, Chapter 1. Therefore, the dependence of hysteresis of the αCD-PyC11 (2, 2) hydrogel on tensile speed was discussed in an appendix at the end of Chapter 3.

3.3.5. Comparison between αCD-R cross-link with slow dynamics and chemical cross-link

As mentioned above, the αCD-R_1-R_2 (2, 1, 1) hydrogel with fast and slow cross-links showed high toughness and a high hysteresis ratio at large strains. To investigate the contributions of slow αCD-R_2 cross-links to related mechanical properties, the author compared the αCD-VC11 cross-link in the αCD-PyC11-VC11 (2, 1, 1) hydrogel with the chemical cross-link *N*, *N*′-methylenebisacrylamide (MBAAm). Therefore, the αCD-PyC11-MBAAm (1, 1, 0.5) and (1, 1, 1) hydrogels, which combined fast reversible cross-link and chemical cross-link, were prepared in a similar way to those in **Figure 3-2c**, and their mechanical properties were evaluated by tensile tests and cyclic tensile tests as previously described (**Figures 3-18–3-20 and Tables 3-24 and 3-25**).

Table 3-24. Amounts of reagents and solvents used in the preparation of the αCD-PyC11-MBAAm (1, 1, 0.5) hydrogel.

	KCl aq. /mL	AAm /mg	αCDAAmMe /mg	PyC11 /mg	MBAAm /mg	KPS /mg	TEMED /μL
αCD-PyC11-MBAAm (1, 1, 0.5) hydrogel	2.0	277	42.2	15.4	3.1	10.8	6.0

Table 3-25. Amounts of reagents and solvents used in the preparation of the αCD-PyC11-MBAAm (1, 1, 1) hydrogel.

	KCl aq. /mL	AAm /mg	αCDAAmMe /mg	PyC11 /mg	MBAAm /mg	KPS /mg	TEMED /μL
αCD-PyC11-MBAAm (1, 1, 1) hydrogel	2.0	276	42.2	15.4	6.2	10.8	6.0

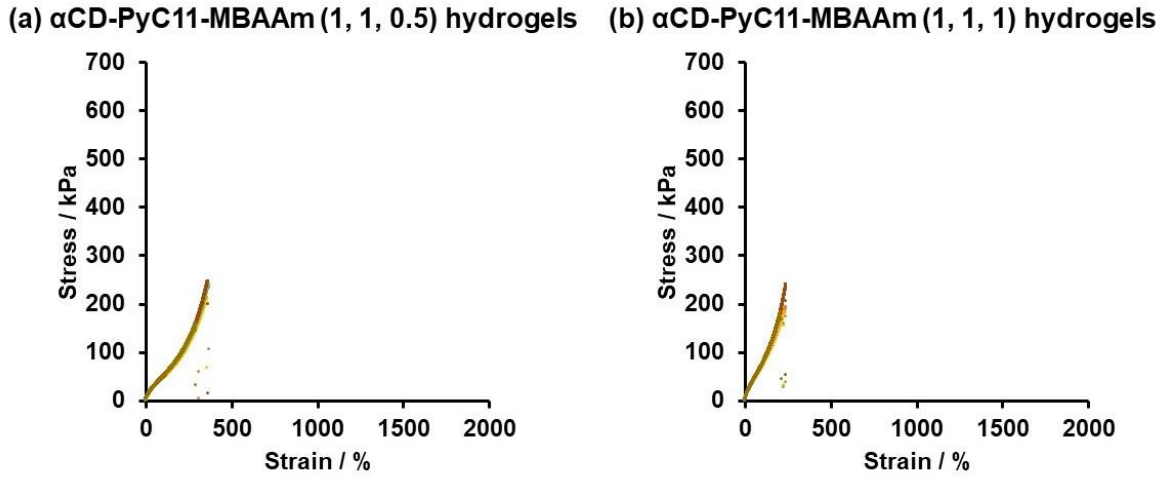

Figure 3-18. Stress–strain curves of **(a)** the αCD-PyC11-MBAAm (1, 1, 0.5) hydrogels (n = 5) and (b) αCD-PyC11-MBAAm (1, 1, 1) hydrogels (n = 5) at 25 °C at a tensile rate of 1.0 mm/s.

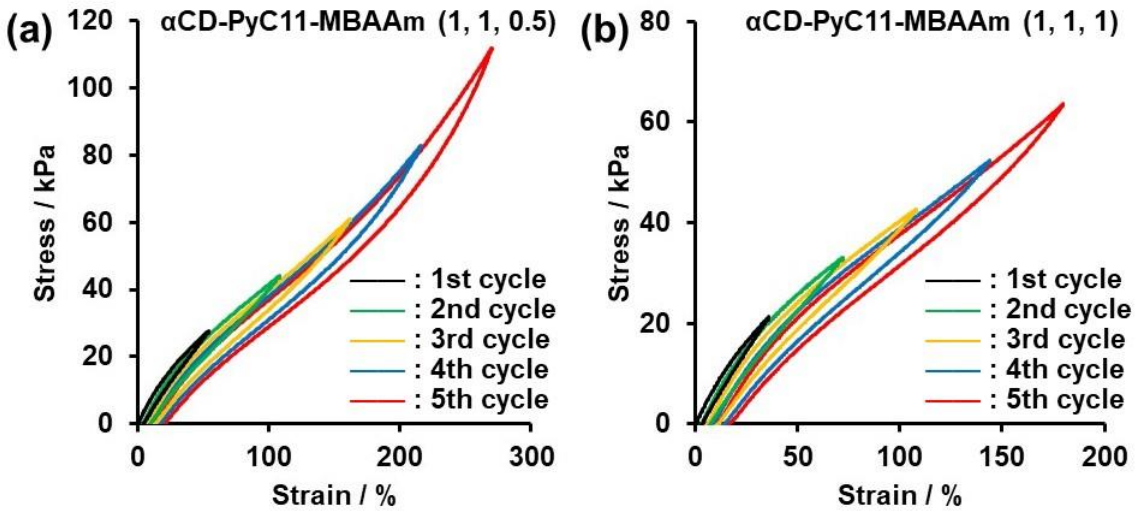

Figure 3-19. Cyclic stress–strain curves of **(a)** the αCD-PyC11-MBAAm (1, 1, 0.5) and **(b)** the αCD-PyC11-MBAAm (1, 1, 1) hydrogels. Maximum strains were set to 16%, 32%, 48%, 64% and 80% of the fracture strain of each gel.

Figures 3-18 and 3-20b–c show the results of tensile tests on the αCD-PyC11-MBAAm (1, 1, 0.5) and (1, 1, 1) hydrogels compared to the αCD-PyC11-VC11 (2, 1, 1) hydrogel. Although the αCD-PyC11-MBAAm hydrogels may be categorized as dual cross-link gel[1] with chemical and physical cross-links, they were brittle (high Young's modulus and low toughness).

Figures 3-19 and 3-20d–e show the results of the cyclic tensile tests. The αCD-PyC11-MBAAm (1, 1, 0.5) and (1, 1, 1) hydrogels showed different hysteresis behaviors than the αCD-PyC11-VC11 (2, 1, 1) hydrogel during cyclic tensile tests. The hysteresis areas and ratios of both αCD-PyC11-MBAAm hydrogels were entirely low. In particular, the hysteresis ratios were almost constant (14~17%) or decreased slightly with increasing the number of cycles, suggesting that they could not dissipate mechanical energy effectively.

The above results for the αCD-PyC11-MBAAm hydrogels address the importance of combining slowly reversible cross-link (not chemical cross-link) and fast reversible cross-link to realize the high toughness of the αCD-R_1-R_2 (2, 1, 1) hydrogel system.

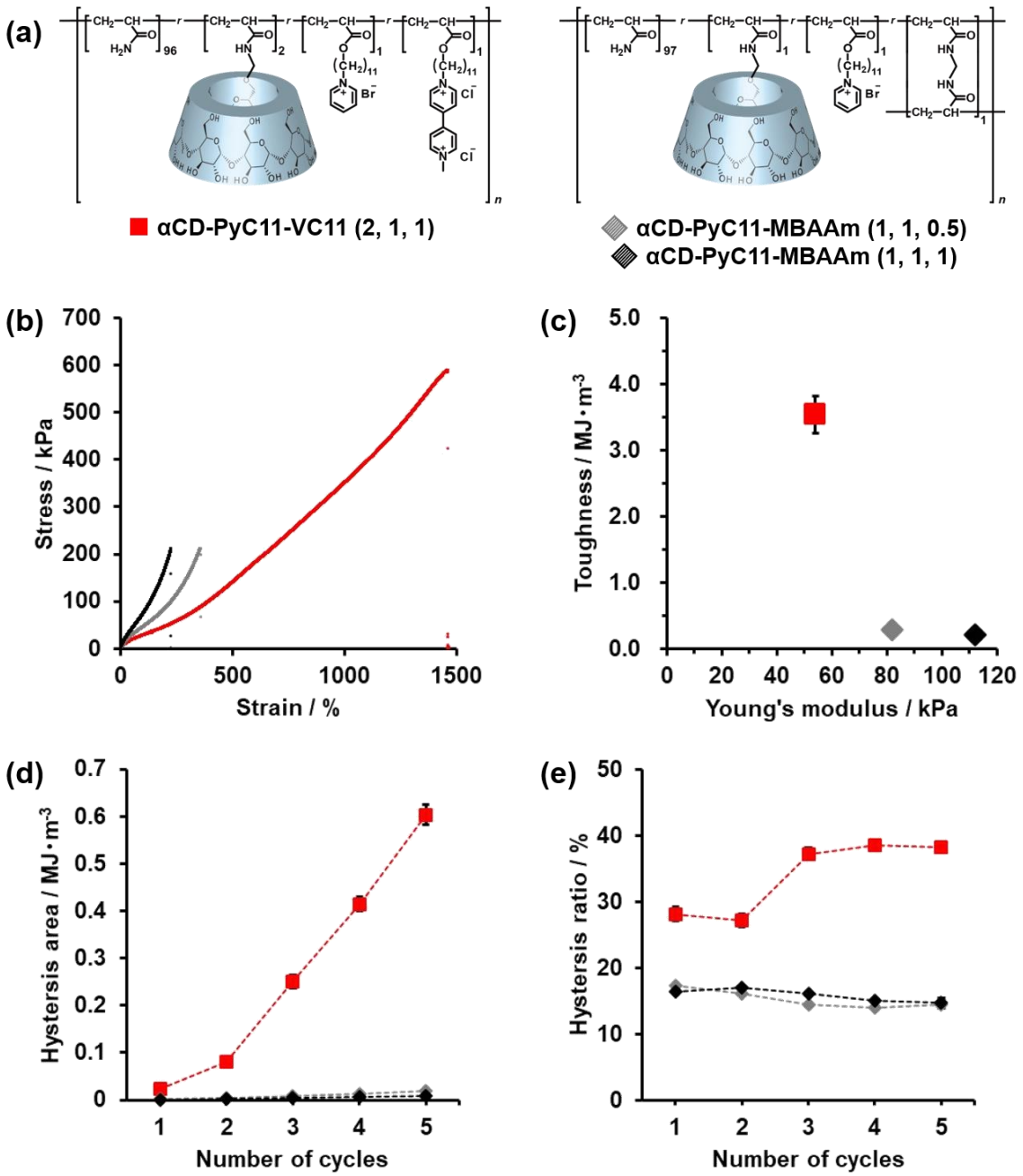

Figure 3-20. Comparison between the αCD-PyC11-VC11 (2, 1, 1), αCD-PyC11-MBAAm (1, 1, 0.5), and αCD-PyC11-MBAAm (1, 1, 1) hydrogels. **(a)** Chemical structures of the hydrogels. **(b)** Stress–strain curves. **(c)** Toughness and Young's modulus. **(d)** Hysteresis areas at each cycle. **(e)** Hysteresis ratios at each cycle.

3.3.6. Structural analyses of αCD-R_1-R_2 hydrogels with *in-situ* SAXS under stretching

To consider the effects of structural changes in the polymer network on toughness, the author analyzed the internal structures of the αCD-R_1-R_2 (2, 1, 1) and αCD-R (2, 2) hydrogels under stretching by *in-situ* small-angle X-ray scattering (SAXS) with a tensile device at the BL40B2 beamline of SPring-8 (**Figures 3-21–3-23**). The hydrogels were stretched at a tensile rate of 0.63 mm/s to adjust the initial strain rate to 0.042 /s. This value was similar to the initial strain rate used in the above tensile tests. Therefore, the effects of hydrogel viscoelasticity on the structural and mechanical properties should be at comparable levels in both SAXS and tensile tests. When the strain (ε_c) reached 0%, 50%, 100%, 200%, 300%, and 400%, ε_c was temporarily fixed, and then the SAXS profiles were recorded. Because of the strain limit of the tensile machine, the author was able to collect SAXS data until 400% strain. The obtained SAXS profiles were converted into absolute intensities (I_{abs}) to eliminate the effects of exposure time (t_e), transmittance (T), and hydrogel thickness (Z).

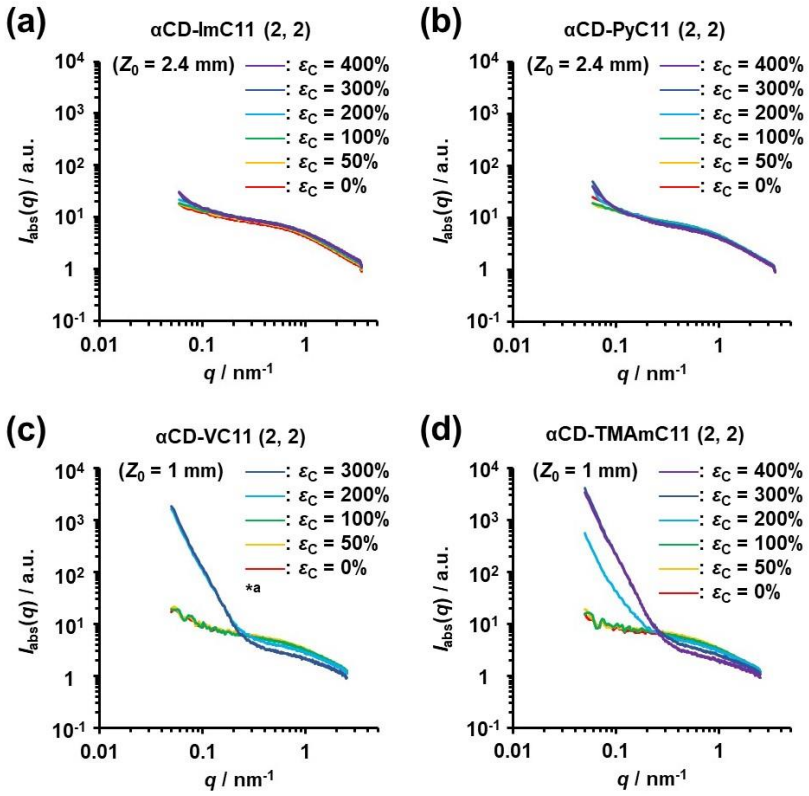

Figure 3-21. SAXS profiles (absolute intensity) of **(a)** αCD-ImC11 (2, 2), **(b)** αCD-PyC11 (2, 2), **(c)** αCD-VC11 (2, 2), and **(d)** αCD-TMAmC11 (2, 2) hydrogels under stretching. (Note) *[a]: The αCD-VC11 (2, 2) hydrogel broke before the strain reached 400%.

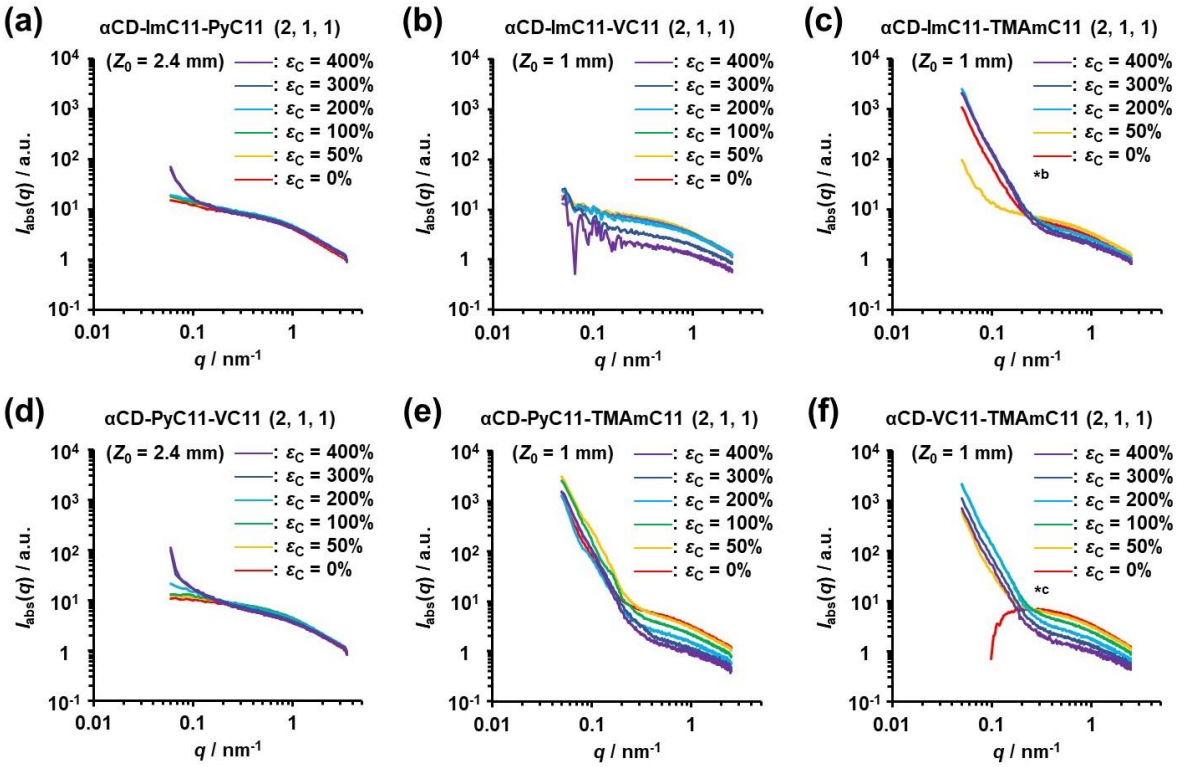

Figure 3-22. SAXS profiles (absolute intensity) of **(a)** αCD-ImC11-PyC11 (2, 1, 1), **(b)** αCD-ImC11-VC11 (2, 1, 1), **(c)** αCD-ImC11-TMAmC11 (2, 1, 1), **(d)** αCD-PyC11-VC11 (2, 1, 1), **(e)** αCD-PyC11-TMAmC11 (2, 1, 1), and **(f)** αCD-VC11-TMAmC11 (2, 1, 1) hydrogels under stretching. (Note) *[b]: SAXS data of the αCD-ImC11-TMAmC11 (2, 1, 1) hydrogel at a strain of 100% were not obtained due to an instrumental error. *[c]: SAXS data of the αCD-VC11-TMAmC11 (2, 1, 1) hydrogel at a strain of 0% was reduced at $q < 0.2$ nm^{-1} due to a small difference from the background.

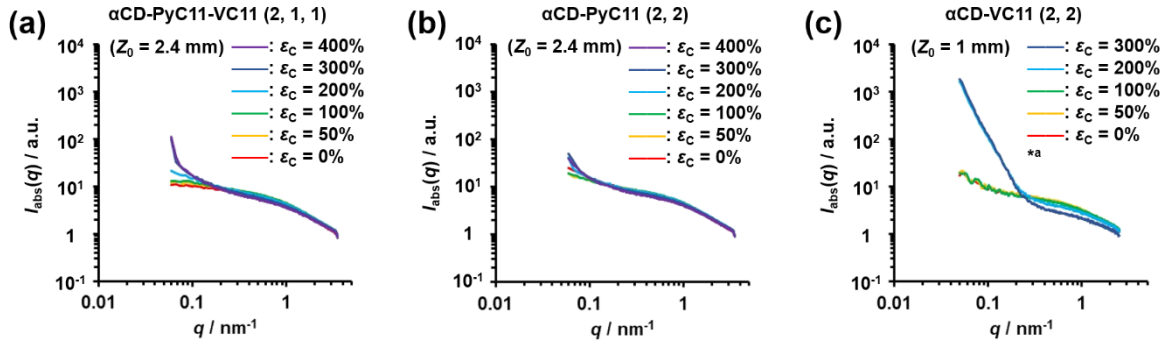

Figure 3-23. SAXS profiles (absolute intensity) for **(a)** the αCD-PyC11-VC11 (2, 1, 1), **(b)** αCD-PyC11 (2, 2), and **(c)** αCD-VC11 (2, 2) hydrogels during stretching. (Note) *[a]: The αCD-VC11 (2, 2) hydrogel broke before the strain reached 400%.

Figure 3-23 shows a comparison of SAXS profiles (I_{abs}) for the tough αCD-PyC11-VC11 (2, 1, 1) hydrogel with those of the αCD-PyC11 (2, 2) and αCD-VC11 (2, 2) hydrogels. In these hydrogels, no characteristic peak was found at the initial state (ε_c = 0%), and no new correlation peak arose under stretching. Furthermore, changes in their profiles were similar: I_{abs} within the scattering vector (q) range of 0.2~1.0 nm^{-1} decreased with increasing ε_c. This trend was also observed for the other hydrogels (**Figures 3-21 and 3-22**). On the other hand, for the αCD-VC11 (2, 2) hydrogel with low fracture strain, I_{abs} within q range of 0.05~0.2 nm^{-1} suddenly increased after ε_c reached 100%, which indicated heterogeneous structure such as crack formation. In addition, in **Figures 3-22c, e, and f**, I_{abs} for the αCD-ImC11-TMAmC11, αCD-PyC11-TMAmC11, and αCD-VC11-TMAmC11 (2, 1, 1) hydrogels at q < 0.2 nm^{-1} was already high at initial state. This indicated that some combinations of the αCD-R cross-links caused heterogeneous structures at the initial state.

These results demonstrated that the αCD-R_1-R_2 (2, 1, 1) and αCD-R_2 (2, 2) hydrogels had similar initial structures (no periodic structure) and showed similar structural changes under stretching regardless of their cross-linking structures. Therefore, the author postulated that their toughness and hysteresis ratios were not attributable to structural changes but to differences in the relaxation behaviors of the reversible αCD-R cross-links.

3.4. Discussion

3.4.1. Proposed mechanism for supramolecular hydrogels with fast and slowly reversible cross-links

Based on the viscoelastic properties and hysteresis properties of the hydrogels, the author proposed an energy dissipation mechanism for tough αCD-R_1-R_2 hydrogels with fast and slowly reversible cross-links, as shown in **Figure 3-24**. First, at low strains, dissociation of the αCD-PyC11 cross-links with short $<\tau>_w$, which was compatible with a high strain rate, caused effective energy dissipation and enabled elongation of the hydrogel, while the αCD-VC11 cross-links with long $<\tau>_w$ then behaved as elastic body and reduced the initial hysteresis ratio. Second, as the strain increased, the strain rate decreased. Therefore, in addition to the αCD-PyC11 cross-links, the αCD-VC11 cross-links could act as viscoelastic bodies and dissociate at large strains (low strain rates), which in turn dissipated energy and improved toughness. In summary, we concluded that additional energy dissipation enabled by dissociation of the αCD-R_2 cross-links with long $<\tau>_w$ at large strains improved the toughness of the αCD-R_1-R_2 (2, 1, 1) hydrogels with fast and slowly reversible cross-links.

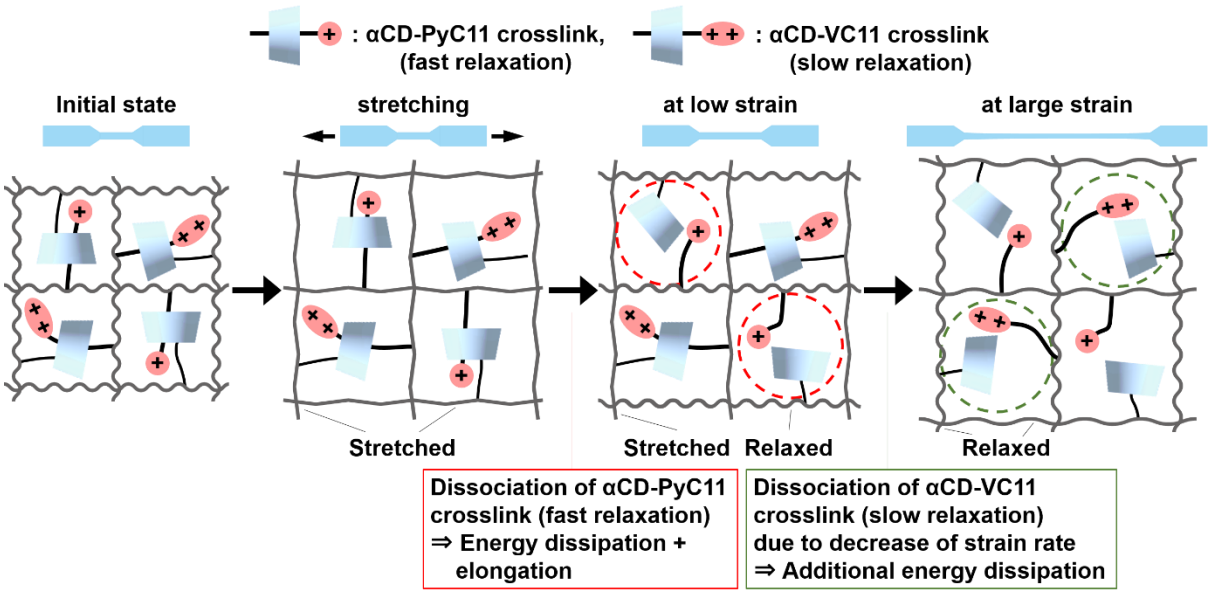

Figure 3-24. Proposed multi-energy dissipation mechanism for the high toughness and unique hysteresis behavior of the αCD-R_1-R_2 (2, 1, 1) hydrogels with fast and slowly reversible cross-links, such as the αCD-PyC11-VC11 (2, 1, 1) hydrogel.

3.4.2. Design of supramolecular hydrogels with triple reversible cross-links

The proposed mechanism in **Figure 3-24** indicates that relaxation by slowly reversible cross-links at large strain should improve toughness. In the case of the hydrogels with dual reversible cross-links, the αCD-PyC11-VC11 (2, 1, 1) hydrogel was the toughest. The author hypothesized that the addition of αCD-TMAmC11 cross-links with $<\tau>_w$ longer than that of the αCD-VC11 cross-links would give a tougher material.

For testing the hypothesis, αCD-PyC11-VC11-TMAmC11 (*w*, *x*, *y*, *z*) hydrogels with triple reversible cross-links were prepared and evaluated as described above (tensile rate = 1 mm/s), where (*w*, *x*, *y*, *z*) denotes the molar ratios of the αCD, PyC11, VC11, and TMAmC11 units, respectively (**Figure 3-25 and Tables 3-26–3-28**). They showed three values for $<\tau>_w$, 1.8, 6.6×10^3, and 9.5×10^3 s. The molar ratios (*w*, *x*, *y*, *z*) were set to (2, 0.67, 0.67, 0.67), (3, 1, 1, 1), and (2, 1, 0.5, 0.5). The αCD-PyC11-VC11-TMAmC11 (2, 0.67, 0.67, 0.67) and (3, 1, 1, 1) hydrogels contained equal amounts of three R guests. The αCD-PyC11-VC11-TMAmC11 (2, 1, 0.5, 0.5) hydrogel contained more PyC11 units and equal amounts of VC11 and TMAmC11 units.

Table 3-26. Amounts of reagents and solvents used in the preparation of the αCD-PyC11-VC11-TMAmC11 (2, 0.67, 0.67, 0.67) hydrogel.

	KCl aq. /mL	AAm /mg	αCDAAmMe /mg	PyC11 /mg	VC11 /mg	TAMmC11 /mg	KPS /mg	TEMED /μL
αCD-PyC11-VC11-TMAmC11 (2, 0.67, 0.67, 0.67) hydrogel	1.2	164	50.7	6.2	7.5	5.9	6.5	3.6

Table 3-27. Amounts of reagents and solvents used in the preparation of the αCD-PyC11-VC11-TMAmC11 (3, 1, 1, 1) hydrogel.

	KCl aq. /mL	AAm /mg	αCDAAmMe /mg	PyC11 /mg	VC11 /mg	TAMmC11 /mg	KPS /mg	TEMED /μL
αCD-PyC11-VC11-TMAmC11 (3, 1, 1, 1) hydrogel	1.2	160	76.0	9.2	11.2	8.7	6.5	3.6

Table 3-28. Amounts of reagents and solvents used in the preparation of the αCD-PyC11-VC11-TMAmC11 (2, 1, 0.5, 0.5) hydrogel.

	KCl aq. /mL	AAm /mg	αCDAAmMe /mg	PyC11 /mg	VC11 /mg	TAMmC11 /mg	KPS /mg	TEMED /μL
αCD-PyC11-VC11-TMAmC11 (2, 1, 0.5, 0.5) hydrogel	1.2	164	50.7	9.2	5.6	4.4	6.5	3.6

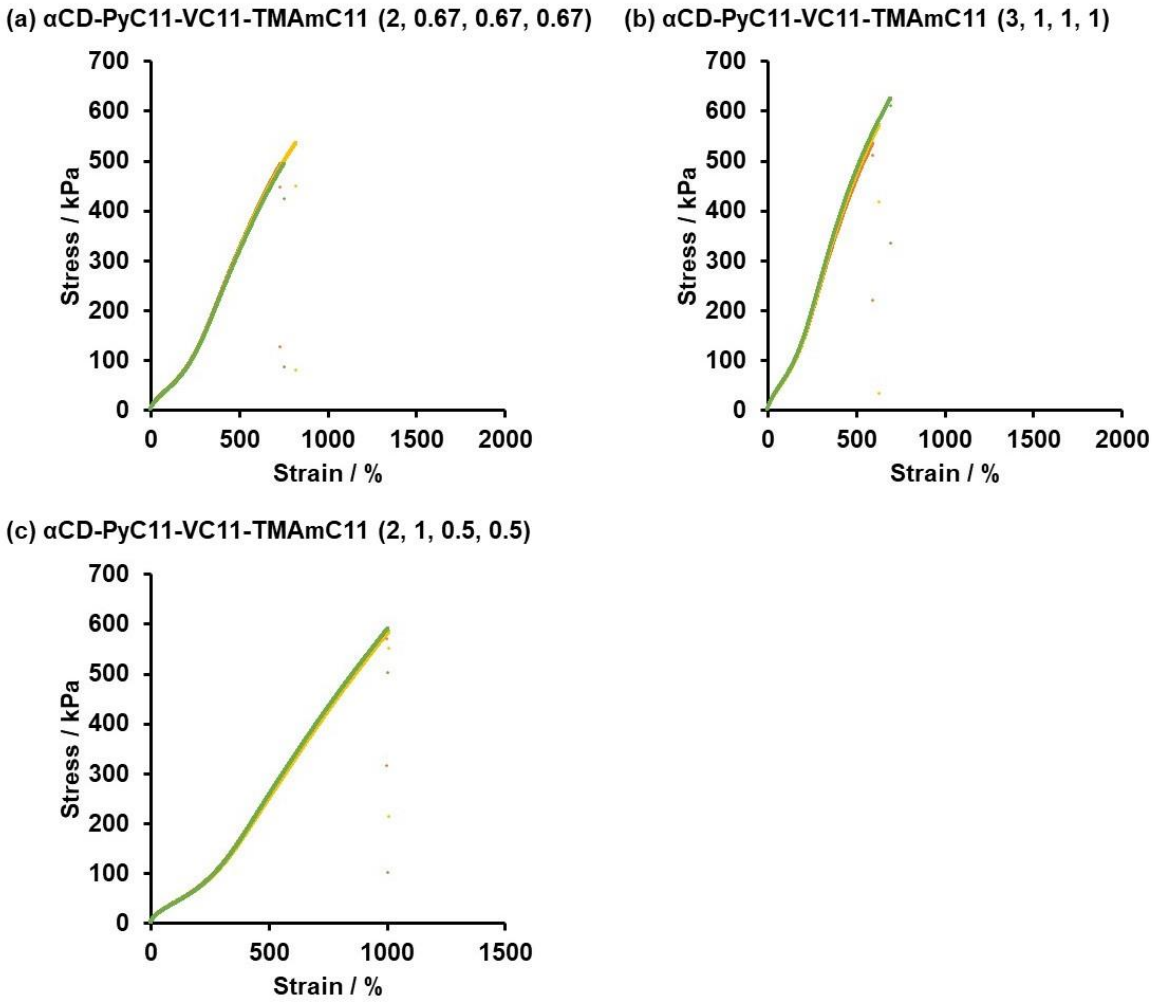

Figure 3-25. Stress-strain curves of **(a)** the αCD-PyC11-VC11-TMAmC11 (2, 0.67, 0.67, 0.67) hydrogel (n = 3), **(b)** the αCD-PyC11-VC11-TMAmC11 (3, 1, 1, 1) hydrogel (n = 3), and **(c)** the αCD-PyC11-VC11-TMAmC11 (2, 1, 0.5, 0.5) hydrogel (n = 3) at 25 ^{o}C at a tensile rate of 1.0 mm/s

Figure 3-26 shows the results of tensile tests on the αCD-PyC11-VC11-TMAmC11 (*w*, *x*, *y*, *z*) hydrogels compared with the αCD-PyC11-VC11 (2, 1, 1) and αCD-PyC11-TMAmC11 (2, 1, 1) hydrogels. The stress-strain curves of the αCD-PyC11-VC11-TMAmC11 (*w*, *x*, *y*, *z*) hydrogels in **Figure 3-26b** were similar to that of the αCD-PyC11-TMAmC11 (2, 1, 1) hydrogel, and their toughness was similarly low (**Figure 3-26c**). The author considered two reasons for the low toughness: high cross-linking density and loss of a synergetic effect of energy dissipation by dissociating cross-links and high stretchability of polymer network.[69] For the αCD-PyC11-VC11-TMAmC11 (3, 1, 1, 1) hydrogels having 3 mol% the αCD-R cross-links, high cross-linking density led to high Young's modulus, which resulted in small fracture strain and decreased toughness like the Lake-Thomas model.[70]

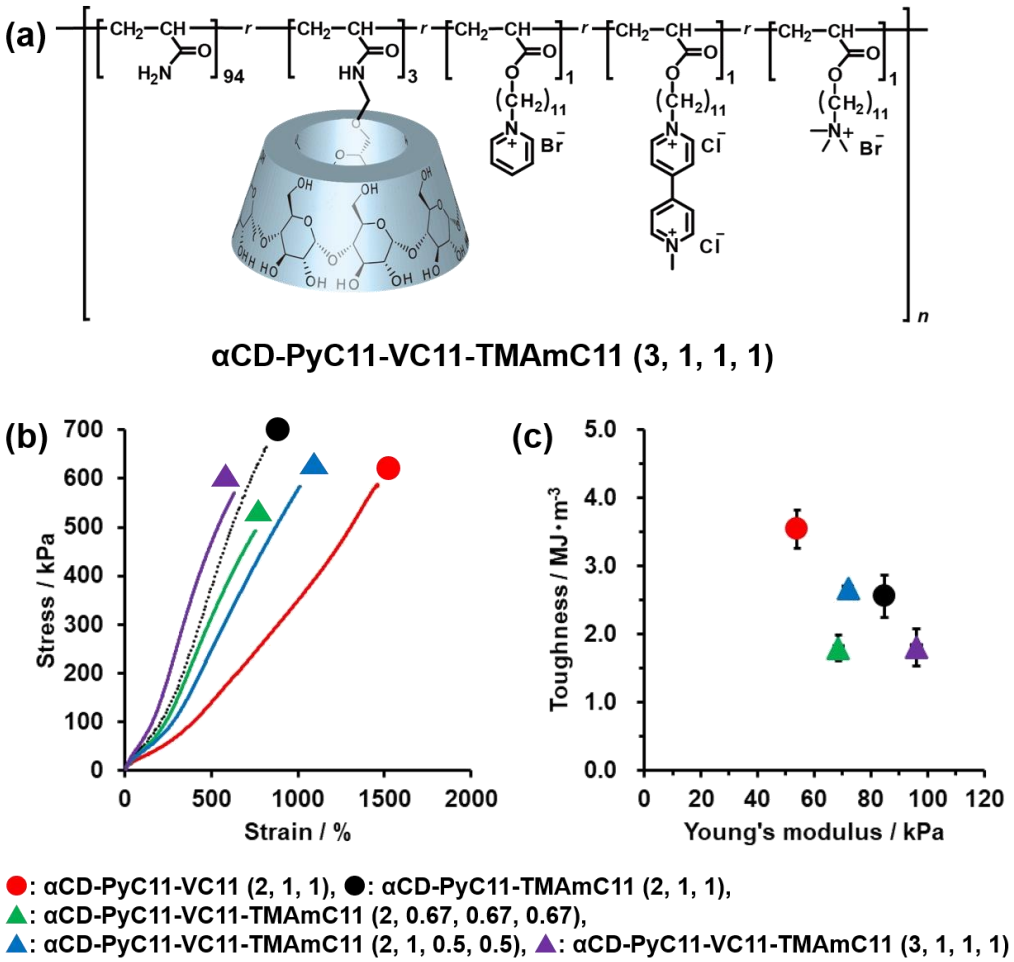

Figure 3-26. Mechanical properties of the αCD-PyC11-VC11-TMAmC11 (*w*, *x*, *y*, *z*), αCD-PyC11-VC11 (2, 1, 1), and αCD-PyC11-TMAmC11 (2, 1, 1) hydrogels. **(a)** Chemical structures of αCD-PyC11-VC11-TMAmC11 (3, 1, 1, 1). **(b)** Stress–strain curves in tensile tests at a tensile speed of 1 mm/s. **(c)** Plots of toughness and Young's modulus.

Next, the stress-strain curve and mechanical properties of αCD-PyC11-VC11-TMAmC11 (2, 1, 0.5, 0.5) hydrogel were approximately intermediate between the αCD-PyC11-VC11 (2, 1, 1) and αCD-PyC11-TMAmC11 (2, 1, 1) hydrogels. For this result, the author considered that the slowest αCD-TMAmC11 cross-links were dominant and reduced the stretchable length of cross-linked polymer chains, although the αCD-PyC11 and αCD-VC11 cross-links could dissociate to dissipate mechanical energy. Therefore, the synergetic effect was lost and the toughness of the αCD-PyC11-VC11-TMAmC11 (2, 1, 0.5, 0.5) hydrogel decreased. Lastly, the αCD-PyC11-VC11-TMAmC11 (2, 0.67, 0.67, 0.67) hydrogel containing less αCD-PyC11 cross-links showed even lower toughness than the αCD-PyC11-VC11-TMAmC11 (2, 1, 0.5, 0.5) hydrogel. Considering the synergetic effect, the ability of energy dissipation decreased with decreasing αCD-PyC11 cross-links, which should result in low toughness of the hydrogel.

The results from linear viscoelastic measurements of the αCD-R_1-R_2 hydrogels in section 3-3 suggested that the three reversible cross-links in the αCD-PyC11-VC11-TMAmC11 (*w*, *x*, *y*, *z*) hydrogels relax independently. However, their toughness was low due to high cross-linking density or the loss of synergy between the energy dissipation mechanism and the high stretchability of the polymer network. In particular, the slowest αCD-TMAmC11 cross-links should dominantly limit the stretchability of polymer chains bound by cross-links. This indicates that the consideration of viscoelastic behavior of the slowest αCD-R cross-link is important for preparing a tougher hydrogel, rather than simply combining three types of cross-links with different $<\tau>_w$. If I utilize the slower relaxation of a reversible cross-link ($<\tau>_w >$ 9500 s) as the third component to design a tougher material, I have to propose a new design concept.

As a result, the αCD-R_1-R_2 (2, 1, 1) hydrogels combining fast and slowly reversible cross-links were competent to improve toughness in the present work. The author found the first condition to improve toughness was to use a cross-link with short $<\tau>_w$ which matched the initial strain rate and then showed viscoelastic behavior. The second condition was to combine it with slowly reversible cross-links having long $<\tau>_w$ to reinforce the energy dissipation mechanism at large strains.

3.5. Conclusion

Supramolecular hydrogels based on host-guest interactions, including αCD-R_1-R_2 (2, 1, 1) with dual reversible cross-links and αCD-R (2, 2) with single reversible cross-links, were evaluated to investigate the effects of combining cross-links with different relaxation times (τ) on the mechanical properties of the hydrogels. The author chose four cation-terminated alkyl chains, ImC11, PyC11, VC11, and TMAmC11, as R guest units. The second-order average relaxation times ($<\tau>_w$) for the αCD-R cross-links were 1.8, 18, 6.6×10^3, and 9.5×10^3 s, respectively. Combinations of fast (R_1 = ImC11 or PyC11) and slowly (R_2 = VC11 or TMAmC11) reversible cross-links effectively increased the toughness by several times. Other combinations, such as two fast cross-links or two slow cross-links, failed to improve toughness effectively.

Cyclic tensile tests revealed that the tough αCD-R_1-R_2 (2, 1, 1) hydrogels with fast and slowly reversible cross-links showed increases in hysteresis ratios from the third to fifth cycles and the highest hysteresis ratios at the fifth cycle (at large strain). This means that much energy in these hydrogels was dissipated at large strain. The author concluded that the energy dissipation mechanism operating at large strain was derived from the relaxation via slow dissociation of αCD-R_2 cross-links in addition to that via fast αCD-R_1 cross-links. This indicated that additional energy dissipation caused by dissociation of αCD-R_2 cross-links with long $<\tau>_w$ at large strain improved the toughness of the hydrogels.

In Chapter 3, the author discovered the usefulness of αCD-R_2 reversible cross-links with slow dynamics for designing tough materials by combining them with fast αCD-R_1 reversible cross-link. The author hopes that material design based on quantitative features such as relaxation time will enable next-generation functional materials regardless of the types of non-covalent bonds.

References

(1) Rodin, M.; Li, J.; Kuckling, D. Dually Cross-Linked Single Networks: Structures and Applications. *Chem. Soc. Rev.* **2021**, *50* (14), 8147–8177.

(2) Liu, H.; Xiong, C.; Tao, Z.; Fan, Y.; Tang, X.; Yang, H. Zwitterionic Copolymer-Based and Hydrogen Bonding-Strengthened Self-Healing Hydrogel. *RSC Adv.* **2015**, *5* (42), 33083–33088.

(3) Taylor, D. L.; in het Panhuis, M. Self-Healing Hydrogels. *Adv. Mater.* **2016**, *28* (41), 9060–9093.

(4) Li, C. H.; Zuo, J. L. Self-Healing Polymers Based on Coordination Bonds. *Adv. Mater.* **2020**, *32* (27), 1–29.

(5) Miyamae, K.; Nakahata, M.; Takashima, Y.; Harada, A. Self-Healing, Expansion-Contraction, and Shape-Memory Properties of a Preorganized Supramolecular Hydrogel through Host-Guest Interactions. *Angew. Chemie - Int. Ed.* **2015**, *54* (31), 8984–8987.

(6) Nair, K. P.; Breedveld, V.; Weck, M. Multiresponsive Reversible Polymer Networks Based on Hydrogen Bonding and Metal Coordination. *Macromolecules* **2011**, *44* (9), 3346–3357.

(7) Yan, X.; Wang, F.; Zheng, B.; Huang, F. Stimuli-Responsive Supramolecular Polymeric Materials. *Chem. Soc. Rev.* **2012**, *41* (18), 6042–6065.

(8) McCune, J. A.; Mommer, S.; Parkins, C. C.; Scherman, O. A. Design Principles for Aqueous Interactive Materials: Lessons from Small Molecules and Stimuli-Responsive Systems. *Adv. Mater.* **2020**, *32* (20), 1906890.

(9) Vázquez-González, M.; Willner, I. Stimuli-Responsive Biomolecule-Based Hydrogels and Their Applications. *Angew. Chemie - Int. Ed.* **2020**, *59* (36), 15342–15377.

(10) Zhao, Q.; Qi, H. J.; Xie, T. Recent Progress in Shape Memory Polymer: New Behavior, Enabling Materials, and Mechanistic Understanding. *Prog. Polym. Sci.* **2015**, *49–50*, 79–120.

(11) Shang, J.; Le, X.; Zhang, J.; Chen, T.; Theato, P. Trends in Polymeric Shape Memory Hydrogels and Hydrogel Actuators. *Polym. Chem.* **2019**, *10* (9), 1036–1055.

(12) Xia, Y.; He, Y.; Zhang, F.; Liu, Y.; Leng, J. A Review of Shape Memory Polymers and Composites: Mechanisms, Materials, and Applications. *Adv. Mater.* **2021**, *33* (6), 1–33.

(13) Kurth, D. G.; Higuchi, M. Transition Metal Ions: Weak Links for Strong Polymers. *Soft Matter* **2006**, *2* (11), 915–927.

(14) Khare, E.; Holten-Andersen, N.; Buehler, M. J. Transition-Metal Coordinate Bonds for Bioinspired Macromolecules with Tunable Mechanical Properties. *Nature Reviews Materials*. Springer US 2021, 421–436.

(15) Thomas, S. The Hydrogen Bond in the Solid State. *Angew. Chemie Int. Ed.* **2002**, *41* (1), 48–76.

(16) Song, P.; Wang, H. High-Performance Polymeric Materials through Hydrogen-Bond Cross-Linking. *Adv. Mater.* **2020**, *32* (18), 1–12.

(17) Varshey, D. B.; Sander, J. R. G.; Friščić, T.; MacGillivray, L. R. Supramolecular Interactions. In *Supramolecular Chemistry*; John Wiley & Sons, Ltd, 2012.

(18) Zheng, J.; Xiao, P.; Liu, W.; Zhang, J.; Huang, Y.; Chen, T. Mechanical Robust and Self-Healable Supramolecular Hydrogel. *Macromol. Rapid Commun.* **2016**, *37* (3), 265–270.

(19) Hu, Y.; Du, Z.; Deng, X.; Wang, T.; Yang, Z.; Zhou, W.; Wang, C. Dual Physically Cross-Linked Hydrogels with High Stretchability, Toughness, and Good Self-Recoverability. *Macromolecules* **2016**, *49* (15), 5660–5668.

(20) Shao, C.; Chang, H.; Wang, M.; Xu, F.; Yang, J. High-Strength, Tough, and Self-Healing Nanocomposite Physical Hydrogels Based on the Synergistic Effects of Dynamic Hydrogen Bond and Dual Coordination Bonds. *ACS Appl. Mater. Interfaces* **2017**, *9* (34), 28305–28318.

(21) Li, X.; Li, R.; Liu, Z.; Gao, X.; Long, S.; Zhang, G. Integrated Functional High-Strength Hydrogels with Metal-Coordination Complexes and H-Bonding Dual Physically Cross-Linked Networks. *Macromol. Rapid Commun.* **2018**, *39* (23), 1–8.

(22) Fan, H.; Wang, J.; Jin, Z. Tough, Swelling-Resistant, Self-Healing, and Adhesive Dual-Cross-Linked Hydrogels Based on Polymer-Tannic Acid Multiple Hydrogen Bonds. *Macromolecules* **2018**, *51* (5), 1696–1705.

(23) Liu, T.; Zou, S.; Hang, C.; Li, J.; Di, X.; Li, X.; Wu, Q.; Wang, F.; Sun, P. Mechanically Strong and Tough Hydrogels with PH-Triggered Self-Healing and Shape Memory Properties Based on a Dual Physically Crosslinked Network. *Polym. Chem.* **2020**, *11* (11), 1906–1918.

(24) Zhou, H.; Jin, X.; Yan, B.; Li, X.; Yang, W.; Ma, A.; Zhang, X.; Li, P.; Ding, X.; Chen, W. Mechanically Robust, Tough, and Self-Recoverable Hydrogels with Molecularly Engineered Fully Flexible Crosslinking Structure. *Macromol. Mater. Eng.* **2017**, *302* (9), 1700085.

(25) Zhao, X. Multi-Scale Multi-Mechanism Design of Tough Hydrogels: Building Dissipation into Stretchy Networks. *Soft Matter* **2014**, *10* (5), 672–687.

(26) Zhang, Y. S.; Khademhosseini, A. Advances in Engineering Hydrogels. *Science* **2017**, *356* (6337), eaaf3627.

(27) Fan, H.; Gong, J. P. Fabrication of Bioinspired Hydrogels: Challenges and Opportunities. *Macromolecules* **2020**, *53* (8), 2769–2782.
(28) Norioka, C.; Inamoto, Y.; Hajime, C.; Kawamura, A.; Miyata, T. A Universal Method to Easily Design Tough and Stretchable Hydrogels. *NPG Asia Mater.* **2021**, *13* (1), 34.
(29) Loveless, D. M.; Jeon, S. L.; Craig, S. L. Rational Control of Viscoelastic Properties in Multicomponent Associative Polymer Networks. *Macromolecules* **2005**, *38* (24), 10171–10177.
(30) Yount, W. C.; Loveless, D. M.; Craig, S. L. Strong Means Slow: Dynamic Contributions to the Bulk Mechanical Properties of Supramolecular Networks. *Angew. Chemie - Int. Ed.* **2005**, *44* (18), 2746–2748.
(31) Yount, W. C.; Loveless, D. M.; Craig, S. L. Small-Molecule Dynamics and Mechanisms Underlying the Macroscopic Mechanical Properties of Coordinatively Cross-Linked Polymer Networks. *J. Am. Chem. Soc.* **2005**, *127* (41), 14488–14496.
(32) Serpe, M. J.; Craig, S. L. Physical Organic Chemistry of Supramolecular Polymers. *Langmuir* **2007**, *23* (4), 1626–1634.
(33) Seiffert, S.; Sprakel, J. Physical Chemistry of Supramolecular Polymer Networks. *Chem. Soc. Rev.* **2012**, *41* (2), 909–930.
(34) Tan, C. S. Y.; Agmon, G.; Liu, J.; Hoogland, D.; Janeček, E. R.; Appel, E. A.; Scherman, O. A. Distinguishing Relaxation Dynamics in Transiently Crosslinked Polymeric Networks. *Polym. Chem.* **2017**, *8* (35), 5336–5343.
(35) Aramoto, H.; Osaki, M.; Konishi, S.; Ueda, C.; Kobayashi, Y.; Takashima, Y.; Harada, A.; Yamaguchi, H. Redox-Responsive Supramolecular Polymeric Networks Having Double-Threaded Inclusion Complexes. *Chem. Sci.* **2020**, *11* (17), 4322–4331.
(36) Konishi, S.; Kashiwagi, Y.; Watanabe, G.; Osaki, M.; Katashima, T.; Urakawa, O.; Inoue, T.; Yamaguchi, H.; Harada, A.; Takashima, Y. Design and Mechanical Properties of Supramolecular Polymeric Materials Based on Host-Guest Interactions: The Relation between Relaxation Time and Fracture Energy. *Polym. Chem.* **2020**, *11* (42), 6811–6820.
(37) Ahmadi, M.; Seiffert, S. Dynamic Model Metallo-Supramolecular Dual-Network Hydrogels with Independently Tunable Network Crosslinks. *J. Polym. Sci.* **2020**, *58* (2), 330–342.
(38) Menyo, M. S.; Hawker, C. J.; Waite, J. H. Rate-Dependent Stiffness and Recovery in Interpenetrating Network Hydrogels through Sacrificial Metal Coordination Bonds. *ACS Macro Lett.* **2015**, *4* (11), 1200–1204.
(39) Grindy, S. C.; Learsch, R.; Mozhdehi, D.; Cheng, J.; Barrett, D. G.; Guan, Z.; Messersmith, P. B.; Holten-Andersen, N. Control of Hierarchical Polymer Mechanics with Bioinspired Metal-Coordination Dynamics. *Nat. Mater.* **2015**, *14* (12), 1210–1216.
(40) Yesilyurt, V.; Ayoob, A. M.; Appel, E. A.; Borenstein, J. T.; Langer, R.; Anderson, D. G. Mixed Reversible Covalent Crosslink Kinetics Enable Precise, Hierarchical Mechanical Tuning of Hydrogel Networks. *Adv. Mater.* **2017**, *29* (19), 1–6.
(41) Ahmadi, M.; Seiffert, S. Thermodynamic Control over Energy Dissipation Modes in Dual-Network Hydrogels Based on Metal-Ligand Coordination. *Soft Matter* **2020**, *16* (9), 2332–2341.
(42) Li, H.; Liu, F.; Li, Z.; Wang, S.; Jin, R.; Liu, C.; Chen, Y. Fingerprintable Hydrogel from Dual Reversible Cross-Linking Networks with Different Relaxation Times. *ACS Appl. Mater. Interfaces* **2019**, *11* (19), 17925–17930.
(43) Zhang, R.; Zhang, C.; Yang, Z.; Wu, Q.; Sun, P.; Wang, X. Hierarchical Dynamics in a Transient Polymer Network Cross-Linked by Orthogonal Dynamic Bonds. *Macromolecules* **2020**, *53* (14), 5937–5949.
(44) Kong, H. J.; Wong, E.; Mooney, D. J. Independent Control of Rigidity and Toughness of Polymeric Hydrogels. *Macromolecules* **2003**, *36* (12), 4582–4588.
(45) Sun, T. L.; Kurokawa, T.; Kuroda, S.; Ihsan, A. Bin; Akasaki, T.; Sato, K.; Haque, M. A.; Nakajima, T.; Gong, J. P. Physical Hydrogels Composed of Polyampholytes Demonstrate High Toughness and Viscoelasticity. *Nat. Mater.* **2013**, *12* (10), 932–937.
(46) Mayumi, K.; Marcellan, A.; Ducouret, G.; Creton, C.; Narita, T. Stress-Strain Relationship of Highly Stretchable Dual Cross-Link Gels: Separability of Strain and Time Effect. *ACS Macro Lett.* **2013**, *2* (12), 1065–1068.
(47) Bose, R. K.; Hohlbein, N.; Garcia, S. J.; Schmidt, A. M.; Van Der Zwaag, S. Connecting Supramolecular Bond Lifetime and Network Mobility for Scratch Healing in Poly(Butyl Acrylate) Ionomers Containing Sodium, Zinc and Cobalt. *Phys. Chem. Chem. Phys.* **2015**, *17* (3), 1697–1704.
(48) Long, R.; Mayumi, K.; Creton, C.; Narita, T.; Hui, C. Y. Time Dependent Behavior of a Dual Cross-Link Self-Healing Gel: Theory and Experiments. *Macromolecules* **2014**, *47* (20), 7243–7250.
(49) Hu, X.; Zhou, J.; Daniel, W. F. M.; Vatankhah-Varnoosfaderani, M.; Dobrynin, A. V.; Sheiko, S. S. Dynamics of Dual Networks: Strain Rate and Temperature Effects in Hydrogels with Reversible H-Bonds. *Macromolecules* **2017**, *50* (2), 652–659.

(50) Chen, H.; Zhang, J.; Yu, W.; Cao, Y.; Cao, Z.; Tan, Y. Control Viscoelasticity of Polymer Networks with Crosslinks of Superposed Fast and Slow Dynamics. *Angew. Chemie - Int. Ed.* **2021**, *60* (41), 22332–22338.
(51) Li, Y.; Zhu, C.; Dong, Y.; Liu, D. Supramolecular Hydrogels: Mechanical Strengthening with Dynamics. *Polymer* **2020**, *210* (June), 122993.
(52) Takashima, Y.; Otani, K.; Kobayashi, Y.; Aramoto, H.; Nakahata, M.; Yamaguchi, H.; Harada, A. Mechanical Properties of Supramolecular Polymeric Materials Formed by Cyclodextrins as Host Molecules and Cationic Alkyl Guest Molecules on the Polymer Side Chain. *Macromolecules* **2018**, *51* (16), 6318–6326.
(53) Takashima, Y.; Sawa, Y.; Iwaso, K.; Nakahata, M.; Yamaguchi, H.; Harada, A. Supramolecular Materials Cross-Linked by Host-Guest Inclusion Complexes: The Effect of Side Chain Molecules on Mechanical Properties. *Macromolecules* **2017**, *50* (8), 3254–3261.
(54) Kakuta, T.; Takashima, Y.; Nakahata, M.; Otsubo, M.; Yamaguchi, H.; Harada, A. Preorganized Hydrogel: Self-Healing Properties of Supramolecular Hydrogels Formed by Polymerization of Host-Guest-Monomers That Contain Cyclodextrins and Hydrophobic Guest Groups. *Adv. Mater.* **2013**, *25* (20), 2849–2853.
(55) Herrmann, W.; Keller, B.; Wenz, G. Kinetics and Thermodynamics of the Inclusion of Ionene-6,10 in α-Cyclodextrin in an Aqueous Solution. *Macromolecules* **1997**, *30* (17), 4966–4972.
(56) Szejtli, J. Introduction and General Overview of Cyclodextrin Chemistry. *Chem. Rev.* **1998**, *98* (5), 1743–1753.
(57) Harada, A. *Supramolecular Polymer Chemistry*; Wiley-VCH: Weinheim, 2012.
(58) Harada, A.; Takashima, Y.; Nakahata, M. Supramolecular Polymeric Materials via Cyclodextrin-Guest Interactions. *Acc. Chem. Res.* **2014**, *47* (7), 2128–2140.
(59) Schmidt, B. V. K. J.; Barner-Kowollik, C. Dynamic Macromolecular Material Design—The Versatility of Cyclodextrin-Based Host–Guest Chemistry. *Angew. Chemie - Int. Ed.* **2017**, *56* (29), 8350–8369.
(60) Sinawang, G.; Osaki, M.; Takashima, Y.; Yamaguchi, H.; Harada, A. Supramolecular Self-Healing Materials from Non-Covalent Cross-Linking Host-Guest Interactions. *Chem. Commun.* **2020**, *56* (32), 4381–4395.
(61) Sinawang, G.; Osaki, M.; Takashima, Y.; Yamaguchi, H.; Harada, A. Biofunctional Hydrogels Based on Host–Guest Interactions. *Polym. J.* **2020**, *52* (8), 839–859.
(62) Xia, D.; Wang, P.; Ji, X.; Khashab, N. M.; Sessler, J. L.; Huang, F. Functional Supramolecular Polymeric Networks: The Marriage of Covalent Polymers and Macrocycle-Based Host-Guest Interactions. *Chem. Rev.* **2020**, *120* (13), 6070–6123.
(63) Saito, H.; Yonemura, H.; Nakamura, H.; Matsuo, T. Stability and Exchange Properties of Through-Ring Cyclodextrin Complexes. Effects of Chain Length in Polymethylene Bis[1-Pyridinium] as Guest Molecules. *Chemistry Letters*. 1990, pp 535–538.
(64) Yonemura, H.; Kasahara, M.; Saito, H.; Nakamura, H.; Matsuo, T. Spectroscopic Studies on Exchange Properties in Through-Ring Cyclodextrin Complexes of Carbazole-Viologen Linked Compounds: Effects of Spacer Chain Length. *J. Phys. Chem.* **1992**, *96* (14), 5765–5770. 1.
(65) Kawaguchi, Y.; Harada, A. An Electric Trap: A New Method for Entrapping Cyclodextrin in a Rotaxane Structure. *J. Am. Chem. Soc.* **2000**, *122* (15), 3797–3798.
(66) Kawaguchi, Y.; Harada, A. A Cyclodextrin-Based Molecular Shuttle Containing Energetically Favored and Disfavored Portions in Its Dumbbell Component. *Org. Lett.* **2000**, *2* (10), 1353–1356.
(67) Kashiwagi, Y.; Katashima, T.; Nakahata, M.; Takashima, Y.; Harada, A.; Inoue, T. Linear Viscoelastic Studies on a Transient Network Formed by Host–Guest Interaction. *J. Polym. Sci. Part B Polym. Phys.* **2018**, *56* (15), 1109–1117.
(68) Leibler, L.; Rubinstein, M.; Colby, R. H. Dynamics of Reversible Networks. *Macromolecules* **1991**, *24* (16), 4701–4707.
(69) Zhao, X.; Chen, X.; Yuk, H.; Lin, S.; Liu, X.; Parada, G. Soft Materials by Design: Unconventional Polymer Networks Give Extreme Properties. *Chem. Rev.* **2021**, *121* (8), 4309–4372.
(70) Lake G. J.; Thomas A. G. The Strength of Highly Elastic Materials. *Proc. R. Soc. London, Ser. A* **1967**, *300* (1460), 108–119.

Appendix

The dependence of hysteresis properties of the αCD-PyC11 (2, 2) hydrogels on tensile speed.

As shown in **Figure 3-16**, hysteresis areas and ratios of the αCD-R (2, 2) and αCD-R_1-R_2 (2, 1, 1) hydrogels varied with the relaxation times of cross-links. Thus, intuitively, the dynamics and hysteresis properties would be also sensitive to strain rate. Although control of constant strain rate is desirable to discuss the sensitivity of bond dynamics, the author cannot perform such control due to the limitation of instrument performance.

However, the author instead performed additional hysteresis tests of the αCD-PyC11 (2, 2) hydrogel at different tensile speeds (0.1, 1.0, and 10 mm/s) for a fixed maximum strain. The maximum strains were set to 122%, 244%, 366%, 488%, and 610%. Note that the number of cycles at a tensile speed of 0.1 mm/s was limited to 3 cycles due to long test time and drying. **Figure 3-A1** shows the results of hysteresis areas and hysteresis ratios. They varied with tensile speed. The hysteresis area of the αCD-PyC11 (2, 2) hydrogel monotonically increased with tensile speed. This order was in accord with that of toughness at different tensile speeds in the Chapter 2, supporting the result in **Figure 3-16b**.

Hysteresis ratio at 0.1 mm/s tensile speed was entirely lower than that at 1 mm/s. This is because the motion of αCD-PyC11 cross-links became more viscous at every cycle, which decreased the ability to dissipate energy. Interestingly, the result at 0.1 mm/s was similar to the hysteresis ratio of the αCD-ImC11 (2, 2) hydrogel at 1.0 mm/s in **Figure 3-16b**. This correspondence supports the relation between viscoelastic behavior of reversible αCD-R cross-links and energy dissipation performance of the αCD-R (2, 2) hydrogels. On the other hand, hysteresis ratios of the αCD -PyC11 (2, 2) hydrogel at 10 mm/s were entirely intermediate. It slightly increased from the first to third cycles, and then slightly decreased from the fourth cycle. The reason for the former is that the αCD-PyC11 cross-links acted as a more elastic body at a tensile speed of 10 mm/s, which decreased the former hysteresis ratio. By contrast, the αCD-PyC11 cross-links can act as a viscoelastic body even in latter cycles due to high tensile speed. This should keep the intermediate hysteresis ratio from the third to fifth cycles.

Hysteresis tests of the αCD-PyC11 (2, 2) hydrogels at different tensile speeds for a fixed maximum strain indicated the effect of viscoelastic behavior of the αCD-R cross-links on energy dissipation performance, which supports the importance to design dynamics for tough materials. However, the author did not add these results at different tensile speeds to the Results and Discussion sections because they would require a more profound discussion.

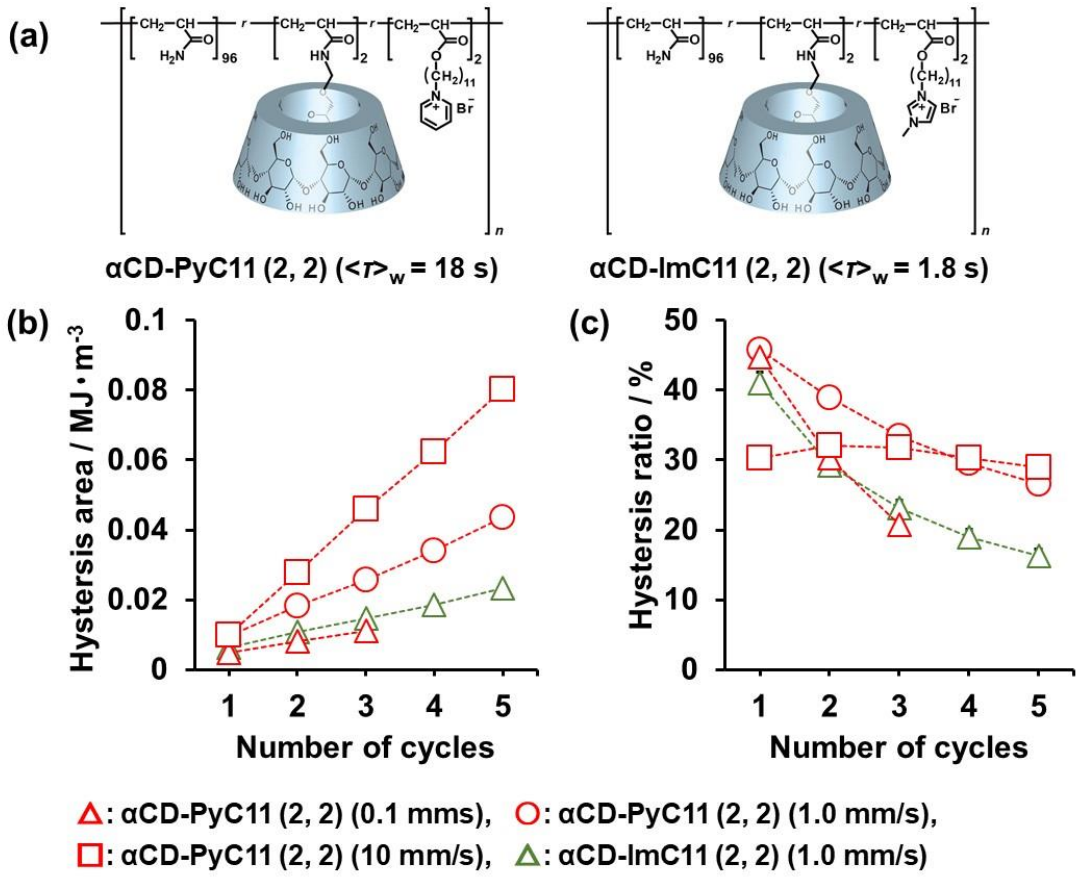

Figure 3-A1. (a) Chemical structures of the αCD-PyC11 (2, 2) and αCD-ImC11 (2, 2) hydrogels. **(b)** Hysteresis areas and **(c)** hysteresis ratios at each cycle of the αCD-PyC11 (2, 2) hydrogels at different tensile speeds (0.1, 1.0, 10 mm/s).

Chapter 4

A Universal Relation between the Relaxation Time and Toughness of Supramolecular Hydrogels cross-linked by Host-Guest Complexations or Metal-Ligand Coordination

4.1. Introduction

In Chapters 2 and 3, the author investigated the effect of relaxation time on the mechanical properties of supramolecular hydrogels cross-linked by host-guest complexations. The viscoelastic behavior of reversible cross-links when the relaxation time matched the initial strain rate was found to be important for toughening of the hydrogels. Such a relation among the dynamics, deformation rate, and macroscopic mechanical behavior of hydrogels has been observed in other studies, including studies of supramolecular hydrogels cross-linked by CB[7][1] and dual cross-link hydrogels.[2,3] Therefore, the author aimed to verify the universality of the concept using supramolecular hydrogels cross-linked by other non-covalent bonds.

The author focused on metal-ligand coordination. As shown in **Figure 1-1** in Chapter 1, metal-ligand coordination bonds have higher association constants (K_a) and binding energies than host-guest complexations. Furthermore, the kinetics of coordination bonds vary widely depending on the structures of the metals, ligands, neighboring ligands, and counterions as well as the external conditions (temperature, pH, light, solvent). For example, the exchange rate constants (k_{ex}) of a water molecule in the first coordination sphere of a metal span 18 orders of magnitude (k_{ex} = 10^{-9}~10^{9} s^{-1}).[4] Therefore, the dynamics of supramolecular polymeric materials have been controlled using the kinetics of different metal-ligand coordination bonds across broad timescales.[5–10] On the other hand, the reversibility of coordination bonds has been incorporated into polymers to develop functional materials with high toughness,[11–14] self-healing,[15–18] and stimulus-responsiveness.[19–21] However, the effects of coordination bonds on linear viscoelasticity or macroscopic nonlinear functionalities are often explored separately. Associating macroscopic properties such as toughness and self-healing with linear mechanical properties is desirable to achieve a fundamental understanding of the role of coordination bonds.[22,23]

In this chapter, the author aimed to expand the relation between linear viscoelasticity and toughness, which was observed in supramolecular hydrogels cross-linked by host-guest complexations, to hydrogels cross-linked by metal-ligand coordination bonds (**Figure 4-1**). To

design reversible cross-links with different dynamics, the author utilized coordination complexes of 5-acrylamidomethyl-5′-methyl-2,2′-bipyridine (BpyAAm) with several transitional metal ions. BpyAAm is a bidentate ligand monomer with a 2,2′-bipyridyl structure. The author prepared supramolecular hydrogels cross-linked by the metal complexes of the 2,2′-bipyridyl units, and assessed their mechanical properties and linear viscoelasticity. Finally, the author compared hydrogels cross-linked by coordination bonds and those cross-linked by host-guest complexations to discuss how the kinetics of non-covalent bonds generally affect the toughness of polymeric materials.

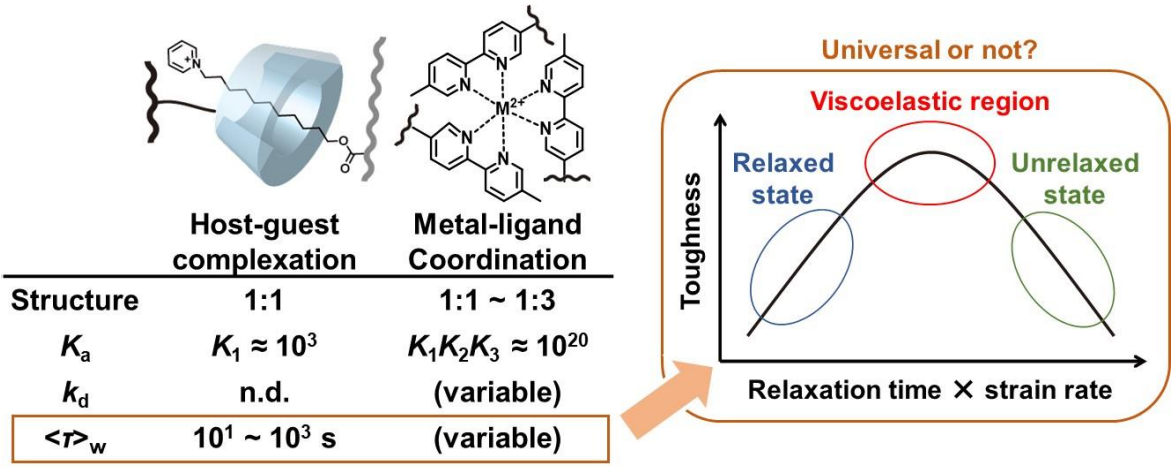

Figure 4-1. Conceptual figure for Chapter 4. The comparison of supramolecular hydrogels cross-linked by host-guest complexations and metal-ligand coordination.

4.2. Experimental

Materials

Acrylamide (AAm), and iron(II) chloride tetrahydrate were purchased from Wako Pure Chemical Industries, Ltd. Methanol, potassium peroxodisulfate (KPS), *N,N,N′,N′*–tetramethylethylenediamine (TEMED), nickel(II) chloride hexahydrate, and zinc(II) chloride were purchased from Nacalai Tesque Inc. IRGACURE 184 was purchased from Tokyo Kasei. The water used for preparing aqueous solutions was purified with a Millipore Elix 5 system. Other reagents were used without further purification. 5-Acrylamidomethyl-5′-methyl-2,2′-bipyridine (BpyAAm) was prepared according to a previous report and provided by Assistant Professor Dr. Nakamura at the University of Tsukuba (**Figure 4-2**).[24]

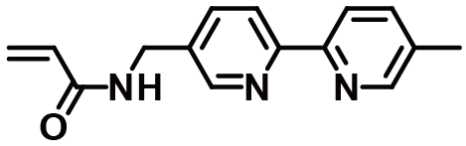

Figure 4-2. Chemical structure of 5-acrylamidomethyl-5′-methyl-2,2′-bipyridine (BpyAAm).

Measurements

Tensile tests: Tensile tests were performed on a universal testing machine [Autograph AG-X plus (Shimadzu Co.)] equipped with a 20 N load cell and 1 N clip grips. The hydrogels were prepared using a type 4 dumbbell-shaped Teflon mold by following the ISO 37 (JIS K6251) standard. Conditions for tensile tests and definitions of toughness and Young's modulus were the same as described in Chapter 2. The error bars (standard deviation) for toughness and the Young's modulus were calculated from the results of more than three experiments.

Rheological measurements: Dynamic viscoelasticity and stress-relaxation properties were measured using an Anton Paar MCR302 rheometer with a parallel-plate fixture (8 mm in diameter). An angular frequency (ω) sweep from 0.1 to 100 rad/s was performed using a parallel-plate fixture with 8 mm in diameter over a temperature range of 0–45 °C. Stress-relaxation tests were performed at 25 °C. The oscillatory shear strain (γ) induced in both ω sweep and stress-relaxation tests was within the range of linear viscoelasticity. Details of the analysis method are described in the below Results section.

4.2.1. Preparation of the metal-ligand complexes of transition metals with BpyAAm

The author complexed transition metals (M^{2+} = Fe^{2+}, Ni^{2+}, Zn^{2+}) with BpyAAm to prepare water-soluble cross-links (**Schemes 4-1–4-3**). Although BpyAAm is insoluble in water, its complexes with metals are soluble in water. Chloride ions (Cl^-) were chosen as the counter anions to the metals. The above transition metals can form 1:1, 1:2, or 1:3 complexes with 2,2′-bipyridyl moieties with high association constants (K_a) (**Table 4-1**).[24] In this study, 1:3 complexes ($[M^{2+}(BpyAAm)_3]Cl_2$) were prepared.

Table 4-1. Association constants of 2,2′-bipyridyl and transition metal ions from the literature.[24] (H_2O, 25 °C, 0.1 mol/L Cl^-, NO_3^-, or ClO_4^-)

Metal ions	log K_1	log K_2	log K_3
Fe^{2+}	**4.2**	**3.7**	**9.55**
Ni^{2+}	**8.2**	**6.8**	**6.4**
Zn^{2+}	**4.3**	**4.5**	**3.7**

Preparation of $[Fe(BpyAAm)_3]Cl_2$

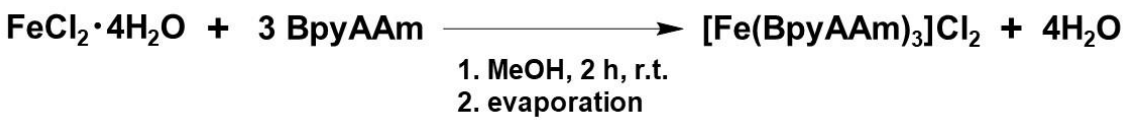

Scheme 4-1. Preparation of $[Fe(BpyAAm)_3]Cl_2$.

Iron(II) chloride tetrahydrate ($FeCl_2 \cdot 4H_2O$; 14.4 mg, 72 μmol, 1 eq.) and BpyAAm (55.0 mg, 217 μmol, 3 eq.) were dissolved in methanol (15 mL), and the mixture was stirred for 2 hours at r.t. The reaction mixture was concentrated to dryness under reduced pressure. After drying under vacuum at 60 °C for 24 hours, the product $[Fe(BpyAAm)_3]Cl_2$ complex was obtained as a mulberry solid (63.6 mg, 99%).

Preparation of $[Ni(BpyAAm)_3]Cl_2$

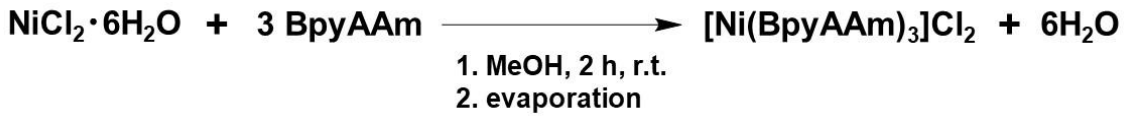

Scheme 4-2. Preparation of $[Ni(BpyAAm)_3]Cl_2$.

Nickel(II) chloride hexahydrate ($NiCl_2 \cdot 6H_2O$; 16.7 mg, 70 μmol, 1 eq.) and BpyAAm (53.4 mg, 210 μmol, 3 eq.) were dissolved in methanol (15 mL), and the mixture was stirred for 2 hours at r.t. The reaction mixture was concentrated to dryness under reduced pressure. After drying under vacuum at 60 °C for 24 hours, the product $[Ni(BpyAAm)_3]Cl_2$ complex was obtained as a pale orange solid (61.8 mg, 99%).

Preparation of $[Zn(BpyAAm)_3]Cl_2$

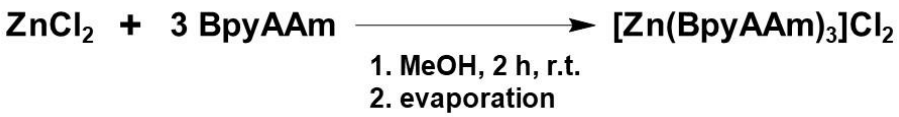

Scheme 4-3. Preparation of the $[Zn(BpyAAm)_3]Cl_2$.

Zinc(II) chloride ($ZnCl_2$; 10.0 mg, 73 μmol, 1 eq.) and BpyAAm (55.7 mg, 220 μmol, 3 eq.) were dissolved in methanol (15 mL), and the mixture was stirred for 2 hours at r.t. The reaction mixture was concentrated to dryness under reduced pressure. After drying under vacuum at 60 °C for 24 hours, the product $[Zn(BpyAAm)_3]Cl_2$ complex was obtained as a colorless ~ pale orange solid (67.6 mg, 102%*).

*: 1 mol% of methanol or hydrate water may remain in the product.

4.2.2. Preparation of the pAAm-M^{2+}(Bpy)$_3$ hydrogels

Supramolecular hydrogels cross-linked by metal-ligand coordination bonds were obtained by free radical copolymerization of acrylamide and $[M(BpyAAm)_3]Cl_2$ monomers with a redox initiator system in water (**Schemes 4-4–4-6**). Acrylamide main monomer (AAm; 97 mol%), $[M(BpyAAm)_3]Cl_2$ monomer (1 mol% = 3 mol% BpyAAm), and potassium peroxodisulfate (KPS; 1 mol%) were dissolved in deionized water. The total concentration of the monomers was set to 2 mol/L. After 1.0 mol% of *N*,*N*,*N*′,*N*′-tetramethylethylenediamine (TEMED) was added, the aqueous solution was shaken quickly and poured into a mold to start gelation. The solution gelated within 10 minutes to afford a self-standing hydrogel.

Preparation of the pAAm-Fe(Bpy)$_3$ hydrogel

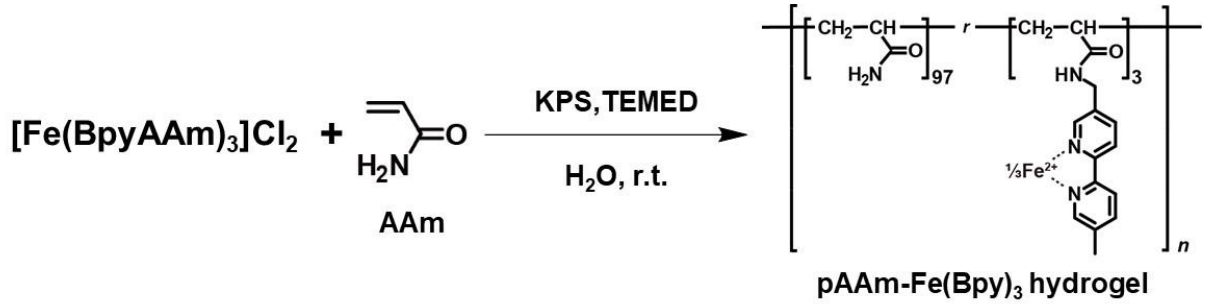

Scheme 4-4. Preparation of the pAAm-Fe(Bpy)$_3$ hydrogel.

$[Fe(BpyAAm)_3]Cl_2$ (21.3 mg, 24 μmol, 1 mol%), AAm (165.5 mg, 2328 μmol, 97 mol%), and KPS (6.5 mg, 24 μmol) were dissolved in water (1.2 mL, total monomer concentration: 2.0 M). TEMED (3.6 μL, 24 μmol) was added to the solution, and then the solution gelated in approximately 15 seconds to afford a mulberry hydrogel. However, due to the rapid gelation, it was difficult to pour the solution into a Teflon mold. Details of the reagents and solutions are presented in **Table 4-2**.

Table 4-2. Amounts of reagents and solvents used in the preparation of the pAAm-Fe(Bpy)$_3$ hydrogel.

	water /mL	AAm /mg	$[Fe(BpyAAm)_3]Cl_2$ /mg	KPS /mg	TEMED /μL
pAAm-Fe(Bpy)$_3$ hydrogel	1.2	165	21.3	6.5	3.6

Preparation of the pAAm-Ni(Bpy)$_3$ hydrogel

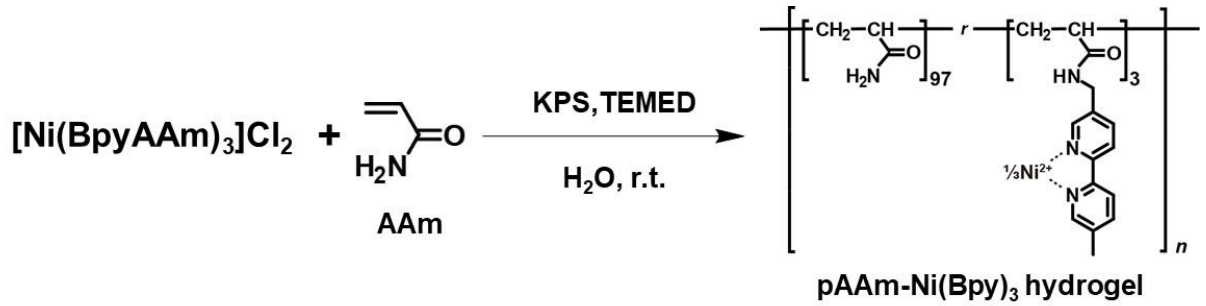

Scheme 4-5. Preparation of the pAAm-Ni(Bpy)$_3$ hydrogel.

[Ni(BpyAAm)$_3$]Cl$_2$ (21.3 mg, 24 μmol, 1 mol%), AAm (165.5 mg, 2328 μmol, 97 mol%), and KPS (6.5 mg, 24 μmol) were dissolved in water (1.2 mL, total monomer concentration: 2.0 M). TEMED (3.6 μL, 24 μmol) was added to the solution. The solution was shaken by a vortex-genie2 for a few seconds and poured into a dumbbell-shaped Teflon mold at r.t. The solution gelated within 10 minutes to afford a pale orange hydrogel. Details of the reagents and solutions are presented in **Table 4-3**.

Table 4-3. Amounts of reagents and solvents used in the preparation of the pAAm-Ni(Bpy)$_3$ hydrogel.

	water /mL	AAm /mg	[Ni(BpyAAm)$_3$]Cl$_2$ /mg	KPS /mg	TEMED /μL
pAAm-Ni(Bpy)$_3$ hydrogel	1.2	165	21.3	6.5	3.6

Preparation of the pAAm-Zn(Bpy)$_3$ hydrogel

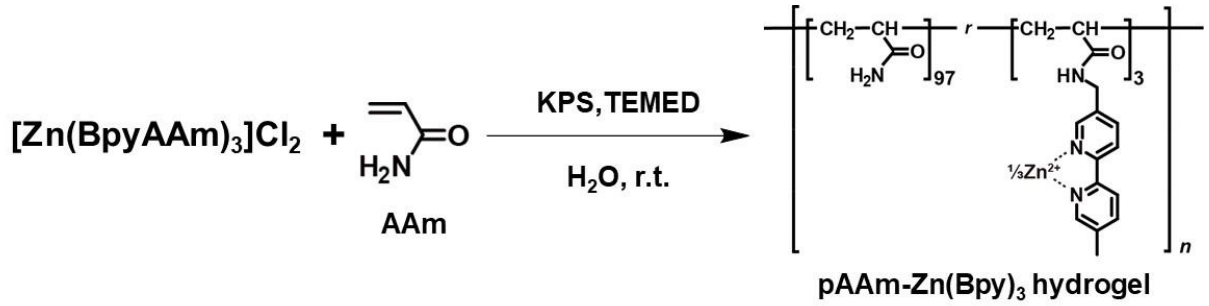

Scheme 4-6. Preparation of the pAAm-Zn(Bpy)$_3$ hydrogel.

[Zn(BpyAAm)$_3$]Cl$_2$ (21.5 mg, 24 μmol, 1 mol%) and AAm (165.5 mg, 2328 μmol, 97 mol%) were dissolved in water (1.2 mL, total monomer concentration: 2.0 M). The addition of KPS (6.5 mg, 24 μmol) to the solution afforded a white suspension. TEMED (3.6 μL, 24 μmol) was added to the suspension. The suspension was shaken by a vortex-genie2 for a few seconds and poured into a dumbbell-shaped Teflon mold at r.t. The solution gelated within 10 minutes to afford a slightly opaque hydrogel. Details of the reagents and solutions are presented in **Table 4-4**.

Table 4-4. Amounts of reagents and solvents used in the preparation of the pAAm-Zn(Bpy)$_3$ hydrogel.

	water /mL	AAm /mg	[Zn(BpyAAm)$_3$]Cl$_2$ /mg	KPS /mg	TEMED /μL
pAAm-Zn(Bpy)$_3$ hydrogel	1.2	165	21.5	6.5	3.6

4.2.3. Preparation of the pDMAA-Fe-Bpy hydrogels

Preparation of the pDMAA-BpyAAm (1) elastomer

As described in Section 4.2.2, copolymerization of AAm and $[Fe(BpyAAm)_3]Cl_2$ monomers using a redox system occurred rapidly, which made it difficult to prepare molded hydrogels for tensile and viscoelastic measurements. Instead, the author synthesized a precursor elastomer for the preparation of a purpose-designed hydrogel. Photoinduced bulk copolymerization of *N*,*N*-dimethylacrylamide (DMAA) and BpyAAm was performed to obtain the pDMAA-BpyAAm (1) elastomer (**Scheme 4-7**).

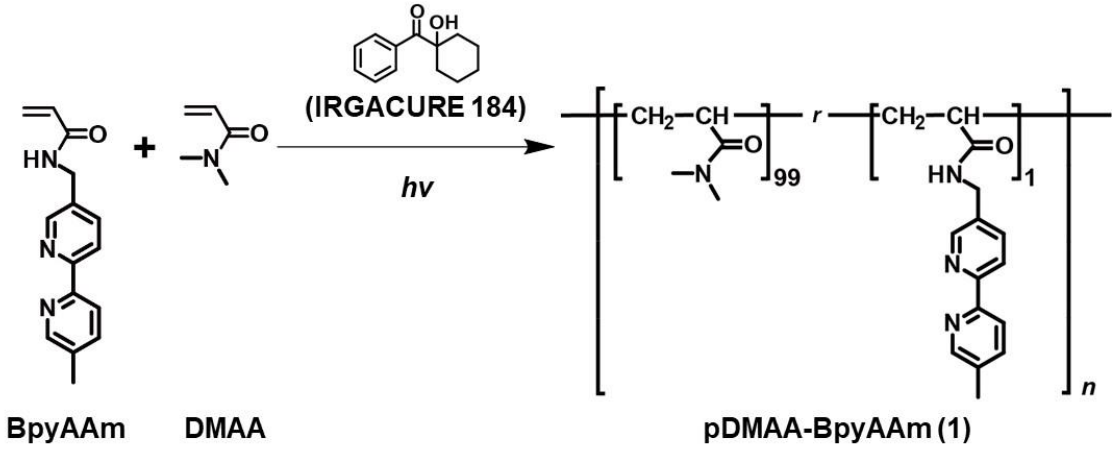

Scheme 4-7. Preparation of the pDMAA-BpyAAm (1) elastomer.

BpyAAm (25.6 mg, 0.10 mmol, 1 mol%) and IRGACURE 184 (20.0 mg, 0.10 mmol) were dissolved in *N*,*N*-dimethylacrylamide (DMAA; 970 mg, 9.78 mmol, 99 mol%). Free radical bulk copolymerization was carried out by UV irradiation with a Hg lamp for 1 hour to generate an elastomer.

Preparation of the pDMAA-Fe-Bpy hydrogel

To prepare a sheet-like hydrogel suitable for tensile and viscoelastic measurements, the pDMAA-Bpy (1) elastomer was swollen in 5 mM $FeCl_2$ aq. for 3 days to load Fe^{2+} ions, followed by swelling in water for 4 days to remove excess Fe^{2+} ions (**Figure 4-3**). The pDMAA-BpyAAm (1) elastomer became red soon after immersion in FeCl aq., indicating the formation of the tris(Bpy) complex $[Fe(Bpy)_3]^{2+}$. The pDMAA-Fe-Bpy hydrogel maintained its red color after immersion in water, indicating that the $[Fe(Bpy)_3]^{2+}$ complexes remained. The elastomer and hydrogel continued to swell in both $FeCl_2$ aq. and water.

Table 4-5 shows the changes in the state and weight of the pDMAA-Bpy elastomer and pDMAA-Fe-Bpy hydrogel. Finally, the swollen pDMAA-Fe-Bpy hydrogel was very soft and fragile but in good shape. Then, the water content of the hydrogel reached 98.8 wt%. Although the amount of Fe^{2+} introduced to the final hydrogel could not be estimated, the equivalent ratio of Fe^{2+} to the Bpy moieties should be no more than 1.3 eq. Therefore, considering the high association constant of the $Fe(Bpy)_3$ complex ($K_3 = 10^{9.5}$ $M^{-1} \gg K_1$, K_2 in **Table 4-1**),[24] most of the Bpy moieties formed $Fe(Bpy)_3$ complexes in the hydrogel after swelling in water.

Before the viscoelastic measurements, the water contents (W_c) of the swollen pDMAA-Fe-Bpy hydrogel were tuned using a moisture analyzer (heating type moisture analyzer MS-70, AND Co., Ltd.). The swollen hydrogels were heated at 70 °C, dried to a specific weight, and left overnight prior to the measurements. W_c was tuned to approximately 97 and 90 wt%.

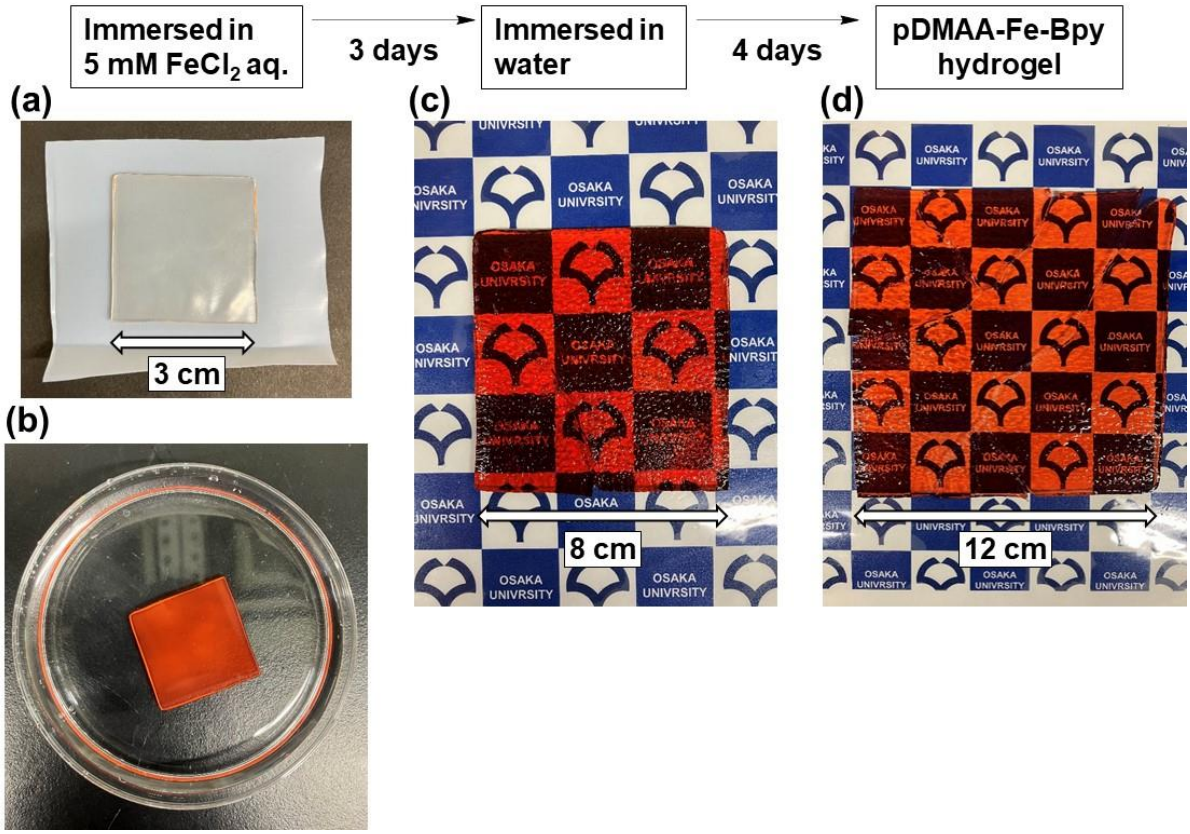

Figure 4-3. Preparation of the pDMAA-Fe-Bpy hydrogel by immersing the elastomer in $FeCl_2$ aq. and water. **(a)** The pDMAA-Bpy elastomer prepared by bulk polymerization. **(b)** The elastomer soon after immersion in $FeCl_2$ aq. (c) The hydrogel three days after swelling in $FeCl_2$ aq. **(d)** The hydrogel four days after swelling in water.

Table 4-5. Changes in the state and weight of the pDMAA-Bpy elastomer and pDMAA-Fe-Bpy hydrogel.

Sample	State	Weight / g	Water content / wt%	Predicted introduction of Fe^{2+} / mmol
(a) Elastomer	–	1.06	n.d.	–
(b) Hydrogel	3 days in $FeCl_2$ aq.	27.20	96.1	0.131* (1.3 eq. to Bpy)
(c) Hydrogel	4 days in water	85.96	98.8	n.d.

*: Introduction of Fe^{2+} was estimated from the amount of absorbed 5 mM $FeCl_2$ aq.

4.3. Results and discussion

4.3.1. Mechanical properties of the pAAm-$M^{2+}(Bpy)_3$ hydrogels.

Uniaxial tensile tests (tensile speed = 1.0 mm/s, room temperature = approximately 25 °C) were performed to evaluate the mechanical properties of the pAAm-Ni$(Bpy)_3$ and pAAm-Zn$(Bpy)_3$ hydrogels (**Figure 4-4**). The toughness of the hydrogels was calculated from the integral of the stress–strain curves, and the Young's modulus was calculated from the initial slope of the curves. **Figure 4-5** shows the plots of the toughness and Young's modulus of these hydrogels compared with the αCD-R (2, 2) and αCD-R_1-R_2 (2, 1, 1) hydrogels described in Chapter 3.

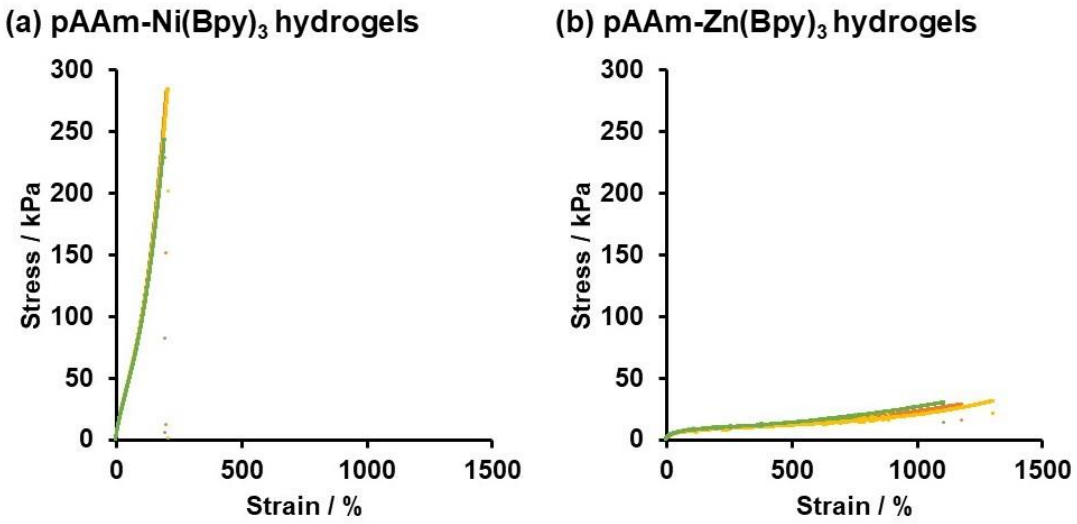

Figure 4-4. Stress–strain curves of the pAAm-$M^{2+}(Bpy)_3$ hydrogels at 25 °C at a tensile rate of 1.0 mm/s. **(a)** pAAm-Ni$(Bpy)_3$ hydrogel (n = 3), **(b)** pAAm-Zn$(Bpy)_3$ hydrogel (n = 3).

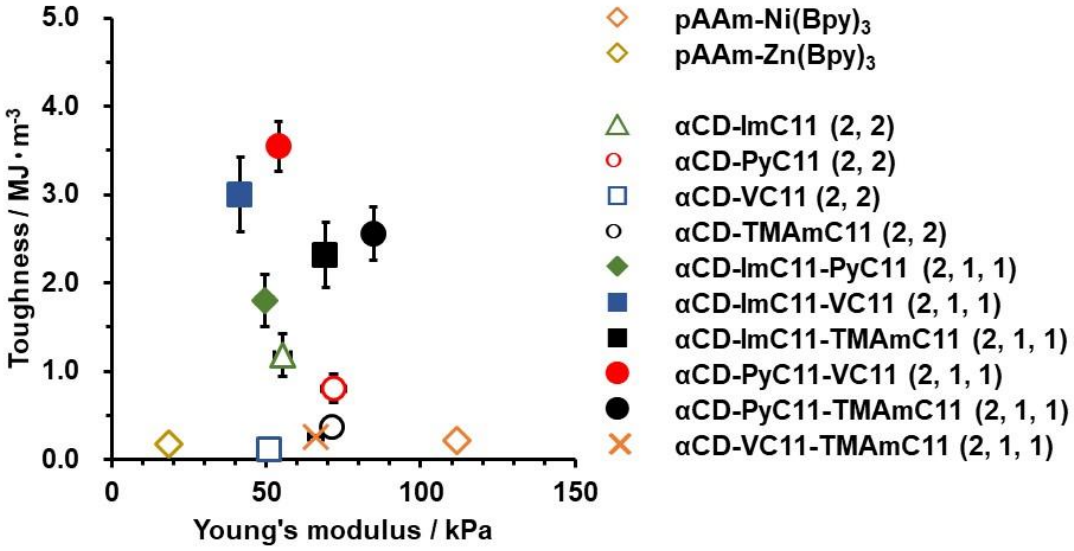

Figure 4-5. Toughness and Young's modulus of the pAAm-Ni$(Bpy)_3$ and pAAm-Zn$(Bpy)_3$ hydrogels compared with those of the αCD-R (2, 2) and αCD-R_1-R_2 (2, 1, 1) hydrogels.

The Young's modulus and toughness of the pAAm-Ni(Bpy)$_3$ hydrogel were 111.6 ± 1.9 kPa and 0.22 ± 0.02 MJ/m^3. The Young's modulus of the pAAm-Ni(Bpy)$_3$ hydrogel was higher than those of the αCD-R (2, 2) and αCD-R$_1$-R$_2$ (2, 1, 1) hydrogels. This was attributed to the high overall association constant ($\beta \simeq 10^{20}$ M^{-3}) of the tris(Bpy) complex, Ni(Bpy)$_3$, and the large number of network chains expanding from one Ni(Bpy)$_3$ reversible cross-link. The toughness was low and similar to that of the αCD-VC11 (2, 2) and αCD-TMAmC11 (2, 2) hydrogels (0.10 ± 0.01 and 0.36 ± 0.05 MJ/m^3, respectively). These results indicate that the kinetics of the Ni(Bpy)$_3$ complex were slow, and that the corresponding reversible cross-links behaved as elastic bodies, resulting in a hard but brittle hydrogel.

In contrast, the pAAm-Zn(Bpy)$_3$ hydrogel showed poor mechanical properties. Its Young's modulus and toughness were 18.5 ± 1.6 kPa and 0.18 ± 0.01 MJ/m^3, respectively. These low values were similar to those of the βCDAAm-AdAAm hydrogel (**Figure 2-41** in Chapter 2) rather than to those of the αCD-R (2, 2) and αCD-R$_1$-R$_2$ (2, 1, 1) hydrogels. Therefore, the author considered that the low modulus and toughness of the pAAm-Zn(Bpy)$_3$ hydrogel were caused by the viscous behavior of the Zn(Bpy)$_3$ reversible cross-links with fast dynamics.

The results of the tensile tests of the pAAm-Ni(Bpy)$_3$ and pAAm-Zn(Bpy)$_3$ hydrogels suggest that the dynamics of reversible cross-links strongly affect the mechanical properties of supramolecular hydrogels, as observed in Chapter 2.

4.3.2. Linear viscoelasticity of the pAAm-$M^{2+}(Bpy)_3$ and pDMAA-Fe-Bpy hydrogels

To determine the relaxation time of reversible cross-links formed by $[M(Bpy)_3]^{2+}$ complexes, linear viscoelastic measurements of the pAAm-$M^{2+}(Bpy)_3$ and pDMAA-Fe-Bpy hydrogels were performed with an Anton Paar MCR302 rheometer. The measurement and analysis methods were the same as those in Chapter 3.

Figure 4-6 shows the results of the frequency-sweep and stress-relaxation tests for the pAAm-$Ni(Bpy)_3$ hydrogel. In the former test, a plateau region of the G' value of the pAAm-$Ni(Bpy)_3$ hydrogel was observed, while $G(t)$ decreased in the long time region. $\langle\tau\rangle_w$ of the pAAm-$Ni(Bpy)_3$ hydrogel was calculated to be 8.7×10^3 s from G_p and τ_p. This value was related to the dissociation of the $[Ni(Bpy)_3]^{2+}$ cross-links and/or disentanglement of the polyacrylamide chains.

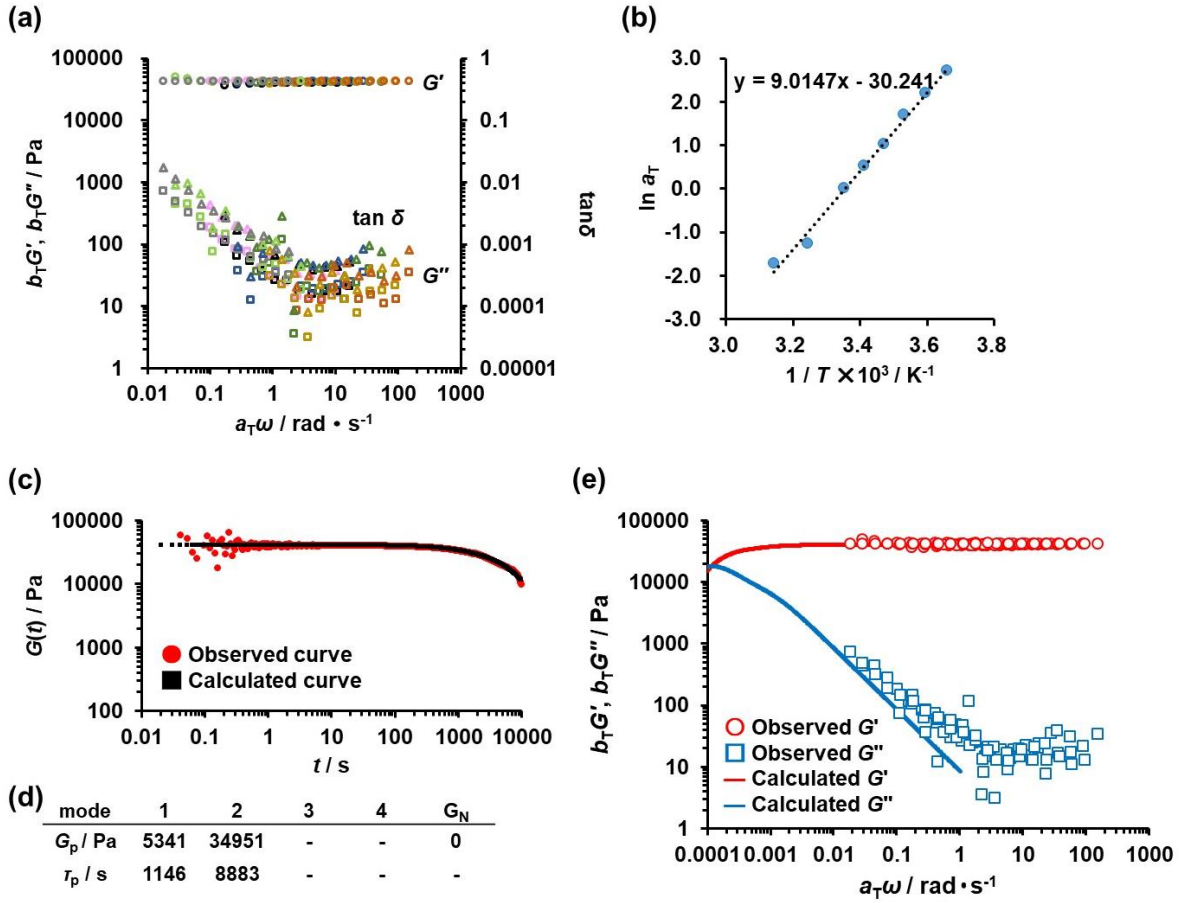

Figure 4-6. (a) Composite curves of G', G'', tan δ for the pAAm-$Ni(Bpy)_3$ hydrogel referenced at 25 °C. **(b)** The Arrhenius plot of a_T used for superposition. **(c)** The stress-relaxation curve of the pAAm-$Ni(Bpy)_3$ hydrogel at 25 °C and curve fitting. **(d)** Parameters G_p and τ_p used for fitting $G(t)$. **(e)** Comparison between the composite curves of G' and G'' and the moduli calculated from G_p and τ_p.

Figures 4-7 and 4-8 show the results of viscoelastic measurements of the pDMAA-Fe-Bpy hydrogels whose W_c values were 97 and 90 wt%. These measurements were performed only at 25 °C. Similar to the pAAm-Ni(Bpy)$_3$ hydrogel, the pDMAA-Fe-Bpy hydrogels with W_c = 97 and 90 wt% showed a plateau of G' values in the ω-sweeps and a decrease in $G(t)$ during the stress-relaxation tests. The $G(t)$ values of both pDMAA-Fe-Bpy hydrogels could be fitted with a single Maxwellian model. The τ (= $<\tau>_w$) values of the pDMAA-Fe-Bpy hydrogels with W_c = 97 and 90 wt% were estimated to be 6.5×10^3 and 8.8×10^3 s, respectively. The observed relaxation modes were derived from the Fe(Bpy)$_3$ cross-links and/or entanglements of pDMAA chains.

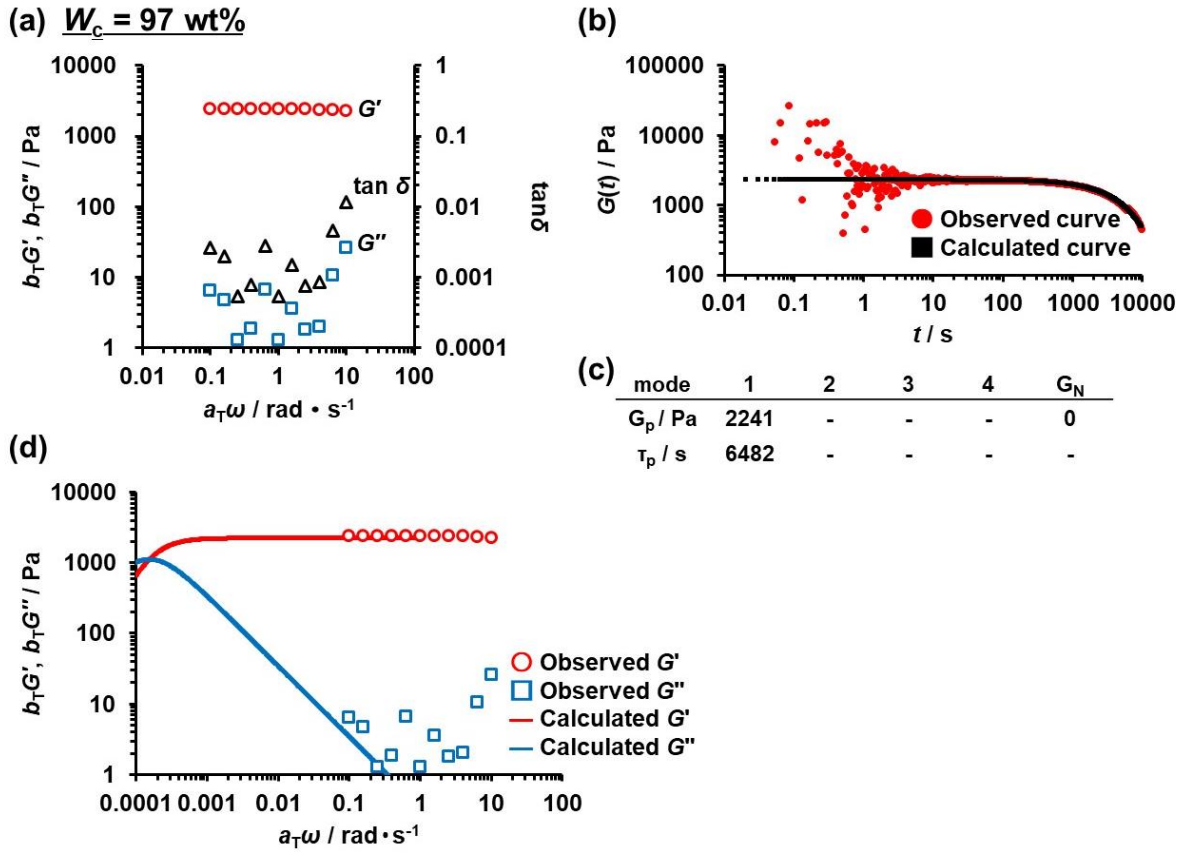

Figure 4-7. Viscoelasticity of the pDMAA-Fe-Bpy hydrogel with W_c = 97 wt%. **(a)** ω dependence of G' and G'' (γ = 0.5%, T = 25 °C). **(b)** The stress-relaxation curve (γ = 0.8%, T = 25 °C) and curve fitting. **(c)** Parameters G_p and τ_p used for fitting $G(t)$. **(d)** Comparison among the observed G', G'', and calculated moduli from G_p and τ_p.

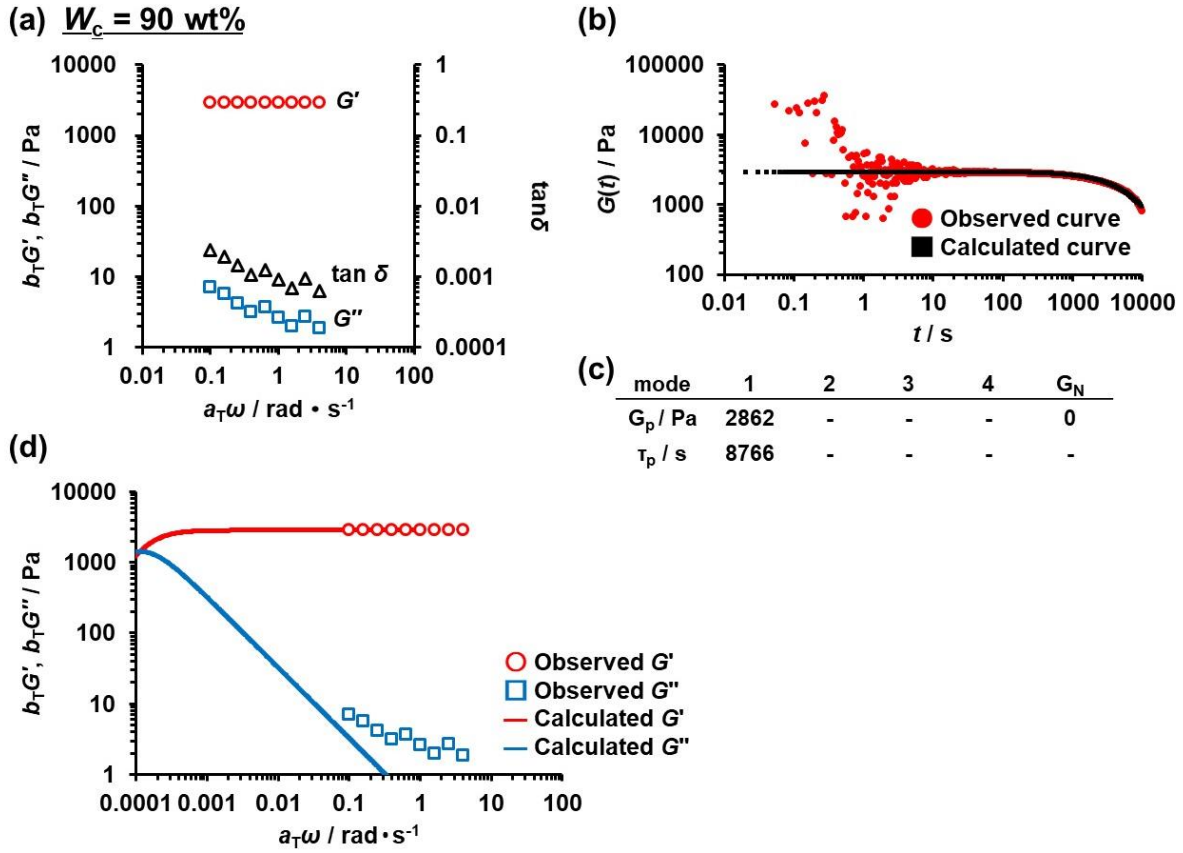

Figure 4-8. Viscoelasticity of the pDMAA-Fe-Bpy hydrogel with W_c = 90 wt%. **(a)** ω dependence of G' and G'' (γ = 0.3%, T = 25 °C). **(b)** The stress-relaxation curve (γ = 0.5%, T = 25 °C) and curve fitting. **(c)** Parameters G_p and τ_p used for fitting $G(t)$. **(d)** Comparison among the observed G', G'', and calculated moduli from G_p and τ_p.

The plateau modulus and $<\tau>_w$ of the pAAm-Ni(Bpy)$_3$ and pDMAA-Fe-Bpy hydrogels are listed in **Table 4-6**. Both hydrogels showed long $<\tau>_w$, whose values were similar to those of αCD-VC11 and αCD-TMAmC11 cross-links (6.6×10^3 and 9.5×10^3, respectively). The plateau modulus of the pDMAA-Fe-Bpy hydrogel increased with decreasing W_c, which was caused by an increase in the cross-linking density. The $<\tau>_w$ of the hydrogel also slightly increased with decreasing W_c, which might be due to state changes in the Fe(Bpy)$_3$ complexes, entanglements, or experimental error.

Table 4-6. Plateau modulus and $<\tau>_w$ of the pAAm-Ni(Bpy)$_3$ and pDMAA-Fe-Bpy hydrogels with different W_c.

Sample	W_c / wt%	Plateau modulus / Pa	$<\tau>_w$ / s
pAAm-Ni(Bpy)$_3$	86* (as-prepared)	4.3×10^4	8.8×10^3
pDMAA-Fe-Bpy	97	2.2×10^3	6.5×10^3
	90	2.9×10^3	8.8×10^3

*: W_c of the pAAm-Ni(Bpy)$_3$ hydrogel was estimated from the amounts of reagents used.

The linear viscoelastic measurements suggested $<\tau>_{w,Ni} \approx <\tau>_{w,Fe}$ for the relation among the dynamics of supramolecular hydrogels cross-linked by $M^{2+}(Bpy)_3$ complexes. In addition, the author estimated the relation $<\tau>_{w,Ni} \approx <\tau>_{w,Fe} \gg <\tau>_{w,Zn}$ from the mechanical properties of the pAAm-$Zn(Bpy)_3$ hydrogel evaluated by a tensile test. This magnitude relation was in accordance with the dynamics of several tetra-PEG hydrogels through coordination bonds. As reported by Messersmith *et al.*[5] and Holten-Anderson *et al*.[6], tetra-PEG hydrogels cross-linked by bis(histidine) complexes with divalent transition metal ions showed distinct relaxation times, $\tau_{Ni} > \tau_{Co} > \tau_{Cu} > \tau_{Zn}$. Furthermore, Ahmadi and Seiffert[7] investigated tetra-PEG hydrogels cross-linked by bis- and tris-phenanthroline complexes and observed the relaxation times $\tau_{Ni} > \tau_{Fe} > \tau_{Co} > \tau_{Cu}$.

4.3.3. Relation between linear viscoelasticity and toughness of the pAAm-Ni(Bpy)$_3$ hydrogel

The pAAm-Ni(Bpy)$_3$ hydrogel was successfully evaluated by linear viscoelastic measurements and tensile tests. To describe the viscoelastic behavior of the pAAm-Ni(Bpy)$_3$ hydrogel during the tensile test, the author utilized the Weissenberg number, which was estimated from the product of $<\tau>_w$ and the initial nominal strain rate ($\dot{\varepsilon}_C$), as described in Chapter 2. $\dot{\varepsilon}_C$ was calculated from the tensile speed (v = 1.0 mm/s) and initial length of a sample ($L_0 \approx 23$ mm) to be $\dot{\varepsilon}_C = v/L_0$. **Figure 4-9** shows the relation between the Weissenberg number $\dot{\varepsilon}_C\langle\tau\rangle_w$ and the toughness of the pAAm-Ni(Bpy)$_3$ hydrogel compared with the those of the αCD-R (2, 2)[25] (**Figure 3-6b** in Chapter 3) and βCD-VC11 (2, 2) hydrogels[26] (**Figure 2-41a** in Chapter 2). Note that the toughness of the αCD-R (2, 2) hydrogels in Chapter 3 differs from that in Chapter 2 due to the replacement of 1 N clip jigs. In particular, the toughness of the αCD-PyC11 (2, 2) hydrogel significantly decreased in Chapter 3, suggesting that the condition of the measuring instrument, as well as material design, strongly influences the measured results. In this chapter, the author used the results from Chapter 3 because the measurement conditions of the tensile tests for the pAAm-Ni(Bpy)$_3$ hydrogel were the same as those used for the αCD-R (2, 2) hydrogels in Chapter 3.

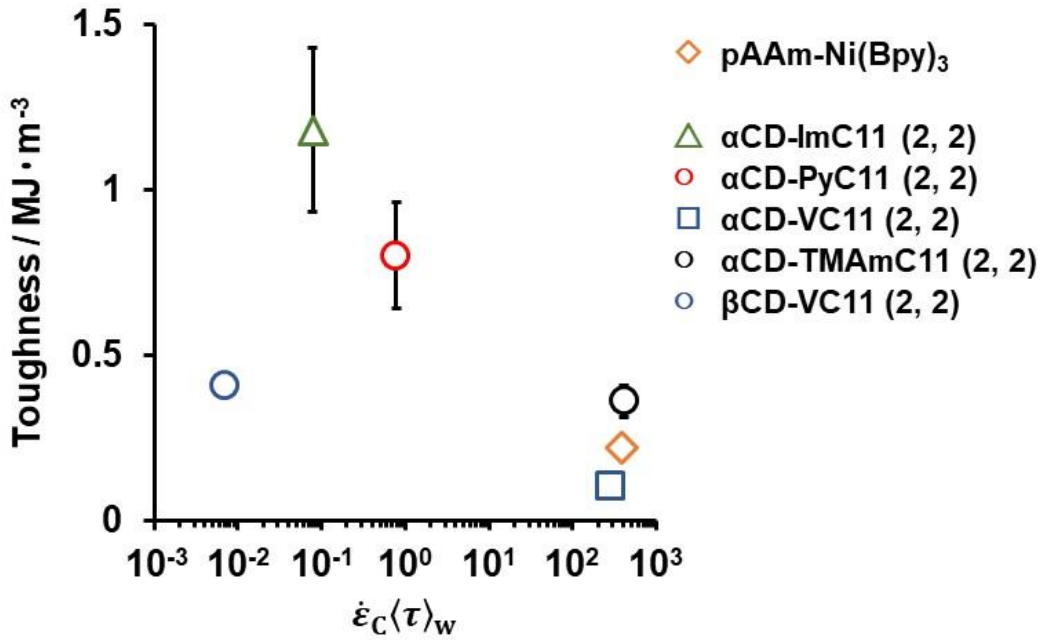

Figure 4-9. Plots of toughness and $\dot{\varepsilon}_C\langle\tau\rangle_w$ of the pAAm-Ni(Bpy)$_3$ hydrogel, the αCD-R (2, 2) hydrogels, and the βCD-VC11 (2, 2) hydrogel.

The data for the pAAm-Ni(Bpy)$_3$ hydrogel were consistent with the relation between $\dot{\varepsilon}_C\langle\tau\rangle_w$ and toughness of the αCD-R (2, 2) hydrogels. The toughness of these supramolecular hydrogels was higher than 0.5 MJ/m^3 in the range of $10^{-2} < \dot{\varepsilon}_C\langle\tau\rangle_w < 10^0$, while it decreased to less than 0.5 MJ/m^3 in the range of $\dot{\varepsilon}_C\langle\tau\rangle_w < 10^{-2}$ and $> 10^2$. This trend indicates that the viscoelastic behavior of reversible cross-links triggers energy dissipation and increases the toughness, whereas the viscous or elastic behavior of the cross-links decreases the toughness, as described in Chapter 2. Therefore, the author considered that the low toughness of the pAAm-Ni(Bpy)$_3$ hydrogel was caused by the elastic behavior of the supramolecular polymer network. Interestingly, the pAAm-Ni(Bpy)$_3$, αCD-VC11 (2, 2), αCD-TMAmC11 (2, 2), and βCD-VC11 (2, 2) hydrogels exhibited similar toughness regardless of the type of non-covalent bond. These hydrogels have several common points of material design: cross-links on side chains, pAAm main chain, monomer concentrations, and initiators. Thus, the similarity of the toughness suggests that the kinetics of non-covalent bonds are more important than the thermodynamics and binding energy for the improvement of toughness.

Figure 4-9 demonstrates to some extent the universality of the relation between linear viscoelasticity and toughness during large deformation of pAAm-based hydrogels cross-linked by host-guest complexes or metal-ligand coordination. However, the author has not yet evaluated the viscoelasticity and mechanical properties of the pAAm-M(Bpy)$_3$ and pDMAA-M(Bpy)$_3$ hydrogels, or their dependence on strain rate, using other metal ions. Such data will ensure the universality of how the kinetics of non-covalent bonds determine the mechanical properties of supramolecular hydrogels with reversible cross-links.

4.4. Conclusion

The author investigated three kinds of supramolecular hydrogels cross-linked by metal-ligand coordination, pAAm-Ni(Bpy)$_3$, pAAm-Zn(Bpy)$_3$, and pDMAA-Fe-Bpy hydrogels, to explore the effects of the coordination bonds on the mechanical properties and viscoelasticity of the hydrogels. The pAAm-Ni(Bpy)$_3$ and pAAm-Zn(Bpy)$_3$ hydrogels were evaluated by tensile tests. The former showed low toughness and a high Young's modulus, while the latter exhibited low toughness and a low Young's modulus. These mechanical properties indicated the elastic behavior of the pAAm-Ni(Bpy)$_3$ hydrogel and the contrasting viscous behavior of the pAAm-Zn(Bpy)$_3$ hydrogel. On the other hand, linear viscoelastic measurements revealed the slow dynamics of the pAAm-Ni(Bpy)$_3$ and pDMAA-Fe-Bpy hydrogels. Their relaxation times ($<\tau>_w$) were approximately 8.8×10^3 s. These slow dynamics of the hydrogels were attributed to the kinetics of the Ni(Bpy)$_3$ and Fe(Bpy)$_3$ complexes. The observed long $<\tau>_w$ of the pAAm-Ni(Bpy)$_3$ hydrogel corresponded to the brittle behavior during the tensile test.

The effect of long $<\tau>_w$ on the toughness of the pAAm-Ni(Bpy)$_3$ hydrogel was demonstrated using a dimensionless parameter $\dot{\varepsilon}_C\langle\tau\rangle_w$. The relation between toughness and $\dot{\varepsilon}_C\langle\tau\rangle_w$ of the pAAm-Ni(Bpy)$_3$ hydrogel agreed with the findings for the αCD-VC11 (2, 2) and αCD-TMAmC11 (2, 2) hydrogels in described in Chapter 3. This consistency suggests that the elastic behavior of reversible cross-links inhibits energy dissipation during stretching and decreases the toughness of supramolecular hydrogels regardless of the type of non-covalent bonds used (host-guest complexation or metal-ligand coordination). The author demonstrated the universal relation between the linear viscoelastic relaxation time and the toughness of supramolecular hydrogels with reversible cross-links. The author believes this concept will be applicable to supramolecular hydrogels with other reversible cross-links and help develop strategies for enhancing mechanical properties.

References

(1) Chen, H.; Zhang, J.; Yu, W.; Cao, Y.; Cao, Z.; Tan, Y. Control Viscoelasticity of Polymer Networks with Crosslinks of Superposed Fast and Slow Dynamics. *Angew. Chemie - Int. Ed.* **2021**, *60* (41), 22332–22338.

(2) Rose, S.; Dizeux, A.; Narita, T.; Hourdet, D.; Marcellan, A. Time Dependence of Dissipative and Recovery Processes in Nanohybrid Hydrogels. *Macromolecules* **2013**, *46* (10), 4095–4104.

(3) Long, R.; Mayumi, K.; Creton, C.; Narita, T.; Hui, C. Y. Time Dependent Behavior of a Dual Cross-Link Self-Healing Gel: Theory and Experiments. *Macromolecules* **2014**, *47* (20), 7243–7250.

(4) Helm, L.; Merbach, A. E. Water Exchange on Metal Ions: Experiments and Simulations. *Coord. Chem. Rev.* **1999**, *187* (1), 151–181.

(5) Fullenkamp, D. E.; He, L.; Barrett, D. G.; Burghardt, W. R.; Messersmith, P. B. Mussel-Inspired Histidine-Based Transient Network Metal Coordination Hydrogels. *Macromolecules* **2013**, *46* (3), 1167–1174.

(6) Grindy, S. C.; Learsch, R.; Mozhdehi, D.; Cheng, J.; Barrett, D. G.; Guan, Z.; Messersmith, P. B.; Holten-Andersen, N. Control of Hierarchical Polymer Mechanics with Bioinspired Metal-Coordination Dynamics. *Nat. Mater.* **2015**, *14* (12), 1210–1216.

(7) Ahmadi, M.; Seiffert, S. Coordination Geometry Preference Regulates the Structure and Dynamics of Metallo-Supramolecular Polymer Networks. *Macromolecules* **2021**, *54* (3), 1388–1400.

(8) Yount, W. C.; Loveless, D. M.; Craig, S. L. Small-Molecule Dynamics and Mechanisms Underlying the Macroscopic Mechanical Properties of Coordinatively Cross-Linked Polymer Networks. *J. Am. Chem. Soc.* **2005**, *127* (41), 14488–14496.

(9) Yount, W. C.; Juwarker, H.; Craig, S. L. Orthogonal Control of Dissociation Dynamics Relative to Thermodynamics in a Main-Chain Reversible Polymer. *J. Am. Chem. Soc.* **2003**, *125* (50), 15302–15303.

(10) Yount, W. C.; Loveless, D. M.; Craig, S. L. Strong Means Slow: Dynamic Contributions to the Bulk Mechanical Properties of Supramolecular Networks. *Angew. Chemie - Int. Ed.* **2005**, *44* (18), 2746–2748.

(11) Zhao, X.; Chen, X.; Yuk, H.; Lin, S.; Liu, X.; Parada, G. Soft Materials by Design: Unconventional Polymer Networks Give Extreme Properties. *Chem. Rev.* **2021**, *121* (8), 4309–4372.

(12) Rodin, M.; Li, J.; Kuckling, D. Dually Cross-Linked Single Networks: Structures and Applications. *Chem. Soc. Rev.* **2021**, *50* (14), 8147–8177.

(13) Means, A. K.; Grunlan, M. A. Modern Strategies to Achieve Tissue-Mimetic, Mechanically Robust Hydrogels. *ACS Macro Lett.* **2019**, *8* (6), 705–713.

(14) Sun, J. Y.; Zhao, X.; Illeperuma, W. R. K.; Chaudhuri, O.; Oh, K. H.; Mooney, D. J.; Vlassak, J. J.; Suo, Z. Highly Stretchable and Tough Hydrogels. *Nature* **2012**, *489* (7414), 133–136.

(15) Burnworth, M.; Tang, L.; Kumpfer, J. R.; Duncan, A. J.; Beyer, F. L.; Fiore, G. L.; Rowan, S. J.; Weder, C. Optically Healable Supramolecular Polymers. *Nature* **2011**, *472* (7343), 334–337.

(16) Shi, L.; Ding, P.; Wang, Y.; Zhang, Y.; Ossipov, D.; Hilborn, J. Self-Healing Polymeric Hydrogel Formed by Metal–Ligand Coordination Assembly: Design, Fabrication, and Biomedical Applications. *Macromol. Rapid Commun.* **2019**, *40* (7), 1–18.

(17) Li, C. H.; Zuo, J. L. Self-Healing Polymers Based on Coordination Bonds. *Adv. Mater.* **2020**, *32* (27), 1–29.

(18) Zechel, S.; Hager, M. D.; Priemel, T.; Harrington, M. J. Healing through Histidine: Bioinspired Pathways to Self-Healing Polymers via Imidazole-Metal Coordination. *Biomimetics* **2019**, *4* (1), 20.

(19) Yan, X.; Wang, F.; Zheng, B.; Huang, F. Stimuli-Responsive Supramolecular Polymeric Materials. *Chem. Soc. Rev.* **2012**, *41* (18), 6042–6065.

(20) Mauro, M. Dynamic Metal–Ligand Bonds as Scaffolds for Autonomously Healing Multi-Responsive Materials. *Eur. J. Inorg. Chem.* **2018**, 2018 (20–21), 2090–2100.

(21) Herbert, K. M.; Schrettl, S.; Rowan, S. J.; Weder, C. 50th Anniversary Perspective: Solid-State Multistimuli, Multiresponsive Polymeric Materials. *Macromolecules* **2017**, *50* (22), 8845–8870.

(22) Khare, E.; Holten-Andersen, N.; Buehler, M. J. Transition-Metal Coordinate Bonds for Bioinspired Macromolecules with Tunable Mechanical Properties. *Nature Reviews Materials.* Springer US 2021, pp 421–436.

(23) Campanella, A.; Döhler, D.; Binder, W. H. Self-Healing in Supramolecular Polymers. *Macromol. Rapid Commun.* **2018**, *39* (17), 1–19.

(24) Nakamura, T.; Takashima, Y.; Hashidzume, A.; Yamaguchi, H.; Harada, A. A Metal-Ion-Responsive Adhesive Material via Switching of Molecular Recognition Properties. *Nat. Commun.* **2014**, *5*, 4622.

(25) Konishi, S.; Park, J.; Urakawa, O.; Osaki, M.; Yamaguchi, H.; Harada, A.; Inoue, T.; Matsuba, G.; Takashima, Y. Multi-Energy Dissipation Mechanisms in Supramolecular Hydrogels with Fast and Slow Relaxation Modes. *Soft Matter* **2022**, *18* (38), 7369–7379.

(26) Aramoto, H.; Osaki, M.; Konishi, S.; Ueda, C.; Kobayashi, Y.; Takashima, Y.; Harada, A.; Yamaguchi, H. Redox-Responsive Supramolecular Polymeric Networks Having Double-Threaded Inclusion Complexes. *Chem. Sci.* **2020**, *11* (17), 4322–4331.

Summary of This Thesis

This thesis has addressed the quantitative design of supramolecular hydrogels that have certain mechanical properties based on the chemistry of non-covalent bonds. In particular, the author has focused on changes in the linear viscoelasticity and tensile toughness of the reversibly cross-linked hydrogels as a result of the kinetics of non-covalent bonds.

In Chapter 2, supramolecular hydrogels with reversible cross-links formed by complexation of αCD with cation-terminated linear alkyl moieties were developed. The toughness, Young's modulus, and relaxation time of the αCD-R hydrogels varied depending on the kinetics of the host-guest complexations. The relation among toughness, relaxation time, and strain rate revealed that the viscoelastic behavior of the reversible cross-links significantly improved the toughness, while their viscous or elastic behavior resulted in low toughness due to a lack of energy dissipation. Chapter 2 demonstrates the importance of the dynamics of polymers, such as relaxation time, in the design of tough polymeric materials.

In Chapter 3, supramolecular hydrogels combining two kinetically distinct reversible cross-links *via* host-guest complexations were investigated to develop improved strategies for establishing tougher materials using reversible cross-links. These hydrogels exhibited hierarchical relaxation behaviors caused by independent dissociation of the two types of reversible cross-links. In particular, the combination of fast ($<\tau>_w \approx 10^{-1}$~10^{1} s) and slowly ($<\tau>_w \approx 10^{3}$ s) reversible cross-links realized effective energy dissipation at large strains, which significantly increased the tensile toughness of supramolecular hydrogels.

In Chapter 4, the author evaluated supramolecular hydrogels cross-linked through metal-ligand coordination to verify whether the relation between linear viscoelasticity and tensile toughness described in Chapter 2 also holds true for hydrogels containing coordination bonds. The polyacrylamide-based hydrogel cross-linked by tris(bipyridine) complexes with Ni^{2+} ions showed a long relaxation time (~ 10^{3} s) in linear viscoelastic measurements and low toughness in tensile tests. These results agreed with those of the αCD-R hydrogels, supporting the universality of how the viscoelastic behavior of reversible cross-links affects the toughness of supramolecular hydrogels.

Throughout this thesis, the author concludes that the kinetics of non-covalent bonds should be considered in the development of tough supramolecular polymeric materials. Compared to the design of numerous polymeric materials with extreme properties, the design of the hydrogels studied in this thesis was simple, and their toughness was not sufficient. However, the author believes that the concept described in this thesis will encourage a considerable amount of research in the field of material science.

List of Supramolecular Hydrogels

Chapter 2

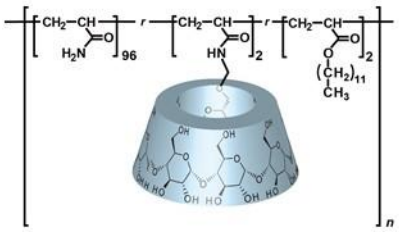

αCD-C12 (2, 2)

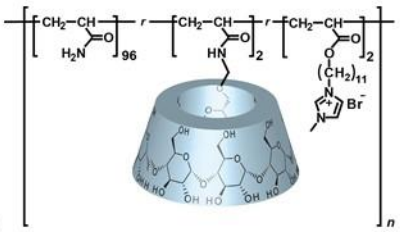

αCD-ImC11 (2, 2)

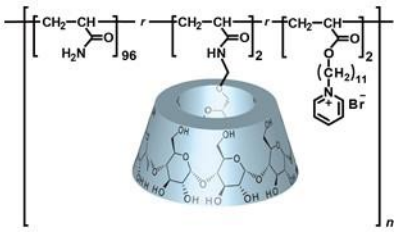

αCD-PyC11 (2, 2)

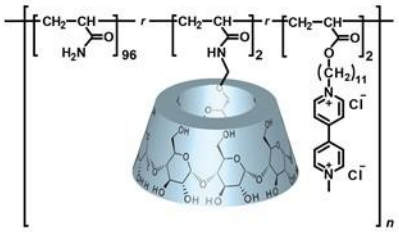

αCD-VC11 (2, 2)

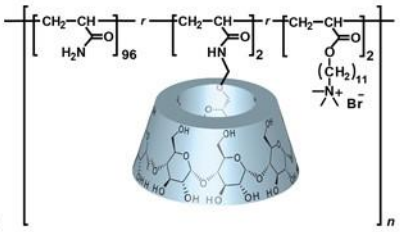

αCD-TMAmC11 (2, 2)

Chapter 4

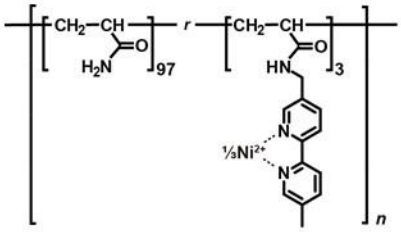

pAAm-Ni(Bpy)$_3$

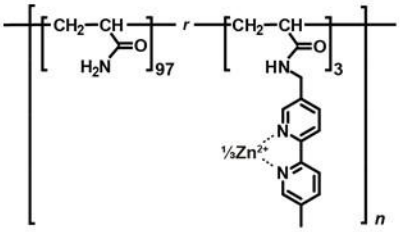

pAAm-Zn(Bpy)$_3$

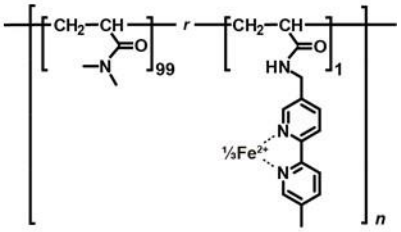

pDMAA-Fe-Bpy

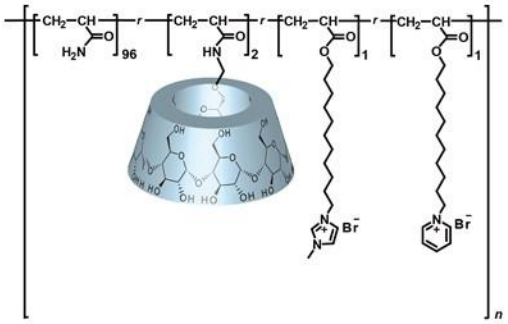

αCD-ImC11-PyC11 (2, 1, 1)

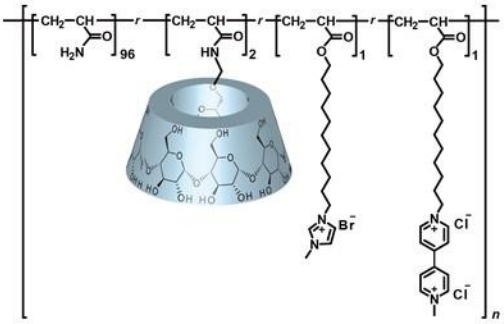

αCD-ImC11-VC11 (2, 1, 1)

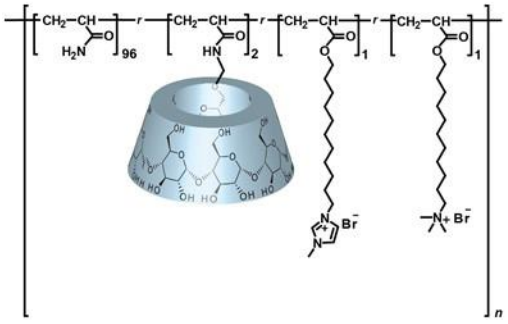

αCD-ImC11-TMAmC11 (2, 1, 1)

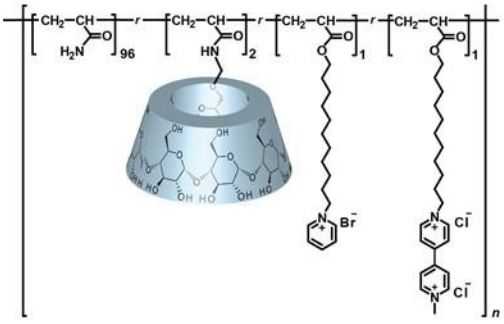

αCD-PyC11-VC11 (2, 1, 1)

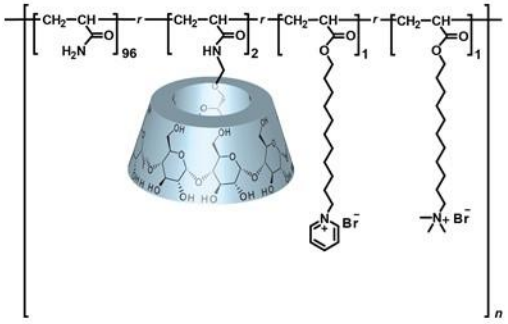

αCD-PyC11-TMAmC11 (2, 1, 1)

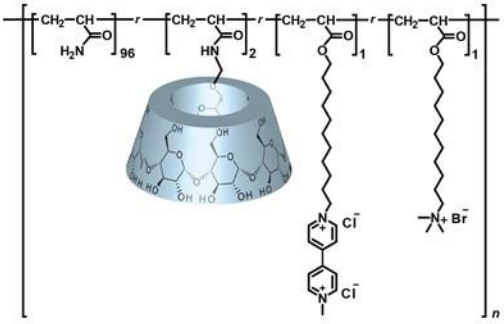

αCD-VC11-TMAmC11 (2, 1, 1)

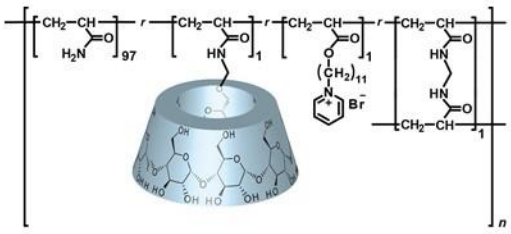

αCD-PyC11-MBAAm (1, 1, 1)

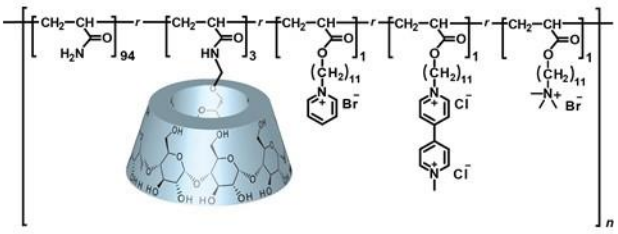

αCD-PyC11-VC11-TMAmC11 (3, 1, 1, 1)

List of Publications

Original papers

1. Konishi, S.; Kashiwagi, Y.; Watanabe, G.; Osaki, M.; Katashima, T.; Urakawa, O.; Inoue, T. ; Yamaguchi, H.; Harada, A.; Takashima, Y. Design and Mechanical Properties of Supramoleuclar Polymeric Materials Based on Host-guest Interactions: the Relation between Relaxation Time and Fracture Energy. *Polym. Chem.* **2020**, *11*, 6811–6820.
2. Konishi, S.; Park, J.; Urakawa, O.; Osaki, M.; Yamaguchi, H.; Harada, A.; Inoue, T.; Matsuba, G.; Takashima, Y. Multi-Energy Dissipation Mechanisms in Supramolecular Hydrogels with Fast and Slow Relaxation Modes. *Soft Matter* **2022**, *18*, 7369–7379.

Related papers

1. Aramoto, H.; Osaki, M.: Konishi, S.; Ueda, C.; Takashima, Y.; Harada, A.; Yamaguchi, H. Redox-Responsive Supramolecular Polymeric Networks Having Double-Threaded Inclusion Complexes. *Chem. Sci.* **2020**, *11*, 4322-4331.
2. Ueda, C.; Park, J.; Hirose, K.; Konishi, S.; Ikemoto, Y.; Osaki, M.; Yamaguchi, H.; Harada, A.; Tanaka, M.; Watanabe, G.; Takashima, Y. Behavior of Supramolecular Cross-Links Formed by Host-Guest Interaction in Hydrogels Responding to Water Contents. *Supramol. Mater.* **2022**, *1*, 100001.

Other publications

1. 小西昴、以倉峻平、大﨑基史、髙島義徳、原田明「可逆性結合を用いた高分子材料の設計とその機能、応用」『重合開始剤,硬化剤,架橋剤の選び方、使い方とその事例』技術情報協会、第3章、第20節（2021年）